POLITECNICO DI TORINO

Corso di Laurea Magistrale in Ingegneria Aerospaziale

Tesi di Laurea Magistrale

Preliminary design of a Thermal and Energy Management Subsystem for hypersonic vehicle concepts

Relatori

Prof.ssa Nicole Viola

Ing. Roberta Fusaro

Ing. Davide Ferretto

Candidato

Paolo Bader

Ottobre 2019

Abstract – English version

Within the framework of the H2020 STRATOFLY project, the feasibility of a hypersonic-speed passenger flight is being studied with the final goal of demonstrating the possibility for a set of key-enabling technologies to reach a technology readiness level (TRL) of 6 by the next decade. This innovative project is providing an interesting challenge for the researchers, since most of the concepts are pioneering comparing to current state of technology, and the idea itself is ambitious and a potential game changer in aerospace industry. The project involves many different skillsets: professors and researchers from all over Europe are sharing their knowledge and expertise in several fields of physics to make it concrete. Over the last year, as part of a dissemination action, Politecnico di Torino kicked-off the STRATOFLY Academy, a way to stimulate the next generations offering topics for Theses and classwork to the worldwide community. The present work is inserted within this context, in particular of the First Challenge.

This thesis focuses on the definition, design, sizing and simulation of the Thermal and Energy Management System, one of the key-enabling technologies identified within the context of the STRATOFLY project. This innovative subsystem, conceived precisely for the hypersonic reference vehicle and never experienced before, brings the utilisation of liquid hydrogen as a fuel to the next level. In fact, thermal issues related to hydrogen storage (cryogenic temperature, necessity to vent, low density and hence increasing fuel tanks mass) are turned to an asset. In particular, this subsystem is meant to be the heuristic sum of several aircraft major subsystems: thermal protection, fuel management, engine cooling, environmental control system and on-board power generation are now integrated in a single comprehensive framework, that will handle these features with a clever management of stored hydrogen.

In details, this thesis aims to analyse this innovative concept in its entirety, starting with mission profile outputs; the target of the work is to define a proper architecture for this subsystem and test its capability and compliance with the expectations. First, aircraft aerodynamics will be considered, in order to evaluate global linearized coefficients in a variety of flight conditions (namely true air speed, altitude, angle of attack and bank angle). In the same way, global thrust data will be estimated in a wide array of working states, to properly describe aircraft behaviour throughout the mission. Two parallel analyses will then be performed: the available literature mission profile data will be compared with a longitudinal-plane flight simulation; the latter consists in applying the equations of flight mechanics to a material point, interpolating the previously prepared aerodynamic and propulsive data over time. This study is only preparatory for a thermal analysis, in which heat loads on the leading edge of the intake (most critical point) and on the whole aircraft (as the average) during the flight will be made. At this point, the reference TEMS configuration can be analysed, and a new one is proposed and described to overcome some disadvantages. Subsequently, a static sizing procedure, benefitting from semi-empiric equations and approximate relation, will be defined. Then, the overall system is dynamically tested throughout the mission. In conclusion, the overall performance of the proposed configuration will be discussed, and new ideas for further development will be recommended.

Abstract – Italian version

Nell'ambito del progetto H2020 STRATOFLY, è in corso uno studio riguardante la realizzabilità di un velivolo da trasporto passeggeri ipersonico; tra i suoi obiettivi figura la dimostrazione che, tramite alcune tecnologie chiave, sia possibile il raggiungimento del livello di preparazione tecnologica (TRL) 6 entro il prossimo decennio. Questo progetto innovativo rappresenta una sfida interessante per i ricercatori, dal momento che la maggior parte dei concept coinvolti sono pionieristici rispetto allo stato attuale della tecnologia, e l'idea stessa è ambiziosa, avendo potenzialmente la possibilità di rivoluzionare l'industria aerospaziale. Il progetto coinvolge diversi ambiti e professionalità differenti: ricercatori e professori da tutta Europa condividono le loro conoscenze e competenze in diversi campi della fisica per realizzare questo progetto. Nel corso dell'ultimo anno, per incentivarne la diffusione, il Politecnico di Torino ha dato il via alla STRATOFLY Academy, ovvero un mezzo per coinvolgere le nuove generazioni, offrendo possibilità di tesi e lavori di gruppo a tutti i livelli di istruzione in ogni parte del mondo. Il presente lavoro è inserito in questo contesto, in particolare in quello della prima sfida.

Questa tesi si concentra sulla definizione, progettazione, dimensionamento e simulazione del Thermal and Energy Management System (TEMS), una delle tecnologie chiave individuate nel contesto del progetto STRATOFLY. Questo innovativo sottosistema, concepito proprio per il veicolo ipersonico di riferimento e mai sperimentato prima, configura un utilizzo rivoluzionario dell'idrogeno liquido (scelto come carburante). Infatti, i problemi termici legati allo stoccaggio dell'idrogeno (temperatura criogenica, necessità di sfiato, bassa densità e quindi aumento della massa dei serbatoi) sono tramutati in punti di forza. In particolare, questo sottosistema rappresenta la somma euristica di alcuni dei principali sottosistemi dell'aeromobile: protezione termica, gestione del combustibile, raffreddamento del motore, sistema di controllo ambientale e generazione di energia a bordo; in tal modo le loro funzioni sono ora adibite ad un unico sistema altamente integrato, che svolgerà le mansioni assegnate tramite una gestione intelligente dell'idrogeno immagazzinato.

In particolare, questa tesi si prefigge lo scopo di studiare questo concept innovativo nella sua interezza, a partire dalla caratterizzazione del profilo di missione; l'obiettivo finale dello studio è definire un'architettura adeguata a questo sottosistema e testarne la capacità e la conformità alle attuali aspettative. In primo luogo, sarà considerata l'aerodinamica dell'aeromobile, al fine di valutare i coefficienti linearizzati globali in diverse condizioni di volo (tra cui TAS, altitudine, angolo di attacco e di sbandamento). Allo stesso modo saranno stimati anche i più importanti indici delle performance del motore in una vasta gamma di condizioni di funzionamento, per descrivere adeguatamente il comportamento degli aeromobili durante tutta la missione. Successivamente verranno effettuate due analisi in parallelo: i dati relativi al profilo di missione disponibili in letteratura saranno confrontati con una simulazione del volo nel piano longitudinale; quest'ultima consiste nell'applicazione delle equazioni della meccanica di volo ad un punto materiale, interpolando nel tempo i dati aerodinamici e propulsivi preparati in precedenza. Questo studio è propedeutico per la successiva analisi termica, in cui si studieranno gli scambi di calore tra corpo e fluido sul bordo di attacco della presa (punto più critico) e sul velivolo intero (mediamente) lungo l'intera missione. A questo punto, si analizzerà la configurazione TEMS di riferimento, e ne verrà proposta e descritta una nuova che rimedi ad alcuni svantaggi della precedente. Successivamente sarà definita una procedura di dimensionamento statico, che beneficia di equazioni semi-empiriche e studi statistici per elaborare un algoritmo di dimensionamento consono ad un livello di design concettuale. In seguito, l'intero sistema viene testato dinamicamente durante tutta la missione, effettuando un'analisi delle performance e della loro evoluzione nel tempo. In conclusione, saranno discusse le prestazioni complessive della configurazione proposta e saranno raccomandate nuove idee per ulteriori sviluppi.

Table of contents

Acknowledgements

This thesis becomes a reality with the kind support and help of many individuals. I would like to extend my sincere thanks to all of them.

Foremost, I must express my very profound gratitude for Prof. Nicole Viola: besides being my mentor in this research, she is the coordinator of the whole STRATOFLY Project and supporter of the STRATOFLY Academy; thanks to this opportunity, I have learned a lot and really enjoyed while working on this thesis.

I would like to express the deepest appreciation to my supervisor, Dr. Roberta Fusaro: she continually and convincingly conveyed a spirit of fascination in regard to research and teaching; without her guidance and persistent help, this dissertation would not have been possible.

I would like to thank Dr. Davide Ferretto for his patience, motivation and immense knowledge. His guidance helped me in overcome many standstills during my research.

My sincere gratitude goes to my parents and my sister for their spiritual and material support, and for always believing in me.

I would like to also mention my dear Silvia: your joy and fondness makes me achieve more.

My thanks and appreciation also go to my teammates, colleagues and friends who have willingly helped me out with their personal and unique abilities.

Paolo Bader

1. Introduction

1.1. Stratofly Project

1.1.1. Horizon 2020

Horizon 2020 is the framework programme for research and innovation (2014-2020). This project main purpose is to promote research and innovation, and in general the actions to be taken to ensure Europe's global competitiveness. Investing in research and innovation means investing in the future of Europe. Research and innovation are encouraged in order to compete globally and improve the daily lives of millions of people in Europe and the rest of the world, helping to solve some of the major social and generational problems. Currently, despite hosting only 7% of the world's population, Europe boasts 20% of world investment in research and innovation, produces one third of all high-quality scientific publications and is a world leader in sectors such as the pharmaceutical industry, chemicals, mechanical engineering and fashion.
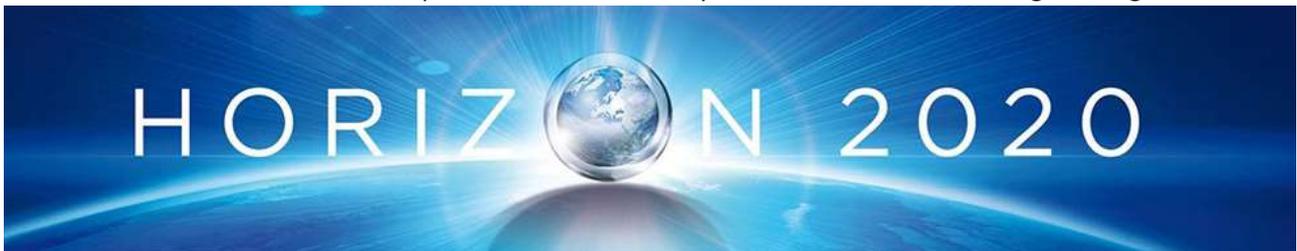
Figure 1: Horizon 2020 logo [1]

Horizon 2020 programme aims to further encourage research and innovation with a financial contribution of 100 billion euros, which will be used to consolidate the results and success of the previous research and innovation programmes and enable the EU to remain at the forefront of research and innovation worldwide. [2] In view of the success that this programme has obtained so far, a new investment plan is being refined for future implementation: his name is "Horizon Europe". It is the new research and innovation programme to succeed Horizon 2020, with a total budget of 100 billion euro for 2021-2027.

Figure 2: Horizon Europe logo [3]

Presented by the European Commission on 7 June 2018, the new Framework Programme for Research and Innovation is part of the next Multiannual Financial Framework (MFF) of the EU (2021-2027). It is a wide-ranging programme, in which both public and private institutions will benefit a wide range of facilitation and investment.

1.1.2. Stratofly project

In the framework of Horizon 2020, a challenging project in the aerospace field is assessed. It is named "STRATOFLY", an acronym that stands for "Stratospheric Flying Opportunities for High-Speed Propulsion Concepts".

This project focuses on the investigation, research and development of a new technology in the field of civil transport, introducing a challenge that has never been addressed before. It is a question of examining the feasibility of an ultra-fast passenger transport aircraft, which will guarantee an antipodal traverse of the globe

in less than three hours; this aircraft will be able to fly in the lower stratosphere (approximately 30 km of altitude, approximately 3 times the current flight altitude of ordinary passenger planes), at a speed of around 10000 km/h, almost at the hypersonic Mach 8 flight regime, which is 8 times faster than sound at that cruise altitude. This innovative project requires, first of all, an in-depth study economic and social in nature, since such an innovation is intended to introduce an entirely new product on the aeronautical market; It is important to attract the support of the general public, so that this project can obtain a good economic response to the costs of developing technologies that have not yet been implemented before. Secondly, a technical study on the real feasibility and safety of the aircraft is being carried out: a two-stage propulsion system powered by liquid hydrogen will be integrated with structural configurations still in phase of research and development, as well as an innovative geometric configuration that manages to deal optimally with the requested mission. A very important aspect of the aircraft will also be the high degree of integration of the systems: for example, the VEMS ("vehicle and Energy Management System"), a single system that exploits the functions (currently performed by different physical systems operating with different logics) of thermal protection, fuel management, environmental control and on-board power generation. The project, although in the conceptual design phase, aims to ensure the aircraft a top-level performance also in the field of passenger safety and noise pollution. In addition to this, the design choices undertaken so far address the project on an eco-sustainable path: the use of liquid hydrogen ensures a lower environmental impact from the point of view of emissions, since the cryogenic fuel offers a high propulsive efficiency (greater than about 15% compared to the current one), and the nature of hydrogen itself presents fewer pollutants than current hydrocarbon fuels (75% to 100% reduction in CO_2 emissions per passenger kilometre, 90% reduction in NO_x emissions) [4].
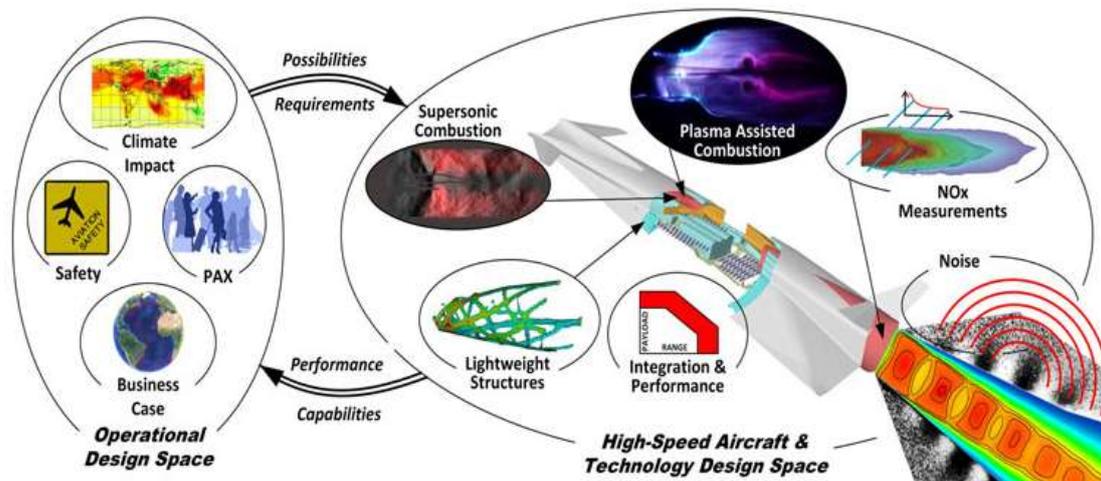

Figure 3: STRATOFLY project shows the positive impact of multidisciplinary analysis and multi-domain integration [5]

The Stratofly project has received financial allocations currently amounting to 4 million euro, and it is expected to reach TRL 6 (technology readiness level, an index that evaluates the maturity of a technology) by 2035: by that date, it is expected that this technology will be demonstrated effective in an industrially relevant environment, that is the earlier stage than the demonstration of a prototype system in an operational environment. In a certain sense, the STRATOFLY project plays the role of bridge between past and future: it originates from the project of the European Space Agency LAPCAT MR2.4, elaborated in the early 2000s but stopped in conceptual design, but aspires to become a point of reference in the field of reusable space transport systems, a rapidly growing sector which is, as never before, the focus of attention on both the academic and the industrial world, but also the general public. It is important to remember that this project is not simply of technical importance: STRATOFLY includes non-technological issues that are of utmost importance for the future of civil passenger transport in the stratosphere; the life cycle costs

estimation of the vehicle, the market analysis, human factors related to the public consensus, safety and airworthiness regulations.

The Polytechnic of Turin plays the role of coordinator of the project that, started on 1/6/2018, will end (at least in the framework of Horizon 2020) on 30/11/2020. Among the many academic and industrial companies around the world taking part in the project, the main European contributors are:

- Politecnico di Torino (POLITO, Italy). Expertise: Aircarft and Systems Design, Life Cycle Cost estimation, Safety Assessment;
- Von Karman Institute for Fluid Dynamics (VKI, Belgium). Expertise: High-speed Propulsion Systems and Noise Emission;
- Centro Italiano Ricerche Aerospaziali (CIRA, Italy). Expertise: High-speed flow analysis;
- Deutsches Zentrum Fuer Luft - Und Raumfahrt (DLR, Germany). Expertise: High-Speed Propulsion Systems and Climate Impact;
- Fundacion de la Ingenieria Civil De Galicia (Spain). Expertise: Structural Analysis and Optimization;
- Office National d'Etudes et de Recherches Aerospatiales (ONERA, France). Expertise: Plasma Assisted Combustion Experiments and Pollutant Emissions;
- Centre National de La Recherche Scientifique (CNRS, France). Expertise: Climate Impact;
- Stichting Nationaal Lucht- En Ruimtevaartlaboratorium (NLR, The Nederlands). Expertise: Noise Emission;
- Totalforsvarets Forskningsinstitut (FOI, Sweden). Expertise: Plasma Assisted Combustion;
- Technische Universitat Hamburg-Harburg (TUHH, Germany). Expertise: Human Factors, Business Plan and Traffic Management.

1.1.3. Stratofly Academy

In the broad context of the Stratofly project, an initiative has been taken to involve the new generations in the project: this idea has the dual aim of introducing new ideas and increasing public acceptance of the project which, being extremely innovative and ambitious, it could arouse initial mistrust or even hostility. This initiative is known as the "Stratofly Academy" and is aimed at all school levels: even primary, intermediate and high school students can participate, sharing essays or drawings on the subject of high-speed passenger transport.

Figure 4: Stratofly Academy logo

However, the initiative is mainly aimed at universities, for which specific challenges have been organised to encourage collaboration and positive competition. In particular, the first challenge, taking place between October 2018 and October 2019, is dedicated to the theme "Design your Future High-Speed transportation". The challenge is announced as follows:

"To shorten the flight time of one order of magnitude (with respect to the state of the art of civil aviation) of at least 300 civil passengers along long haul and antipodal routes, through the preliminary design of a Mach

8 vehicle, flying at stratospheric altitudes within a future CNS/ATM scenario, enhancing existing on---ground infrastructures, in compliance with environmental compatibility and safety issues, assessing the overall economic feasibility of the solution".

Students are divided into international teams made up of a mixed set of doctoral candidates, bachelor and master undergraduates, coordinated by an impartial supervisor from one of the research entities involved in the STRATOFLY project. Each student, who can take part in the challenge with his thesis, is invited to contribute to the design of the aircraft under study, providing an in-depth analysis of one of its subsystems; this is precisely the context of this thesis, the aims of which are briefly listed in the next paragraph.

1.2. Purpose of the work and thesis baseline

The aim of the thesis is an in-depth conceptual design study of the VEMS system.

The present work is organized in such a way as to convey the analysis, in the most natural way possible, from the input data currently available in literature up to the results of the simulations carried out. As the VEMS system is currently designed exclusively on a theoretical level, there is a complete lack of bibliography and dedicated studies. For this reason, this work has been carried out in a design perspective: starting from the current idea of its structure, a new architecture has been developed and tested. It should be noted that, in accordance with the rest of the project, this study is part of a conceptual design concept, that is the first stage of the project: as there is still little information available on the whole aeroplane and other systems, a first sizing and performance estimation will be provided, which will then be refined and deepened in a long iterative and recursive process.

The thesis is divided into the following points which reflect the subdivision into chapters:

- Literature review, analysis, modification and acquisition of currently existing aircraft performance data. In particular, this study focuses on the aerodynamic and propulsive characteristics of the aircraft along its concept of operation. The analysis also focuses on various techniques for evaluating the thermal exchange between the body and the external environment, which will be essential for the good outcome of this work;
- Revision of the current planned mission profile for the aeroplane. With the help of analytical techniques and the numerical implementation of the aerodynamic and propulsive data (properly settled in the previous part), a new mission profile is developed. Such analysis is carried out with a flight simulation of the longitudinal plane of the aircraft, trying to respect the constraints imposed from the references in literature and the aeronautical regulations in the field of civil transport. Finally, the results obtained are compared with a similar simulation, which is elaborated through a dedicated software developed by the European Space Agency;
- Study of the main physic-chemical characteristics of hydrogen, in particular the conditions of coexistence of the liquid and gaseous phase. An in-depth study of storage techniques and a description of the phenomenon known as "boil-off". Finally, a detailed database is built which presents the main physical, chemical, mechanical, optical and electrical characteristics of hydrogen in a wide combination of temperature and pressure conditions;
- Investigation of the main active and passive components of aerospace turbomachinery. In particular, an analytical and semi-empirical methodology is outlined for the parametric study of these components, in order to develop an algorithm combining the required performance characteristics with an initial estimate of the geometrical and physical characteristics of the turbo machines. This study, carried out also at the statistical level, allows to carry out a first attempt sizing of the main components of a fluid machine in a specific operating condition.
- Study of the current VEMS system structure, definition of the system's scope and potential, and introduction of a new configuration. Thermal analysis of the aeroplane during the mission, and subsequent analysis and sizing of the whole VEMS system, divided into the following parts:

       o   Fuel system: management of tanks and liquid fuel;

       o   Gas assembly: management of turbomachinery and gaseous fuel;

       o   Engine interface

Definition of analytical, empirical and numerical tools for estimating the performance of each subsystem considered, depending on the operating conditions. Integration of the individual parts and development of a dynamic simulation of the whole system, in which it is possible to directly correlate the inputs of the analysis (heat flows on the fuselage during the flight) with the performance of the turbo machines and the impact on the fuel stored on board.

- Conclusions, summary of the main results obtained, and identification of possible further developments.

In the following picture, a basic roadmap of the thesis is outlined

Roadmap: thesis storyline and carried out studies

AERODYNAMICS
- Literature review; hypersonic flight;
- Aerodynamic forces and moments coefficients acquisition
- Data interpolation in a wider and denser array of Mach numbers and angles of attack
- Evaluation and choice of the best fitting results, comparing CFD analyses

PROPULSION
- Literature review: ATR and DMR engines
- Propulsive characteristics of both engine are acquired, and then interpolated in any foreseeable flight condition

MISSION DEFINITION
- Literature review; Lapcat mission and possible trajectories
- Data acquisition, selection and interpolation in a denser time array

HEAT TRANSFER
- Definition of dynamic pressure along the trajectory
- Intake geometrical definition; leading edge radius and thermal properties alternatives identification
- Heat exchange analysis based on empirical law (Scott's and Zoby's)
- Skin temperature determination
- Leading edge radius and emissivity choice

MISSION SIMULATION
- Literature review; mission profile and optimized trajectory
- Detailed definition of main flight phases, in terms of vertical and horizontal navigation
- Implementation of longitudinal flight mechanics equations
- Interpolation of aerodynamic and propulsive data as function of instantaneous flight conditions
- Reference mission data vs flight time used as a driver
- Simulation of the actual mission
- Definition of the vertical trajectory and flight conditions in each time step

HYDROGEN
- Literature review: liquid and gaseous hydrogen features and issues identification
- Chemical and physical properties definition in a multidimensional array of pressure and temperature
- Boil-off phenomenon description and characterization

TEMS: introduction
- Literature review: original configuration
- Definition of requirements and specifications of the subsystem
- New architecture design
- Necessary components identification

TEMS: static sizing
- Literature review: parametric methods for turbomachinery preliminary sizing
- Review of empirical algorithms for the estimation of several geometrical features of components and performances:
    - Heat exchanger
    - Pipe
    - Pump
    - Tank
    - Gas turbine
- Sizing of those elements in the foreseen most critical flight condition, namely the hypersonic cruise

TEMS: dynamic sizing
- Literature review: differential equations to describe hydraulic and mechanics main components
- TEMS architecture implementation in a dynamic simulation software
- Mission boundary conditions definition
- Dynamic simulation
- Results analysis and inputs adjustment to fulfill mission requirements and system design specification
- Most demanding flight condition identification
- Subsystem performance test
- Work still in progress!

Figure 5: thesis roadmap

13

2. Literature review and data acquisition

This chapter focuses on the review of the LAPCAT MR2.4 project in its current state of development, so as to first understand the technological landscape in which this programme was born, the stages of development, the technical (and not) to which it went against, and finally the purpose of the project itself. In fact, before its cancellation, the study carried out by the European space agency on hypersonic civil transport had reached a relatively high degree of maturity, although not having completed the conceptual design part: the most important characteristics of the aeroplane have been defined in a rather accurate way, up to the definition of a computerized model of the aircraft. In this process, a number of global aspects of the aircraft have been carefully assessed, including predominantly aerodynamics, propulsion and the concept of operation. Such definitions are in fact essential during the design of an aircraft, since they are the most qualifying elements of the performance and the desired effectiveness of the mission. The analysis of the subsystems of the aircraft was less accurate, since these are aspects that, while of primary importance, play a chronologically and logically secondary role along the correct design path of a new aircraft. In the course of this thesis we will try to take a step forward in the definition and sizing of the TEMS subsystem, whose performance and design specifications strongly depend on the conditions to the contour, or the environment surrounding the aircraft and its flight configuration. For this reason, in this first chapter, all those aspects relating to aerodynamics, propulsion and thermal exchanges will be considered which, although not directly related to the TEMS system itself, are essential for a correct definition of the same and the operating conditions that it will face. In particular, these aspects will be assessed by existing studies on the subject, the salient data of which are given; however, during the course of the chapter, will show how it was necessary a careful work of review and reorganization of the previous works, both for reasons of practicality in the subsequent use that will be made in this project, and for reasons of technical correctness. Each section will be organized respectively with a short introduction on the subject, a presentation of the data from literature, and a subsequent reworking and graphic representation.

2.1. Aerodynamics

2.1.1. Introduction

The aircraft's design is based on waverider configuration, that is the best configuration for hypersonic flight. Nevertheless, the choice of this configuration must not hinder other aircraft's features, like the integration with engines and other subsystems, nor the performance at subsonic and supersonic flight, which will represent a non-negligible part of the concept of operation.
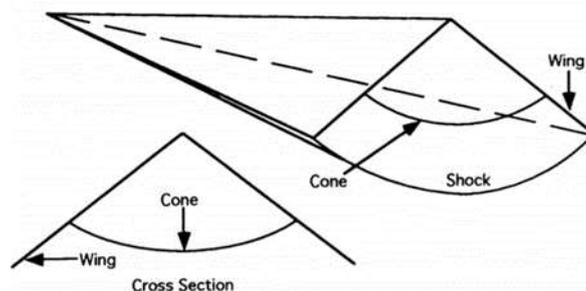

Figure 6: idealized cone-derived waverider [6]

To gain better understanding of the waverider concept consider the simplest model, the idealized cone-derived waverider. The body is a section of a cone. The wing, which is infinitesimally thin, extends out from the body to the shock that is induced by the conical body. The upper surface is parallel to the free-stream, called the free-stream surface, and the lower surface, called the compression surface, is completely immersed in the conical flow field. Since the shock is attached to the wing tips there is no flow leakage between the free-stream and the compression surface. The flow fields on the upper and lower surface are

completely independent of each other. The upper surface is subject only to free-stream pressure, and the lower surface of the body and the wing are subject to the pressure of conical flow field.
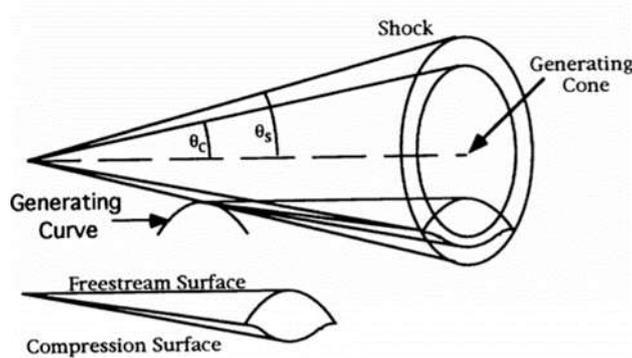

Figure 7: conical waverider generation [6]

The waverider can be described by first considering a conical flow field created by an imaginary cone. The leading edge of the waverider is the 3-D intersection of the shock and a generating curve. The generating curve can be any shape. The free-stream surface is defined by locus of streamlines which start at the shock but follow a free-stream path. The compression surface is defined by locus of streamlines which start at the shock and follow the paths defined by conical flow field. These two surfaces form a waverider. The shape of the waverider can be completely determined if are know the generating cone angle, θ_c, the generating curve and the Mach number, which determines the shock angle ϑ_s. [6]

It is necessary to adopt the osculanting cone method for every osculanting plane of the cone to generate the correct compression surface. First of all, the flow design conditions must be defined in order to calculate:

- cone radius, R;
- maximum angle of the osculanting planes;
- shock wave angle β
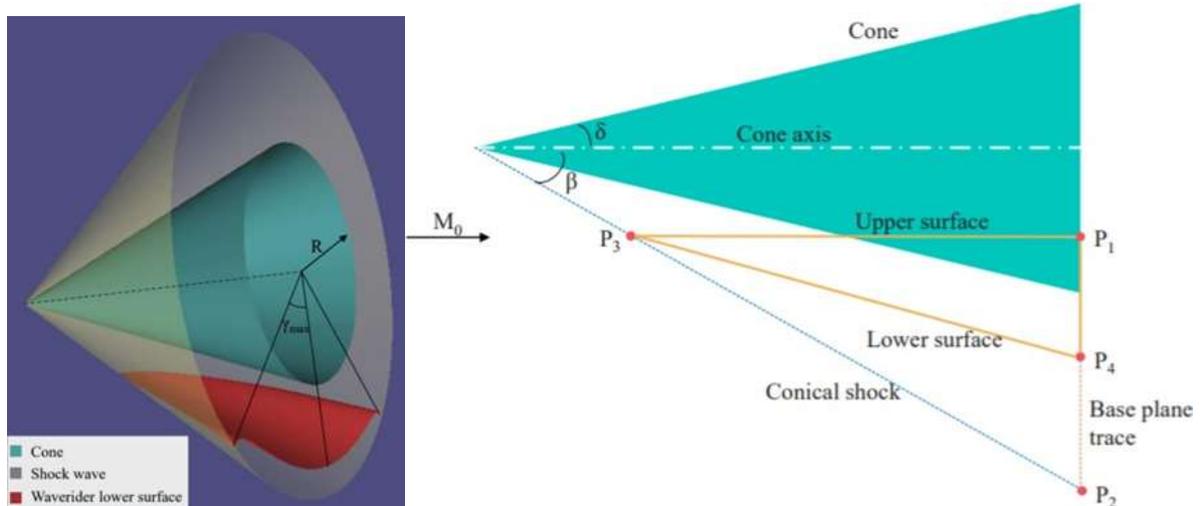
Figure 8: conical waverider generation [7]

For every osculating planes, the position of four points are determined. The first point that can be generated is P2, which is localized at the intersection between the conical shock wave trace in the osculating plane and the base plane trace. The base plane is simply the plane which contains the cone base. Then, P1 position can be set: vertically aligned with P2, but its distance from that point is a degree of freedom of the algorithm. This means that it is possible to create different waverider configurations assigning different values to the P2

15

– P1 distance (with some geometrical constraints). The positioning of the next point (P3) is based on the upper surface characteristics, in our case the upper surface has been set aligned with the free stream, minimizing the drag effect. Finally, P4 can be determined tracing the parallel to the cone curved surface, passing through P3. This step corresponds to the design of the local lower surface, constituted by the segment P3P4. Since this segment is aligned with the cone, it is guaranteed to have the same flow conditions we will find close to the cone surface. This fact also ensures that the aerodynamic calculations can be performed solving the supersonic cone problem. [7]

Waverider configuration, apart its aerodynamic benefits, still present the problems of structural integrity, reduced internal volume and integration with onboard systems. The current cross-section of the vehicle is the result of some trade-offs:

- first configuration (blue): slender design to minimize wave drag losses. Its drawback is a large wetted area, that increases friction drag: in these condition waverider is no more practical, since it presents all the previously mentioned problems (namely passenger cabin and tanks integration, complex structure), with no aerodynamic advantage;
- second configuration (green): evolution of waverider design, with improved volumetric efficiency;
- third configuration (red): elliptical cross-section, hence further improvement in terms of volumetric efficiency and the distribution of loads through hoop stresses; however, it introduces a more complex leading-edge configuration;
- fourth configuration (black): MR2-4 definitive configuration [8].
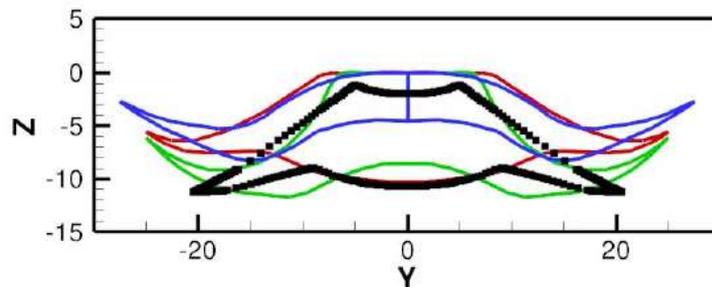
Figure 9: comparison of cross-section of various waverider configuration. Blue: MR2-1, Green: MR2-2, Red: MR2-3, Black: MR2-4 [8]

2.1.2. Literature review

Current analysis is based on an aerodynamic database for hypersonic cruisers developed by the private company Gas Dynamics Ltd for the LAPCAT project, using a customised tool which includes a surface inclination method to compute the inviscid drag and the lift of supersonic and hypersonic configurations. This analysis was led taking account of several parameters:

- Mach number: each coefficient was evaluated for the following array of Mach numbers

$$M = [0.3, 0.5, 0.7, 1.5, 2, 2.5, 3, 3.5, 4, 4.5, 5, 5.5, 6, 6.5, 7, 7.5, 8]$$

First, it is possible to see that this discretisation is quite approximate, since involves a limited number of values; moreover, transonic speed is not characterised, leaving one of the most critical flight phases open.

- Angle of attack (aerodynamic incidence): each coefficient was evaluated for each integer number in the range $-12° < \alpha < 24°$ for subsonic Mach numbers, or in the range $-6° < \alpha < 6°$ for supersonic and transonic Mach numbers, since it is unlikely to meet high aerodynamic incidence at high speeds;

16

- Sideslip angle: each coefficient was evaluated for $\beta = -4°, 0°, 4°$. Since this analysis will consider only longitudinal motion, these data will be considered only at null sideslip angle.

The first targets of this analysis were the body-axis force and moments coefficient, evaluated with a CFD analysis. It is now appropriate to define them, prior to evaluate the main aerodynamic coefficients.

The reference coordinate system is body-fixed and right-handed, with the origin in the centre of mass of the aircraft. In particular, the chosen model is shown in the following picture
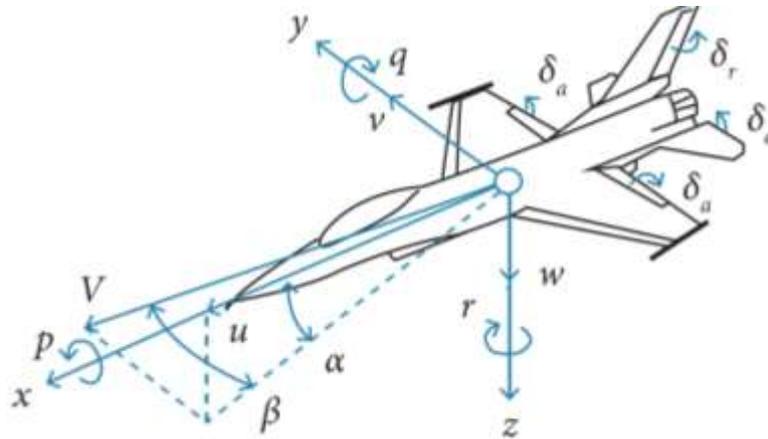
Figure 10: body-fixed aircraft axis, speed, and angle [9]

Force equations of motion for the vehicle can be developed by writing Newton's second law for each differential element of mass in the vehicle, and then integrating over the entire vehicle. The resulting force is the sum of propulsive, aerodynamic and propulsive forces. Moment equation of motion are obtained as the product of the net torque in each axis and the rate of change of angular momentum, with no contribution of gravity, since the body-axis system is centred in the centre of mass of the aircraft.

If it is possible to assume of small perturbations around a flight equilibrium condition, it is possible to simplify those coupled and nonlinear equation; in particular, a condition of longitudinal equilibrium (in which the velocity and gravity vectors lie in the plane of symmetry of the vehicle) is chosen. This is a good approximation for steady flight phases, and it is very handful in a conceptual design stage. On the other side, perturbations in aerodynamic forces and moments are functions of both the perturbations in state variables and control inputs.

On a more global scale (on which this whole aerodynamic analysis is made), force and moment coefficients can be expressed as follows

$$C_X = \frac{X}{qS}$$

$$C_Y = \frac{Y}{qS}$$

$$C_Z = \frac{Z}{qS}$$

$$C_l = \frac{L}{qSb}$$

$$C_m = \frac{M}{qSc}$$

17

$$C_n = \frac{N}{qSb}$$

In which each coefficient considers the dimensional force or moment to which it is related to (forces in axis x y, z, moment around axis x, y, z respectively), the vehicle reference area S (usually the planform area, namely the product of wing mean aerodynamic chord and wing span) and the dynamic pressure, defined as follows

$$q = \frac{1}{2} \cdot \rho \cdot V^2 = \frac{1}{2} \cdot \rho_{SL} \cdot V_{eq}^2$$

Moments equation also are referred to their own reference moment arm, namely the wing span for rolling and yawing, and mean aerodynamic chord for pitching moment.

Finally, longitudinal forces can be written in an established fashion as vector sum of lift and drag, which coefficients are evaluated as follows

$$C_L = \frac{L}{qS} = -C_z \cdot \cos(\alpha) + C_x \cdot \sin(\alpha)$$

$$C_D = \frac{D}{qS} = -C_z \cdot \sin(\alpha) - C_x \cdot \cos(\alpha)$$

In which the angle of attack is the angle between the instantaneous vehicle velocity vector and the x-axis; it is also assumed that the propulsive thrust is aligned with the x-axis. [10]

In addition to main aerodynamic coefficients (lift and drag), some other useful physical quantities are evaluated:

- Aerodynamic efficiency, whose definition is the ratio between lift and drag coefficient

$$E = \frac{C_L}{C_D}$$

- Aerodynamic centre position, referring to the whole wing length (94 m)

$$x_{ac} = -\frac{C_m}{C_z} \cdot L_{wing}$$

The longitudinal force coefficient is not always empirically derived (with CFD analysis), but it is evaluated (for supersonic Mach numbers) from the sagittal axis as a function of local wing twist

$$C_x = \frac{C_z}{\sin(\theta_{wing})}$$

In order to carry out a more appropriate analysis, the calculation of the previous results shall be carried out on each surface of the aeroplane in such a way as to simplify its shape and deepen the study on more regular surfaces; then, under the linearity hypothesis of the aerodynamic coefficients, the principle of effects overlapping is used, in order to obtain the results for the entire aeroplane and for the moving surfaces. The breakdown carried out was

- Body and rudders
- screw lugs
- canard

As shown in the next figure
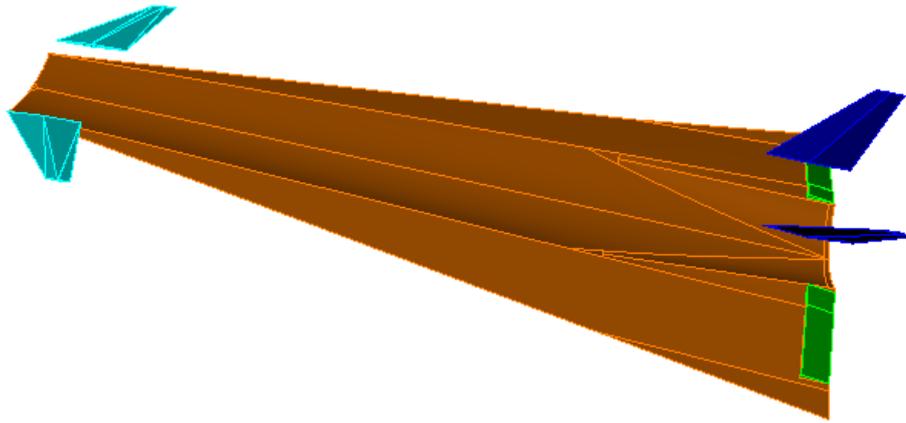
Figure 11: aircraft surface breakdown

This analysis, carried out with the hypothesis of incompressible fluid, is corrected (only on the longitudinal force coefficient, cx) taking into account the viscous and thermal effects, in particular of the wall friction (evaluated as a function of dynamic pressure) and heat exchange (assessed as a function of static wall temperature, estimate with some approximation). This corrective contribution is also treated in the same way as the others, hence added to the individual relevant coefficients each a portion of the aircraft, to obtain the respective overall aerodynamic coefficient. Hence

$$C_{x_{tot}} = C_{x_{body}} + C_{x_{canard}} + C_{x_{aileron}} + C_{x_{viscous}}$$

$$C_{y_{tot}} = C_{y_{body}} + C_{y_{canard}} + C_{y_{aileron}}$$

$$C_{z_{tot}} = C_{z_{body}} + C_{z_{canard}} + C_{z_{aileron}}$$

$$C_{l_{tot}} = C_{l_{body}} + C_{l_{canard}} + C_{l_{aileron}}$$

$$C_{m_{tot}} = C_{m_{body}} + C_{m_{canard}} + C_{m_{aileron}}$$

$$C_{n_{tot}} = C_{n_{body}} + C_{n_{canard}} + C_{n_{aileron}}$$

The estimation of coefficients by simple algebraic sum provides an indication of the first approximation of the aerodynamic behaviour of the aeroplane. For the calculation of the actual forces acting on the aeroplane, each section of the aeroplane and control area should be considered as the relevant surfaces; the most up-to-date results are as follows: (estimated from the CAD model of the final aeroplane)

Aircraft section		Area (m^2)
Body	wetted surface	5210,91
	aerial projection	2305,34
Canard	wetted surface	200,86
	aerial projection	100,4
Elevon	wetted surface	124,76
	aerial projection	59,46
V-tail (fixed part)	wetted surface	112,79
	aerial projection	32,02
Rudder	wetted surface	112,54
	aerial projection	28,14
Total (no canard, no tail)	wetted surface	5335,67
	aerial projection	2364,8

This far, the Gas Dynamics Ltd aerodatabase has been analysed, evaluating the global aircraft lift and drag coefficients with a simple, linear formulation. A further improvement has been made, merging those data with another independent CDF analysis, which was focused on subsonic flight [11]. In fact, this work seemed more extensive and relevant in that flight regime, and hence it was chosen to replace the subsonic data already available with the new ones. Unfortunately, even this works offers a limited amount of data, with a different discretization: in fact, only data for $M = 0.3, 0.5, 075$ were available, each one for a limited set of angles of attack ($\alpha_{M=0.3} = -2°, 0°, \alpha_{M=0.5} = -4°: 16°, \alpha_{M=0.75} = 0°, 1°$). To overcome this inconvenience, and properly integrate those data with the pre-existing aerodatabase, the following procedure was utilised:

- available data were plotted as single points on a chart, for each aerodynamic coefficient. Each angle of attack is related to the Mach number it was calculated for;
- an interpolant curve was chosen for the angles of attack at $M = 0.5$, since this Mach number presents the majority of available data (other Mach number have only two available angles of attack in which aerodynamic coefficients were evaluated). A polynomial interpolation was performed due to its ease of elaboration; a cubic spline-fit was chosen, since it achieved a good fit, and further degree of deepening resulted in no remarkable improvement in accuracy;
- as a first attempt, the resulting curve was translated up to match one of the aerodynamic coefficients, for each Mach number. This operation resulted in good accuracy for $M = 0.75$, but insufficient precision for $M = 0.3$ (as showed in the following pictures)
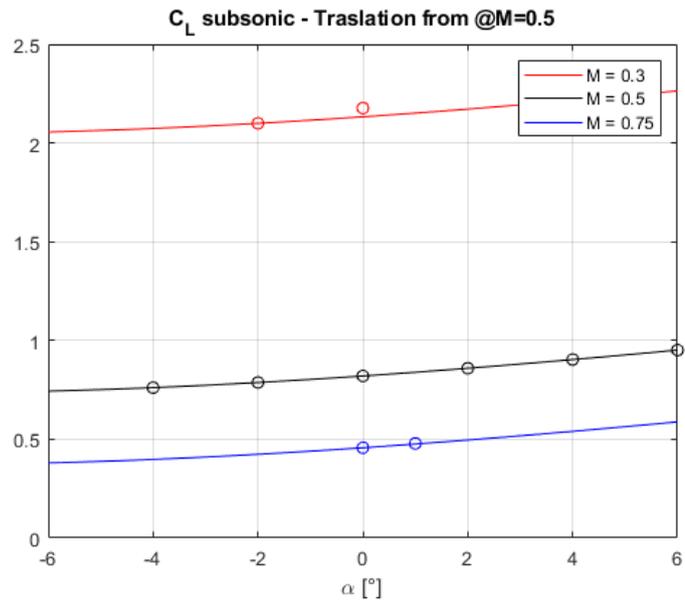
Figure 12: lift coefficient for subsonic flight - interpolation at Mach = 0.5 and subsequent vertical translation
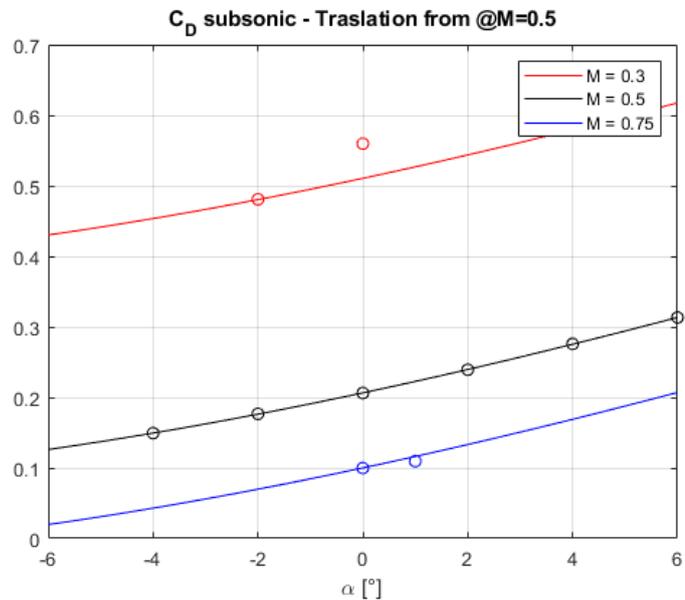
Figure 13: drag coefficient for subsonic flight - interpolation at Mach = 0.5 and subsequent vertical translation

- as a second attempt, the definition of a new interpolating curve for both $M = 0.3$ and $M = 0.75$ is performed. A third order polynomial curve is desired, for similarity to $M = 0.5$ trend. In this algebraic problem there are two equations in four variables, since the curve requires four coefficients (since it is a third order), and it is possible to force the passage of the function through two points.

$$\begin{cases} ax_1^3 + bx_1^2 + cx_1 + d_1 = y_1 \\ ax_2^3 + bx_2^2 + cx_2 + d_2 = y_2 \end{cases}$$

Since this problem provides ∞^2 solutions, two more conditions are applied, namely the coefficients a and b; they are defined iteratively as a multiple of the respective coefficients of the curve at $M = 0.5$. The results are satisfactory and are shown below
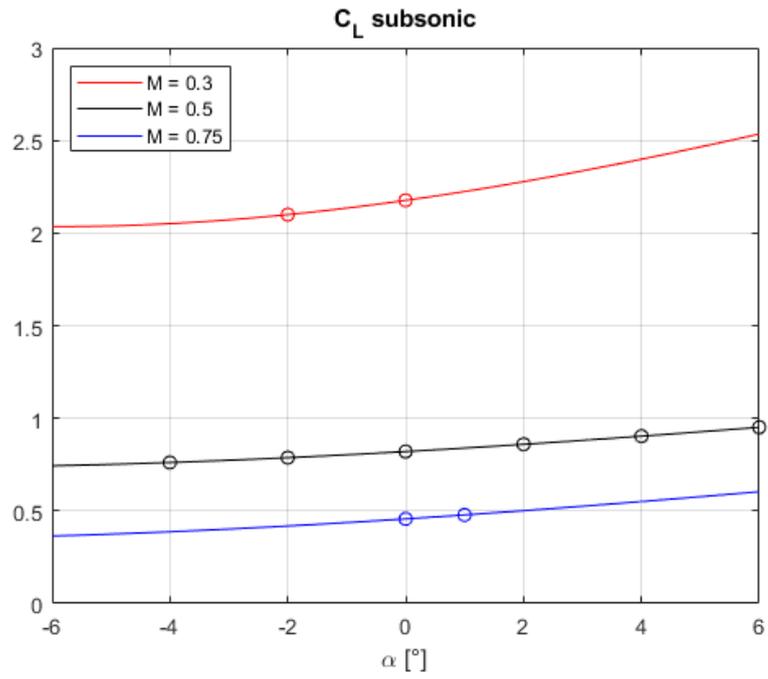
Figure 14: lift coefficient in subsonic regime. Each curve is interpolated from the available data (points)
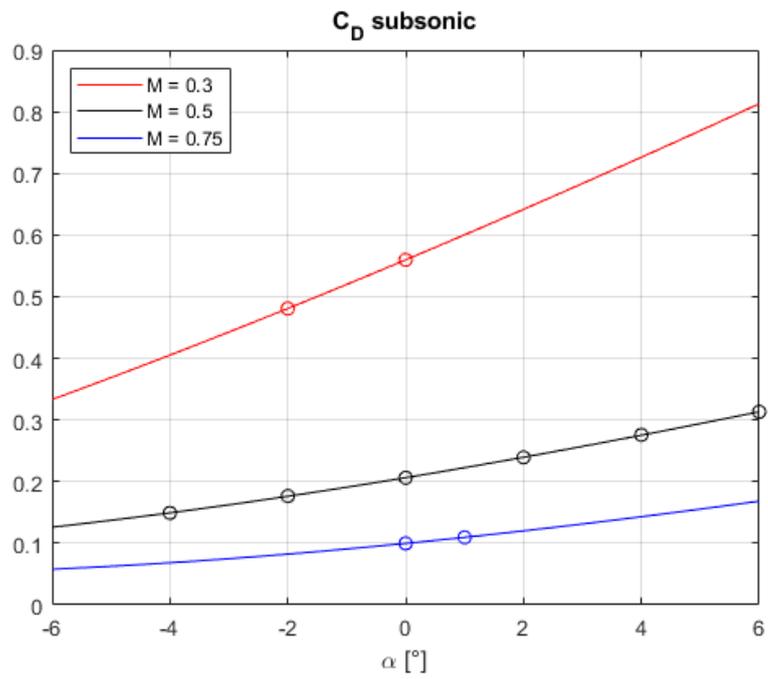
Figure 15: drag coefficient in subsonic regime. Each curve is interpolated from the available data (points)
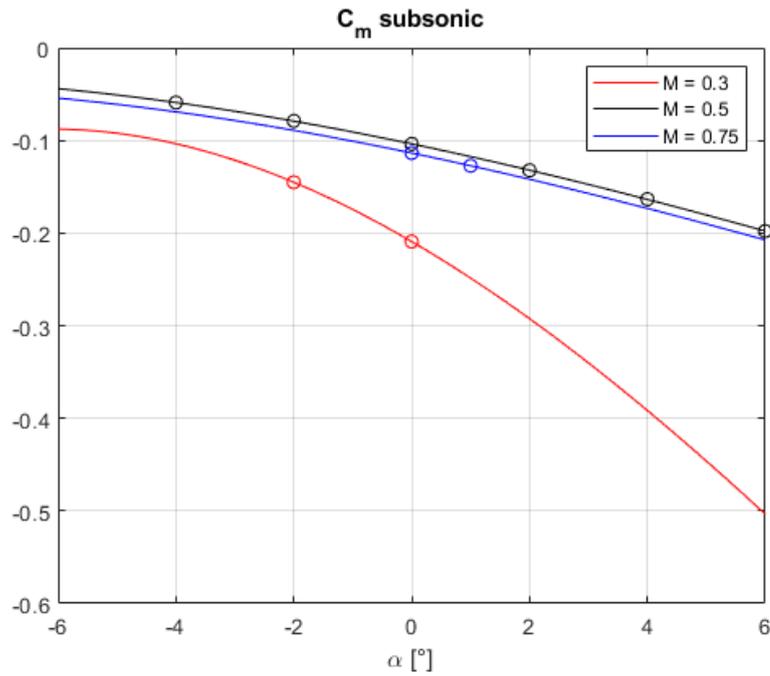
Figure 16: pitch coefficient in subsonic regime. Each curve is interpolated from the available data (points)

- the pre-existing aerodatabase is consequently filled with data relieved from this interpolation. In particular, they are evaluated in each point of discretization from the respective curve equation.

2.1.3. Revision and results display

In this section, some of the many aerodynamic coefficients evaluated are shown
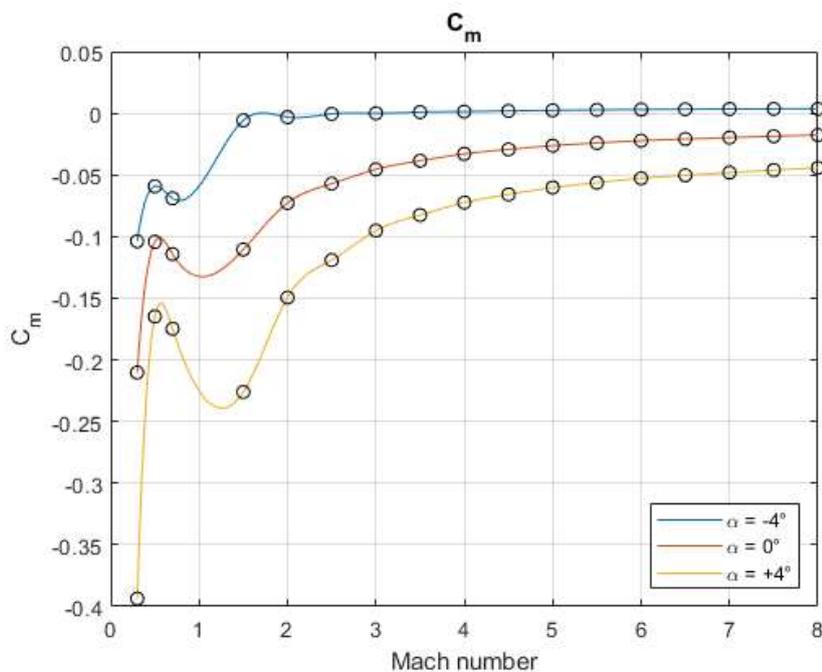
Figure 17: pitch coefficient as a function of Mach number, for different angles of attack, interpolated from available data (black points)
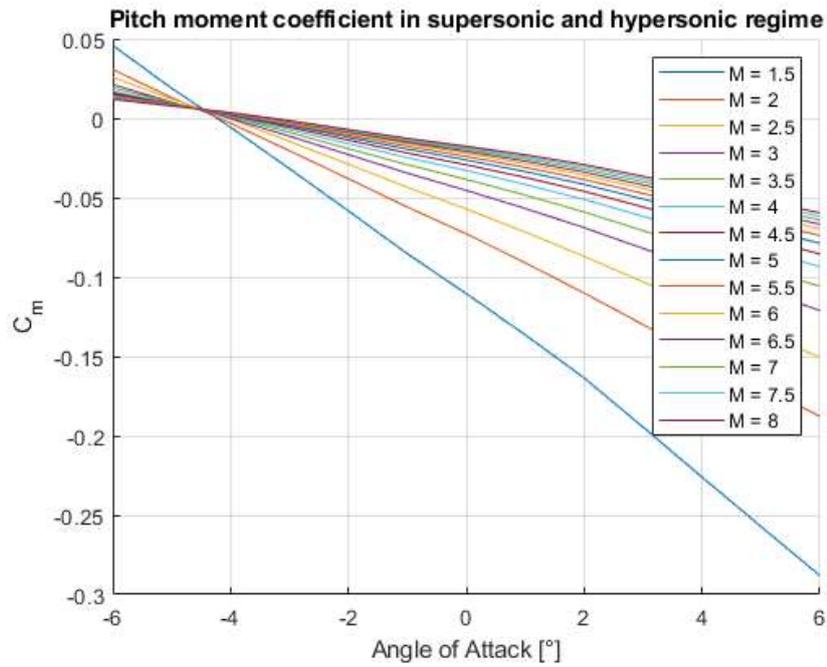
Figure 18: pitch moment coefficient as a function of angle of attack number, for different Mach number
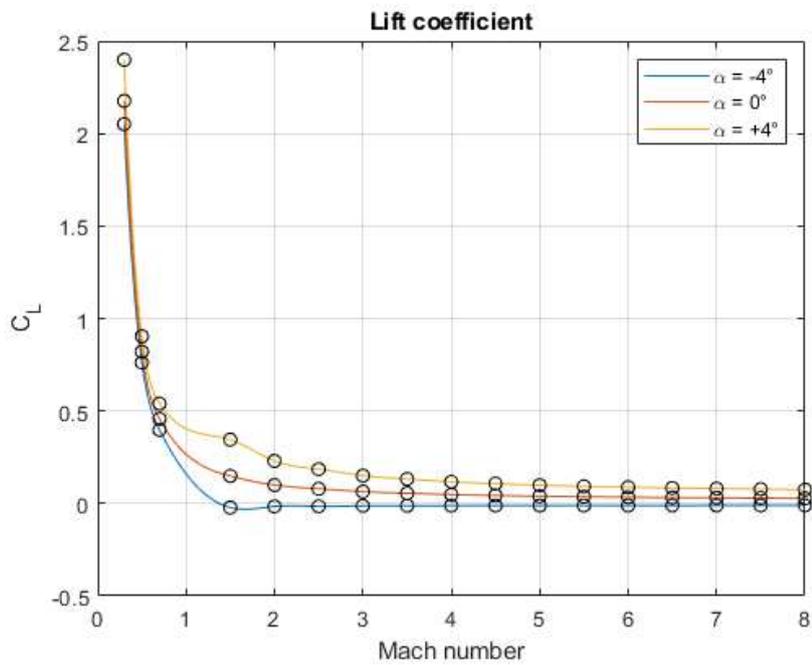
Figure 19: lift coefficient as a function of Mach number, for different angles of attack, interpolated from available data (black points)
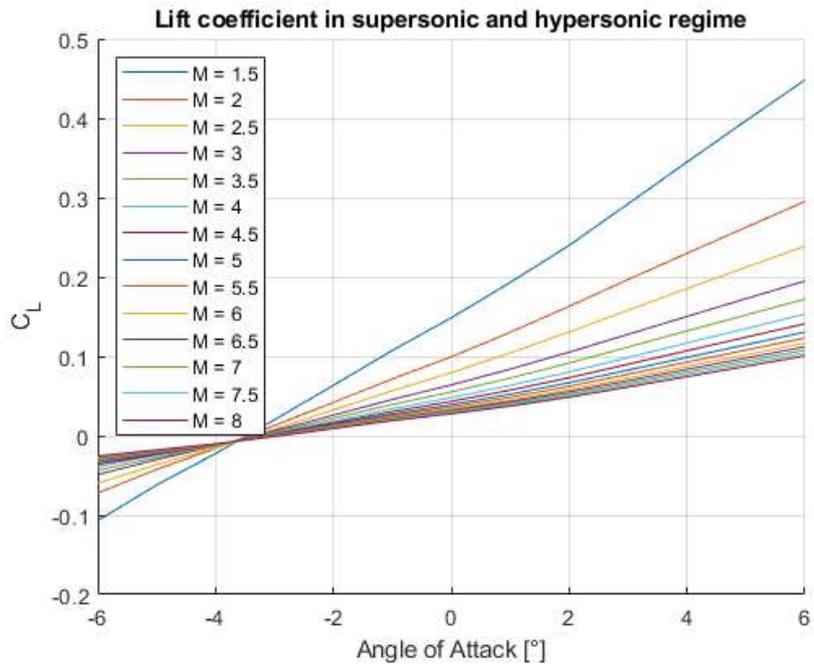
Figure 20: lift coefficient as a function of angle of attack number, for different Mach number
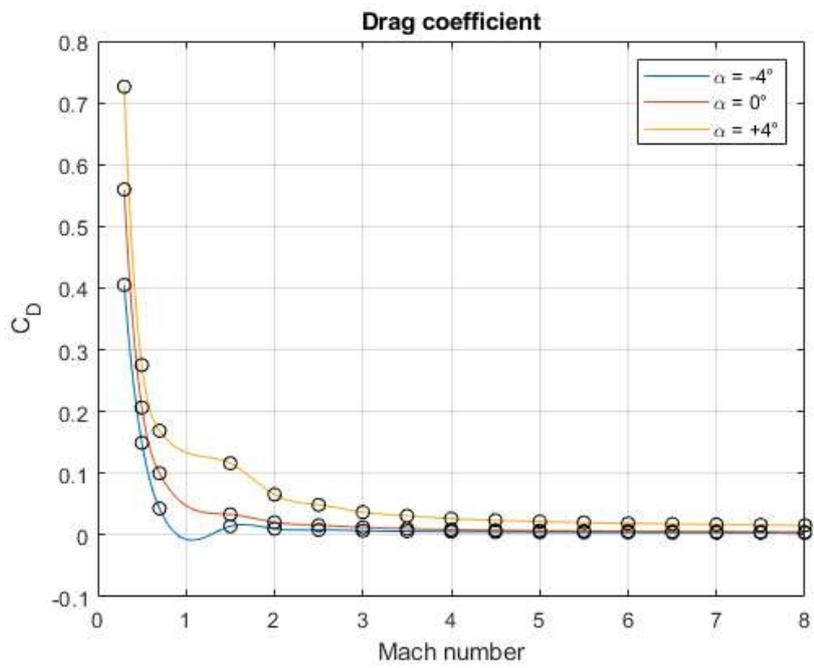

Figure 21: drag coefficient as a function of Mach number, for different angles of attack, interpolated from available data (black points)
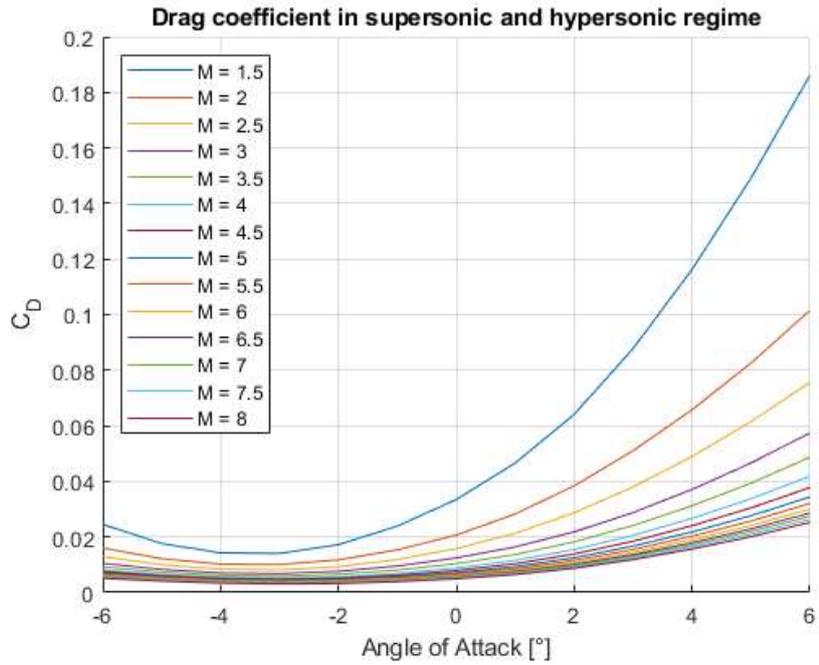
Figure 22: : drag coefficient as a function of angle of attack number, for different Mach number
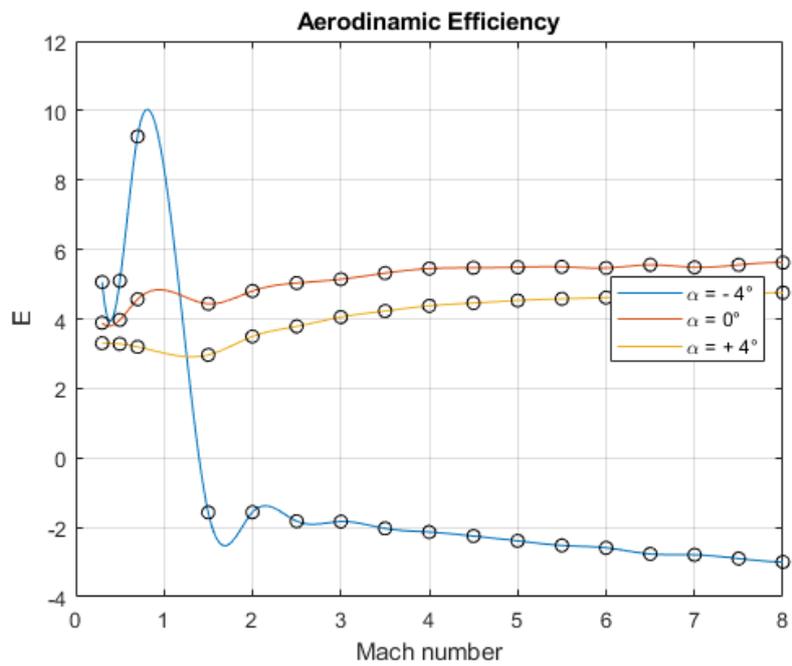
Figure 23: aerodynamic efficiency as a function of Mach number, for different angles of attack, interpolated from available data (black points)
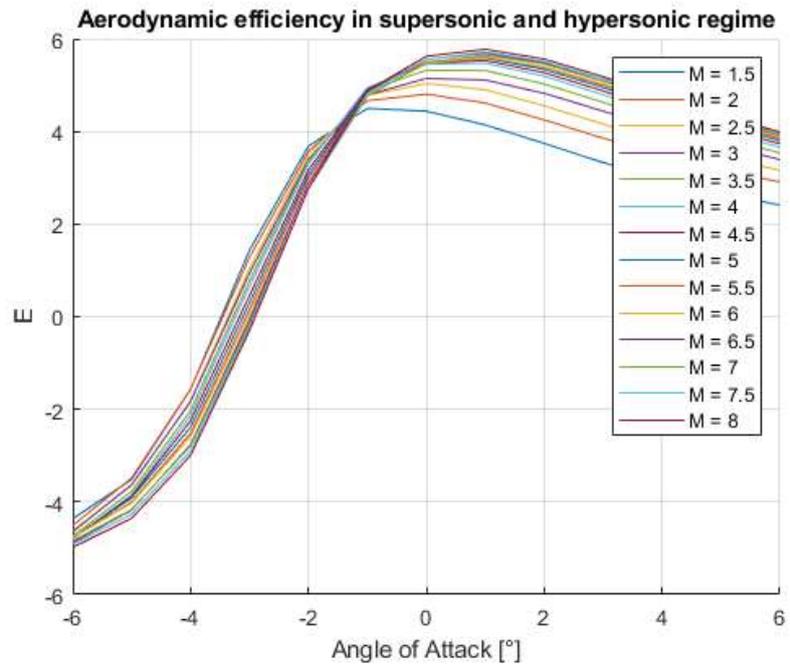
Figure 24: aerodynamic efficiency as a function of angle of attack number, for different Mach number

2.2. Propulsion

2.2.1. Introduction

An accurate description and analysis of the propulsive plant involved in this mission is far beyond the purpose of this thesis; however, since the global propulsion data will be necessary for a logical progression of the work, a brief description of this matter will be made.

The current propulsion system is composed by two different engine type, since it is necessary to provide high thrust level in the different flight phases:

- ATR, or air-turbo ramjet, are used to reach Mach 4,5. ATR engine is a combined propulsion system born by the union of a classical turbojet engine and a ramjet; their different physical principles are therefore exploited. The first phase follows classical turbojet engine performance; it is necessary to provide thrust during take-off, subsonic and low supersonic phases. The impossibility to reach Mach number above 1.6 without afterburner and the excessive fuel consumption in supersonic flight phase, make the turbojet inefficient beyond this point. It is then necessary to use of the second type of engine, the ramjet. Its working principle is straightforward, as it is essentially a variable section duct that takes advantage on the dynamic pressure of the high-speed air flow instead of compressor stage, and then equipped with an injector system as "combustion chamber". The duct geometry is optimized in order to have a subsonic combustion, which means a convergent-divergent profile. The ramjet engine works efficiently around Mach 3 and it's used up to Mach 4.5. This engine's biggest limit is the low available thrust level at high Mach number, due to the overheat of compressor blades, making the engine less efficient.
- DMR, or dual mode ramjet, is used up to Mach 8. Its architecture is straightforward, it is composed of a constant section duct and the injectors; no moving parts are required , the dynamic compression of the high-speed air flow is exploited. During the last climb segment, a bypass in the intake section is activated to provide air to the DMR, , which is started and used in the last climb segment and for all the cruise phase and stopping the air flow to the ATRs engine.

2.2.2. Revision and results display

Von Karman Institute for Fluid Dynamics (VKI) carried out the performance analysis of the propulsion plant in a wide array of operative conditions. These data have not been modified, but just reorganised in a more convenient way for this thesis purposes (see next chapter). In addition to this, all available data is interpolated with a spline-fit as to be available in a denser array of values.

In this section, a few results concerning engine performance will be showed.
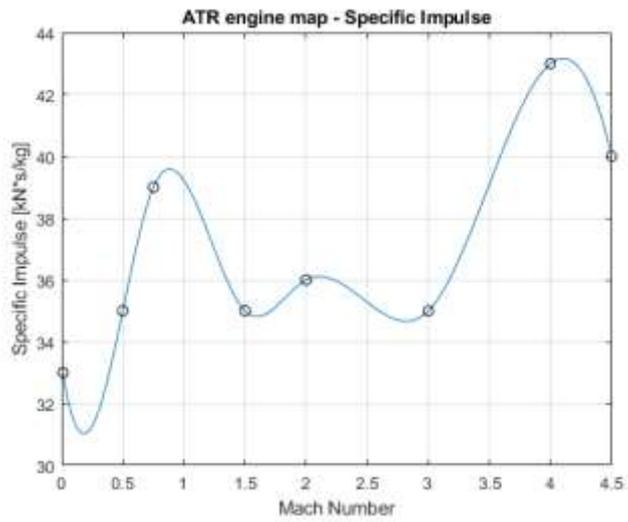
Figure 25: ATR engine, specific impulse as a function of Mach number. Interpolation from CFD data (black points)
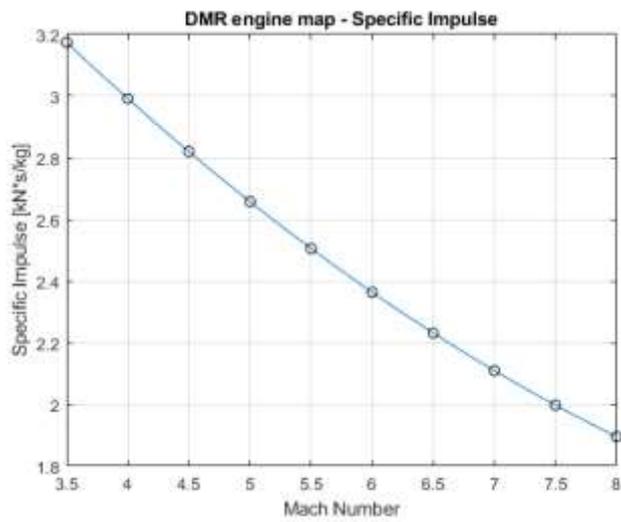

Figure 26: DMR engine, specific impulse as a function of Mach number. Interpolation from CFD data (black points)
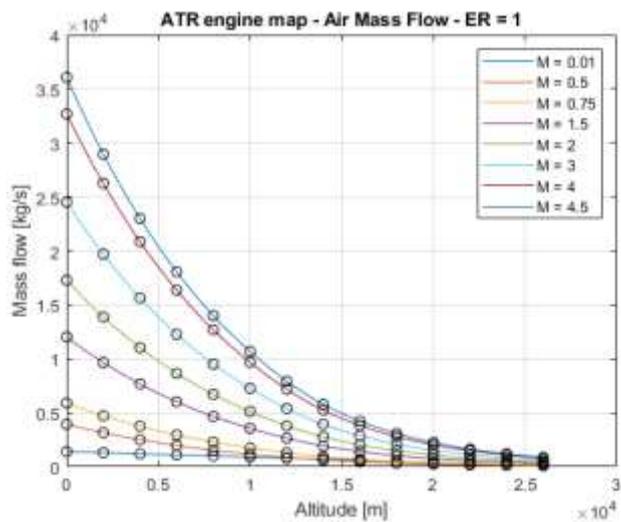

Figure 27: ATR engine, air mass flow at ER = 1, as a function of altitude. Interpolation from CFD data (black points)
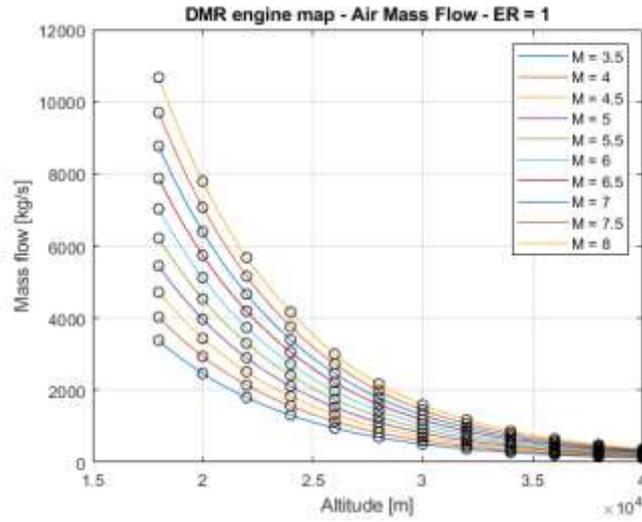
Figure 28: DMR engine, air mass flow at ER = 1, as a function of altitude. Interpolation from CFD data (black points)
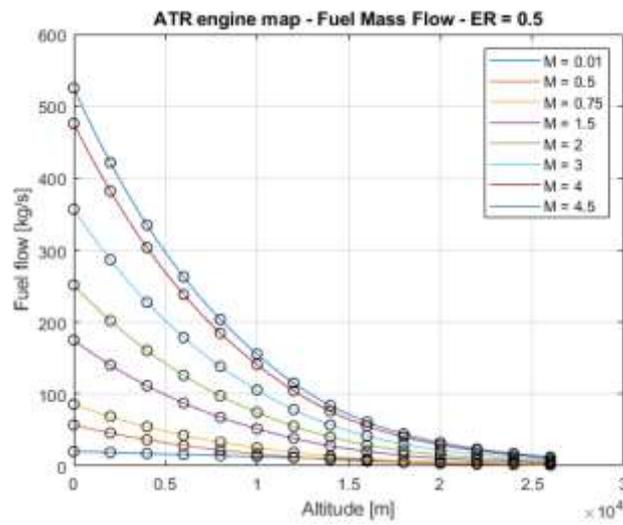
Figure 29: ATR engine, fuel mass flow at ER = 0.5, as a function of altitude. Interpolation from CFD data (black points)
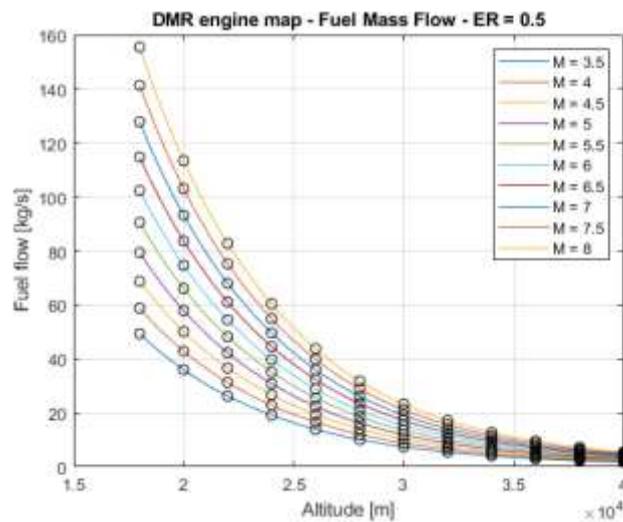

Figure 30: DMR engine, fuel mass flow at ER = 0.5, as a function of altitude. Interpolation from CFD data (black points)
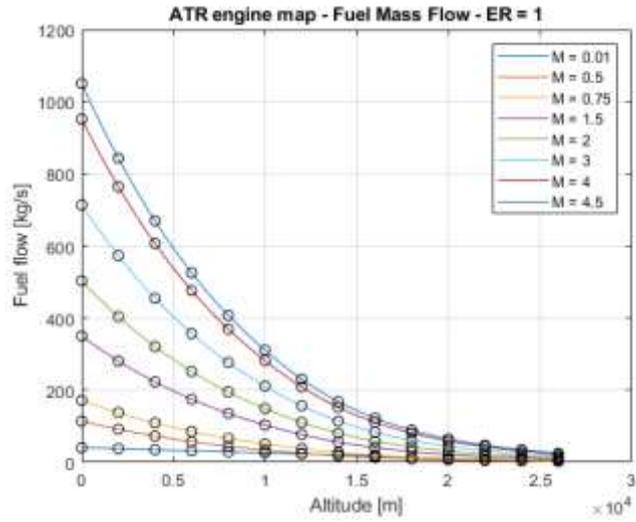
Figure 31: ATR engine, fuel mass flow at ER = 1, as a function of altitude. Interpolation from CFD data (black points)
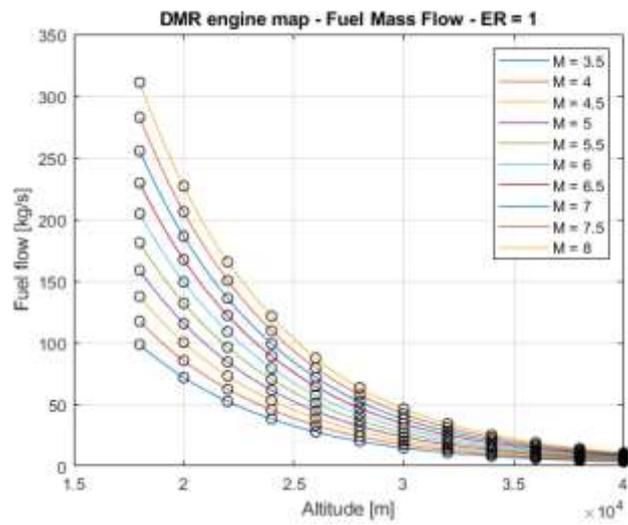

Figure 32: DMR engine, fuel mass flow at ER = 1, as a function of altitude. Interpolation from CFD data (black points)
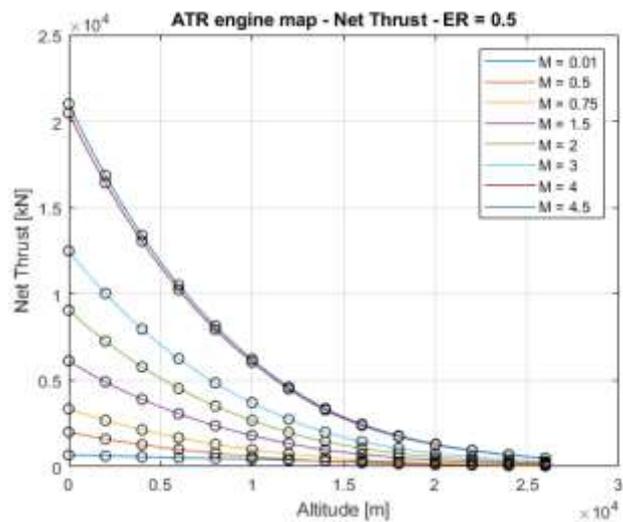

Figure 33: ATR engine, net thrust at ER = 0.5, as a function of altitude. Interpolation from CFD data (black points)
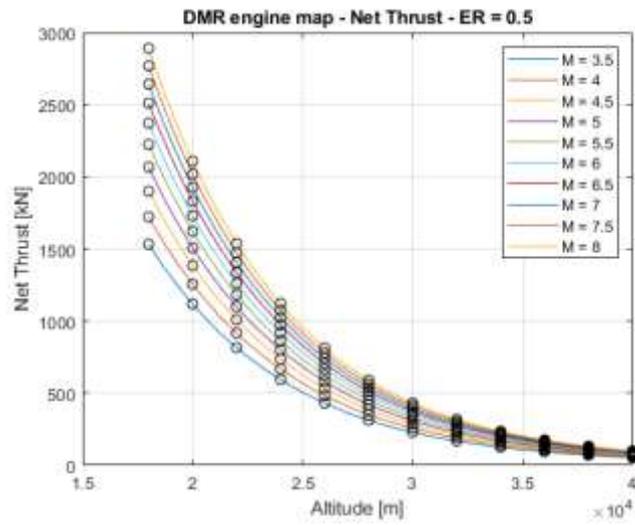
Figure 34: DMR engine, net thrust at ER = 0.5, as a function of altitude. Interpolation from CFD data (black points)
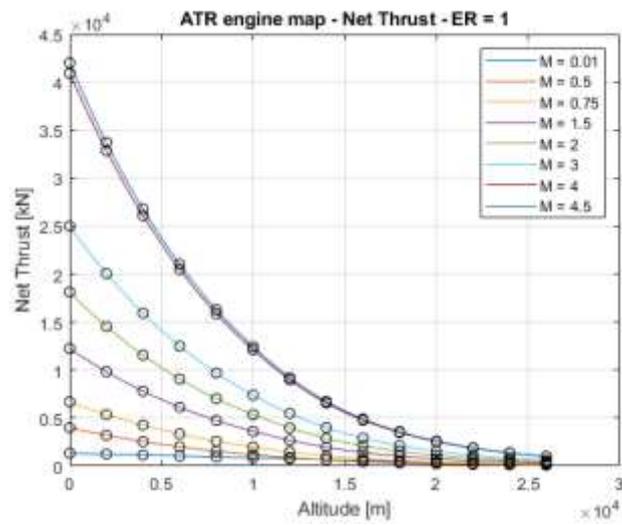

Figure 35: ATR engine, net thrust at ER = 1, as a function of altitude. Interpolation from CFD data (black points)
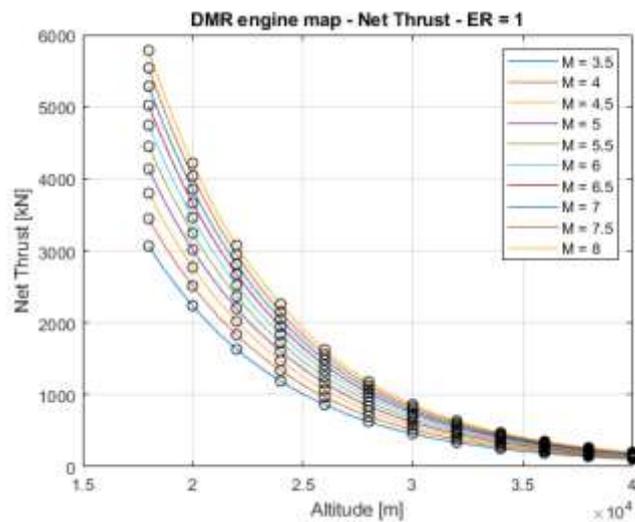

Figure 36: DMR engine, net thrust at ER = 1, as a function of altitude. Interpolation from CFD data (black points)

2.3. Thermal loads

2.3.1. Introduction

The complex topic of thermal loads on the aircraft external shell is addressed first with some general considerations on the nature of the phenomenon. In the first place, a simplified zero-dimensional analysis will be used to estimate thermal loads. At first glance heat fluxes on the aero shell during the mission are somehow proportional to the product of the dynamic pressure of air affecting the vehicle and its flight speed, as follows

$$\dot{Q} \propto q_{dynamic} \cdot V_\infty = \frac{1}{2} \cdot \rho \cdot V_\infty^3$$

However, experimental evidence shows that the thermal flux during Mach 8 flight is only 25 to 35% higher than Mach 5 flight; in addition to this, the reduced flight time spent at Mach 8 instead of Mach 5 leads to another reduction of integrating load during the mission: these inconsistencies are the source of the so-called "thermal paradox" [12], which states that the integrated heat load decreases with increasing flight Mach number.

It is possible to assess a zero-dimensional analysis, in which an energy balance equation is written in each flight condition, to study the thermal equilibrium at any given time of the mission; hence, it is possible to identify the most critical flight phase on the external temperature point of view, in order to size the thermal insulation consequently. This analysis neglects supersonic and hypersonic phenomena occurring within the air at high speed; for the sake of clarity they are now listed, even if their effect was neglected in this study, as it is a first attempt of conceptual design, and those phenomena require proper and accurate characterisation.

<u>High speed effects on aerothermodynamics</u>

Hypersonic flow (considered as the flight regime between Mach 5 and Mach 10) requires a more evolved approach for the evaluation of aerodynamics and thermal performance, since it involves a set of physical phenomena not existing (or at least negligible) in other flight regimes, such as:

- Effect of entropy on the boundary layer. With increasing supersonic speed, the intensity of each shock occurring on the fuselage rises, and hence a stronger entropy gradient is created; the consequence is the creation of a high-vortical flow that mixes, due to its proximity, with the boundary layer.
- Viscous and thermal interaction within the boundary layer. The high-speed flight involves a remarkable amount of kinetic energy, which is transformed, though the viscosity, in internal fluid energy, which causes a temperature rise. Since the pressure gradient normal to the flow within a boundary layer is approximately zero for low to moderate hypersonic Mach numbers, the increase of temperature through the boundary layer coincides with a decrease in density. This causes the bottom of the boundary layer to expand, so that the boundary layer over the body grows thicker and can often merge with the shock wave near the body leading edge.
- Interaction between shocks and boundary layer. As speed increases, oblique shocks tend to become stronger and closer to aircraft fuselage; this proximity causes both an interaction between the shock and the boundary layer and a design hurdle, since the whole vehicle must be included in the Mach cone to avoid structural and aerodynamic complications.
- High temperatures effects. The amount of kinetic energy transformed in internal energy (and hence temperature) and the skin friction (which is proportional to flight speed) cause the gas to assume a different behaviour. This is known as "non-equilibrium

chemical flow", and it involves some real gas effects, such as dissociation and ionization of molecules. In this sense, it is more appropriate to describe the hypersonic flow in terms of aerothermodynamics, since these two disciplines are not detachable in the considered flight regime. A few thermal phenomena related to high speed are now briefly described:

- Gas dissociation: polyatomic gases dissociate as they come into contact with the bow shock generated by the body. This event causes a large energy drop, and changes dramatically the fluid properties; this is the first phenomenon occurring as speed increases.
- Gas ionisation. The ionized electron population of the stagnated flow becomes significant, and the electrons must be modelled separately. In this flight regime, gases behave like a non-radiating plasma.
- Radiation-dominated regime. This regime changes the main mean of thermal exchange between the body and the fluid: as it was conduction (in form of forced convection), now the radiation heat exchange becomes dominant. The modelling of this regime is difficult, since the emitted radiation can be both absorbed by the fluid or represent a significant energy source applied to the body.

In addition to this, hypersonic flight regime in rarefied gas does not follow the Navier-Stokes equations. [13]

Heat transfer balance consists in an equilibrium equation, in which several phenomena are taken into account:

- Convective heat exchange within the boundary layer: it considers wall recovery and actual temperature, and a proper heat transfer coefficient;
- Radiation of heat from the aircraft outer layer: it is considered through the Stephan-Boltzmann radiation equation of a grey body;
- Conduction of heat through the outer layer and insulation towards the inside of the aircraft: it is solved through the conductive heat exchange between a plate with two isothermal surfaces at different temperatures. The inner wall is represented by the tanks (since they are placed on the outer fuselage, directly facing the outer environment), so the reference temperature is taken as liquid hydrogen's.

The resulting equilibrium equation is

$$h_{conv} \cdot (T_{rec} - T_w) = \epsilon \cdot \sigma \cdot T_w^4 + \frac{k}{t} \cdot (T_w - T_{LH_2})$$

In which

- h_{conv} is the convective heat transfer coefficient, evaluated as follows
- $h_{conv} = St \cdot \rho_\infty \cdot V_\infty \cdot c_p$
- St is the Stanton number
- c_p is the specific heat at constant pressure
- T_{rec} Is wall recovery temperature
- T_w is wall actual temperature
- ϵ is the emissivity
- σ is the Stephan-Boltzmann constant
- k is the insulation layer thermal conduction
- t is the insulation layer thickness

The heat flux conducted into the cryogenic tank will eventually be absorbed by the liquid hydrogen. The passive cooling results in fuel boil-off within the self-pressurized tanks. For a more extensive dissertation of this topic, please refer to the last chapter of this work, in which a routine for the estimation of outer skin temperature is accurately described.

The method used in literature for the evaluation of aeroshell viscous heating uses a quite different technique. In fact, it is based on the Eckert enthalpy method [12], and takes account of several semi-empiric equations for the evaluation of thermal and transport properties. Reference enthalpy is calculated as a function of wall, free stream and recovery enthalpy as follows

$$h_{ref} = h_\infty + 0.5 \cdot (h_w - h_\infty) + \frac{11}{50} \cdot (h_r - h_\infty)$$

Recovery enthalpy is calculated as a function of recovery and free stream enthalpy, and Prandtl number

$$h_r = h_\infty + Pr^{1/3} \cdot (h_\infty^0 - h_\infty)$$

Total enthalpy is

$$h_\infty^0 = h_\infty + \frac{1}{2} \cdot V_\infty^2$$

If air can be modelled as ideal and calorically semi-perfect gas and no compressibility correction is considered, these relations provide conservative estimations of thermic loads. The convective heat transfer coefficient is then expressed as a function of the convective heat transfer parameter (k_{conv}, which depends on boundary layer conditions and wall temperature) and the distance to the leading edge in which the laminar-turbulent transition occurs (x)

$$h_{conv} = k_{conv} \cdot x^{-1/5}$$

Heat exchange rate is computed as follows

$$\dot{q}_{conv} = h_{conv} \cdot (T_r - T_w) = k_{conv} \cdot x^{-1/5} \cdot (T_r - T_w)$$

Total convective heat load is then evaluated as the integral of the heat exchange rate over a planar element of the aircraft aeroshell

$$\dot{Q}_{conv} = \iint \dot{q}_{conv} \, dA = \iint k_{conv} \cdot x^{-1/5} \cdot (T_r - T_w) \, dA = k_{conv} \cdot (T_r - T_w) \iint x^{-1/5} \, dA$$

The aeroshell has been discretised into a set of planar surfaces, on which the application of the previous equilibrium equation is possible; depending on the location of the finite element of area, flow conditions are assumed to be those of the free-stream, Prandtl-Meyer expansion or an oblique shock.

2.3.2. Literature review

The previous paragraphs showed a method for the estimation of global heat loads affecting the whole aircraft. However, a first analysis of leading-edge thermal load should be carried on with sufficient precision, in order to properly identify the magnitude of the hoarded heat on the most critical point, namely the stagnation point (from thermal point of view).

A parametric stagnation-point heat transfer study, since it involves early stages of a design, requires simple empirical methods with good agreement with experimental results. In this section, a few engineering methods for stagnation-point heating assessment are listed and explained.

The basic parameters involved in the stagnation-point heat transfer are expressed in Fay-Riddell equation

$$\dot{q}_0 = \eta \cdot \mathrm{Pr}^{-0.6} \cdot (\rho_w \mu_w)^{0.1} \cdot (\rho_e \mu_e)_s^{0.4} \cdot (h_e - h_w) \cdot \left(\frac{du_e}{dx}\right)_s^{0.5}$$

Where the subscript "e" denotes external conditions. In this analysis the most critical point (i.e. the stagnation point) will be considered; hence the subscript will be "t_2".

This equation can be simplified exploiting the proportionality of those variables as follows:

- According to perfect gas equation

$$\rho_{t_2} \propto \frac{p_{t_2}}{z_{t_2} T_{t_2}}$$

$$\rho_{w_t} \propto \frac{p_{w_t}}{z_{w_t} T_{w_t}}$$

- According to Sutherland law

$$\mu_{t_2} \propto T_{t_2}^E$$
$$\mu_{w_t} \propto T_{w_t}^E$$

  Where $E \cong 0.5$.

- For high temperature flows at hypersonic speed

$$h_e - h_w \cong h_e \cong \frac{V_\infty^2}{2}$$

- Since $p_{t_2} = z_{t_2} \rho_{t_2} R T_{t_2} \gg p_2$

$$\left(\frac{du_e}{dx}\right)_{t_2} = \frac{1}{R_N} \sqrt{\frac{2(p_{t_2} - p_1)}{\rho_{t_2}}} \cong \frac{1}{R_N} \sqrt{\frac{2p_{t_2}}{\rho_{t_2}}} \cong \frac{1}{R_N} \sqrt{2 z_{t_2} T_{t_2}}$$

Hence it is possible to write the following relation

$$\dot{q}_0 = K \cdot \left(\frac{\rho_\infty}{R_N}\right)^{0.5} \cdot V_\infty^3$$

In which K is a proportionality constant, which takes account of the effect of the thermodynamic and transport gas properties at the wall and external to the boundary layer.

$$K = \eta \cdot 2^{0.25} \cdot Pr^{-0.6} \cdot \left[\frac{T_{w_t}^{0.1E} \cdot T_{t_2}^{0.1E}}{\left(z_{w_t} T_{w_t}\right)^{0.1} \cdot \left(z_{t_2} T_{t_2}\right)^{0.15}}\right]$$

In the relation expressed before, the heat transfer rate is a function of free-stream physical quantities and the stagnation-point radius, R_N. The parameter K has been estimated in several different engineering correlations [14]:

- Scott equation

$$\dot{q}_0 = 18300 \cdot \left(\frac{\rho_\infty}{R_N}\right)^{0.5} \cdot \left(\frac{V_\infty}{10^4}\right)^{3.05} \qquad \left[\frac{W}{cm^2}\right]$$

- Detra equation

$$\dot{q}_0 = \frac{11030}{\sqrt{\rho_{SL}}} \cdot \left(\frac{\rho_\infty}{R_N}\right)^{0.5} \cdot \left(\frac{V_\infty}{V_{circ}}\right)^{3.05} \qquad \left[\frac{W}{cm^2}\right]$$

  In which ρ_{SL} is the density at sea level, and V_{circ} is the circular orbit velocity.

- Zoby equation [15]

$$\dot{q}_0 = 3.88 \cdot 10^{-4} \cdot \left(\frac{p_{t_2}}{R_N}\right)^{0.5} \cdot (H_{t_2} - H_w) \qquad \left[\frac{W}{m^2}\right]$$

In which:

- H_{t_2} is the stagnation point enthalpy, J/g
- H_w is the wall enthalpy, J/g
- $\dot{q}_0$ is the heat transfer rate, $\frac{J}{cm^2 \cdot s}$
- R_N is the radius of curvature, cm
- p_{t_2} is stagnation pressure, atm
- $K = 3.879793 \cdot 10^{-4} \; \frac{kg}{m^{3/2} \cdot s \cdot Pa^{1/2}}$, is the constant evaluated experimentally for air

This formula is valid only in the stagnation point, which is approximated as a sphere of constant radius: hence, this formula considers the three-dimensional effect of heat transfer around a blunt body.

- Anderson equation

$$\dot{q}_0 = 1.83 \cdot 10^{-4} \cdot \left(\frac{\rho_\infty}{R_N}\right)^{0.5} \cdot \left(1 - \frac{H_w}{H_e}\right) \qquad \left[\frac{W}{m^2}\right]$$

2.3.3. Revision and results display

For the following discussion, the most critical flight phase is considered

Altitude	Mach number	Angle of attack	Flight path angle	Pitch angle	Dynamic pressure
32-33.5 km	8	0°	0°	0°	50 kPa

The most critical stagnation point is considered to be the intake leading edge; for a first analysis, it is assumed to be spherical, with the following test radiuses: $R_{LE} = 6.25, 11.3, 22.5 \; mm$, and the following emissivities for the calculation of radiative equilibrium: $\epsilon = 0.7, 0.8, 0.9$. Then, some of the previous formulas (in particular Scott's and Zoby's, also referred as "cold wall" and "hot wall")are used for the estimation of both heat flux and temperature on the leading edge, taking account of all the combinations of geometrical and thermal properties listed earlier. This study is extended in all cruise conditions, as to provide a thermal assessment of the intake leading edge alongside the whole mission. In this section, a few results are showed. Since the possible combinations are many, the following charts are focused on the definitive configuration chosen for the intake leading edge radius, namely $R = 11.3 \; mm$ and $\epsilon = 0.8$.

Two main aspects are immediately noted:

- Scott's theory ("cold wall") predicts a heat flow and temperature higher than Zoby's theory ("hot wall") about 3 times, in any presented condition;
- Both theories provide very high temperature values (not less than twice as high as the temperatures found in the literature for the free surface convective heat exchange [12]). These values therefore demonstrate the need for an appropriate thermal protection system to protect the edge of the attack from excessive temperatures.
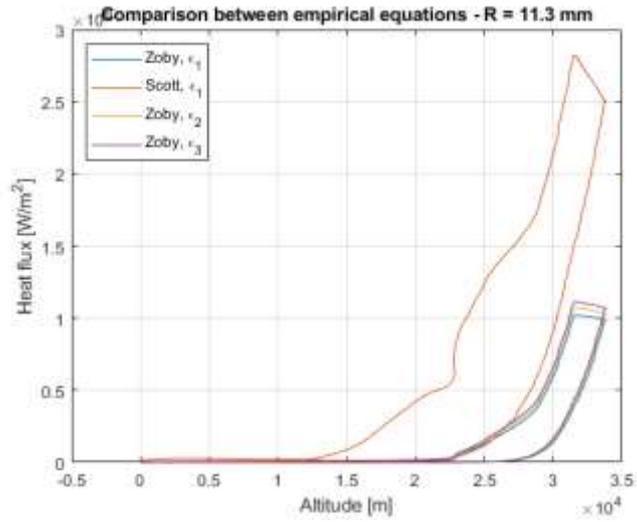
*Figure 37: heat flux as a function of altitude, for R = 11.3 mm, according to Scott and Zoby's theories*
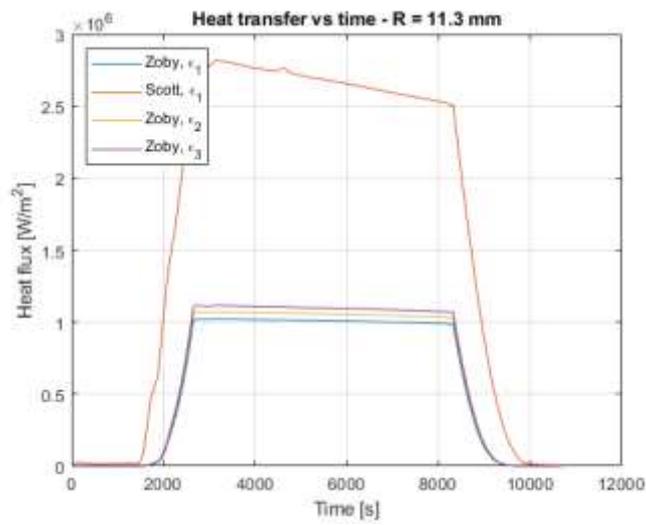
Figure 38: heat flux as a function of flight time, for R = 11.3 mm, according to Scott and Zoby's theories
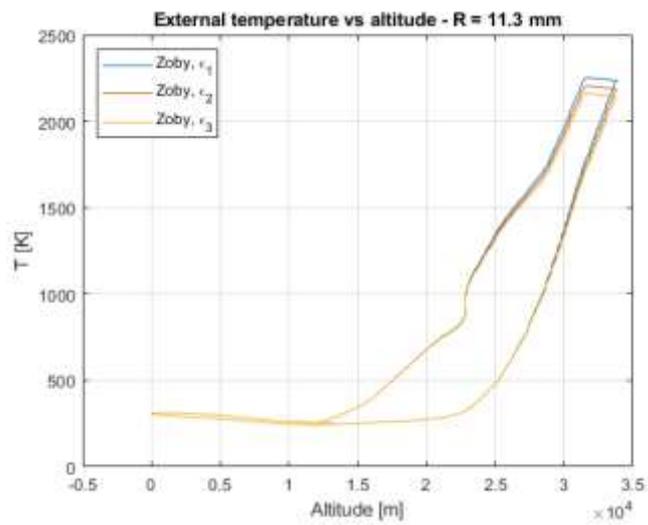

Figure 39: external temperature as a function of altitude, for R = 11.3 mm, according to Zoby's theory, for several emissivity values
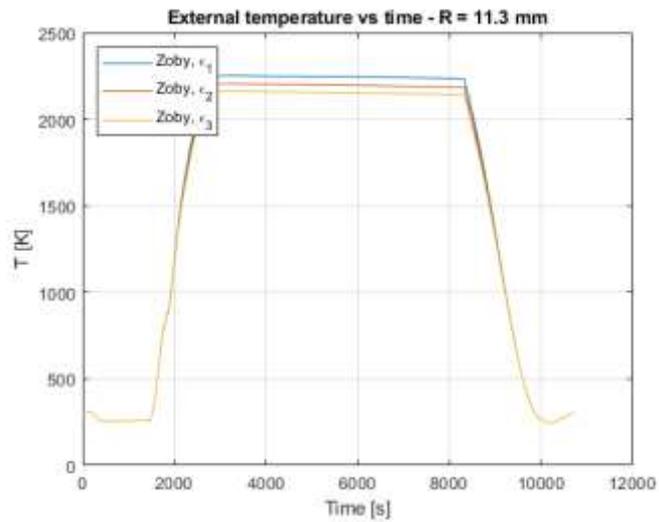
Figure 40: external temperature as a function of time, for R = 11.3 mm, according to Zoby's theory, for several emissivity values
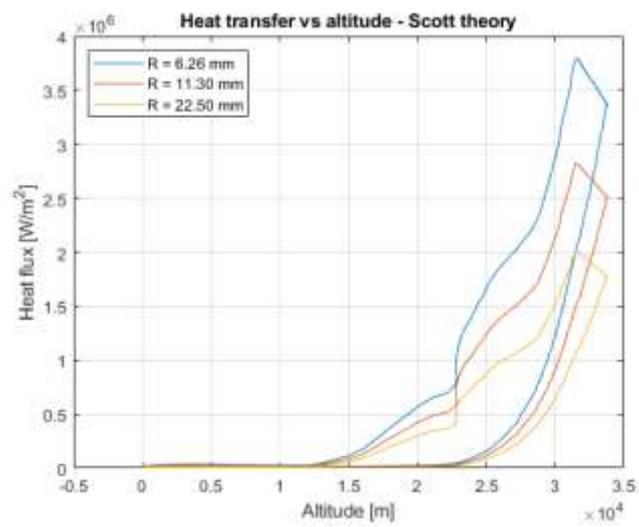

Figure 41: heat flux as a function of altitude, according to Scott's theory, for several radius values
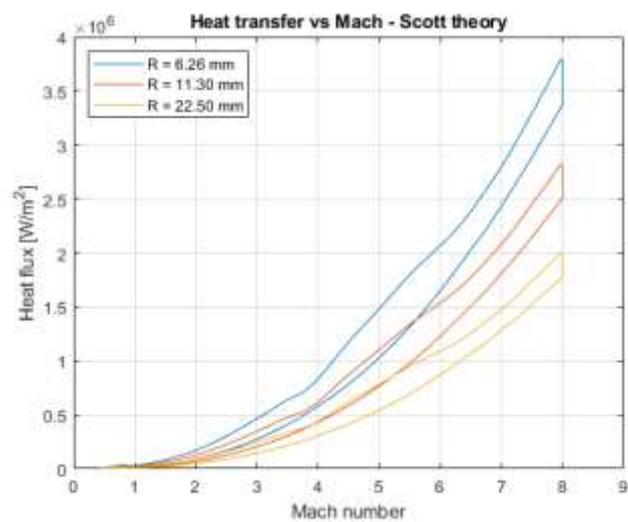

Figure 42: heat flux as a function of Mach number, according to Scott's theory, for several radius values
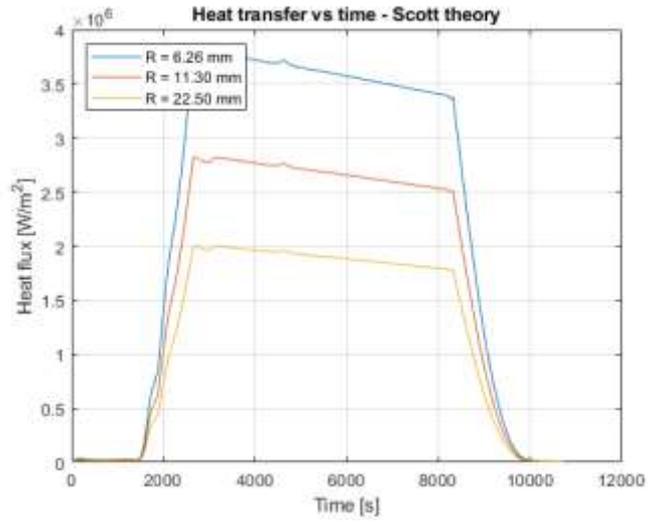
Figure 43: heat flux as a function of flight time, according to Scott's theory, for several radius values
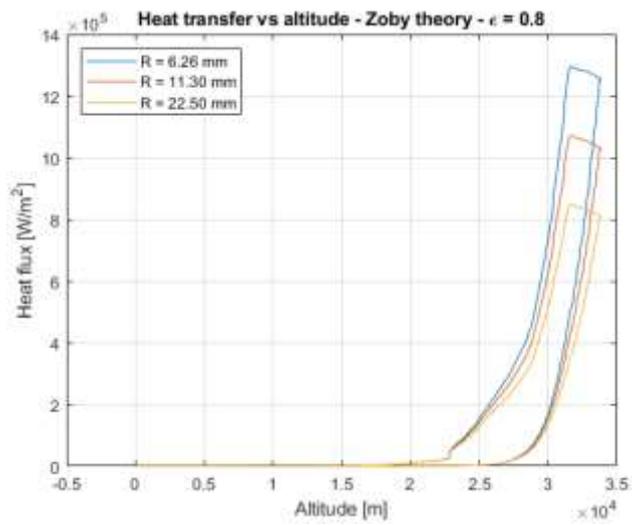

Figure 44: heat flux as a function of altitude, according to Zoby's theory, for several radius values
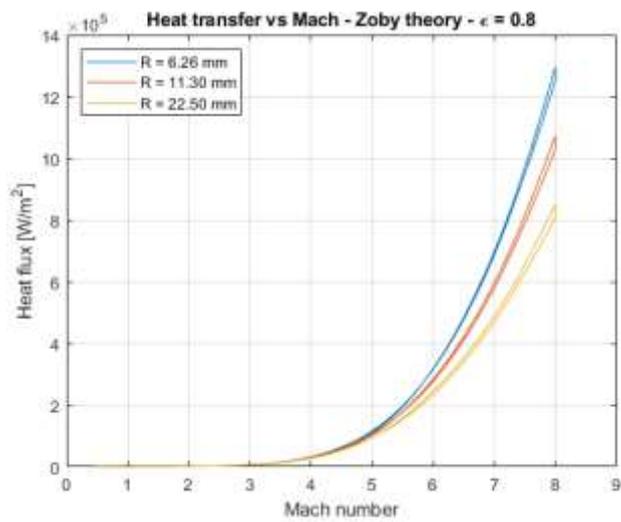

Figure 45: heat flux as a function of Mach number, according to Zoby's theory, for several radius values
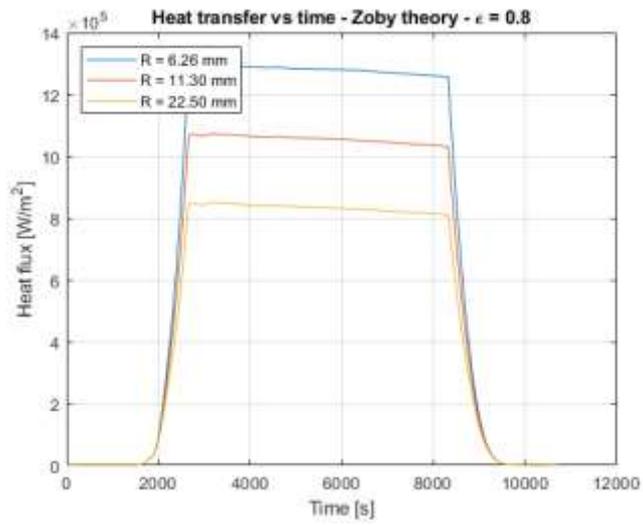
Figure 46: heat flux as a function of flight time, according to Zoby's theory, for several radius values
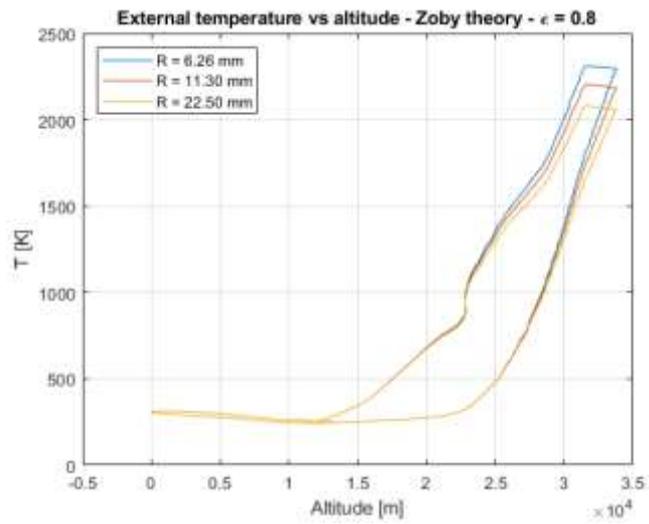

Figure 47: external temperature as a function of altitude, according to Zoby's theory, for several radius values
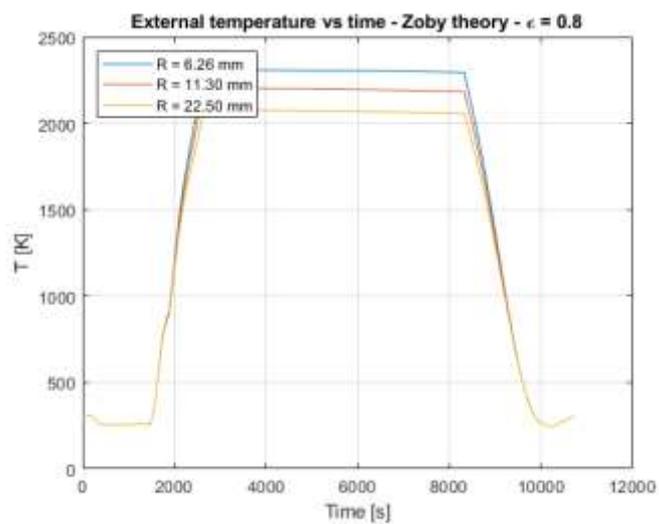

Figure 48: external temperature as a function of flight time, according to Zoby's theory, for several radius values

3. Aircraft performance and trajectory evaluation

3.1. Literature review

Hypersonic flight regimes are worthwhile only if engaged for very long-range trajectories since these allow the aircraft to keep flying at high speed for a longer period and therefore increasing the beneficial effect of higher flight regimes rather than traditional subsonic ones. The flight path was indeed designed in order to enhance the potential for hypersonic cruises: the adopted baseline is a flight from Brussels Airport (BRU) to Sydney International Airport, which are at antipodal distance (18734 km). If a hypersonic aircraft is considered, the optimal flight root will necessarily be different from what normally implemented for traditional planes, due to aeroacustic limits imposed by several regulations for inhabited areas. Those restrictions are linked to sonic booms and ground overpressure: it must not exceed the maximum tolerable value (50 kPa). For this reason, roots for supersonic civil aircrafts shall limited to a few oceanic areas, a critical aspect which undermines business capabilities of similar vehicles. ESA technical papers about LAPCAT A2 report [16] that the aircraft's overpressure values are:

- 85 kPa at the beginning of the first cruise phase at Mach 5;
- 70 kPa at the second hypersonic cruise phase.

As a result, like previous supersonic attempts, the study case in considerably limited in terms of root possibilities to the areas with low density of population such as Artic and oceanic regions. In short, hypersonic civil air transport has to meet a few constraints in a more restrictive way than traditional subsonic flights, namely:

- requirements for horizontal take-off and landing;
- take-off and landing maximum field range;
- environmental regulations;
- aeroacustic issues (sonic booms);
- comfort and safety of passengers.

In order to prove the feasibility of this vehicle on its reference mission (antipodal flight) it is mandatory to simulate its trajectory including all flight phases. In particular, a few constraints have been pointed out:

- lift-off speed is $V_{LOF} = 150 \ ^m/_s$
- take-off speed is $V_{TO} = 90 \ ^m/_s$
- first turbojet ascent must be limited under $M = 0.95$, at least until a minimum distance from take-off of $400 \ km$, in order to avoid a sonic boom generation over land
- turbojet acceleration ends when $M = 4$ is reached; then ATR engines are deactivated gradually, and DMR engine is used for main propulsion (up to $M = 8$)
- Due to sonic boom requirements it is necessary to avoid flying over inhabited land and therefore a simple great circle route from the departure airport to the destination is not possible. It has been chosen as a shortest alternative to head north from a European destination, fly over the arctic region and then pass between Asia and North America at the Bering Strait;
- The descend consists of unpropelled gliding flight, with the deactivation of the whole propulsion plant
- maximum acceleration consistent with passengers' comfort is selected to be $a_{max} = 3 \ ^m/_{s^2}$

in this case study the antipodal route is selected, but for this project economic feasibility also other trajectories were considered; unfortunately, it was shown that missions across the Atlantic (Europe – North America) are not very efficient when aiming at cruising at $M = 8$, because of the short range required and the relatively long acceleration and deceleration phases [17].

3.2. Current state of the design

3.2.1. Aircraft performance evaluation

The determination of the performance of the aircraft is a fundamental stage in the project, as it allows to properly size the airplane geometry and propulsion plant for a most cost-effective concept of operations, but also to verify the compliance of current aircraft configuration to the desired mission. In this section, an empirical set of equations will be presented: it has been obtained thanks to an analytic study of the optimal concept of operations and statistical analysis of existing airplanes for civil transport. The result is a set of equations to be used as a general principle in the definition of an aircraft mission; this approach has a sufficient accuracy but doesn't require too many parameters to be used, and it is suitable for a conceptual design phase.

3.2.1.1. Introduction

All civil aircraft must comply with airworthiness standards and ensure minimum performance for the user. The mission profile is a graph that summarizes the evolution in time or space of the single flight, from the taxiing phase to the landing.
The main flight phases are

1. Start-up and taxi-out
2. Take off
    1. Transition to climb
    2. Climb up to 1500 ft
3. Climb up to 5000 ft
4. Climb up to 15000 ft
5. Climb up to 24000 ft
6. Climb up to 11000 m
7. Subsonic cruise
8. Climb up to 25000 m
9. Supersonic cruise
10. Climb up to 35000 m
11. Hypersonic cruise
12. Descent
13. Approach e landing
    1. Flare
    2. Ground roll

The following picture show the typical mission profile for civil aircrafts
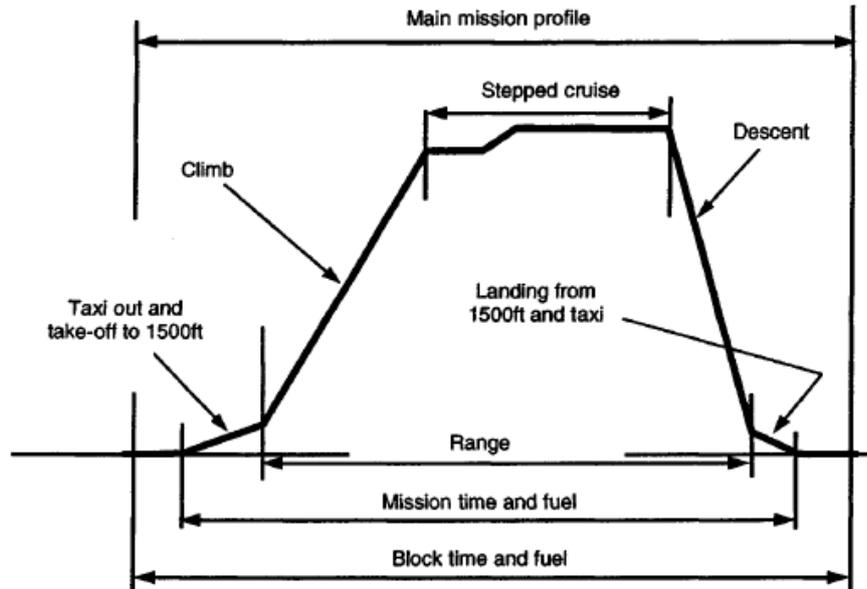
Figure 49: typical mission profile for civil aircraft [18]

Additional phases of mission are also provided, in case it is necessary to extend the flight due to problems at the landing or for a change of route:

14. Hold for a specific time at a speed calculated for minimum consumption
15. Rise to a new cruise altitude
16. Cruise at a speed that maximizes the range
17. Descent to 1000 ft
18. Increase in fuel safety rate required for nominal mission (around 10%)

In the following picture are shown the addition necessary to a traditional mission profile to handle an out-of-nominal scenario, namely after a failed approach and a new landing at some distance from the first attempt.
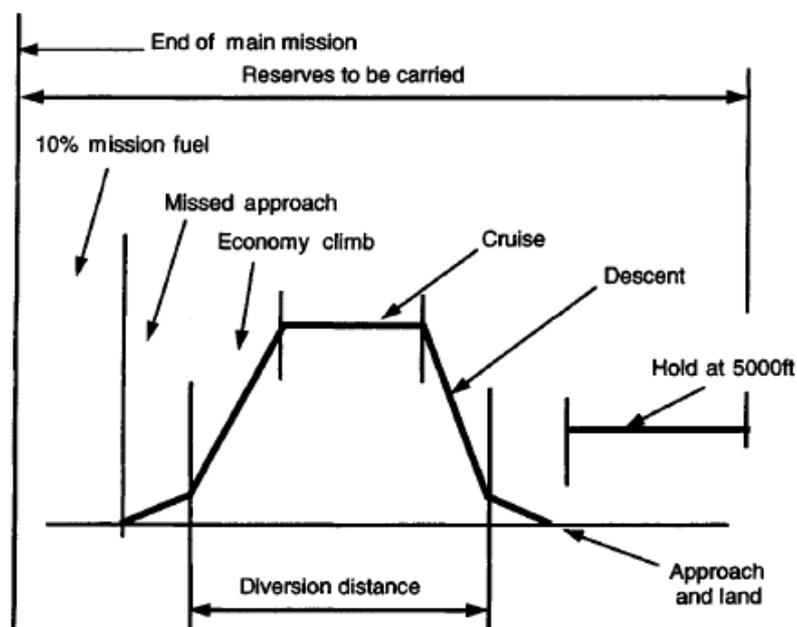

Figure 50: typical mission profile for civil aircraft, in the event of a failure [18]

Each important segment of the mission profile will now be defined in order to derive its considerations.

3.2.1.2. Start-up e taxi-out

This phase does not contribute to the real mission in terms of range, but requires a considerable amount of fuel expenditure, as well as a time necessary not negligible (Typically the limits allowed by airport infrastructure managers are 9 minutes for domestic flights and 12 minutes for international flights).

3.2.1.3. Take off

These phases are critical from the safety point of view, but do not significantly affect the mission range. The consumption at this stage should be considered, as the engine is used at its maximum power (i.e. maximum power consumption) for a few minutes (typically 2).

Take-off distance
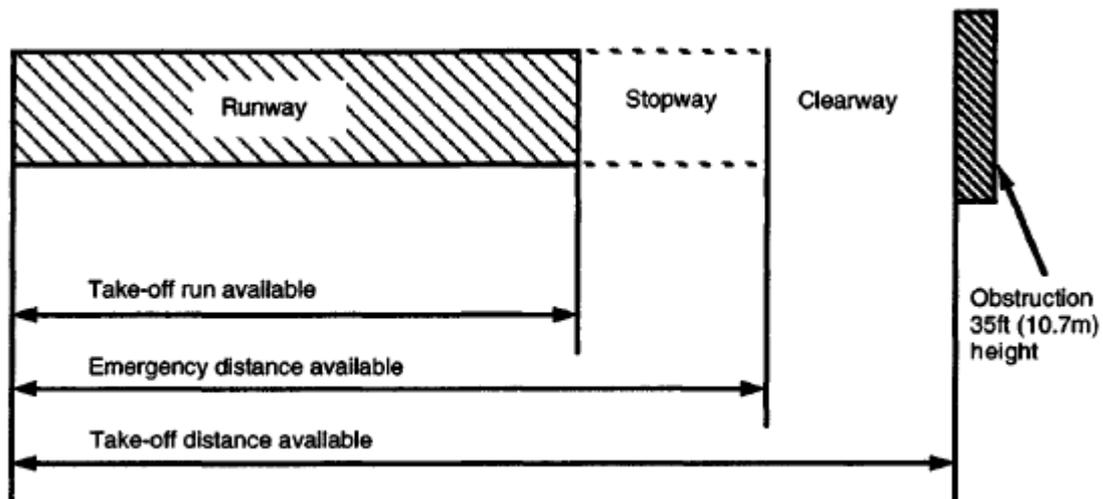
Figure 51: runway length compared to take-off distances in different scenarios [18]

The take-off distances are divided as follows:
- Take-off run available: asphalted track length
- Emergency distance available: sum of the previous and the length of the stopway, or an obstacle-free zone placed immediately after the first
- Take-off distance available: sum of the previous and the length of the Clearway, that is the space between the end of the stopway and the first obstacle higher than 35 feet (10.7 meters).

The take-off phases may be further specified according to mission needs:

- Take-off run required: distance between the start of the take-off run to the lift-off point (lifting), increased by one third of the distance between the lift-off point and the obstacle at the end of the track
  - Take-off run required with all engines running: the previously defined distance is multiplied by a safety factor of 1.15, respecting the take-off run available
  - Failure of an engine: in this case you can present two possible scenarios, depending on the speed reached when the damage is felt
    - o Continued take off after failure (accelerate and go): distance defined as before, but in order to consider the failure and the consequent variation of the performances. The distance thus specified must be less than the available take-off run distance.
    - o Rejected take off after failure (accelerated and stop): distance between the start of the take-off run until failure occurs, to which is added the distance necessary to brake the plane up

to a zero speed using only the brakes of the undercarriage. The distance thus specified must be less than the available take-off run distance.

Continued take-off (accelerate–go)

climbing with one engine failed

Acceleration

35 ft

(engine failure at speed V_1)

Rejected take-off (accelerate–stop)

Acceleration

Stopping

$V = 0$

(engine failure at speed V_1)
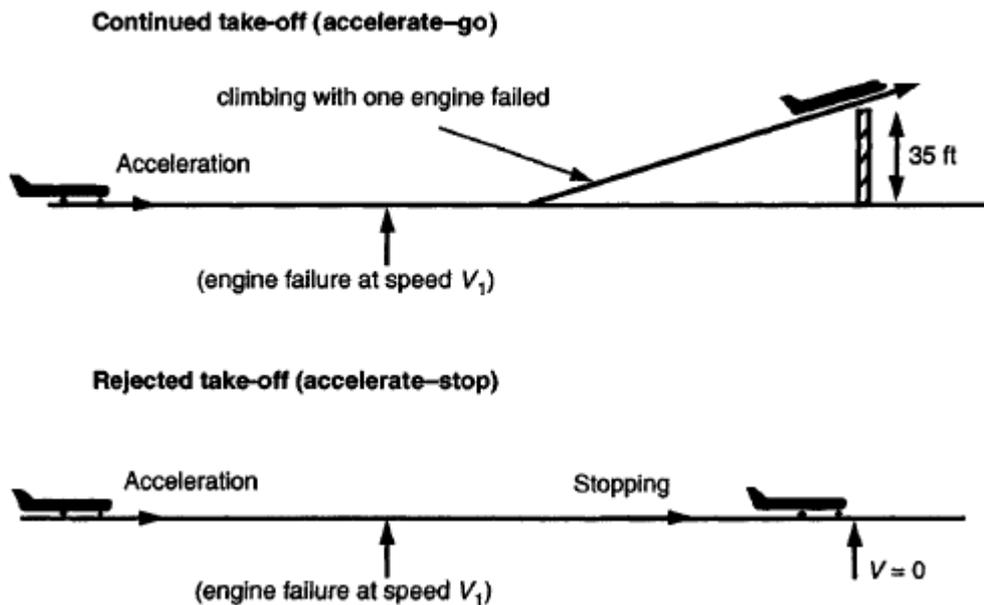
Figure 52: comparison between failure during take-off scenarios: accelerate-go (up) and accelerate-stop (bottom) [18]

Essential speed steps during take-off

The take-off situation with all operating engines is relatively simple from the conceptual point of view, as it is a linear acceleration of the aircraft, crossing several remarkable speeds, and then overcome the obstacle at the end of the track. The main phases are described with reference to the figure

V_0

V_S

V_{mc}

V_1

V_r

V_{mu}

V_{LOF}

V_2

Obstruction 35ft (10.7m) height
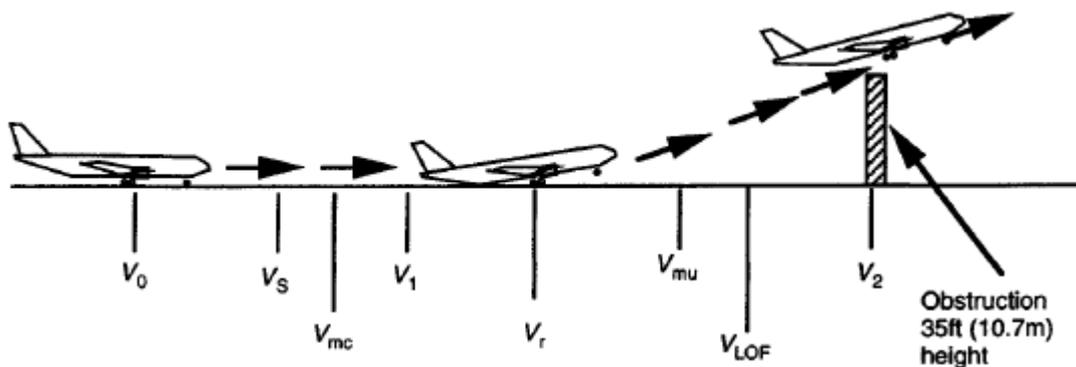
Figure 53: nominal take-off phase, with significant speed values [18]

- $V_0 = 0$; the plane usually starts at a standstill, and accelerates along the track with the front wheel of the carriage resting on the track, with a low incidence angle;
- V_S, aeroplane stalling speed in take-off configuration; at this speed flaps are extended in take-off mode;
- V_{mc}, aeroplane minimum control speed: if an engine failure occurs at this speed, the aeroplane may be controlled without embarking and with roll angles of less than 5°
- V_1, critical speed of decision, in case of failure of the propulsive system;

- V_R, rotation speed; may be the same as the previous one but must be at least 5% higher than V_{mc}. When this speed is reached the aeroplane is rotated by raising the front carriage from the runway; the rotation angle is limited to avoid the tail strike on the runway;
- V_{mu}, minimum unstick speed; due to the interference between the tail and the ground the previous speed may not be enough to the lift-off, due to the limitation of the rotation angle of the aeroplane;
- V_{LOF}, lift-off speed; at this speed the aircraft is able to generate sufficient lift capacity to sustain its weight. If all engines are operational must have a margin of 10% compared to V_{mu}, otherwise it is reduced to 5%;
- V_2, speed reached when crossing the obstacle cross the track; there must be a margin of 10% with respect to the V_{mc}, and a margin of 15-20% with respect to the stall speed.

Take off performance – all engine operative
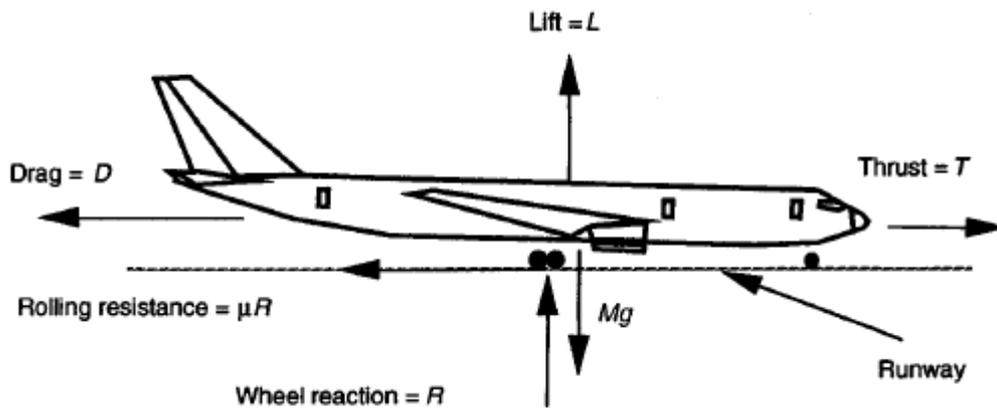
Figure 54: force equilibrium on the aircraft [18]

The equilibrium of horizontal and vertical forces implies that

$$T = D + M\frac{dV}{dt} + \mu R$$

$$R = Mg - L$$

Combining them

$$T = D + M\frac{dV}{dt} + \mu(Mg - L)$$

The required acceleration is obtained

$$\frac{dV}{dt} = -\frac{1}{M}[D + \mu(Mg - L) - T]$$

Replacing lift aerodynamic lift and drag expressions

$$\frac{dV}{dt} = -\frac{1}{M}\left[\frac{1}{2}\rho V^2 S C_D + \mu\left(Mg - \frac{1}{2}\rho V^2 S C_L\right) - T\right]$$

$$\frac{dV}{dt} = -\frac{1}{M}\left[\frac{1}{2}\rho V^2 S(C_{D_0} + kC_L^2) + \mu\left(Mg - \frac{1}{2}\rho V^2 S C_L\right) - T\right]$$

$$\frac{dV}{dt} = g\left[\left(\frac{T}{W} - \mu\right) + \frac{\rho}{2\frac{W}{S}}(-C_{D_0} - kC_L^2 + \mu C_L)V^2\right]$$

It is possible to obtain the necessary distance to the take-off stroke by integrating the previous equation between zero speed and lift-off speed. However, it should be noted that the incidence of the aeroplane is constant in the take-off run phase, so that the load bearing factor can be assumed to be constant and directly proportional to V 2; In addition, the thrust also assumes an approximately constant course during the run, so the calculations are conducted at a speed of 0.707*V (as the integration is done with the speed square). 2 coefficients can therefore be defined approximately constant

$$K_T = \frac{T}{W} - \mu$$

Coefficient μ c considers rolling friction in dry runway conditions depending on the type of pavement of the runway; civil transport uses only paved runways, so it can be assumed that $\mu = 0.02$.

$$K_A = \frac{\rho}{2\frac{W}{S}}(-C_{D_0} - kC_L^2 + \mu C_L)$$

Hence, acceleration at take-off becomes

$$\frac{dV}{dt} = g[K_T + K_A V^2]$$

Stall speed is evaluated by imposing lift and weight equilibrium

$$L = W$$

$$\frac{1}{2}\rho S V_{stall}^2 C_{L_{max}} = MTOW$$

$$V_{stall} = \sqrt{\frac{2 * MTOW}{\rho S C_{L_{max}}}}$$

The minimum lift-off speed is obtained by requiring it to be 10% higher than the stall speed

$$V_{LOF} = 1.1 * V_{STALL}$$

Integrating between the starting speed (zero) and the lift-off speed, the distance necessary to reach is

$$s_G = \frac{1}{2gK_A}\ln\left[\frac{K_T + K_A * V_{LOF}^2}{K_T}\right]$$

The result obtained is in accordance with the available track length.

Take off performance – one engine operative

In the case of a failure of an engine during the take-off that renders it totally inoperative, therefore necessary aborting the mission, it is possible to undertake two approaches:

1. Maximum thrust reversal, extended airborne brakes and bogie brakes maximised in the possibilities to stop the aircraft before the end of the runway;
2. Continuation of the take-off run in order to continue the take-off if the aeroplane cannot be stopped before the end of the runway.

Both procedures consist of a first section of nominal acceleration until the failure occurs, a reaction time of the driver equal to 2 seconds, and then divide in the choice to continue or stop the race.

A Matlab script has been implemented to calculate the distance from the start of the track (and at what speed) an accelerated and go approach is needed. The results show that the speed of decision (above which it is necessary to continue taking off) is

$$V_{dec} = 58.45 \ m/s$$

3.2.1.4.   Transition to climb

Durant this flight phase, the aircraft accelerates from lift off speed, V_{LOF}, to climbing speed, V_2. A simplified method is used to predict the distance to the ground necessary for the transition: first of all, it is assumed to fly along an arc of perfect circumference with a coefficient of portance equal to

$$C_L = 0.9 \ C_{L_{max}}$$

Climbing speed is equal to

$$V_2 = 1.15 * V_{stall}$$

Average speed during the manoeuvre is

$$V_{TRANS} = \frac{V_{LOF} + V_2}{2}$$
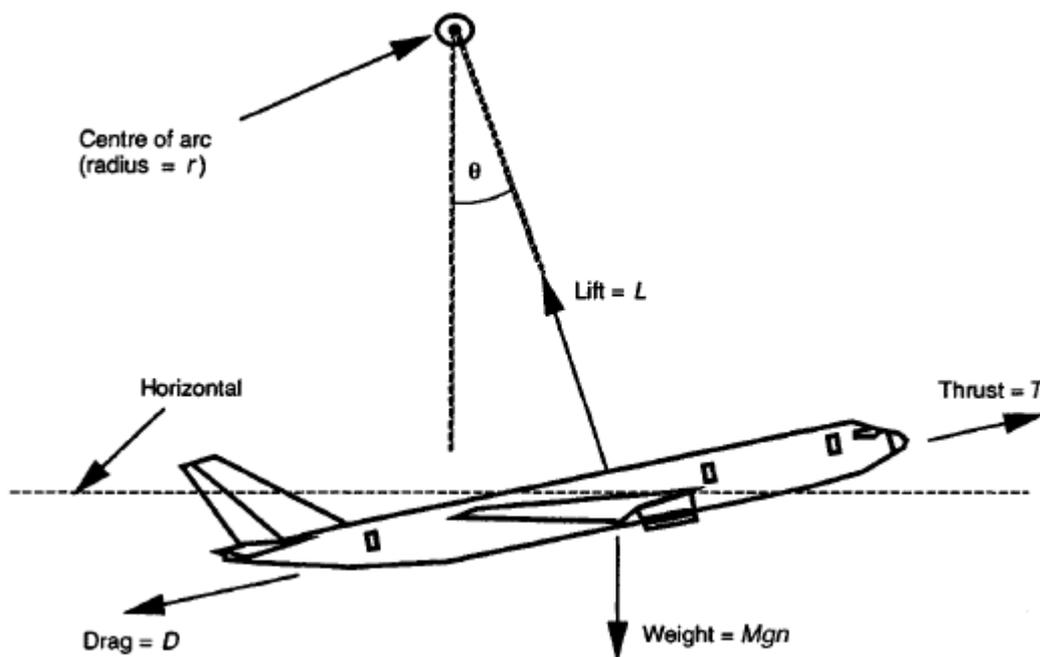
Figure 55: transition to climb, force diagram [18]

Equilibrium equation states that

$$L = Mgcos\theta + \frac{MV_{TRANS}^2}{r}$$

With r equal to the radius of the circular trajectory, M is the mass of the aeroplane and θ is the trim angle. The load factor is defined as (also introducing the lift formula)

$$n = \frac{L}{W} = \frac{\frac{1}{2} * \rho * V_{TRANS}^2 * S * 0.9 * C_{L_{max}}}{W}$$

For small trim angles $\cos\theta \sim 1$, so

$$L = Mg + \frac{MV_{TRANS}^2}{r}$$

By replacing this last expression in the load factor formula, it is obtained that

$$n = \frac{L}{W} = \frac{Mg + \frac{MV_{TRANS}^2}{r}}{Mg} = 1 + \frac{V_{TRANS}^2}{rg}$$

Hence

$$r = \frac{V_{TRANS}^2}{g(n-1)}$$

Assuming a typical value for final climbing gradient $\gamma = 12° = 0.21\ rad$, the ground clearance required for the transition is equal to

$$s_t = r * \sin(\gamma)$$

The height at the end of the transition is calculated as

$$h_t = r * (1 - \cos\gamma)$$

The distance to the obstacle is calculated as

$$s_s = \sqrt{(r + h_s)^2 - r^2}$$

3.2.1.5. Climb up to 1500 ft

The requirements impose a cruising altitude of more than 10000 m; in this case a cruising altitude of 11000 m is assumed.

A standard subdivision of this flight phase into four segments is applied, as shown in the following table

Segment	Height	Flap	U/C	Rating
1st	0–35 ft	TO	Down	TO
2nd	400 ft	TO	Up	TO
3rd	400+ ft	Variable	Up	Max. Cont.
4th	1500 ft	En-route	Up	Max. Cont.

Figure 56: high-lift devices typical usage [18]

The second stage shall end when the main bogie is retracted; during this segment the aeroplane shall maintain a speed at least 15% higher than the stalled one.

Considering the figure below
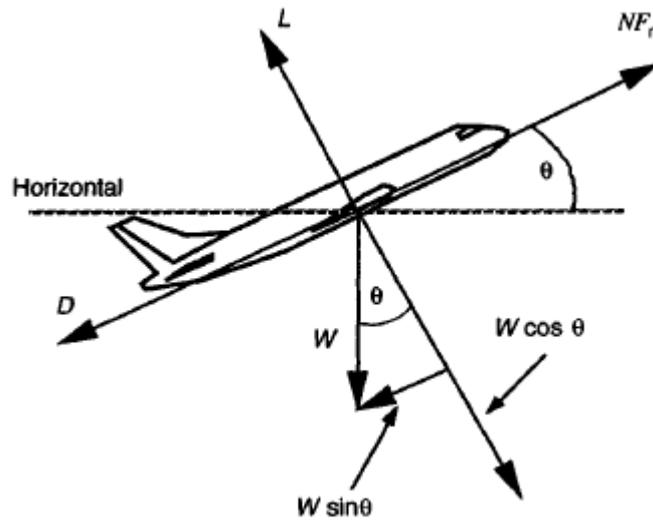
Figure 57: equilibrium of forces on the climbing airplane [18]

It is possible to calculate the climb gradient to determine how much space 1500 ft will be reached.

From balance to horizontal travel (thrust, drag and weight)

$$NF_n - D = W sin\theta$$

Hence, climbing gradient is equal to

$$\theta = \frac{\frac{T_{TOT}}{2} - D}{W}$$

The norm prescribes that it is greater or equal to 0.024 also in case of failure: the requirement turns out therefore respected. The approach that will be adopted in the phases of ascent, regarding the speed, is that of the least direct operating cost, applying the typical rates of climb used in civil field.

During this phase the EAS speed remains constant: this necessarily implies that the TAS increases with the increasing of the altitude. An average climb rate is assumed, according to current Airbus320 common practise, as

$$roc = 2500 \ {}^{ft}\!/_{min}$$
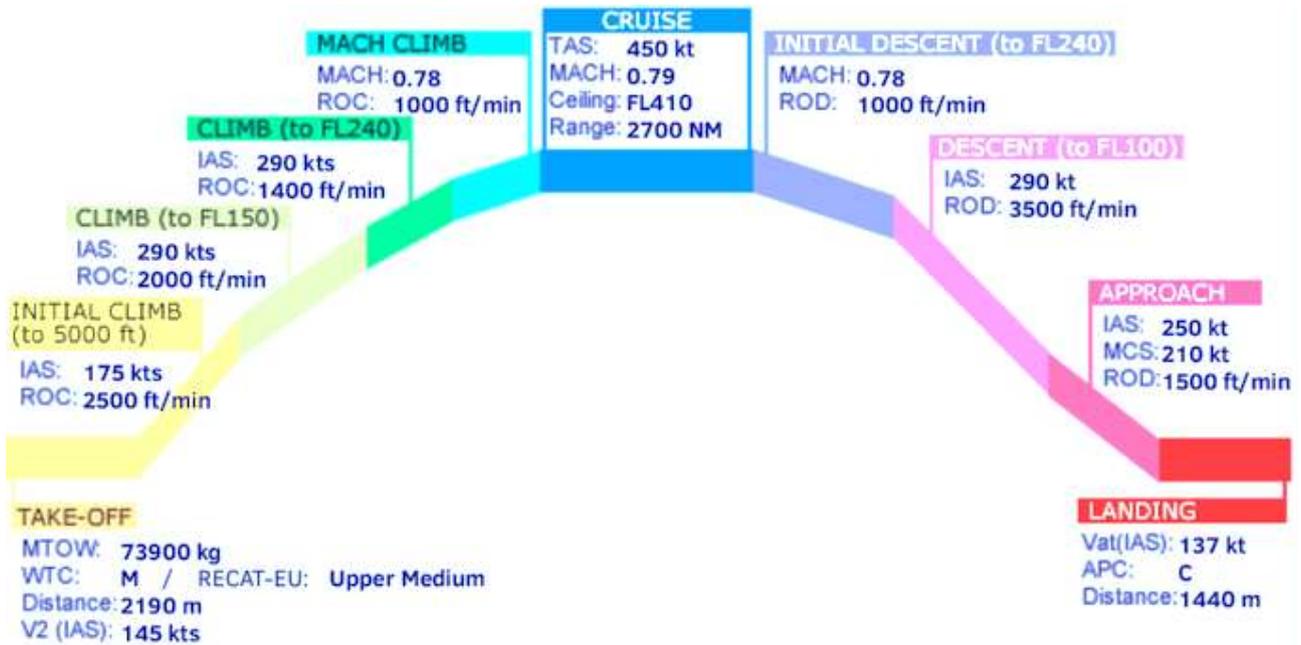
Figure 58: A320 step cruise, suggested rates of climb [19]

The following climb steps, in the same way, are described with an average rate of climb, which is more gradual as the aircraft approached the first cruise altitude. They are defined as follows:

- Climb to 5000 ft:
- Climb to 15000 ft:
- Climb to 24000 ft:
- Climb to 11000 m:

3.2.1.6.   Subsonic cruise

In this phase we do not see a change in altitude, nor significant linear accelerations; we consider a Mach of flight and a constant altitude. This subsonic cruise is necessary to provide enough physical distance between the airplane and any inhabited land; in fact, according to literature review trajectory, it is necessary to travel at least 360 km along the expected route to reach Netherlands coast from Brussels airport. In this analysis, the subsonic cruise is carried on until the aircraft reaches a safe distance from the airport of 965 km, in which it is in the middle of the Northern Sea, were ground overpressure are not regulated.

In phase of cruise the attainable autonomy hour is calculated using the available data on the necessary power, the resistance, the consumption of the propellers (c) and the amount of fuel on board. The decrease in aircraft weight over time is expressed as

$$\frac{dW}{dt} = -c * T$$

Level flight (?)

$$\frac{dW}{dt} = -c * D * \frac{W}{L}$$

$$dt = \frac{1}{c} * \frac{L}{D} * \frac{dW}{W}$$

Integrating between the initial and final weight of the aeroplane (considered in case a reserve of 8% in case of necessity remains and a deposition of 5% of the total fuel) we obtain the classical equation of the autonomy of Breguet, that is

$$t = \frac{1}{c} * \frac{L}{D} * \ln\left(\frac{W_1}{W_2}\right) = s = m$$

The maximum mileage is calculated through the temporal range through the cruising speed (supposed to be calculated at $M =$) as follows

$$dR = V_{cruise}\, dt = m = nm$$

Replacing the expression of speed, under the hypothesis of levelled flight

$$dR = \sqrt{\frac{2W}{\rho S C_L}}\, dt$$

And using Breguet formula

$$dR = \sqrt{\frac{2W}{\rho S C_L}} * \frac{1}{c} * \frac{L}{D} * \frac{dW}{W}$$

Since $\frac{L}{D} = \frac{C_L}{C_D}$

$$dR = \sqrt{\frac{2W}{\rho S C_L}} * \frac{1}{c} * \frac{C_L}{C_D} * \frac{dW}{W}$$

$$dR = -\sqrt{\frac{2}{\rho S}} * \frac{1}{c} * \frac{\sqrt{C_L}}{C_D} * \frac{dW}{\sqrt{W}}$$

Integrating between initial and final weight

$$R = \frac{2}{c} * \sqrt{\frac{2}{\rho S}} * \frac{\sqrt{C_L}}{C_D} * (\sqrt{W_1} - \sqrt{W_2})$$

$$W_2 = \left(\sqrt{W_1} - \frac{R}{\frac{2}{c} * \sqrt{\frac{2}{\rho S}} * \frac{\sqrt{C_L}}{C_D}}\right)^2$$

Or, more easily

$$M_{fuel} = M_{maximum\ take\ off} * \left(1 - e^{-c*\left(\frac{D}{L}\right)*\left(\frac{R}{V}\right)}\right) = kg$$

$$M_{fuel_{totale}} = M_{fuel} + 0.13 M_{fuel} = kg$$

In which an increase of the transported mass of fuel of 8% for eventual additional segments of cruise is considered (change destination, attended in the landing circuit) and a further increase of 5% considering the fuel unusable in the tank (pump draught, sedimentation).

From the previous formula you get that the maximum range is obtained when

$$\frac{\sqrt{C_L}}{C_D} = max$$

53

That happens when

- $C_{L_{max\ range}} = \sqrt{\dfrac{C_{D_0}}{3k}}$
- $C_{D_{max\ range}} = \dfrac{4}{3} C_{D_0}$

3.2.1.7. Climb up to 25000 m

This is a first segment climb, in order to reach a less dense atmosphere layer, and hence achieve a most cost-effective flight. The great amount of thrust provided by the engines allows even a linear acceleration during the ascend. This phase has no restriction in terms of rate of climb, but the previously mentioned limits for compliance with civil regulation must be respected.

3.2.1.8. Supersonic cruise

This flight phase is approximately at constant speed, and it is useful to accelerate the aircraft and gain speed. This phase end when the total speed of the airplane reached $M = 4$: when this condition is met, a sudden deactivation of ATR engine and the DMR engine ignition happens, in order to use each propulsor in the surrounding his design point. Actually, the shut off of ATR and activation of DMR are not sudden but follows a gradual procedure of switching on and off; in this analysis, since the exact activation procedure is still unknown, a sudden change of propulsive technique will be simulated.

3.2.1.9. Climb up to 35000 m

This is the final climb segment, that achieves the final flight altitude. As stated before, this phase has no restriction in terms of rate of climb, but the previously mentioned limits for compliance with civil regulation must be respected.

3.2.1.10. Hypersonic cruise

This phase is considered to happen at rather constant speed, which is the maximum velocity envisaged by the project ($M = 8$). Force balance on the aircraft shows substantial equilibrium, and the airplane proceeds at constant speed. It is possible to see a slight altitude rise, due to the fact that, while at constant speed and flight configuration (hence constant lift force), the aircraft weight decreases due to fuel consumption: "vertical" forces are no more at equilibrium. The phase continues until in proximity of the final destination airport; the distance from the take-off is estimated to be $17000\ km$, hence leaving $1650\ km$ for the final approach stage. In literature, this is supposed to be the last propelled phase, since the descent is supposed to happen gliding; hence, the fuel should end at the conclusion of this phase, since no more power plant activation is foreseen.

3.2.1.11. Descent

Literature review proposed a mission profile with a relatively steep descent trajectory. In order to comply with passenger's physiology and comfort, a first-attempt rate of climb of $3500\ ft/min$ is chosen [19], in similitude with A320 average descent profile. It is important to remember not to exceed a total acceleration (in the gravity centre) of $3\ ^m/_{s^2}$, for compliance with civil aircraft regulations.

3.2.1.12. Landing

The landing phase should be divided into sections so that the distance needed for each should be more accurately calculated; this subdivision is then scaled to take into account the uncertainty related to the weather conditions and the performance of the pilot. The breakdown is shown in the figure below
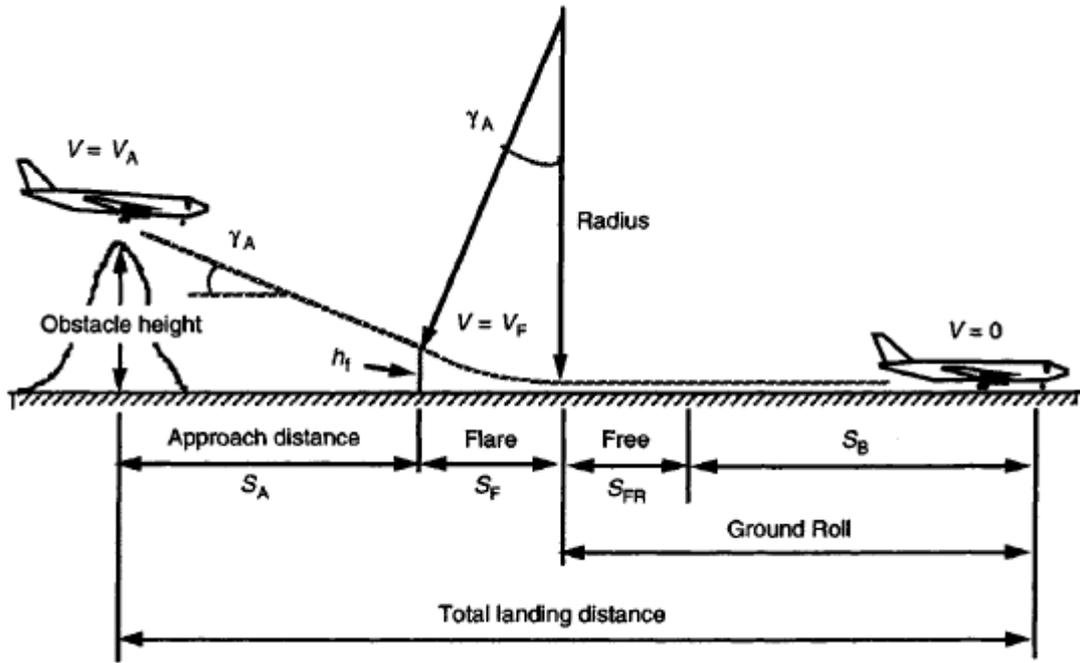
Figure 59: typical landing procedure [18]

3.2.1.12.1. Approach

In the case of passenger transport, this stage is covered with a descent angle of $\gamma_a = 3°$ (called "approach gradient").

This phase starts at the high obstacle 50 ft and ends at the flare height, calculated as

$$h_F = \frac{r * \gamma_A^2}{2}$$

The distance to the ground covered at this stage is

$$s_A = \frac{h_{obstacle} - h_F}{tan\gamma_A}$$

3.2.1.12.2. Flare

During this phase the aeroplane decelerates from the approach speed V_A up to touch-down speed, V_{TD}.

Tipicamente la velocità di touch-down è pari a

$$V_{TD} = 1.15 \, V_S = 1.15 \sqrt{\frac{MLW}{\frac{1}{2}\rho_{SL}SC_{L_{landing}}}}$$

Typically, the touch-down speed is equal to

$$V_F = \frac{V_A + V_{TD}}{2} = \frac{V_S(1.15 + 1.3)}{2}$$

The radius of manoeuvre is calculated by considering a load factor of $n = 1.2$

$$r = \frac{V_F^2}{g(n - 1)}$$

The distance to the ground covered at this stage is

55

$$s_F = r * \gamma_A$$

3.2.1.12.3. Ground roll

This phase takes place in contact with the track, but before the driver activates the brakes and spoilers; the distance covered is called '"free rolling distance", equal to

$$s_{FR} = t_{FR} * V_{TD}$$

3.2.1.12.4. Braking

The distance necessary to stop the aeroplane with the use of brakes is calculated by means of two coefficients:

- $K_A = \frac{\rho}{2\frac{W}{S}}\left(-C_{D_0} - kC_L^2 + \mu C_L\right)$

  A zero-lift coefficient is considered due to the full extension of the wings.

- $K_T = -\mu$

A value of the coefficient of friction relative to a wet paved track is considered; the coefficient takes this form as there is no thrust in this phase of mission.

The distance relative to this phase turns out therefore

$$s_B = \frac{1}{2gK_A}\ln\left(\frac{K_T + K_A V_{TD}^2}{K_T}\right)$$

3.2.1.12.5. Conclusion

The total horizontal distance required for the landing, starting from the obstacle of 50 ft, is

$$s_{LANDING} = s_A + s_F + s_{FR} + s_B$$

The norm previews however to consider a factor of safety of 1.66 in order to consider possible adverse environmental conditions and a potential not-optimal technical performance of the pilot.

Please note that the calculation of the total landing distance takes the following simplifications:

- The approach distance does not depend on the speed of the aeroplane but only on the angle of approach;
- The flare distance is function only of V 2 and normal acceleration;
- The ground roll distance is only a function of V 2 and the braking force available;
- All aeroplanes shall be subject to the same flare acceleration;
- The mass distribution between main trolley and bow trolley is similar;
- Spoilers have the same efficiency

3.2.2. Flight simulation

A Matlab simulation is run using the previous hypothesis and restriction. A few notes are necessary:

- The aircraft is approximated as a material point moving alongside its trajectory;
- Mission is simulated with a time step of $\Delta t = 1\ s$;
- Aerodynamic coefficients (lift and drag coefficients) are interpolated from the existing Aero-database as a function of flight speed, altitude and angle of attack;
- Propulsive physical quantities (namely net thrust, specific fuel consumption, specific impulse) are interpolated from the existing Propulsive database as a function of flight Mach number and altitude;
- Aerodynamic forces are evaluated using linear equations evaluated in the surrounding of an equilibrium point, considering small perturbations;
- Equilibrium equations of force and moments are evaluated with simple flight mechanics equations, to evaluate the consequent motion of the rigid body;
- Only the longitudinal motion (in the aircraft longitudinal plane, x-z) is considered in this analysis;
- Simulation input and restrains are completely independent from existing Astos simulation input and results (the differences between them will be evident).
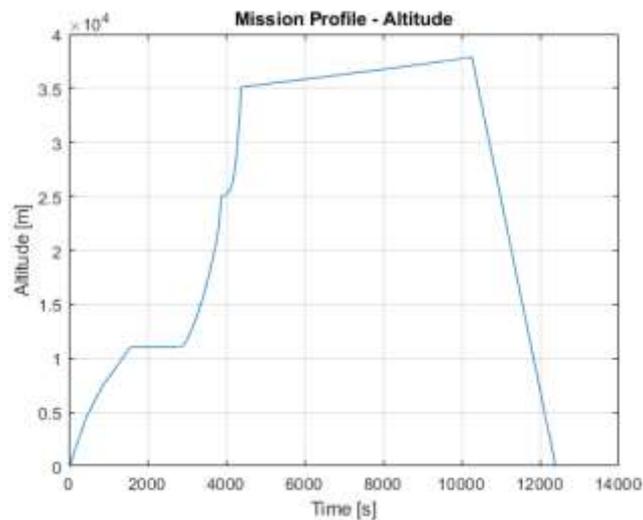

*Figure 60: mission profile, altitude vs time*
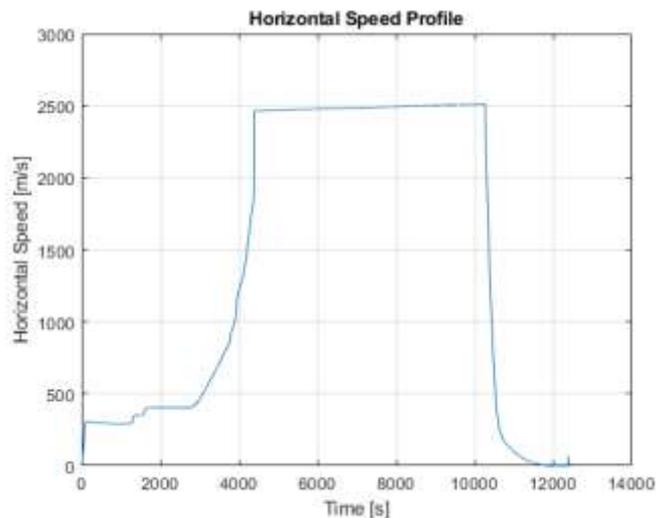

Figure 61: horizontal speed profile
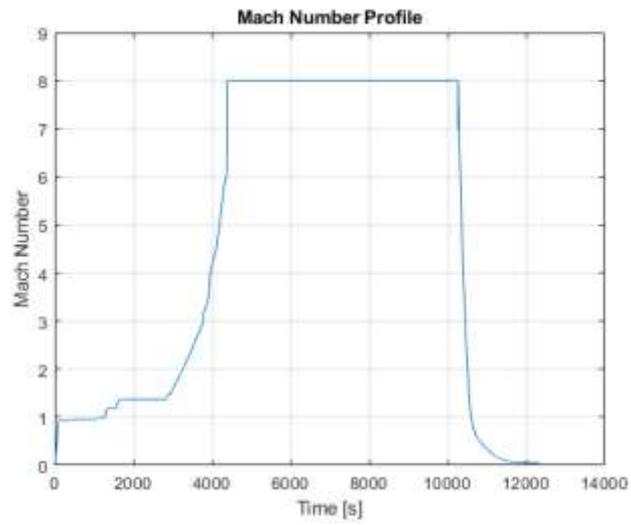
Figure 62: Mach number profile
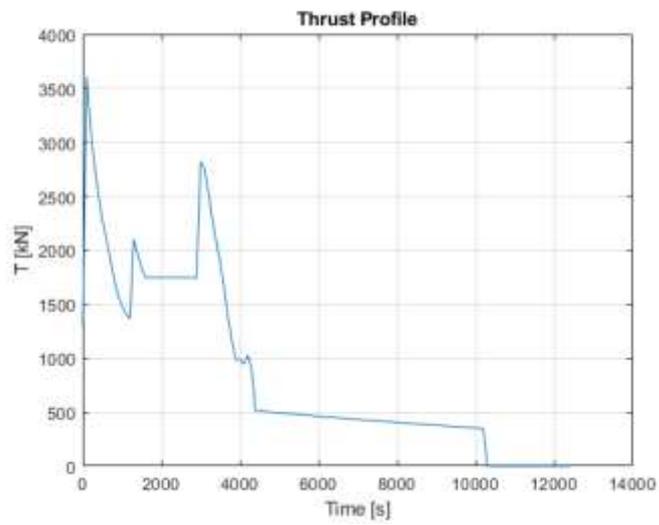

Figure 63: thrust profile
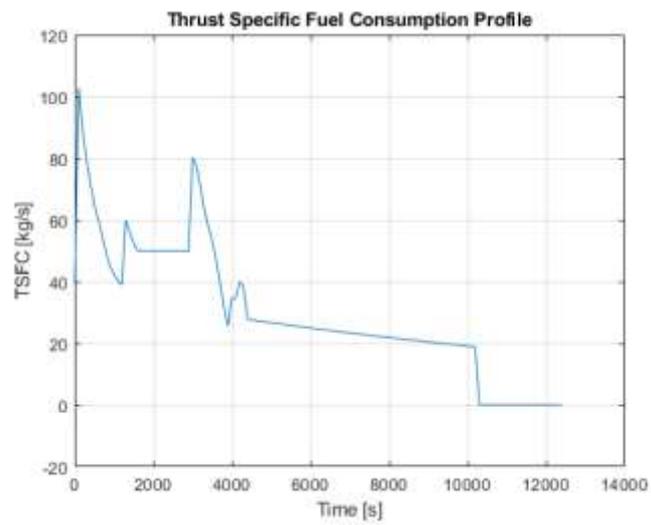
*Figure 64: thrust specific fuel consumption profile*
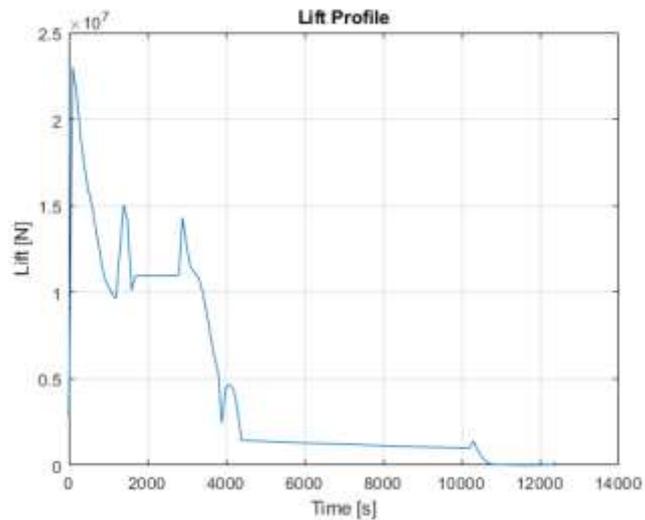
Figure 65: lift force profile
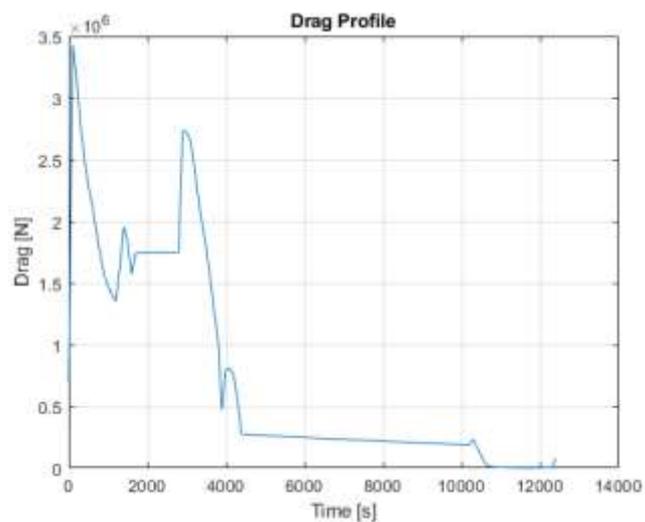
Figure 66: drag force profile

As a final comment about this simulation, it is possible to see that it is not compliant with literature mission profile: in the altitude vs time chart, it is possible to see that the proposed concept of operations provides a $4000\ s$ longer flight (this result, however, shows good matching with more advanced trajectory simulation techniques; for further data, see the next paragraph). Each physical quantity involved shows rapid oscillations, due to the unrefined discretisation of Propulsive and Aero Databases from which the data were interpolated. However, the results show a good approximation of the foreseen mission profile. This analysis was made for the further development of this thesis, in order to achieve a good flight path prediction in order to evaluate thermal loads on the aircraft. However, this study is still an approximation of reality, and since official data evaluated with dedicated software are available and recently updated, the latter will be used to grant more accuracy to the following thermal analysis.

3.3.   Trajectory optimisation

Within the framework of the Stratofly Academy, further research work has been carried out to accurately assess the evolution of mission and trajectory; such a study has been carried out using ASTOS software. It is a software for the optimization and simulation of trajectories for various missions, developed within the European space agency. This program, although specialized in the elaboration of orbital trajectories for rocket-propelled spacecraft, has been adapted to a mission in the lower stratosphere with airbreathing engines. The result of this work was primarily the optimization of the trajectory (with careful evaluation of overflight of inhabited areas), but also a study of the best concept of operation, in which any out-of-nominal scenarios have not been neglected). Some results are shown below
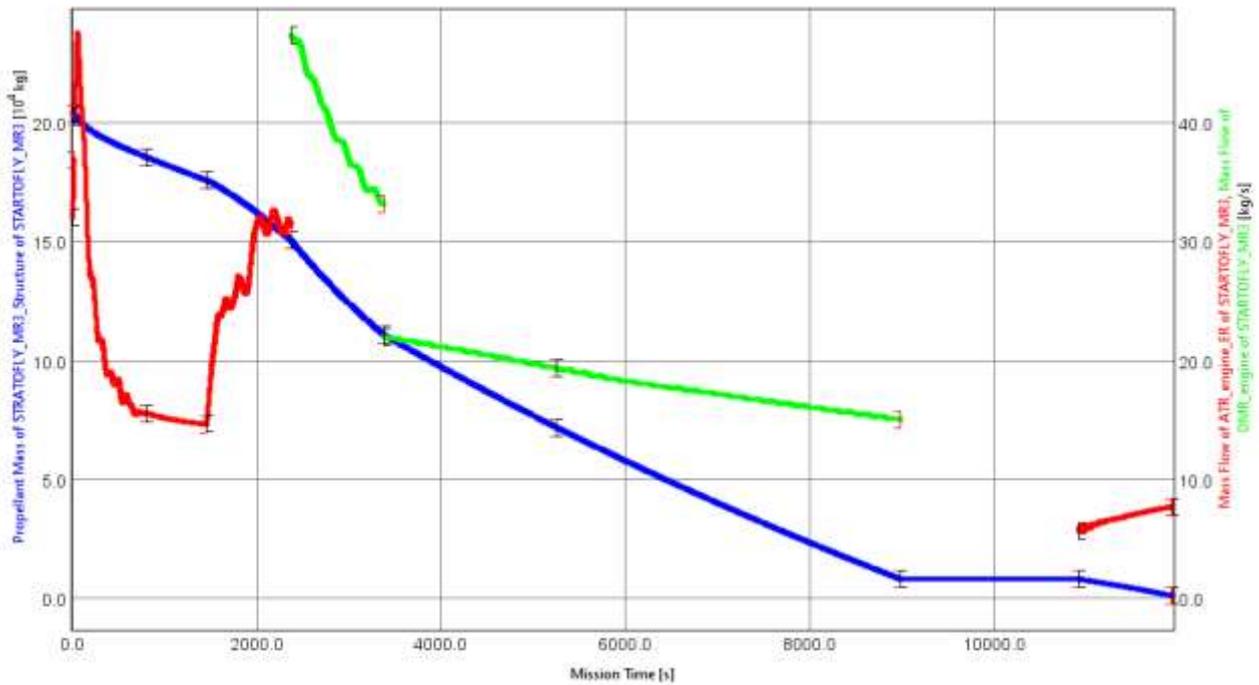
*Figure 67: propellant (blue line), air in the ATR (red line) and DMR (green line) mass flow rate as a function of mission time [20]*
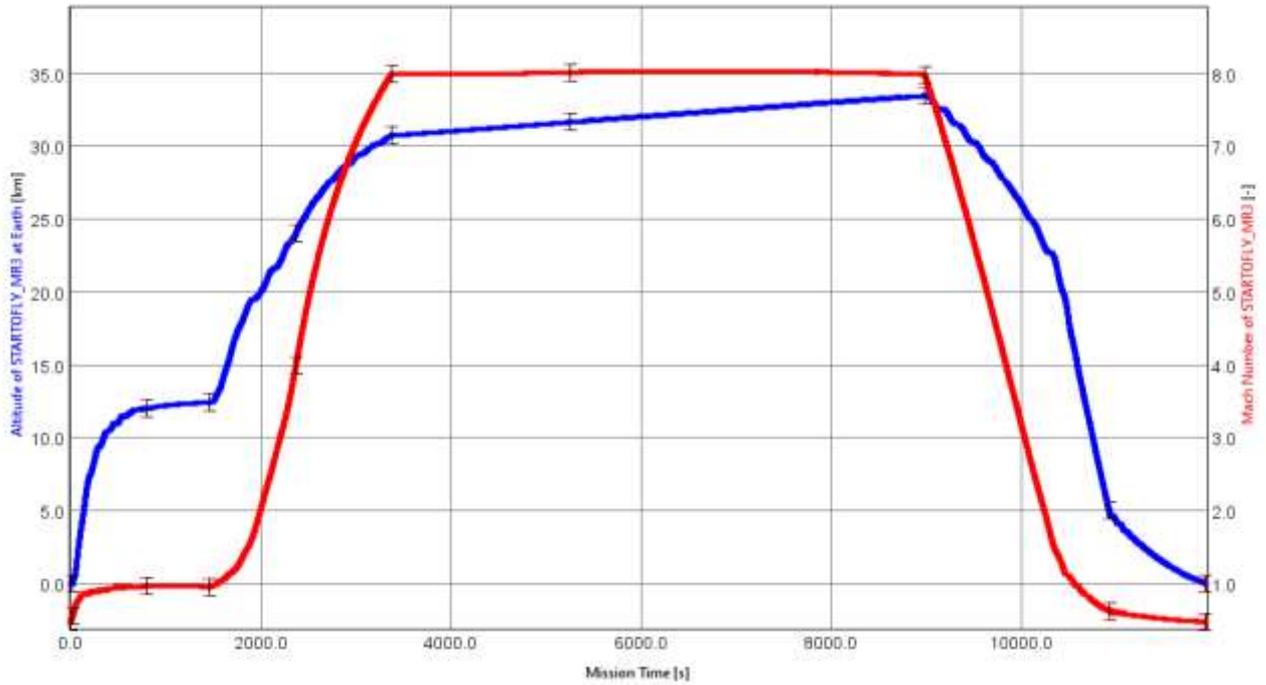
Figure 68: altitude profile (red line) and Mach number profile (blue line) as a function of flight time [20]
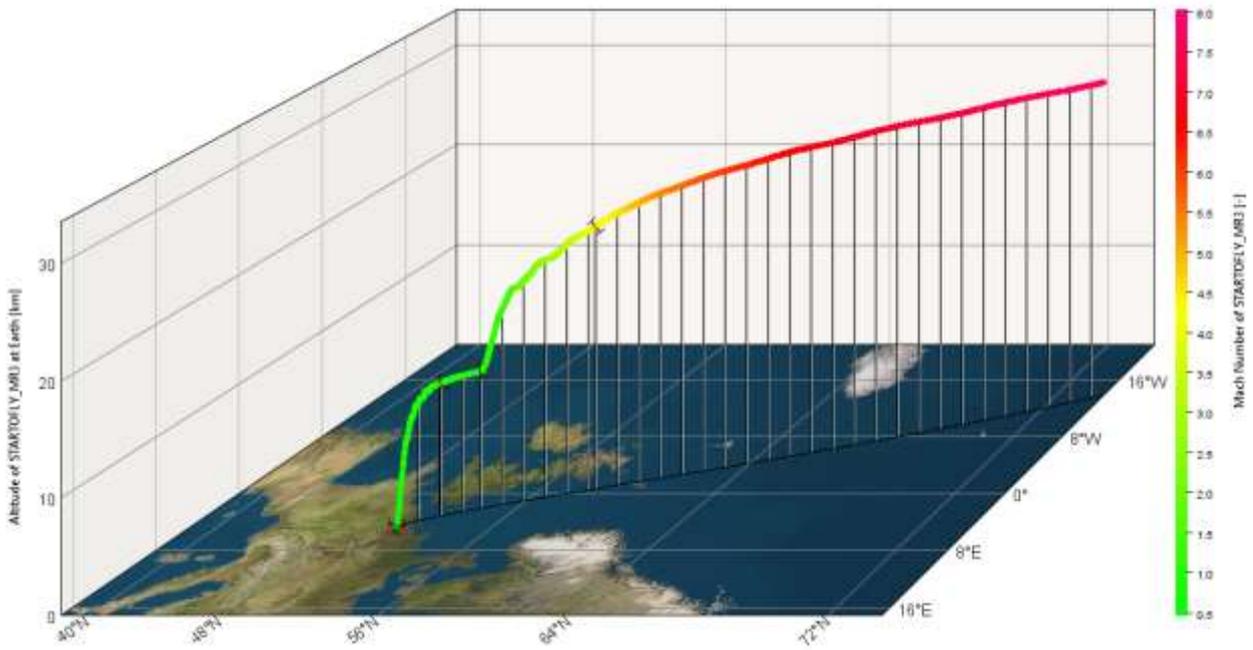

Figure 69: three-dimensional detail of altitude and speed profile on a map of northern Europe [20]
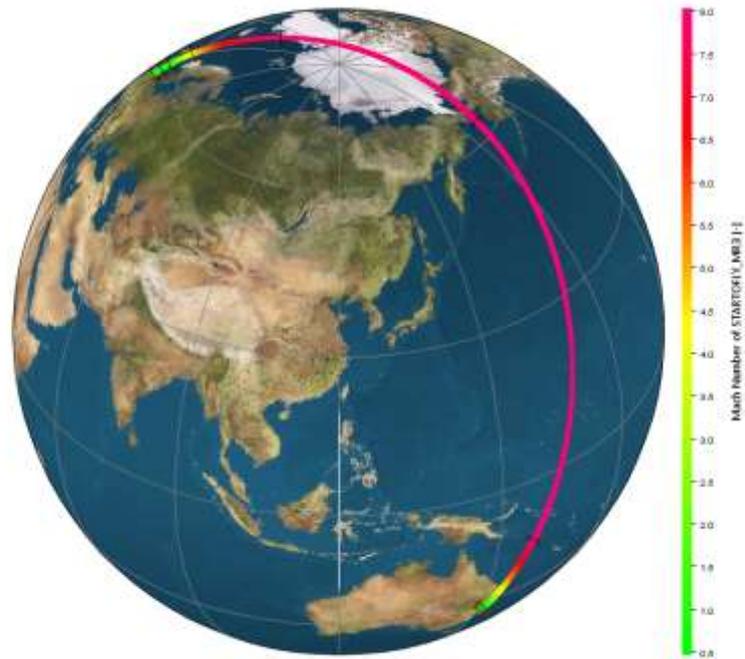
Figure 70: flight trajectory showed on a world map [20]

4. Hydrogen characterisation

4.1. Introduction

Hydrogen is the most abundant element in the observable universe, forms up to 75% of matter by mass and more than 90% by number of atoms. It's the main component of stars in the plasma state: 90% of the Sun is made of hydrogen. This element plays a vital role in providing energy to the universe: through nuclear fusion processes, huge amounts of energy are released in the form of electromagnetic radiation when the combination of two hydrogen nuclei into one of helium takes place.

When subjected to exceptionally high pressures, such as those at the centre of the gas giants (Jupiter for example), molecules lose their identity and hydrogen becomes a liquid metal (metallic hydrogen). On the contrary, under extremely low-pressure conditions, H_2 molecules may be dissociated and, if irradiated at an appropriate frequency, individual atoms may survive for sufficient time to be detected. Clouds of H_2 form and are associated with the birth of stars.

On Earth hydrogen is present in water, in most organic matter (which includes all known life forms), fossil fuels and natural gas. Hydrogen is very rare in the Earth's atmosphere (1 ppm) and practically non-existent as H_2 on the surface and underground, so it must be produced for its various uses. It is obtained in the laboratory by the reaction of acids with metals such as zinc and, industrially, by the electrolysis of water, the reforming of natural gas (from methane, which is a by-product of organic decomposition) and gasification of oil refinery residues. In particular, dihydrogen is used in the production of ammonia, in the hydrogenation of vegetable oils, in aeronautics (in the past as filling gas in airships, now as alternative fuel) and as a source of energy for fuel cells. [21]

4.2. Physical Properties

The most common isotope of hydrogen (also known as "Great Uncle") does not have neutrons, but there are two others: deuterium, with a neutron, and tritium (radioactive), with two. Those isotopes are stable, with the exception of tritium. Hydrogen is the only element given different names for some of its isotopes.

Hydrogen atoms naturally combine to pairs to form the dihydrogen, which has H_2 brute formula. Under normal conditions it is presented as a colourless, odourless and flammable gas in a wide concentration range. Alternative H_2 nomenclatures are: molecular hydrogen, diatomic hydrogen, diatomic hydrogen and dihydrogen.

Under normal conditions dihydrogen is a mixture of two different types of molecules, which differ depending on whether the spins of the two atomic nuclei are parallel or antiparallel. These two forms are respectively known as ortho-hydrogen and para-hydrogen. Under standard conditions, the ratio between ortho and para is about 3 to 1 and the conversion from one form to another is so slow that it does not take place in the absence of a catalyst. The two forms differ in terms of energy, which causes small differences in their physical properties. For example, the melting and boiling points of parahydrogen are about 0.1 K lower than ort-hydrogen. [22]

The existence of these two forms poses a drawback to the industrial production of liquid hydrogen: when it is liquefied, dihydrogen is generally a para-orto mixture of about 25:75; left alone, over a month the mixture is enriched with the para form, which becomes 90%; this free heat conversion which evaporates much of the dihydrogen, which is lost. To obviate this, the liquefaction of dihydrogen is conducted using a catalyst such as iron trioxide, activated carbon, platinized asbestos, rare earth metals, uranium compounds, chromium trioxide, or some nickel compounds to facilitate the transition to the para form.
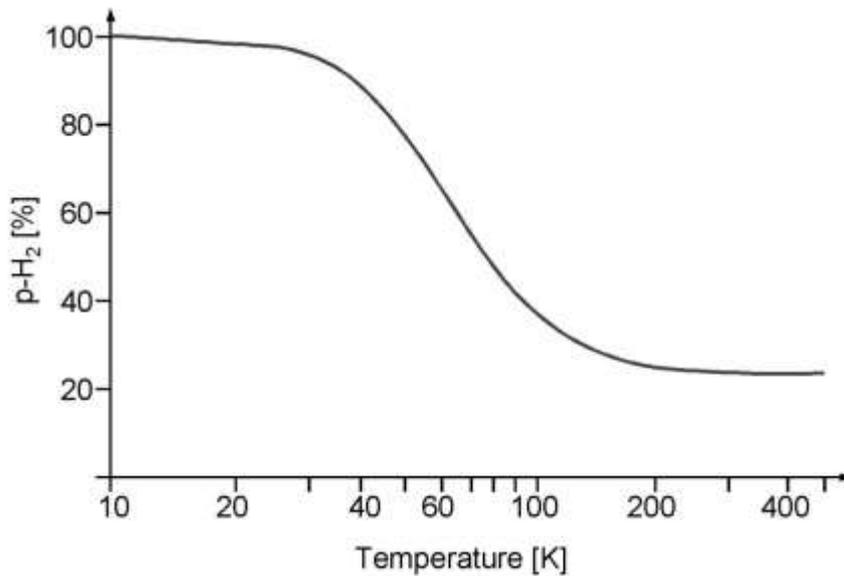
Figure 71: amount of para-hydrogen (p-H2) in the equilibrium composition, as a function of temperature [23]

Some physical and chemical properties are now listed.

	Temperature	Pressure	Latent heat of fusion	Density	Latent heat of vaporisation
	[K]	[Pa]	[kJ/kg]	[kg/dm^3]	[kJ/kg]
Triple point	13,95	7042,1	58,16	n/a	n/a
Critical point	33,24	1297,1	n/a	0,031	n/a
Boiling point	20,38	n/a	n/a	0,071	447,6

Figure 72: thermal properties of some important conditions

Thermal conduction	Specific heat at constant pressure	Specific heat at constant volume
[μW/cm/K]	[J/mol/K]	[J/mol/K]
1819,2	28,85	20,534
Calorific power		
[kJ/m^3]		
Lower	Upper	
10760	12770	

Figure 73: chemical properties of hydrogen (at 25° C)

4.3. Hydrogen: energy carrier

In general, the use of dihydrogen as fuel has several advantages: it burns air when its concentration is between 4 and 75% of its volume, the temperature of spontaneous combustion is relatively high ($858\,K$) and reacting with oxygen produces only water, avoiding harmful emissions. In fact, currently dihydrogen is used in some prototypes of cars as fuel for internal combustion engines, in fuel cells that allow electricity to be obtained without any thermal combustion process and in the aerospace field.

The main disadvantages of dihydrogen are:

- atomic and molecular hydrogen is very scarce in nature because it is combined with other elements in various compounds on the earth's crust, can be produced artificially only by using energy, so it is not a primary source of energy as natural gas, oil and coal are. Using current technologies,

dihydrogen has a production cost, in energy terms, much higher than its efficiency to obtain energy; its use is therefore more correctly definable as an energy carrier.

- energy density of liquid or gaseous dihydrogen (at usable pressure) is significantly lower than conventional fuels, and therefore requires larger tanks and to be compressed at higher pressures during storage. Liquid hydrogen has less energy density by volume than hydrocarbon fuels such as gasoline by approximately a factor of four. This highlights the density problem for pure hydrogen: there is Actually about 64% more hydrogen in a litre of gasoline ($116\ g\ H_2$) than there is in a litre of pure liquid hydrogen ($71\ g\ H_2$). The carbon in the gasoline also contributes to the energy of combustion.

4.4. Storage

For the practical purposes of the above it is necessary to liquefy dihydrogen for all uses of this mobile fuel.

Liquid hydrogen is in demand today in applications requiring high levels of purity, such as in the chip industry. As an energy carrier, LH_2 has a higher energy density than gaseous hydrogen, but it requires liquefaction at $20.268\ K$ (at atmospheric pressure), which involves a complex technical plant and an extra economic cost. When storing liquid hydrogen, the tanks and storage facilities have to be insulated in order to prevent boil off, that occurs if heat reaches the stored content, in terms of conduction, radiation or convection. Tanks for LH_2 are used today primarily in space travel.

For the needs of aerospace activities, NASA is setting up, with works begun at the end of 2018, at the Kennedy Space Centre in Florida an innovative system, IRaS.

Integrated refrigeration and storage, or IRaS, is a refrigeration system allowing control of the fluid inside the storage tanks. This approach provides direct removal of heat energy using an integrated heat exchanger together with a cryogenic refrigeration system. Studies of the new technology began with analysis, modelling and a series of laboratory research tests.

The new technology also is being coupled with new glass "bubble" insulation to replace perlite powder. Based on various field demonstration tests completed at Kennedy and NASA's Stennis Space Centre in Mississippi in 2015, with glass bubble insulation, liquid hydrogen losses through boil off can be Reduced by as much as 46 percent. If IRaS is employed, boil off can be eliminated altogether. This will be especially important for the new liquid hydrogen tank that will hold 1.25 million gallons. [24]
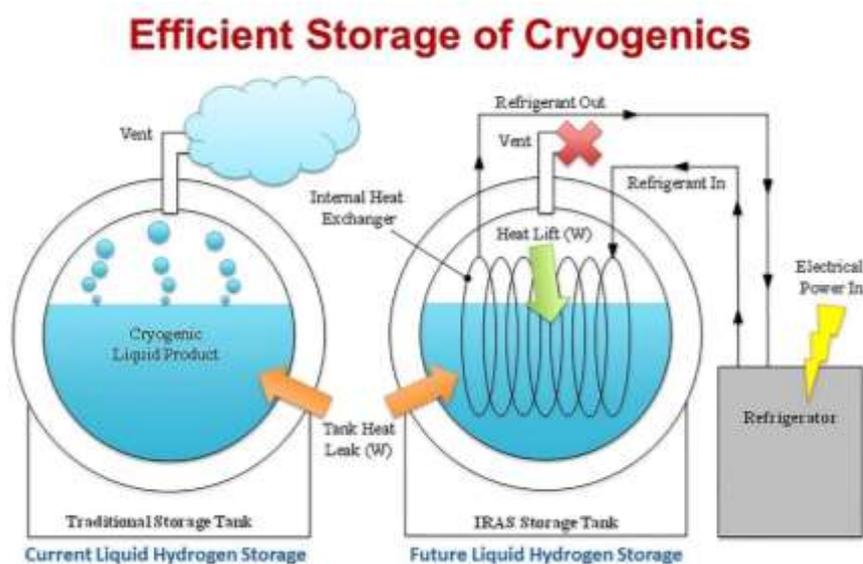

Figure 74: comparison between traditional hydrogen tank and IRaS configuration [25]

Comparatively speaking, it's like going from storing ice in a foam cup to keeping it in a freezer. While insulation in a foam cup will slow melting, it won't stop it and there is no control. Similarly, cryogenic liquids evaporated when stored in an insulated container, even one with the highest performance vacuum-jacketing. In a freezer with temperature control, ice can be stored indefinitely.

To support fuelling of NASA's SLS rocket, Kennedy's EGS Program soon will begin construction of the new liquid hydrogen storage tank at Pad 39B. The SLS rocket is designed to launch the agency's Orion spacecraft, sending humans to distant destinations, such as the Moon and Mars. The SLS core stage and in-space stage will require 730,000 gallons of liquid hydrogen and liquid oxygen to fuel the four-core stage and single upper stage engine.
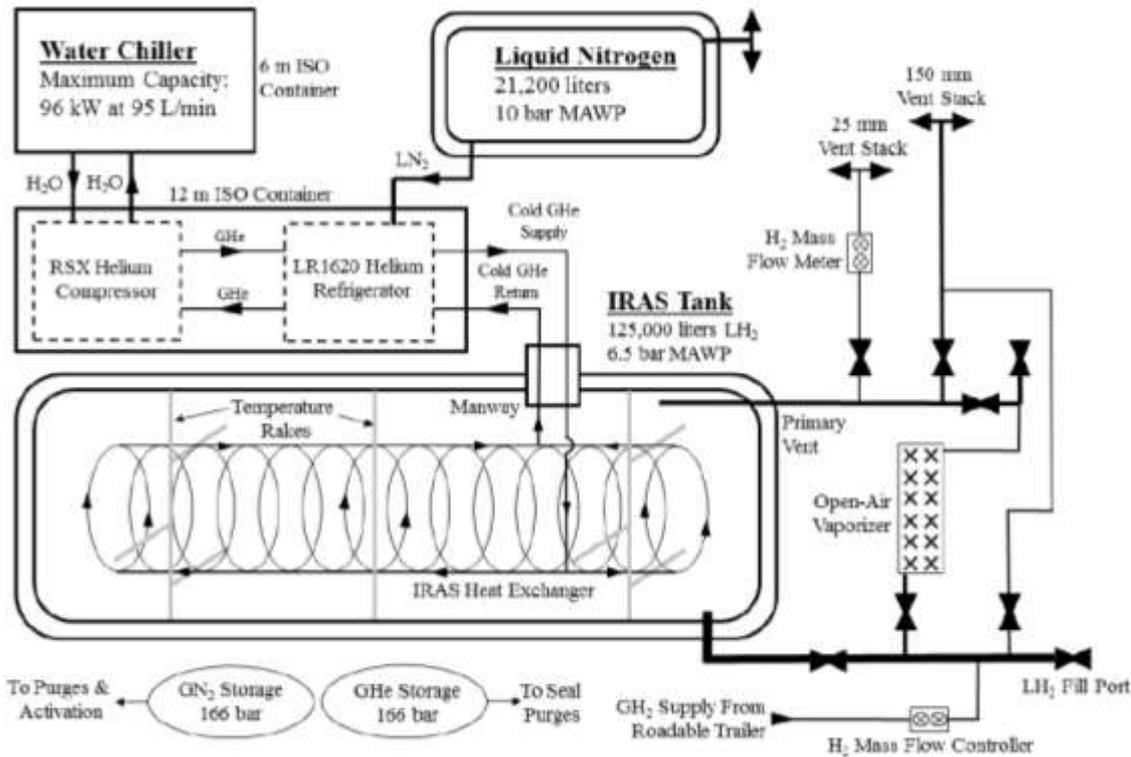

Figure 75: IRaS working scheme [24]

The larger tank will allow the attempt SLS launches on three consecutive days, while the past, it was necessary to stand down after two attempts so additional liquid hydrogen could be trucked in and loaded into the storage tank. [25]

The choice of spherical tanks is obviously aimed at optimizing the thermal insulation because this form allows to maximize the ratio between the available volume and the external surface, through which the heat exchange with the surrounding environment takes place. Various alternatives are being studied for storage on land, such as metallic hydride sponges, carbon nanostructures and crystal microspheres, all of which are being tested.

For in-flight transport, tanks made of materials that withstand a low temperature and an atmospheric pressure of an order of magnitude may be used. These tanks must primarily provide excellent thermal insulation, for example by making an inner chamber containing LH2 and an outer liner separated by an air chamber, In the most sophisticated solutions, there is also a cooling circuit to compensate at least partially for the heat absorbed by the external environment.

Because dihydrogen, both in liquid and gaseous form, makes metals fragile, because it fixes on metal atoms within the interstitial spaces of the molecular lattice, shells shall be constructed with an excess of thickness. Because of its very low atomic weight, dihydrogen is able to spread through virtually every coating material used for its containment, climbing into the inside of the container wall and going through it to get out. In any case, therefore, tanks should be periodically checked for potential damage caused by hydrogen leakage.

4.5.   Boil-off phenomenon

In storage tanks, part of the dihydrogen liquid is lost by evaporation due to the heat absorbed by the external environment and the transition between the two para and ortho-hydrogen forms; both of these phenomena contribute to boil-down off.

To counteract the phenomenon of evaporation of LH_2 in static storage sites, large spherical reservoirs are constructed to minimize the relationship between external walls and volume, an outer sleeve is created to form an air chamber with a rarefied atmosphere and the absorption of the energy of the solar rays is avoided as much as possible by using particular coatings of the surfaces exposed to the radiation. In the tanks used in mobility these advanced devices are not all realistically implementable, therefore maintenance of the temperature for the stored dihydrogen that remains liquid is ensured by the heat dissipation for unavoidable boil-off.

In addition to this, the transition from the ortho form to the para form occurs spontaneously at the temperature of the liquid dihydrogen. There is a slow but definite change in the mixture chemical composition even in absence of external heat flow, which complicates the problem of keeping the liquid for any great length of time. The exothermic heat of conversion of ortho to parahydrogen at $20\,K$ is about $254\ ^{cal}/_{mol}$, whereas the endothermic heat of vaporization of liquid hydrogen is $216\ ^{cal}/_{mol}$.

In summary, since conversion from ortho to parahydrogen is accompanied by energy release ($703\ ^{J}/_{g}$ at $20\,K$), this phenomenon should be minimised and, as mentioned above, catalysts are used in the process of condensation of dihydrogen in order to convert as much as possible to the para form. It should however be considered that under standard conditions the ortho form is present at 75%, while at 20 K the equilibrium condition corresponds to 99.8% of the para form. Therefore, although the technology is well developed, the presence of the ortho form in LH2 is higher than the percentage of 0,2 % equilibrium and the exothermic process of conversion, generating an intrinsic heat input, to be always compensated with boil-off.

The total amount of dihydrogen subject to the boil-off depends strictly on the storage conditions, can be estimated only after designing the reservoir and known the conditions to the contour. However, based on usage experience in recent years, it can be estimated that it is 1% per day for standstill spherical tanks on land. The boil off, in addition to generating a cost for the energy wasted, also constitutes a risk for the safety; before the release into the air, the evaporated dihydrogen is usually passed through a catalyst which converts it into water vapor.

4.5.1.   Optimal tank configuration

In this study case, it is not possible to use any of the previously mentioned ground infrastructure, since a flying tank could not afford the weight of a dedicated cooling system. The analysis of tank designer is hence focused on the development of an economical, lightweight, safe, efficient, reliable and reusable insulation system for the tank walls, in order to minimise the boil-off phenomenon during the flight. One of the most recent configurations suggests the use of a nitrogen purged, layered insulation system with nonpermeable closed-cell insulation surrounding it [26]. This solution requires minimum flight preparation, but also guarantees structural integrity and reusability.

The thermal protection systems now described consists (from the external layer to the fuel itself) in

- Outer heat shield: it should be able to withstand high wall temperatures, and have a small ρK product (average density times average thermal conductivity) in order to better insulate the inner layers from the outer environment
- Inert purge gas: nitrogen has been chosen, due to its low freezing point (77 K), which reduces the thickness of the frost layer; it is also readily available and relatively cheap
- Two layers of insulation: they should effective as thermal insulators, but also contain the cryodeposit of the inert gas on the tank wall
- Hydrogen tank wall.

The following picture shows a scheme of a portion of the overall predicted thermal protection system
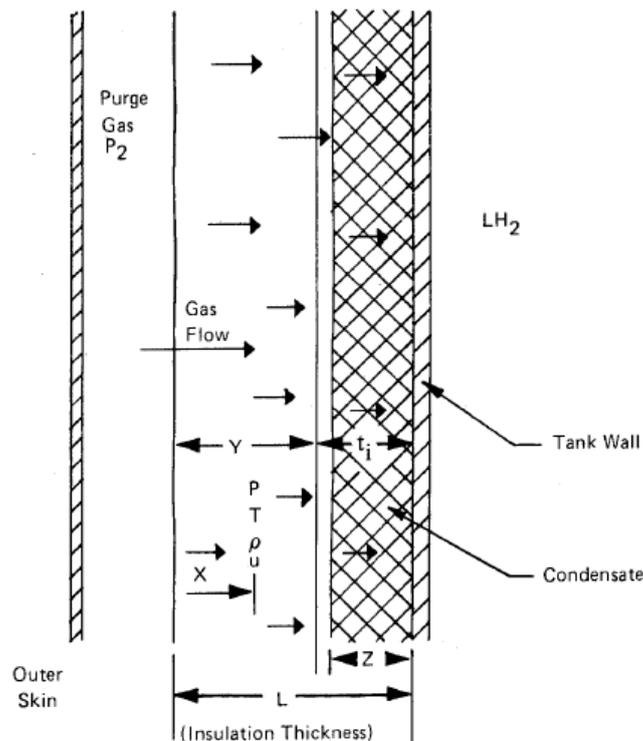
Figure 76: thermal protection system with purged gas, scheme [26]

In this section, a one-dimensional model is assessed to show the heat exchange mechanism in a real insulation system. One of the major problems affecting this configuration is the cryodeposited frost on the outer side of the tank wall, which heavily modifies the heat transfer profile throughout the layers. However, this frost layer absorbs a large amount of the incoming heat, preventing it to affect the liquid hydrogen inside the tank, and hence reducing the amount of boiled-off fuel.

For the further analysis, two conditions will be envisaged:

- Wet tank: the liquid hydrogen is in direct contact with the tank wall, hence its temperature will start rising, and eventually boil-off happens;
- Dry tank: only hydrogen gas is in contact with the tank wall. An adiabatic condition essentially exists, and the incoming heat flow will just increase tank wall temperature.

For the wet condition, incoming heat start melting the deposited frost; when this layer vaporisation chases, the equilibrium temperature is reached. The heat balance at the frost layer states that

$$k_f \cdot \frac{T_f - T_c}{z_1} = k_i \cdot \frac{T_s - T_f}{l - z_1}$$

In which

- k_f is the thermal conductivity of frost
- k_i is the thermal conductivity of inner insulation
- T_f is the condensation temperature of frost
- T_c is the cryogenic fuel storage temperature
- T_s is the outer surface temperature
- z_1 is the flight equilibrium frost thickness (obtained from ground equilibrium equations)
- l is the thickness of the thermal protection system

Hence

$$z_1 = \frac{l}{\left(\frac{T_s - T_f}{T_f - T_c}\right) \cdot \left(\frac{k_i}{k_f}\right) + 1}$$

If the rate of frost evaporation is constant, the purge gas flow rate can be expressed as

$$\dot{w} = \frac{v \cdot \rho_f \cdot (z_0 - z_1)}{t_1}$$

In which

- $\dot{w}$ is the purge gas flow rate
- ρ_f is the frost density
- z_0 is the initial frost thickness
- t_1 is the time to reach equilibrium condition (for a wet tank)

The heat flow to the frost line is evaluated with the following approximated formula

$$Q = \frac{v \cdot \rho_f \cdot c_p \cdot (z_0 - z_1) \cdot (T_s - T_f)}{1 - e^{\frac{v \cdot \rho_f \cdot c_p \cdot (z_0 - z_1) \cdot (l - 0.5 \cdot (z_0 + z_1))}{k_i t_1}}}$$

In which

- Q is the heat flow
- c_p is the specific heat at constant pressure of the purge gas

The previous equation states that frost thickness is the key parameter to estimate heat flow through the frost layer. Hence, it is possible to write a time-dependant heat equilibrium equation

$$Q = \frac{k_f \cdot (T_f - T_c) \cdot t_1}{0.5 \cdot (z_0 + z_1)} + v \cdot (z_0 - z_1) \cdot \rho_f \cdot \left(h_{fg}\right)_g$$

In which $\left(h_{fg}\right)_g$ is the combined heat of fusion and evaporation of purge gas.

This equation allows the determination of t_1. There is then a double possibility:

1. $flight\ time > t_1$
   The mean frost thickness is given by

$$z_m = 0.5 \cdot \left(\frac{t_1}{t_t}\right) \cdot z_0 + z_1 \cdot \left[1 - 0.5 \cdot \left(\frac{t_1}{t_t}\right)\right]$$

2. $flight\ time < t_1$
   The mean frost thickness is given by

$$z_m = 0.5 \cdot \left(\frac{t_t}{t_1}\right) \cdot z_1 + z_0 \cdot \left[1 - 0.5 \cdot \left(\frac{t_t}{t_1}\right)\right]$$

Using the right value of mean frost thickness, the resulting frost weight is

$$W_f = \rho_f \cdot z_m$$

Boil-off weight of hydrogen is

$$W_B = \frac{k_f \cdot (T_f - T_c) \cdot t_t}{z_m \cdot \left(h_{fg}\right)_{H_2}}$$

In which t_t is the total flight time.

For the dry condition, the incoming heat is absorbed by the thermal protection system (which makes its average temperature rise) and by the frost layer. First, the time to evaporate all the frost is evaluated, under the hypothesis that, at that time, tank wall will be at the frost vaporisation temperature. Assuming that the frost boil-off and heat flow to the frost vary linearly during the time interval t_2, the cumulative heat input to the frost can be estimated by utilizing the heat flux at time $\frac{t_2}{2}$, given by

$$Q = \frac{v \cdot \rho_f \cdot c_p \cdot \frac{z_0}{t_2} \cdot (T_s - T_f)}{1 - e^{\frac{v \cdot \rho_f \cdot c_p \cdot z_0 \cdot \left(l - \frac{z_0}{2}\right)}{k_i t_2}}}$$

Equating the total heat input during time t_2 to the increase in internal energy of the insulation system plus the heat vaporisation of the complete frost thickness, the following equation is obtained

$$t_2 = \frac{v \cdot \rho_f \cdot c_p \cdot z_0 \cdot \left(l - \frac{z_0}{2}\right)}{k_i \cdot \ln\left[\frac{1 + v \cdot \rho_f \cdot c_p \cdot z_0 \cdot (T_s - T_f)}{v \cdot \rho_f \cdot c_p \cdot z_0 \cdot \frac{T_f - T_c}{2} + \rho_w \cdot c_{pw} \cdot t_w \cdot (T_f - T_c) + v \cdot \rho_f \cdot h_{fg} \cdot z_0}\right] - e^{\frac{v \cdot \rho_f \cdot c_p \cdot z_0 \cdot \left(l - \frac{z_0}{2}\right)}{k_i t_2}}}$$

In which

- ρ_w is the tank wall density
- c_{p_w} is the specific heat at constant pressure of tank wall
- t_w is the tank wall thickness

This equation allows the determination of t_2. There is then a double possibility:

1. $flight\ time > t_2$
   The average frost thickness is given by

$$z_m = 0.5 \cdot \left(\frac{t_2}{t_t}\right) \cdot z_0$$

2. $flight\ time < t_2$
   The average frost thickness is given by

$$z_m = z_0 \cdot \left[1 - 0.5 \cdot \left(\frac{t_t}{t_2}\right)\right]$$

In the case of dry tank, its wall temperature risks to exceed thermal and structural limits during the flight; hence, an estimation of dry tank temperature is necessary. Assuming that the heat flow to the tank wall varies linearly with time, tank wall temperature can be obtained by the iterative resolution of the following non-linear equation

$$\left[\frac{\rho_0 \cdot c_{p_0} \cdot y^2}{2 \cdot l} + \frac{\rho_i \cdot c_{p_i} \left[y + \frac{t_i}{2} \right]}{l} + \rho_w \cdot c_{p_w} \cdot \theta \right] \cdot \left(T_w - T_f \right) = \frac{U_0 \cdot (t_t - t_2)}{l} \cdot [T_s - 0.5 \cdot (T_w - T_f)]$$

This equation is nonlinear since the overall conductance is dependent on each of the insulation thermal conductivity values, which are related to the mean temperature level of the insulation which, in turn, are dependent on the wall temperature. If wall temperature exceeds thermal limits, an additional wall thickness should be provided for better insulation, with a weight rise of the TPS system.

In conclusion, when even the frost layer thickness is known, the geometrical definition of the system is complete; it is then possible to evaluate actual heat flow from the outer environment to the liquid hydrogen through the insulation. This method is shown in the fifth chapter of this thesis, and it consists in a heat balance involving a "heat resistance", obtained as the sum of a series of local heat resistances of the single layer, which are a function of its thickness and thermal insulating properties. In general, the problem is then considered as a heat flow analysis on a solid plate with the opposite surfaces at constant temperature

$$Q = m \cdot c \cdot \Delta T$$

4.6.   Physical properties

Liquid and gaseous hydrogen physical properties are now plotted as a function of both storing pressure and temperature. These features are considered in a wide array of operating conditions, namely

$$p = [0.01, 0.08, 0.101325, 0.25, 0.5, 0.75, 1, 3, 7, 14, 24, 40, 65, 100] \, MPa$$

$$13.8 \, K \leq T \leq 3000 \, K$$

In these graphs the transition between gaseous and liquid phase is particularly evident. [27]
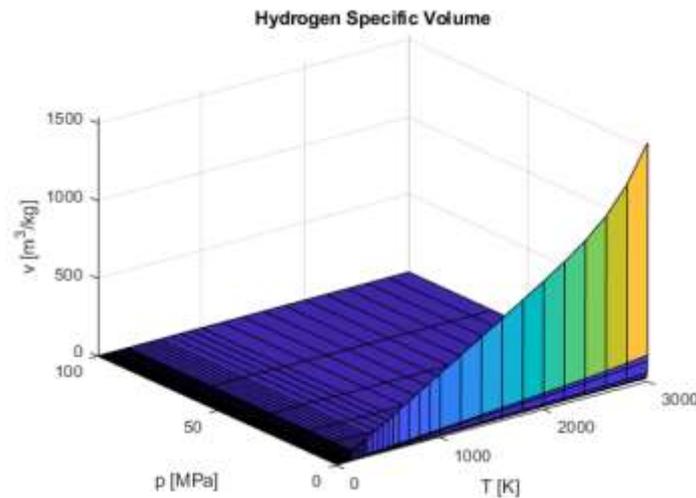

Figure 77: hydrogen specific volume chart
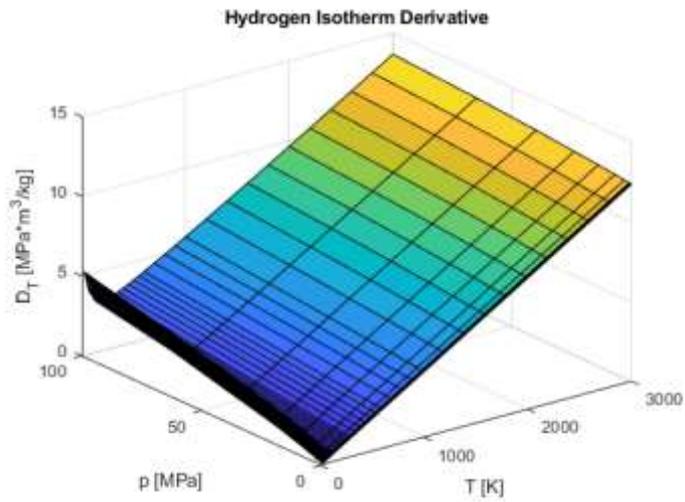
*Figure 78: hydrogen isotherm derivative chart*
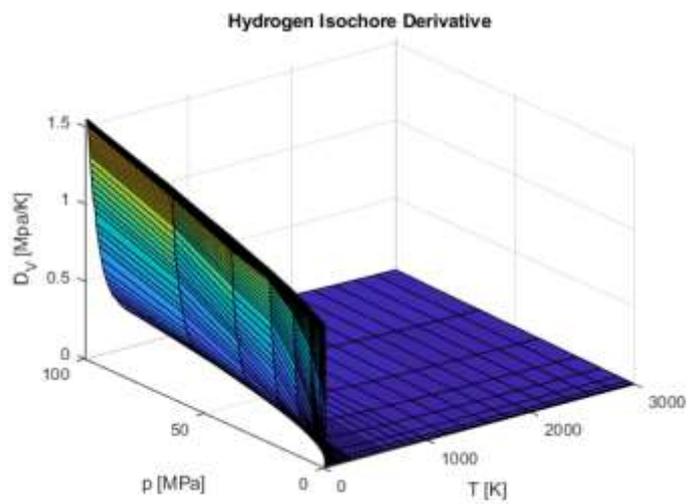
*Figure 79: hydrogen isochore derivative chart*
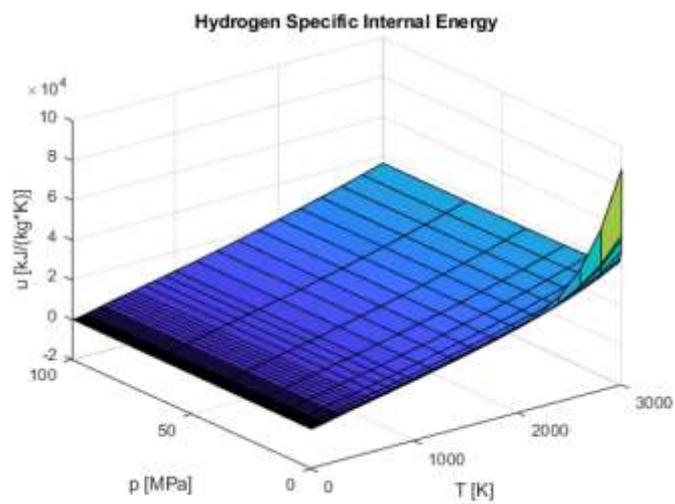
*Figure 80: hydrogen specific internal energy chart*
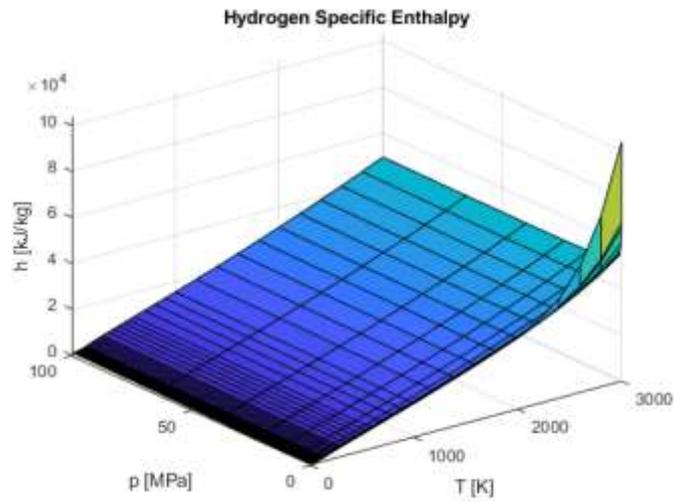
*Figure 81: hydrogen specific enthalpy chart*
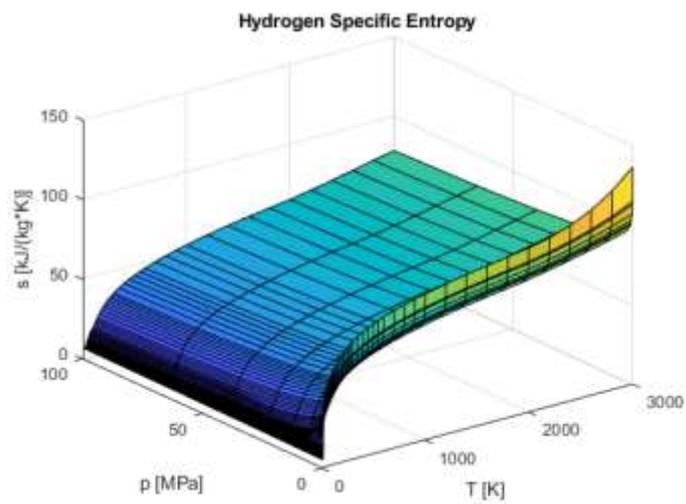
*Figure 82: hydrogen specific entropy chart*
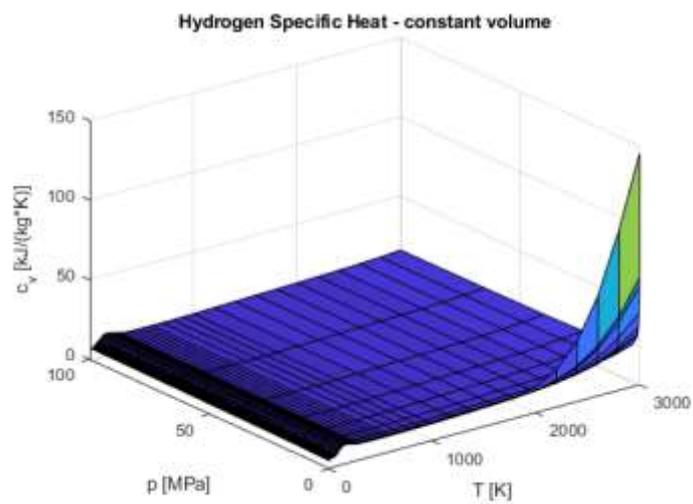
Figure 83: hydrogen specific heat at constant volume chart
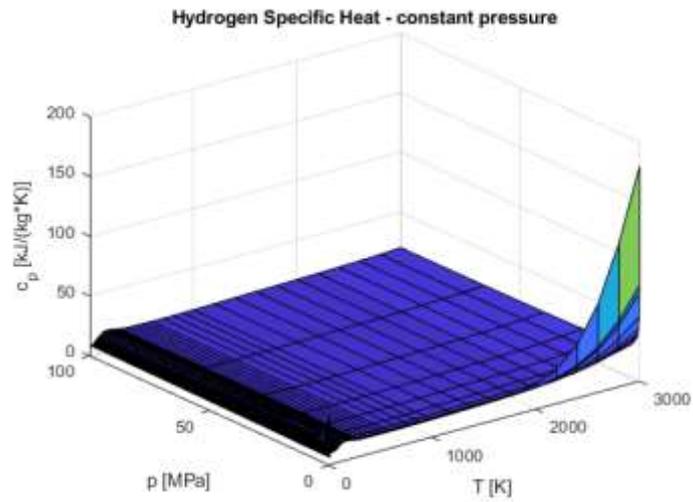
Figure 84: hydrogen specific heat at constant pressure chart
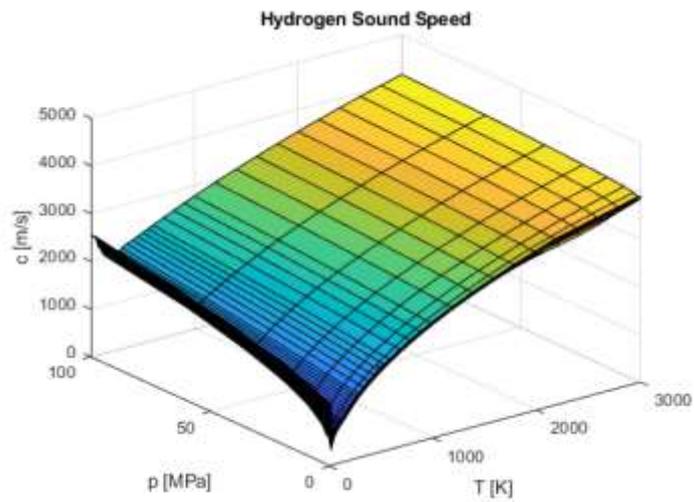
Figure 85: hydrogen sound speed chart
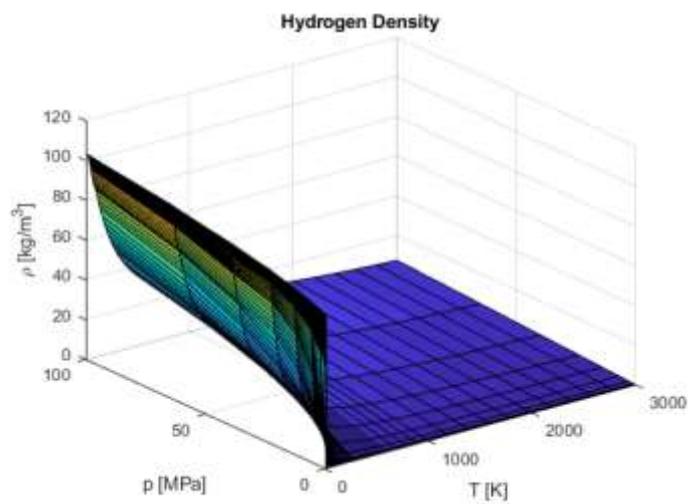
Figure 86: hydrogen density chart

Hydrogen Specific Heat Input
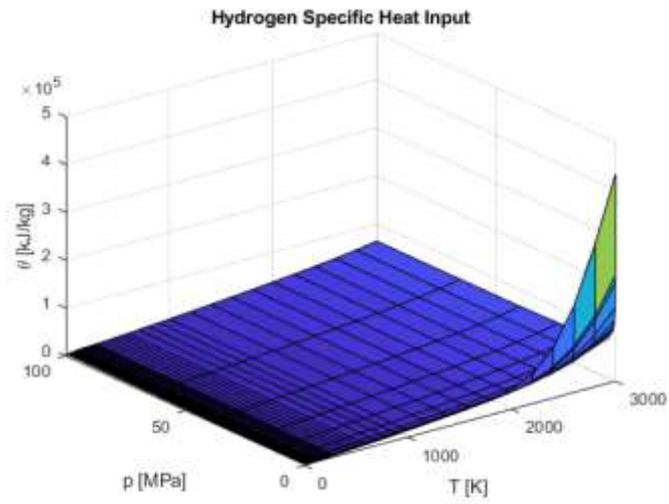
Figure 87: hydrogen specific heat input chart

Hydrogen Energy Derivative
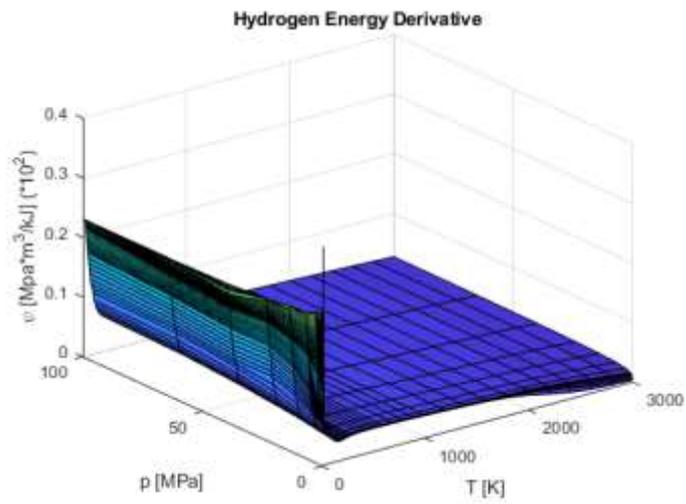
Figure 88: hydrogen energy derivative chart

Hydrogen Isothermal Bulk Modulus
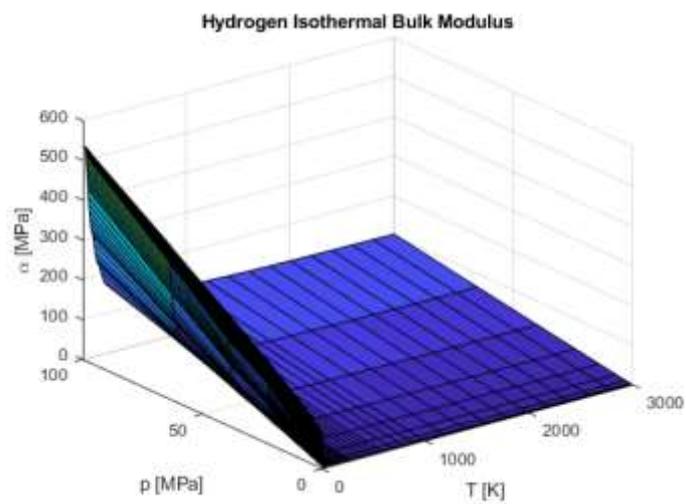
Figure 89: hydrogen isotherm bulk modulus chart
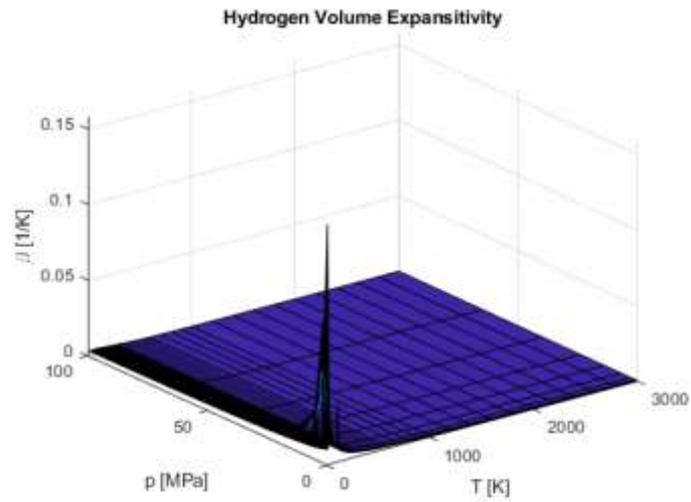
Figure 90: hydrogen volume expansitivity chart
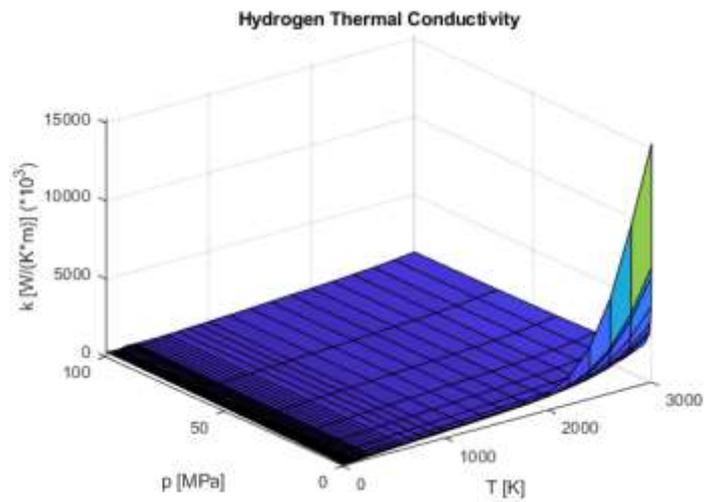
Figure 91: hydrogen thermal conductivity chart
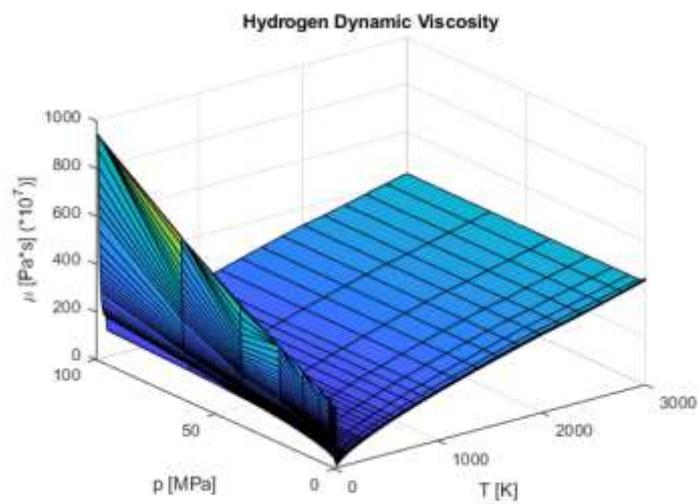
Figure 92: hydrogen dynamic viscosity chart
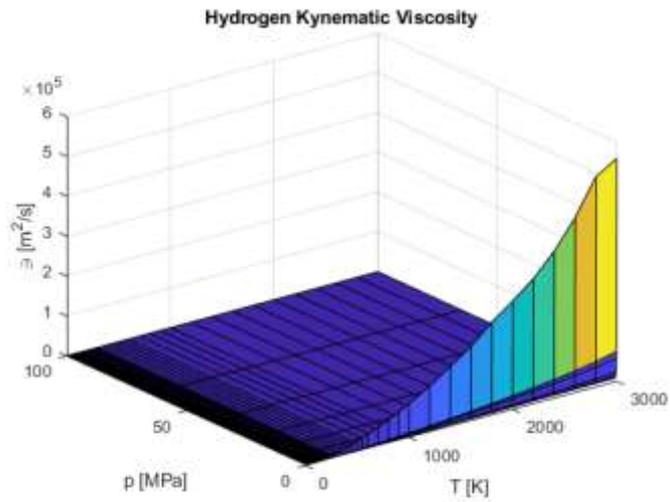
Figure 93: hydrogen kinematic viscosity chart
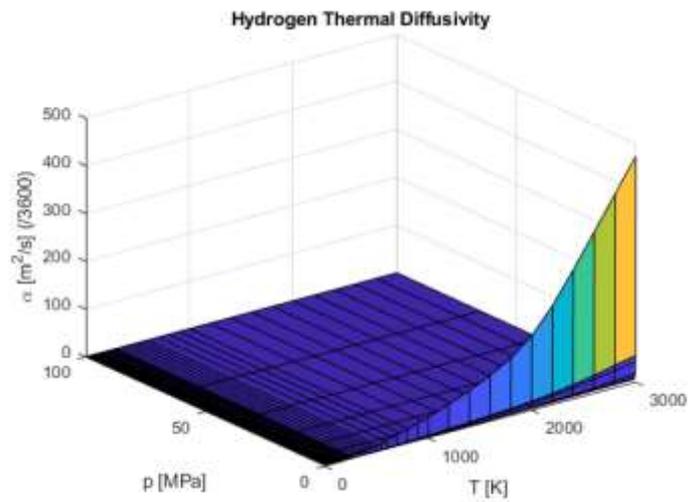
Figure 94: hydrogen thermal diffusivity chart
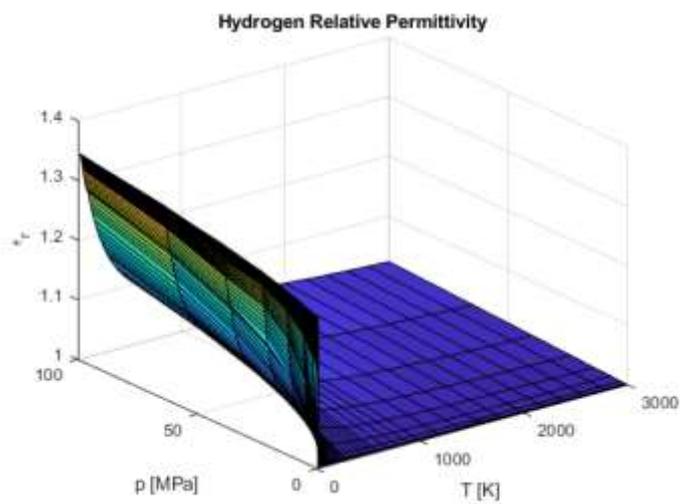
Figure 95: hydrogen relative permittivity chart
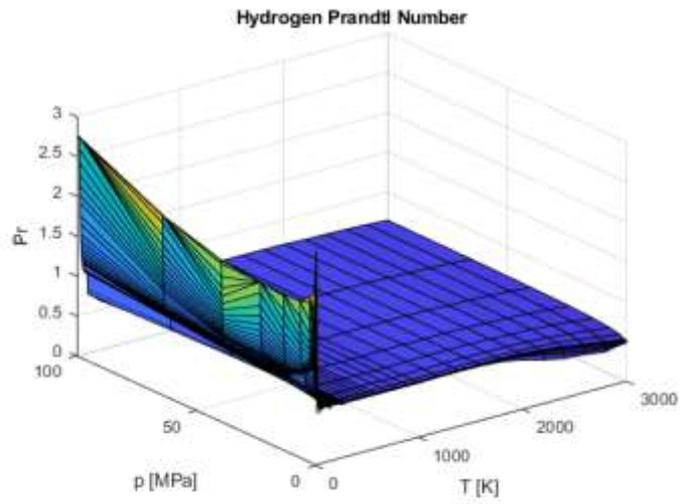
Figure 96: hydrogen Prandtl number chart

5. TEMS: introduction and static sizing

5.1. Introduction

As showed earlier in previous chapters about the Mission Profile and Performances, the vehicle considered spends most of the operational flight time performing a hypersonic cruise. This feature, that gives our project his uniqueness, is also one of the main problem designers must deal with: although the cruise flight altitude is included in the stratosphere (in which temperatures falls under 240 K and air density is almost negligible) the skin friction due to the high speed and the solar radiation transmit a very large amount of heat to the aircraft. In addition to this, the engines produce a huge amount of heat to drain because the DMR needs high temperatures to work well; another problem is that this source is placed almost inside the aircraft, transmitting heat to the main structure directly by conduction.

Designers must face these problems in order to avoid materials to lose their mechanical properties (or melt, in some highly-stressed areas of the fuselage) and allow the mission to be performed without problems inside the aircraft, both for equipments (that represent another large heat source to deal with) and for the occupants of the aircraft. The first part of this analysis needs to find the best cruise trajectory in order to minimize flight time and optimize skin and shape drag; this step is necessary and has been made for the best in the dedicated chapter, but unluckily is not enough to resolve the issue.

These problems will be treated drawing inspiration from spacecrafts, whose re-entry phase is always critical by the point of view of the thermal control and management. On the hypersonic vehicle a passive thermal protection system like the Shuttle's, an active thermal control system and a special environment control and life support system will be implemented.

In this section a new concept of TPS will be analysed, in order to better manage the energy produced onboard and minimize fuel losses; in addition to this, it is possible to take advantage on this system to generate onboard power usable by other equipments.

5.1.1. A new concept of TCS

The thermal protection system has by now be seen as a mandatory subsystem to guarantee the survival and good operative condition to the aircraft and the occupants, at the price of high energy request and very intrusive structures.

New trends aim to find a thermodynamic cycle able to cool both the airframe and the onboard equipment, as well to provide onboard power source throughout the flight within the same hardware. The risk of this concept is to make a heavy and large system, hard to integrate within the aircraft. Another difficult to deal with is the integration of this system within the aircraft, in order to provide all needed cooling for passenger cabin in a narrow range of comfort but also for onboard equipment while facing high heat fluxes on almost the whole external surface of the fuselage, as well as inside the propulsion system: the system need to be extremely pervasive to fulfil his purpose effectively.

In the main part of the flight, consisting in hypersonic cruise, the DMR is unable to provide the suitable amount of mechanical and electrical energy to feed all the energy consumers on board, whose peak request can be in the order of tens of megawatts. These requirements are going to be satisfied with an innovative concept of thermal protection system involving the fuel (liquid hydrogen), despite his low thermal capacity.

5.1.2. Current configuration

The solution implemented is shown in the following scheme
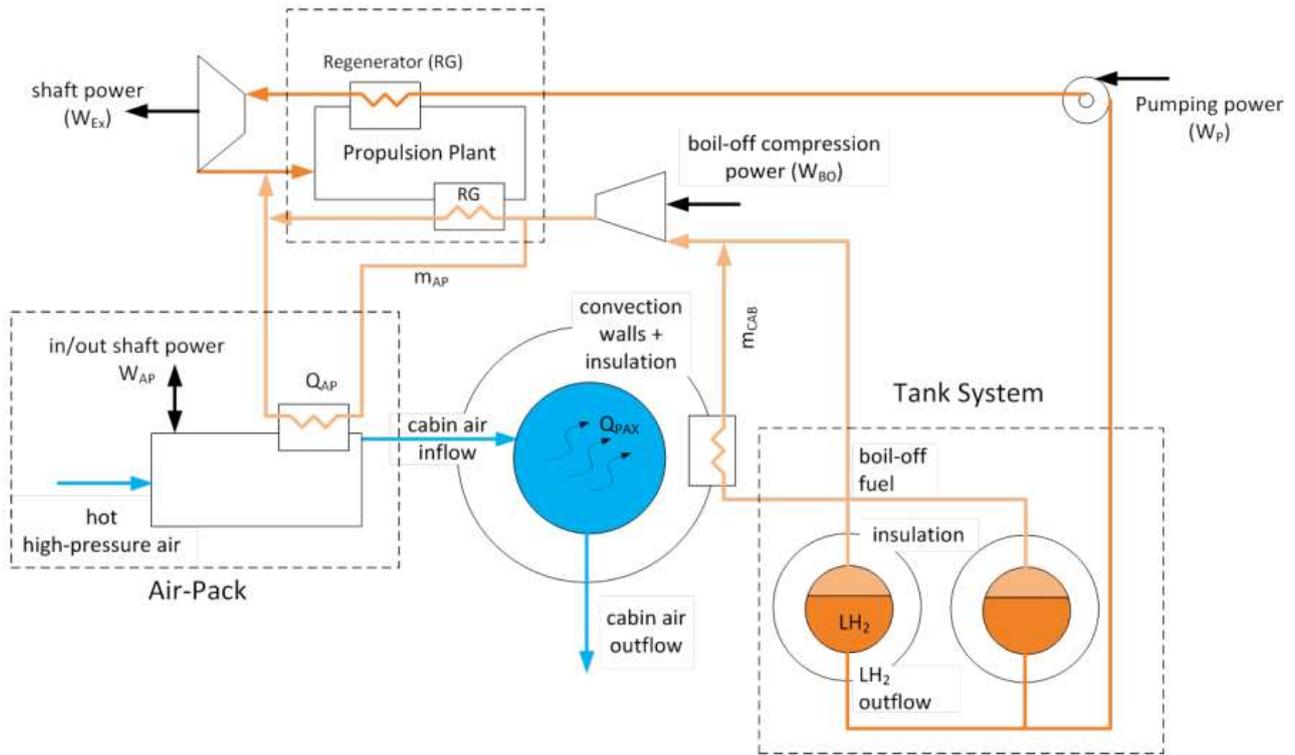
Figure 97: VEMS schematics [28]

The heat load which penetrates the aeroshell despite the insulation layer generates boil–off within the cryogenic tanks. A fraction of this gaseous fuel provides cooling to the cabin and is subsequently compressed upon mixing with the remaining fuel boiled off. The compressed boil–off is used as coolant within the air–pack and the propulsion plant, where it is finally injected. On the other hand, the high-pressure liquid hydrogen cools the propulsion plant and is subsequently expanded through a turbine to provide mechanical power. The fuel is then injected into the combustion chamber.

At first glance is possible to understand that this configuration allows strong integration between subsystems; the overall hydrogen circuit and the boil-off phenomenon, in fact, manages at the same time:

• Active Thermal Protection System (TPS), by the cooling of the airframe and the propulsive plant;

• Environmental Control System (ECS), by the cooling of the air-pack air extracted from engines in order to guarantee cabin comfort in terms of temperature and humidity;

• Onboard power generation, through the expansion of compressed gaseous hydrogen in a turbine.

These subsystems are individually described in following sections.

This solution allows to take maximum advantage on the available fuel and to turn his weaknesses into an advantage. In fact, cryogenic temperatures, guaranteed by complex insulation systems and expensive refuelling infrastructure on the ground, allow the cooling of the whole systems, and the parasite phenomenon consisting in the evaporation of tank's content is used to make the fluid circulate and cover great distances within the aircraft.

It is otherwise clear that there is a dangerous dependency of 3 main subsystems on the fuel systems, and a likely failure of it can preclude on-board main power generation, TPS and ECS. It is in fact necessary to

implement a high degree of redundancy both of system feeding lines and pumps in order to guarantee a proper safety margin in case of failure.

5.2. Turbomachinery characterisation and sizing

In a Joule-Brayton based thermal machine, some major components can be identified, namely compressor, combustor and turbine.

For the analysis of off-design conditions, each type of propeller is characterized by a given set of design parameters, which can be used to evaluate its performances. It is possible to get rid of the geometrical characteristics of the machine by referring to specific project performances or non-dimensional. Several parameters will be considered:

- environmental conditions: pressure, temperature, humidity due to variations in altitude or climatic conditions;
- flight speed;
- the regulation of
  - o throttle, in terms of fuel injected, machine revolutions per time unit, pitching of the propeller blades
  - o variable geometry and active control of the various components
- installation features (bleed, power off-take, ...)
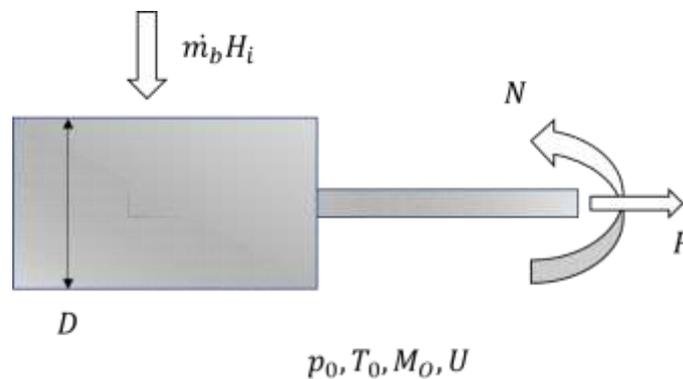
Figure 98: generic turbomachinery schematics, with external conditions and performance parameters

Since fluid dynamic and thermal properties of the fluid experience little variation within the engine, and its geometrical features are fixed, actual performances will be described in terms of specific performance. A dimensional analysis will be made to understand how many parameters influence the specific and non-dimensional performance.

During performance determination, especially when considering on-design conditions, it is a common procedure to refer to specific performance, in order to be independent from the dimensions of the machine.

The dimensional analysis assumes some knowledge on the considered machines; in this case, it is characterised by

- generated power, P;
- shaft of revolutions per time unit, N;
- prevalent dimension, D;
- environmental conditions (temperature and pressure), p_0, T_0;
- flight conditions (speed and Mach number), U, M_0;
- energy input (fuel mass flow times the net calorific value).

The main parameters that influence the global functioning of the motion are now defined. Buckingham π theorem provides a method for computing sets of dimensionless parameters from the given variables, or non-dimensionalization; it states that if there is a physically meaningful equation involving a certain number n of physical variables and k physical elementary dimensions, then the original equation can be rewritten in terms of a set of $p = n - k$ dimensionless parameters π_1, π_2, ... π_p constructed from the original variables. [29]

In this case, fundamental quantities are length, mass and time; the seven physical variables involved have been already stated before. Hence, the resulting application of Buckingham theorem will result in 3 dimensionless numbers and the specific performance considered. The governing equation of the non-dimensional performance power is

$$P_{nd} = \frac{P}{D^2 p_0 \sqrt{RT_0}}$$

Which is a function of several quantities

$$P_{nd} = f(M_0, N_{nd}, \dot{m}_{b_{nd}}) = g\left(\frac{U}{\sqrt{RT_0}}, \frac{ND}{\sqrt{RT_0}}, \frac{\dot{m}_b H_i}{D^2 p_0 \sqrt{RT_0}}\right)$$

It is important to remember that:

- dimensional analysis assumes a knowledge of the phenomenon;
- power is also a function of the viscosity through the Reynolds number and of the conductivity by Prandtl number, but the dimensional analysis does not take it into account. This approximation can be accepted since the variation of the Reynolds and the Prandtl number is negligible;
- dimensional analysis does not consider other coefficients, such as the performance of the combustor efficiency or γ;
- dimensional analysis must be followed by a study of the components and the throttle management. [30]

The analytic expression of the previous expression is

$$P_{nd} = f(M_0, N_{nd}, \dot{m}_{b_{nd}}) = \frac{U}{\sqrt{RT_0}} \cdot \frac{ND}{\sqrt{RT_0}} \cdot \frac{P_q}{D^2 p_0 \sqrt{RT_0}}$$

Where P_q is the general expression of the thermal energy entering the system. This formulation is valid at conceptual design to first evaluate the features of the machine; under the hypothesis of direct drive architecture (no mechanical transmission between compressor and turbine) and the same working fluid flowing through them. When designing a new machine, the diameter is a crucial parameter to determine; hence, from the previous equation

$$D = \frac{u P_q}{NP}$$

In which u is the working fluid speed.

In the following paragraphs, a parametric model for the estimation of turbomachinery performance will be considered. These results are just valid at conceptual design level, since they will be conservative if compared to the real size of the machine upon installation.

5.2.1. Compressor
5.2.1.1. Description

In this analysis, axial compressors will be considered. The following picture shows a simplified view of an axial compressor, in which rotor and stator stages are pointed out. From now on, a rotor blade row plus a succeeding stator blade row will be considered as a single compression stage. Blade length varies along the section of the compressor, since the desired condition of axial velocity requires that the annular flow area at the entrance to each stage vary inversely with density.
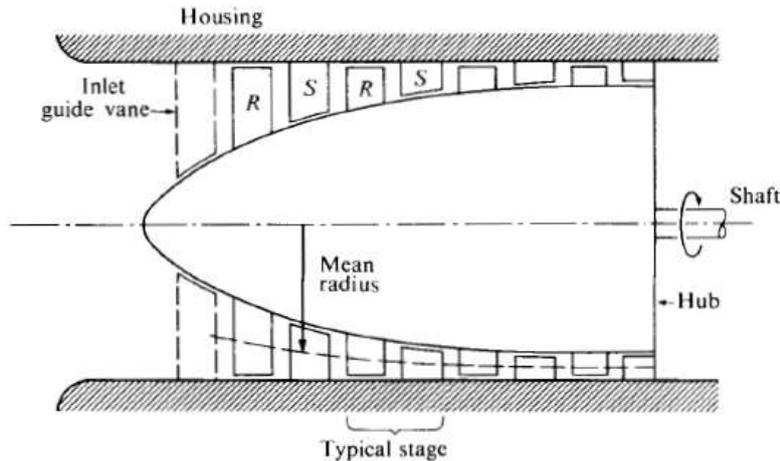

Figure 99: schematic of a section of an axial compressor

Since the in-depth analysis of compressor internal details is far beyond the purpose of this study, its performances will be studied with a set of general variables that fit each any blade geometry and describe in general the compressing of a gas. In fact, it is possible to define the overall features in terms of stagnation pressure at compressor outlet and its adiabatic efficiency as a function of few variables

$$p_{02}, \eta_c = f(\dot{m}, p_{01}, T_{01}, \Omega, \gamma, R, v, design, D)$$

In which

- p_{02} is the outlet stagnation pressure
- η_c is the adiabatic efficiency
- p_{01} is the inlet stagnation pressure
- T_{01} is the inlet stagnation temperature
- Ω is the rotational speed of the shaft
- γ, R and v denote the most important gas properties, namely specific heat ratio, specific gas content and kinematic viscosity, respectively
- D is the characteristic size
- $design$ stands for the complete specification of the geometric shape of the machine

Those listed variables are independent, which means that each variable in the set can be varied without necessarily altering the value of any other member of the set. to reduce the complexity of the problem, dimensional analysis is performed. Since there are four significant primary variables (mass, length, time and temperature) in this thermodynamic problem, it is possible to reduce the statement of physical dependence to one in which each (dimensionless) dependent variable is seen to be a function of only 5 dimensionless independent variables. A lot of possible combinations are possible; below the chosen one is shown

$$\frac{p_{02}}{p_{01}}, \eta_c = f\left(\frac{\dot{m}\sqrt{RT_{01}}}{p_{01}D^2}, \frac{\Omega D}{\sqrt{RT_{01}}}, \frac{\Omega D^2}{\nu}, \gamma, design\right)$$

To further reduce the number of variables (and hence the complexity of the problem), a few assumptions are made:

- γ doesn't vary appreciably across the compressor
- Reynolds number variation affects minimally the pressure ratio and efficiency (viscosity change is almost negligible at high Reynolds numbers)
- Diameter of the compressor is fixed [31]

Hence, a simpler relation con be expressed

$$\frac{p_{02}}{p_{01}}, \eta_c = f\left(\frac{\dot{m}\sqrt{T_{01}}}{p_{01}}, \frac{N}{\sqrt{T_{01}}}\right)$$

Where N is the shaft revolution per minute. It is possible to relate those performance index to standard atmospheric conditions at sea level (standard day)

$$\theta = \frac{T_{01}}{(T_{01})_{st\_day}}$$

$$\delta = \frac{p_{01}}{(p_{01})_{st\_day}}$$

Hence

$$\frac{p_{02}}{p_{01}}, \eta_c = f\left(\frac{\dot{m}\sqrt{\theta}}{\delta}, \frac{N}{\sqrt{\theta}}\right)$$

Those parameters can then describe the compressor performance in terms of maps, like the following one, whose meaning will be deepened in the following chapter, when they will be actually used for the testing and sizing of the TEMS system
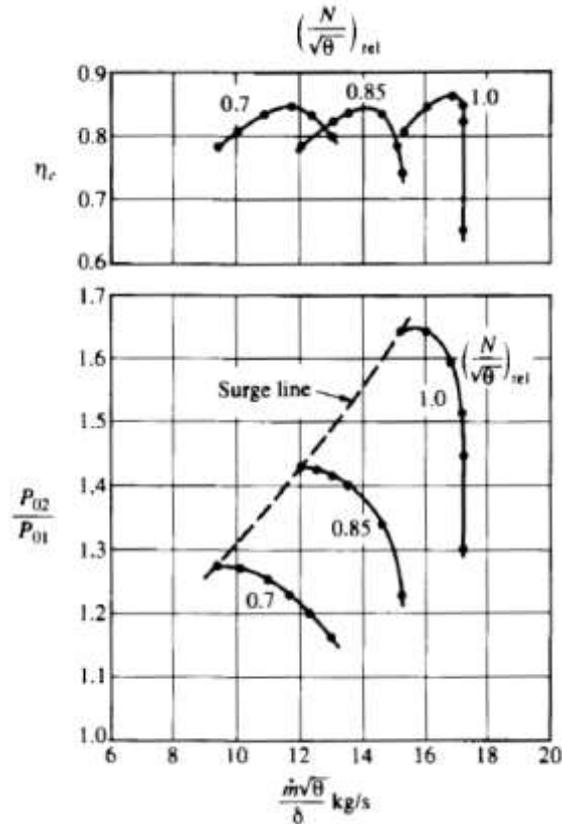
Figure 100: compressor map example [31]

5.2.1.2.   Sizing procedure

The compressor isn't usually the largest element of the machine, but its performance it's strongly influenced by it. First, the power required by the compressor is

$$P_C = \eta_{m,c} \frac{1}{\eta_C} \dot{m} c_p T_{i,c} \left(\beta_c^{\frac{\gamma-1}{\gamma}} - 1 \right)$$

Where

- $\eta_{m,c}$ is the mechanical efficiency of the compressor
- η_c is the compressor adiabatic efficiency
- $T_{i,c}$ is the temperature at compressor inlet
- β_c is the compressor pressure ratio

It is then possible to evaluate the compressor diameter through the following formula, after assuming a few parameters

$$D_c = \frac{u_c P_q}{N P_c}$$

It is then possible to implement a few semi-empirical methods for the estimation of gas generator components mass, breaking it down into its main parts, whether the turbomachinery involved is in the following operating range

Variable	Range
Number of stages	2 - 14
Inlet hub-tip diameter ratio	$0.38 - 0.83$
Pressure ratio	1.5 - 15
Average stage pressure ratio	$1.15 - 1.46$
Mean diameter	$0.34 - 0.98$ m
Length to inlet mean diameter ratio	$0.29 - 1.4$

Figure 101: range of applicability for the following semi-empiric method [32]

The compression rate of a single stage can be evaluated with the following semi-empirical equation

$$\beta_{c,stage} = 1 + \left(\frac{U/\sqrt{\theta}}{A} - C\beta_c^{1.8} + B - 1 \right)$$

In which

- U is the tangential blade velocity (m/s)
- $\theta = \dfrac{T°}{T_{static}}$ is the ratio of total to static temperature at inlet
- A is the reference mean tangential blade speed (assumed as $466\ m/s$)
- B is the dimensionless number to consider loading levels (assumed in the range $0.676 - 0,588$)
- C is the statistical coefficient to hold constant mean diameter of compressors (assumed as $6.54 \cdot 10^{-4}$)

The number of compression stage is estimated as follows

$$\aleph = \frac{\ln(\beta_c)}{\ln(\beta_{c,stage})}$$

The length-to-inlet-mean-diameter ratio is evaluated as follows

$$\frac{L_C}{D} = 0.2 + \left(0.234 - 0.218 \cdot D_{hi,c} \right) \cdot \aleph$$

In which $D_{hi,c}$ is the hub-tip diameter ratio that shall be provided as input (in the range of $0.38 - 0.83$ to be consistent with the model). The diameter is already known, and then it is possible to derive the compressor length

$$L_C = \left({L_C}/{D} \right) \cdot D$$

And the volume, assuming the compressor as a cylinder

$$V_C = \frac{L_c \pi D^2}{4}$$

Compressor mass is estimated through the following formula

$$M_C = 24.2 \cdot D^{2.3} \cdot \aleph^{1.2} \cdot \left[1 + \frac{{L_C}/{D}}{\left({L_C}/{D} \right)_{ref}} \right]$$

In which $\left({L_C}/{D} \right)_{ref} = 0.2 + 0.081 \cdot \aleph$. [32] [33]

Length of compressor vs Number of compressor stages
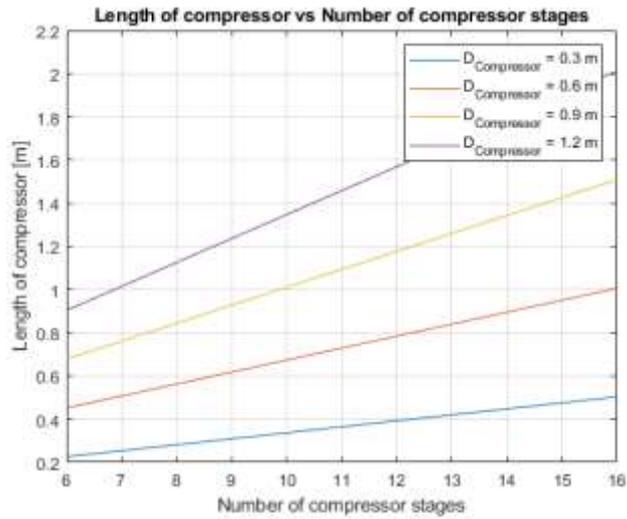

Figure 102: compressor length, as a function of the number of stages, for several diameters

Compressor mass vs Rotational speed
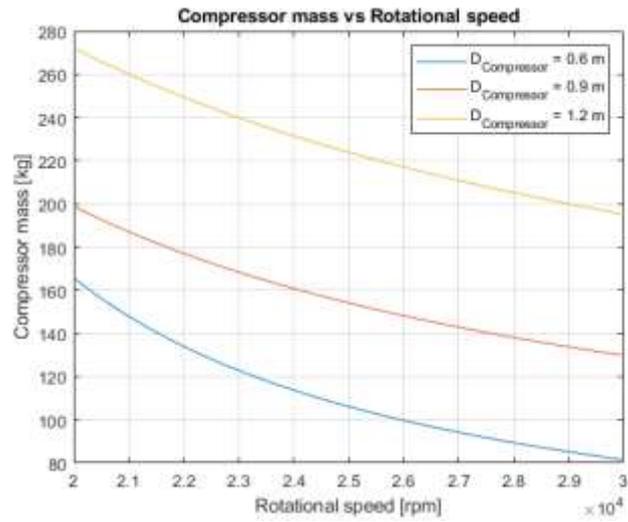
Figure 103: compressor mass, as a function of the rotational speed, for several diameters

Compressor mass vs Diameter
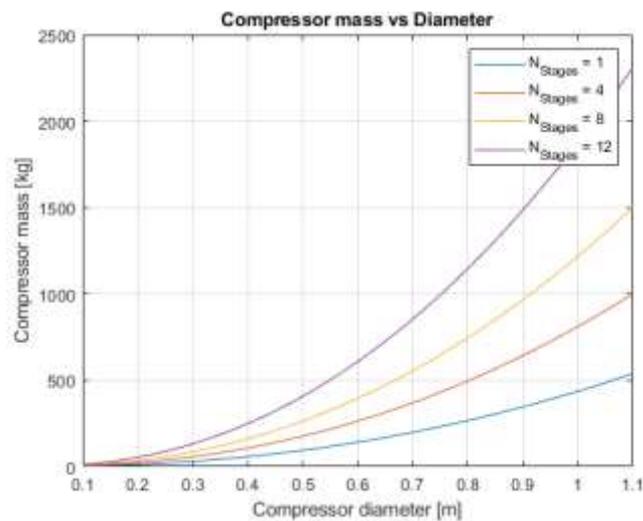
Figure 104: compressor mass, as a function of its diameter, for several numbers of stages

5.2.2. Turbine

5.2.2.1. Description

Using the same logical steps adopted in the evaluation of compressor corrected performance, turbine expansion ratio can be expressed as a function of the following variables [31]

$$\frac{p_{04}}{p_{05}}, \eta_t = f\left(\frac{\dot{m}\sqrt{T_{04}}}{p_{04}D^2}, \frac{\Omega D}{\sqrt{\gamma R T_{04}}}\right)$$

Turbine performance could be effectively described in terms of corrected parameters with a map, like the one shown in the following picture
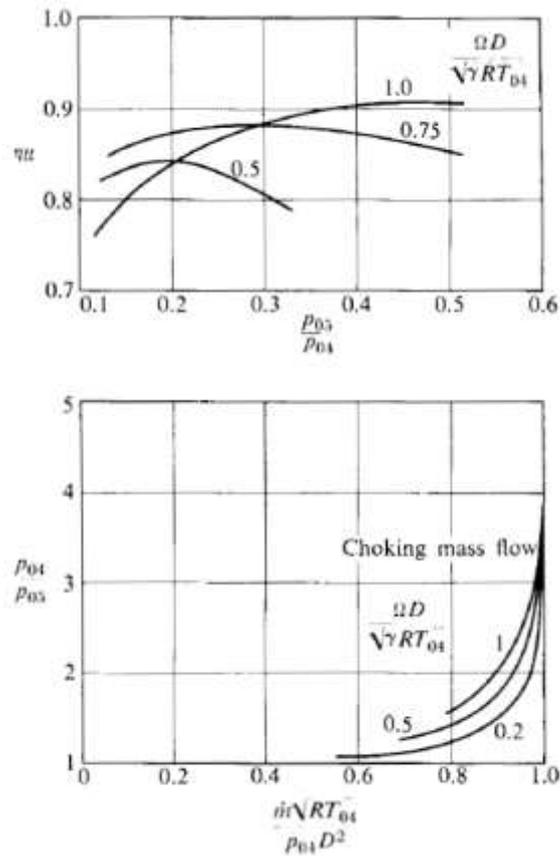
Figure 105: turbine map example [31]

5.2.2.2. Sizing procedure

The turbine usually is the largest element of the machine, since it has to expand the working fluid through the exhaust. First, the power produced by the turbine is

$$P_T = \eta_{m,t}\eta_T \dot{m} c_p T_{i,t}\left(1 - \frac{1}{\beta_c^{\frac{\gamma-1}{\gamma}}}\right)$$

Where

- $\eta_{m,t}$ is the mechanical efficiency of the turbine
- η_t is the turbine adiabatic efficiency
- $T_{i,t}$ is the temperature at turbine inlet

- β_t is the turbine expansion ratio

It is then possible to evaluate the turbine diameter through the following formula, after assuming a few parameters

$$D_t = \frac{u_t P_q}{N P_t}$$

It is then possible to implement a few semi-empirical methods for the estimation of gas generator components mass, breaking it down into its main parts, whether the turbomachinery involved is in the following operating range

Hub-tip diameter ratio	0.52 - 0.89
Mean diameter	0.43 – 1.2 m
Number of stages	1 – 6
Mean blade tangential velocity	120 – 510 m/s

Figure 106: range of applicability for the following semi-empiric method [32]

First, the blade axial aspect ratio is defined

$$AR_x = A' + B' \cdot \frac{D_{h,T}}{D_{t,T}}$$

In which

- A' is the dimensionless coefficient to correct aspect ratio depending on spool pressure (expected in the range 10.45 – 13.36)
- B' is the dimensionless coefficient to correct hub-to-tip ratio depending on spool pressure (expected in the range 6.45 – 10.95)
- $D_{h,T}$ is the hub diameter (m)
- $D_{t,T}$ is the tip diameter (m)

Hence, it is possible to determine the standard axial chord length value for both rotor blade and stator gap (namely C_{x_r} and C_{x_s}) [33]

$$C_x = \frac{D_{t,T} - D_{h,T}}{2 \cdot AR_x}$$

There is some additional clearance between rotor stages, evaluated with the following formula

$$S_T = \alpha_T \cdot C_x$$

Where α_T is a proportionality constant for gaps computation depending on axial chord length (considered in the range $0.2 – 1$).

In the end, the length of rotor blade is estimated as

$$L_T = \aleph_T \cdot \left(C_{x_r} - C_{x_s}\right) + (2 \cdot \aleph_T - 1) \cdot S_T$$

In this expression, the turbine number of revolutions $\aleph_T$ is hypnotised as a free parameter; its volume, assuming the turbine as a cylinder, is

$$V_T = \frac{L_t \pi D^2}{4}$$

Turbine mass is expressed as [32]

$$M_T = 7.9 \cdot D^{2.5} \cdot \aleph_T \cdot U_T^{0.6}$$

Results display
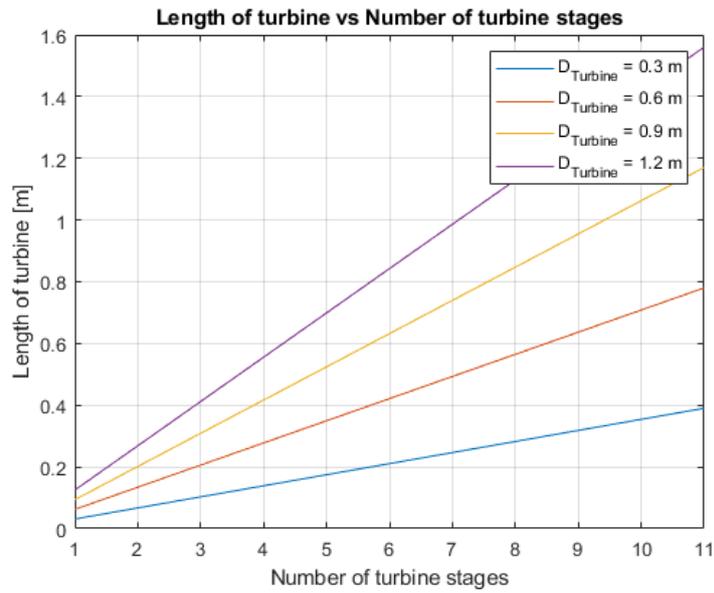
*Figure 107: : turbine length, as a function of the number of stages, for several diameters*
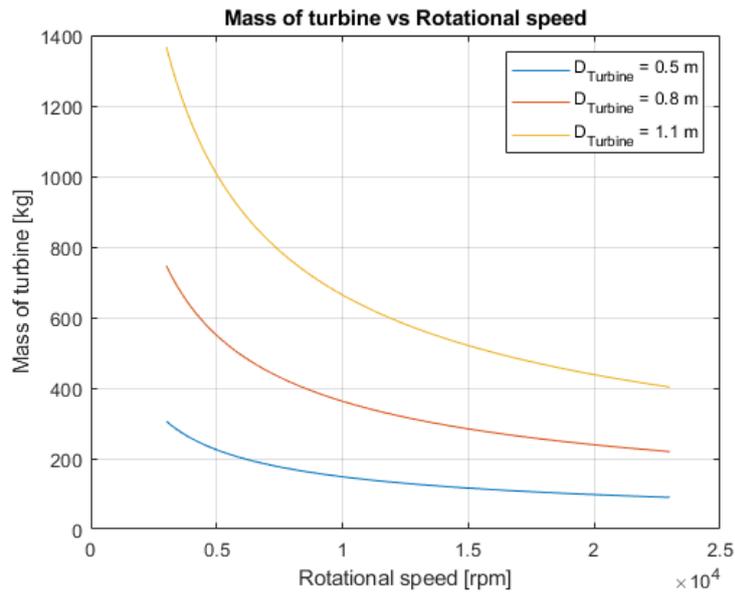
*Figure 108: turbine mass, as a function of the rotational speed, for several diameters*
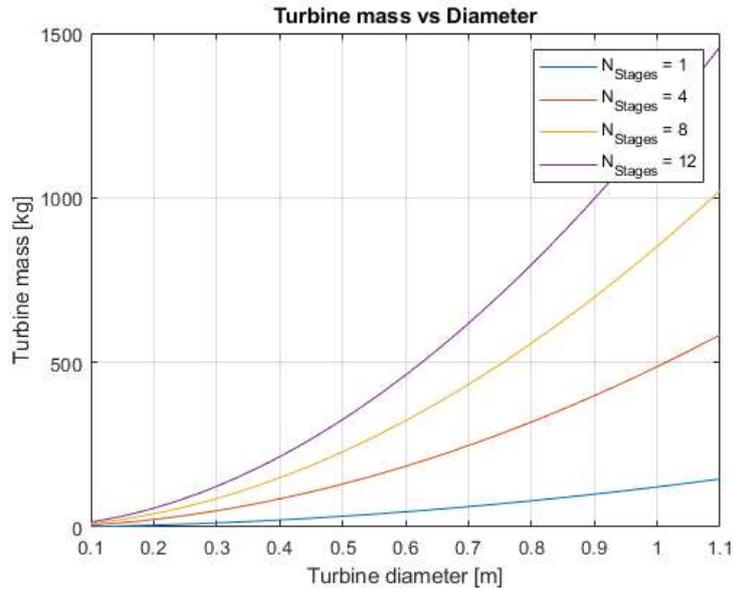
Figure 109: turbine mass, as a function of its diameter, for several numbers of stages

5.2.3. Total

5.2.3.1. Sizing Procedure

In the computation of the total mass of the gas assembly, it is important to consider also accessories, control and support structure. It is possible to demonstrate that often the mass of controls and accessories is between $9 - 30\,\%$ of the total mass of the engine, while the mass of support structure is between $10 - 18\,\%$.

In the end, the total mass of the engine is the sum of compressor, turbine, accessories and controls, and support structure, respectively [32]

$$M_{TOT} = M_C + M_T + M_{CA} + M_S$$

5.2.3.2. Results display
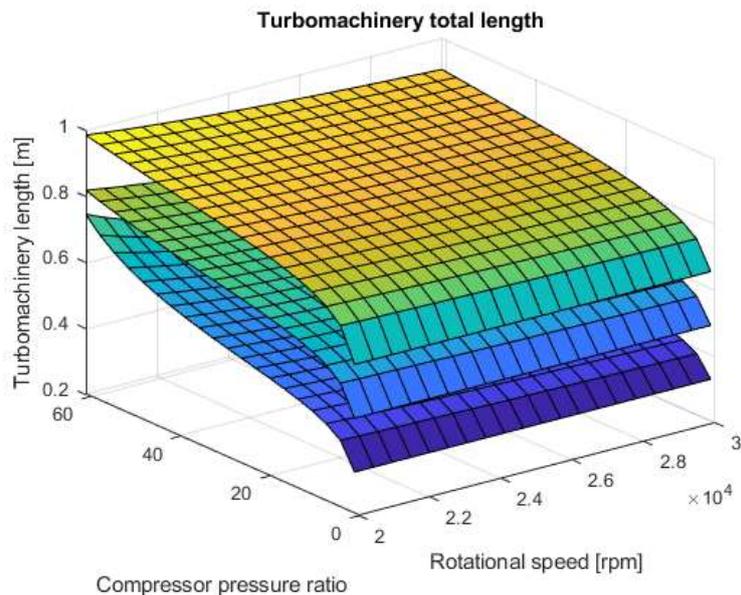
Figure 110: total length of turbomachinery assembly (compressor and turbine), as a function of both compressor pressure ratio and rotational speed (D = 0.6 m, D = 0.9 m, D = 1.2 m)
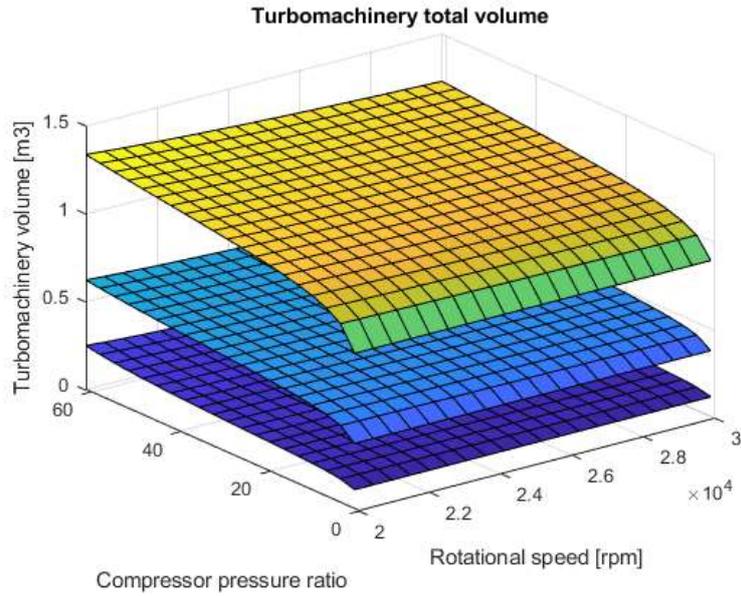
Figure 111: total volume of turbomachinery assembly (compressor and turbine), as a function of both compressor pressure ratio and rotational speed (D = 0.6 m, D = 0.9 m, D = 1.2 m)
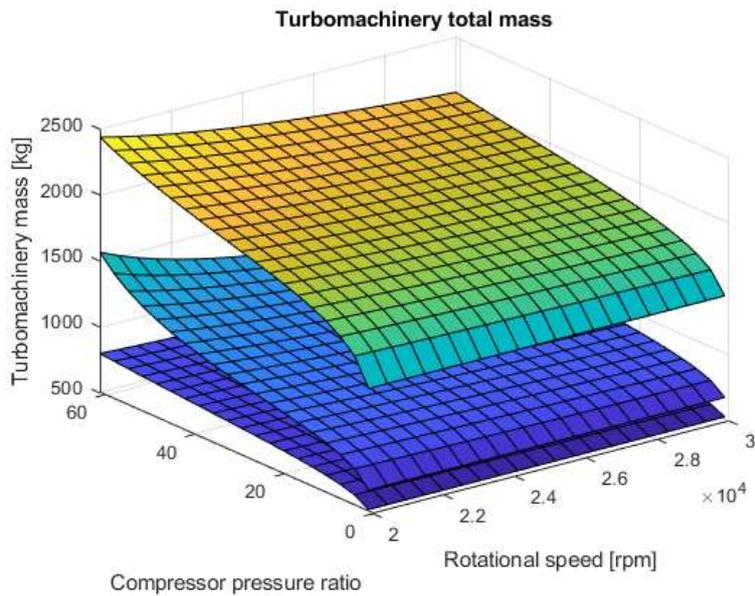
Figure 112: total mass of turbomachinery assembly (compressor and turbine), as a function of both compressor pressure ratio and rotational speed (D = 0.6 m, D = 0.9 m, D = 1.2 m)

5.3. Turbopump sizing

5.3.1. Description

In the following paragraph, the considered pump consists of a single centrifugal stage preceded by an axial inducer running on the same shaft. Even in this case, dimensional analysis technique is used. Pump pressure rise and efficiency depend essentially on the following variables

$$\Delta p_0 = f(\Omega, \dot{m}, \rho, \mu, design, D)$$

$$\eta_p = g(\Omega, \dot{m}, \rho, \mu, design, D)$$

Where

- η_p is the pump efficiency, calculated as

$$\eta_p = \frac{\dot{m}\Delta p_0}{\rho P}$$

- P is the pump power input
- Ω is the pump rotational speed
- ρ is the working fluid density
- μ is the working fluid viscosity
- D is the size or scale of the pump, for example rotor tip diameter.

According to dimensional analysis, the performance of the pump can be represented as

$$\frac{\Delta p_0}{\rho \Omega^2 D^2} = f\left(\frac{\dot{m}}{\rho \Omega D^3}, \frac{\rho \Omega D^2}{\mu}, design\right)$$

$$\eta_p = g\left(\frac{\dot{m}}{\rho \Omega D^3}, \frac{\rho \Omega D^2}{\mu}, design\right)$$

Hence, the number of independent variables is reduced to two. For a given design, they are the head rise coefficient ψ and the mass flow coefficient ϕ

$$\psi = \frac{gH}{\Omega^2 D^2} \propto \frac{\Delta p_0}{\rho \Omega^2 D^2}$$

$$\phi \propto \frac{\dot{m}}{\rho \Omega D^3}$$

In which H is the hydraulic heat of the pump. If viscosity is expressed in terms of Reynolds number, the previous equation become

$$\psi = f(\phi, Re, design)$$

$$\eta_p = f(\phi, Re, design)$$

5.3.2. Sizing procedure

The performance of turbopumps will be expressed (as suggested in literature) in terms of specific speed

$$N_s = \frac{N\sqrt{Q}}{H^{3/4}}$$

And specific diameter

$$D_s = \frac{DH^{1/4}}{\sqrt{Q}}$$

Where

- N is the rotating speed (rpm)
- Q is the volumetric flow rate (gpm)
- H is the head rise (ft)
- D is the diameter of the machine (ft)

Those performance index can be used to compare different machines on the Balje diagram, which acts as a sort of map, as shown in the following picture
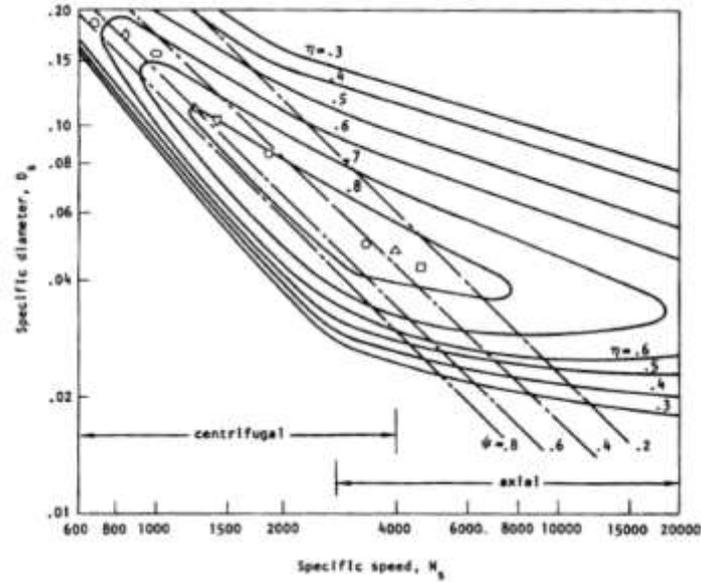
Figure 113: Balje diagram for turbopump (example)

The reference diameter is one of the most important physical parameters of the turbopumps when trying to characterize its volume and mass. This is due to the fact that, in general, the diameter of the machine can be related to the other physical features by means of semi-empirical models. The following semi-empirical formulation for multi-stages impellers mounted on the same shaft is used for the estimation of the impeller diameter

$$D_{p_{imp}} = \frac{D_S \sqrt{Q}}{(gH)^{1/4}} \sqrt{\frac{1}{n_{stage}}}$$

This formulation assumes that:

- All stages rotate at the same speed
- They handle the same fluid and develop the same head as an ideal single stage user
- Pump volume flow rate varies directly with the rotational speed
- Pump-developed head varies directly as the square of speed
- The heat developed by a single stage is equal to the total head over the number of stages, namely the stages are fluid dynamically equal.

Overall pump diameter can be estimated as a function of the impeller diameter, since others pumps components size can be derived from it. In particular, the following components will be considered

- Diffuser
- Inlet
- Outlet
- Other elements, like connectors
- Components integration, such as casing and insulation

Hence

$$D_P = D_{p_{imp}} \cdot (1 + k_{diff} + k_{inlet} + k_{outlet} + k_{other} + k_{integration})$$

A similar approach is here suggested to evaluate the overall length of the turbopump on the basis of its constituent components. In particular, the following components will be considered

- Impeller
- Pre-burner
- Inducer
- Bearings
- Turbine
- Outlet section of the turbine
- Accessories and other components

Hence

$$l_P = l_{imp}\left(1 + k_{pb} + k_{ind} + k_{other}\right) + l_b + l_t$$

Where the impeller contribution is usually estimated on the basis of the mass flow that the pump should handle and remembering that the length of the impeller is in proportion with the inlet pump diameter

$$l_{imp} = 0.7 \cdot \frac{r_{in}}{2}$$

Which is, on turn

$$r_{in} = n_{stages}\sqrt{\frac{\dot{m}}{\rho u \pi}}$$

Bearing contribution is evaluated as follows

$$l_b = 2 \cdot D_{shaft} = 2 \cdot \frac{u_{shaft}}{\pi n_t} = 2 \cdot \frac{0.1 u_t}{\pi n_t}$$

Turbine contribution is evaluated as follows

$$l_t = 0.083 \cdot n_{stages}$$

Whether the pump could be considered as a cylinder, its volume can be expressed as

$$V_P = \frac{l_p \pi D_P^2}{4}$$

A similar approach is here suggested to evaluate the overall mass of the turbopump on the basis of its constituent components. In particular, the following components will be considered

- Technology parameter
- Casing
- Impeller
- Rotor
- Shaft

Hence

$$M_P = I \cdot (M_{cas} + M_{imp} + M_{rot} + M_{shaft})$$

Considering each component as a cylinder, each component mass can be expressed as follows [33] [32]

$$M_{cas} = \rho_{cas}\left(\pi R_{imp}^2\right)l_P$$

$$M_{imp} = \rho_P\left(\pi R_{imp}^2\right)l_{imp}$$

$$M_{rot} = \rho_{rot}(\pi R_T^2)l_T$$

5.3.3. Results display

This analysis involves many parameters, and the most of them is often not yet known in a conceptual design level of detail. Therefore, it is now presented a statistical analysis of existing turbopumps on actual spacecrafts [32]. Data are rather scattered, since this turbopumps involve different architecture, design points, interfaces with other components and purpose. The analysis is led to have a benchmark to generally direct the conceptual design of this subsystem in the same field of operation.
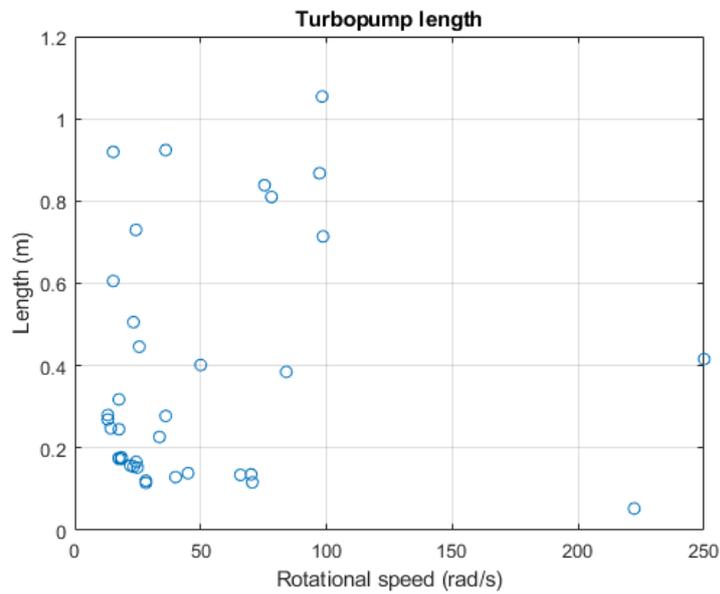
Figure 114: statistical analysis of spacecraft turbopumps length
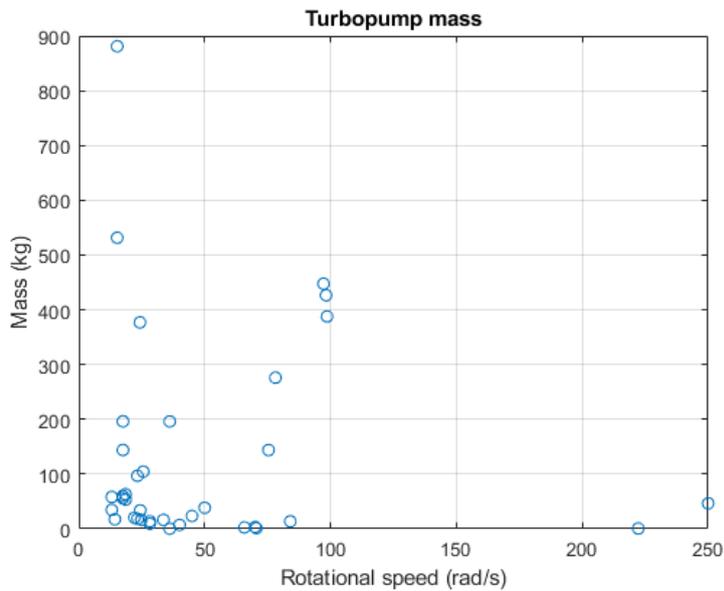
Figure 115: statistical analysis of spacecraft turbopumps mass
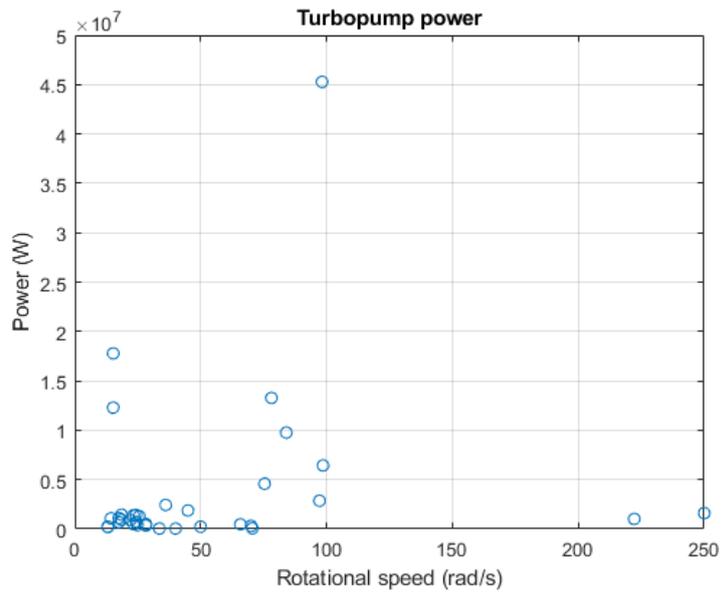
Figure 116: statistical analysis of spacecraft turbopumps consumed power

6. TEMS: new architecture and dynamic sizing

6.1. Current configuration vs new draft

6.1.1. Introduction

In the previous chapter the current configuration of the Thermal and Energy Management System [34] was shown and explained.
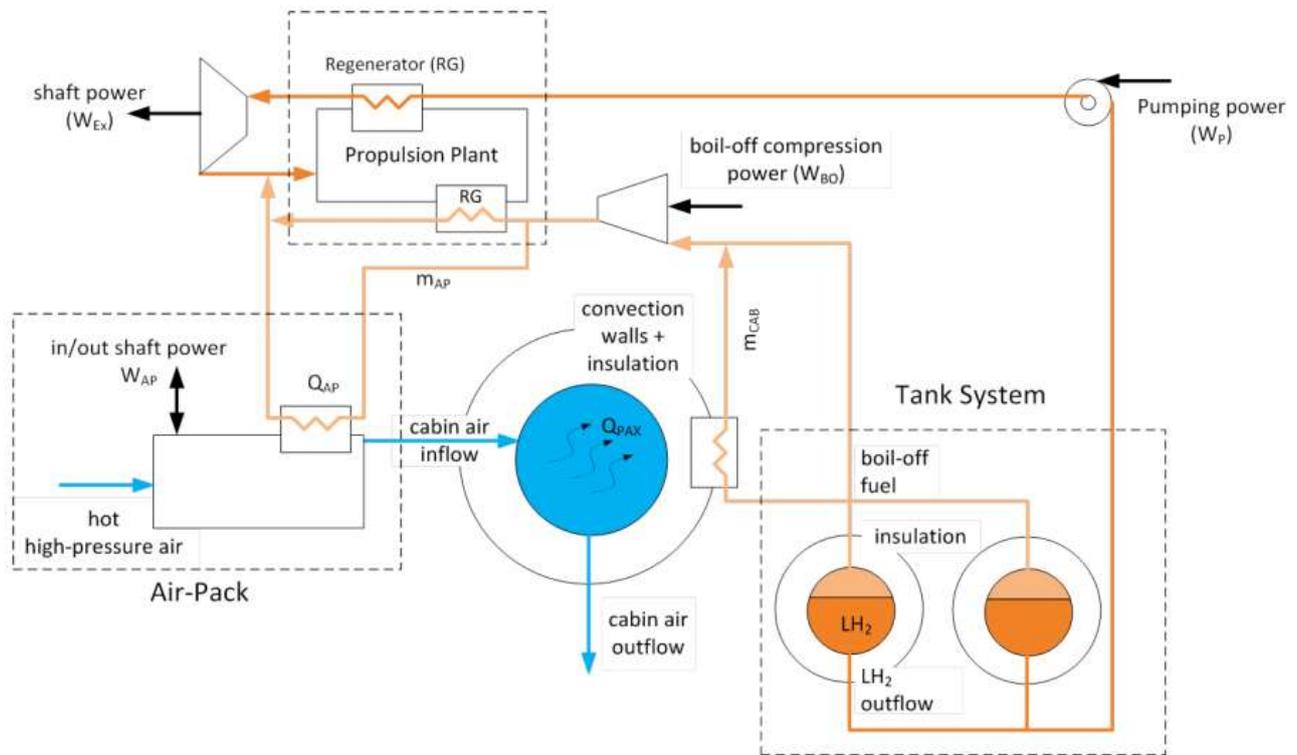
Figure 117: current TEMS configuration [1]

This is a conceptual design configuration, since a lot of technical details and ideas are still not well defined. The most outstanding example is how do the propulsion plant regenerator and turbine will work: although the heat to be assimilate is considerable, in the scheme liquid hydrogen remains so even after the regeneration. In the other hand, it was shown in the previous hydrogen chapter that the temperature range in which H_2 is liquid (at least at $p = 0.5\ MPa$) is narrow. In addition to this, it is still unclear how will the subsequent turbine generate useful power: the pressure of the liquid hydrogen in that line is fully provided by the preceding turbopump, that has to be fed with the turbine output shaft power; the regenerator will give the liquid a certain amount of thermal energy, but the output fluid cannot expand in a turbine since it is still liquid. In the likely chance that the hydrogen would evaporate after the regenerator, the expansion becomes possible, but still there is no considerable energy source between the compressor and the turbine to make the gas cycle worthwhile.

Since some questions are arisen, a new architecture will be tested; it will be slightly different from the original, but a few changes will be implemented.

6.1.2. New architecture

The following picture shows the new concept of Thermal and Energy Management System:
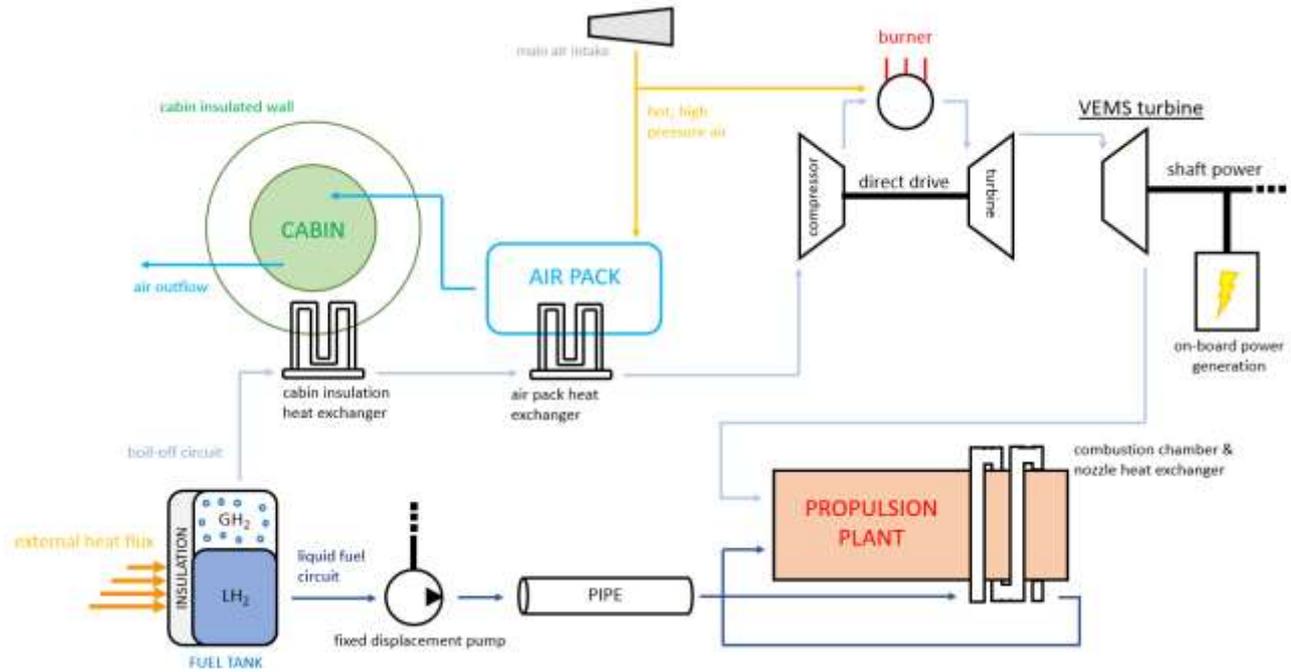
Figure 118: new TEMS configuration

It is first necessary to state that each component shown here stands as a conceptual example of the behaviour of several physical elements, namely:

- The single tank is fictional, since the large amount of stored hydrogen is spread all along the vehicle in a multitude of smaller containers. The latter solution is adopted to make an external aerodynamic shape possible, since a single cylindrical container could not fit the fuselage along with passengers, propulsion plant duct (whose size is remarkable) and other aircraft subsystems. According to initial estimations, fuel tanks should be symmetrical around the aircraft's longitudinal axis, but they will be spread all along the delta wing length: this solution forces the tanks to fit the multi-lobe structure, making their shape irregular and not constant along aircraft's x body axis. In addition to this, each tank could have a different purpose, hence a different structure and configuration: primary tanks feed directly the engine, while secondary tanks are provided with transfer pumps to delivery fuel to the first ones. Further studies on the subject are already in progress within the overall STRATOFLY project, and an accurate definition of tanks emptying sequence will be soon available. The current approximation of a large, single tank that contains all the fuel mass allow to describe the overall system and global phenomena, but is of course inaccurate, since it does not take account of some additional hardware (tanks physical elements, pumps, pipe, valves and fittings, sensors, …) and friction generated heat. Once the final fuel system architecture will be defined, a more accurate model will be implemented;
- Pipes are inserted in the model as a physical element that occurs a single time in each pipeline, with an appropriate length that takes account of the overall pipe length in the subsystem. This is a first attempt hypothesis, since it does not take account of pipe diameter variation and possible local restriction. This simplification is made to take account of friction head losses and pressure drops due to the pipe, still not knowing exactly their configuration, length and approximate diameter;

- Pump, compressor and turbine are represented as a single component with a single turbomachinery stage. This is a simplification, since the large amount of fuel is most likely be handled with a series of pumps, and both Brayton cycle compressor and turbine will implement a few compression/expansion stages to manage the boil off mass flow rate with a better efficiency. Within this model, those elements will be represented as an equivalent single element able to process the whole mass; this approximation is made as a conceptual design choice, since no further data are available.

A few overall hypotheses have been discussed; a further definition of every design choice is going to be made in the following section, while describing each part of the system individually. It is first necessary to describe the overall behaviour of the global TEMS subsystem in the new proposed architecture.

First, external heat due to aerodynamic friction and outer radiation flows inside the tanks through an insulation layer, that prevents the tank external walls to exceed structural limit temperature. The heat flow increases liquid hydrogen temperature and eventually makes it evaporate: this is an artificial increase of the natural inclination of hydrogen to boil-off. Tanks are considered kept at constant pressure, since the boiled-off hydrogen self-pressurize the tank, and a pressure relief valve allow the gaseous hydrogen surplus to flow into the upper circuit. Liquid hydrogen is driven by several pumps through a pipeline and other fuel transfer tanks; eventually it flows around the main combustion chamber and nozzle for cooling purposes, and then it is injected in the propulsion plant to provide thrust.

Gaseous hydrogen flows in several heat exchangers in series: the first cools down the air layer that insulates passenger's cabin and cockpit from the engine and the external skin, and the second is part of a sub-freezing cold air unit known as "air pack" to provide a suitable environment onboard. Hydrogen, that is now much hotter due to heat exchange, is then compressed. The gas goes through a combustion chamber, that burns part of the hydrogen to provide the rest of the gas thermal energy and speed. The amount of burned hydrogen is set as required introducing a variable amount of air spilled from the intake, since the burning reaction takes place only in stoichiometric conditions. The resulting gas is now a high energetic mixture of unburned hydrogen and reaction products, namely water. Gas flows into a first turbine that mechanically drives the compressor, and then through a free turbine, whose architecture is like turboshaft engines: it can be connected to an electrical power generator to feed onboard users. The unburned hydrogen is then injected in the combustion chamber.

6.2. Initial conditions

6.2.1. Thermal assessment during the mission

The optimized Lapcat MR2 Brussels–Sydney mission profile provided necessary boundary conditions and the freestream conditions for the calculation of the airframe heat loads. In the following picture both flight altitude profile and fuel mass flow rate are shown (solid lines):
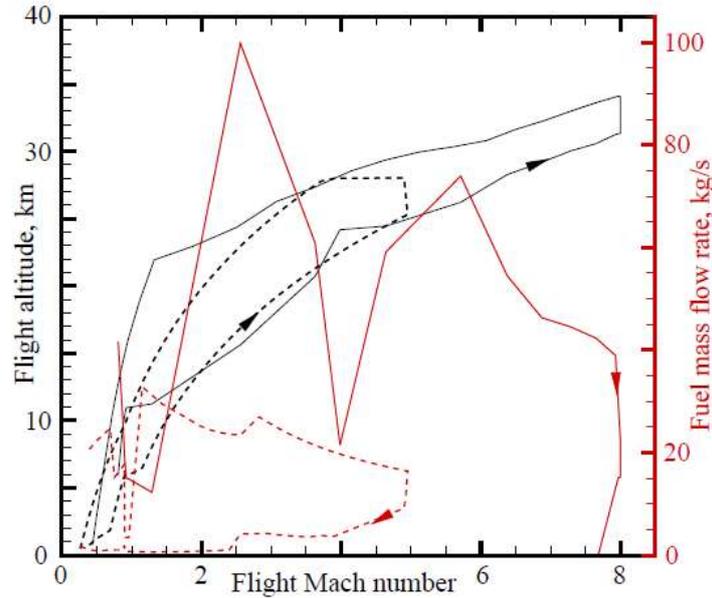
Figure 119: flight altitude and fuel mass flow rate for standard Lapcat MR2.4 mission profile (solid line) [34]

Absorbed heat load can be then estimated analytically considering free-flow speed and altitude, using a zero-dimensional technique and neglecting supersonic and hypersonic thermodynamic issues (as described in the aerodynamic database section): it is computed by time–integrating the heat flux across all the aeroshell panels. A total of 26 GJ of heat were absorbed by the fuel tanks by the end of the Mach 8 mission [34], to which the contribution of the ascent and descent phases amounted to respectively 2.4 GJ and 3.4 GJ, whereas the cruise segment contributed with 20.2 GJ of thermal energy.
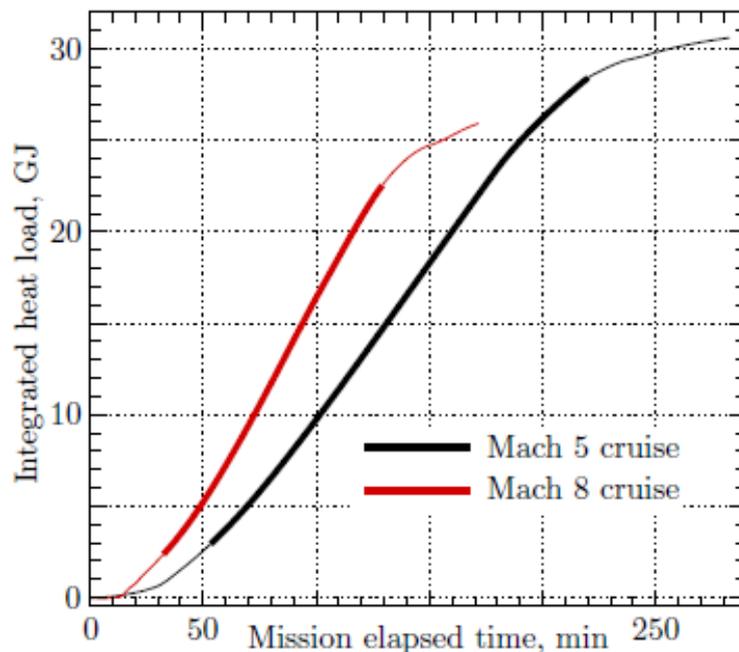
Figure 120: integrated heat load during MR2.4 mission (red line) [34]

A thermal evaluation, lead with the techniques already exposed in this thesis, lead to a first attempt estimation of both external temperature (outer wall of the aeroshell) and internal (inner wall, inside the insulation layer). These results are shown in the following picture
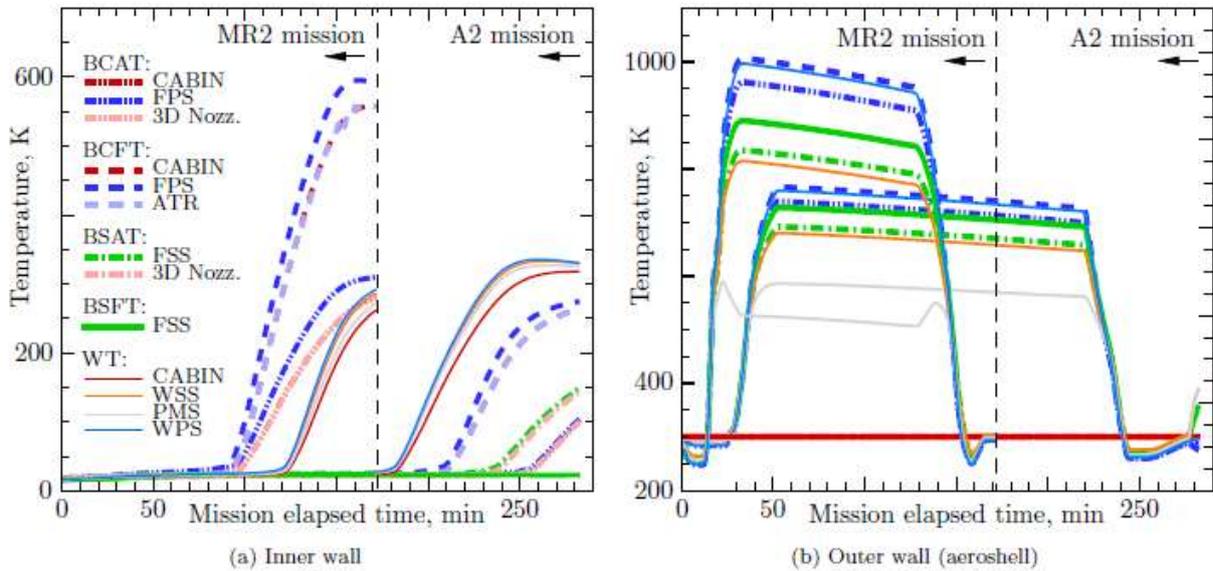
Figure 121:Tank inner and outer wall temperatures along the interfaces with the aeroshell, the cabin and the propulsion plant [34]

Internal temperature starts approximatively around stored hydrogen temperature, since the thermal situation is supposed steady around an equilibrium point. Its evolution starts slow since the cryogenic fuel still absorbs most of the external heat; temperature starts then rising due both to tank depletion and mission progression (more heat flux incoming). A peak of 550-600 K is observed for the MR2 mission at the interfaces between the body center forward tank (BCFT) and the passengers' cabin (PAX), the fuselage pressure side (FPS) and the propulsion duct of the air–turbo rocket (ATR). The walls of the wing (WT) and the body center aft tank (BCAT) reached a peak temperature of 300 K upon depletion. On the other hand, the body side aft (BSAT) and forward (BSFT) tanks, where the reserve fuel is allocated, remained cryogenic until the end of the mission. [34]

The difference between external and internal temperature is due to the choice of insulation material and layer thickness; this is a remarkable design decision to make, since

- A thin layer of insulation permits a lighter structure, less maintenance and lower building expense. In the context of Thermal and Energy Management System it allows a greater amount of heat to penetrate the shell and make liquid hydrogen evaporate, setting boil-off mechanics in motion. On the other hand, it could represent a risk, since the structure could face temperatures too high to withstand mechanical loads properly, since metals and composites suffer a large loss of mechanical properties when their working temperatures approaches even half of their fusion point. An additional external layer of insulation could be provided for proper thermal protection purposes, but in this analysis such possibility was not evaluated;

- A thick layer of insulation (or a choice of better insulating materials) can better protect the inner structure of the aircraft from high temperatures, with the drawback of increasing mass and cost. A trade off choice must be undertaken in order to better regulate boil-off phenomenon, still taking advantage of its features.

6.2.2. Tank system

The following tables show interfacing areas between main aircraft sections and the size of the tank (whether it could be modelled as a cylinder), respectively.

	Aeroshell						Intake	Propulsion plant			Cabin	Total lateral surface
	Wing suction side	Surface on the wing suction side	Prandtl-Meyer expansion	Wing pressure side	Fuselage pressure side	Fuselage suction side		ATR duct	3D nozzle	2D nozzle		
Cabin	-	-	-	-	276	-	124	76	76	-	-	853
Body centre aft tank	-	-	-	-	58	-	-	-	58	-	28	160
Body centre forward tank	-	-	-	-	129	-	102	14	-	14	77	369
Body side aft tank	-	-	-	-	-	125	-	-	209	-	-	418
Body side forward tank	-	-	-	-	-	143	143	-	-	-	-	286
Wing tank	328	161	489	-	-	-	-	-	-	-	183	1245

Table 1: Interfacing areas (m^2) between the aeroshell, the propulsion plant, the tank system and the cabin

	Volume, m^3		Equivalent length, m	Single unit cross section		
	Single unit	Total		D_h, m	A, m^2	b/a
Body centre aft tank	153	153	21	2	7.2	7
Body centre forward tank	568	568	44	3.2	12.9	4
Body side aft tank	210	420	27	2.1	7.7	7
Body side forward tank	117	233	29	1.7	4.1	5
Wing tank	678	1357	58	2.2	11.8	10
	Total	2731				

Table 2: tank volumes, equivalent length and cross section characteristics

Different temperatures were considered for the interfaces between the tank and each subsystem, namely the aeroshell elements, the cabin or the propulsion plant. The interface with the propulsion plant was considered isothermal at 300 K, since a regenerative cooling of the walls was foreseen. The cryogenic fluid was modelled as a homogeneous mixture of vapor and liquid in thermodynamic equilibrium. Since pressurization is needed from a structural point of view, the saturation pressure of the bulk liquid is always below the tank pressure. [28].

Hence, the initial state of the fuel has been established as

- Initial pressure: $p_0 = 1\ bar$
- Initial temperature: $T_0 = 15\ K$

That is to say, hydrogen stand steady in a sub-cooled situation, with a density of 76 $\frac{kg}{m^3}$. [34]

6.3. Dynamic simulation environment

6.3.1. Simulink

Simulink is a MATLAB-based graphical programming environment for modelling, simulating and analysing multidomain dynamical systems. Its primary interface is a graphical block diagramming tool and a customizable set of block libraries. It offers tight integration with the rest of the MATLAB environment and can either drive MATLAB or be scripted from it. Simulink is widely used in automatic control and digital signal processing for multidomain simulation and model-based design. [35]

6.3.2. Simscape

Simscape software is a set of block libraries and special simulation features for modelling physical systems in the Simulink environment. It employs the Physical Network approach, which differs from the standard Simulink modelling method and is particularly suited to simulating systems that consist of real physical components. Simulink blocks represent basic mathematical operations. When Simulink blocks are connected, the resulting diagram is equivalent to the mathematical model, or representation, of the system under design, based on the Physical Network approach. According to this approach, each system is represented as consisting of functional elements that interact with each other by exchanging energy through their ports. These connections are nondirectional, they mimic physical connections between elements. Connecting Simscape blocks together is analogous to connecting real components, such as pumps, valves, and so on. In other words, Simscape diagrams mimic the physical system layout.

The mathematical representation of the just mentioned physical system contains ordinary differential equations (ODEs), algebraic equations, or both:

- ODEs govern the rates of change of system variables and contain some or all the time derivatives of the system variables. The system is differential if there are no algebraic constraints;
- Algebraic equations specify functional constraints among system variables but contain no time derivatives of system variables. The system is algebraic if there are no ODEs;
- With ODEs and algebraic constraints, the system is mixed differential-algebraic (DAEs). A system variable is differential or algebraic, depending on whether its time derivative appears in the system equations or not. [36]

In the framework of Simscape modelling environment, pre-existing libraries and custom functions will be implemented. Within this work, most used libraries are:

- Mechanical: contain blocks for the mechanical rotational and translational domains, organized into rotational and translational elements, mechanisms, sources, and sensors;
- Hydraulic: contain blocks for the hydraulic domain. Fluid properties are assumed to be constant during simulation time;
- Gas: contain blocks for the gas domain. This category provides the following levels of idealization: perfect gas, semiperfect gas, and real gas;
- Thermal liquid: contain blocks for the gas domain. Within this library it is possible to take account for thermal effects in a fluid system, even the temperature dependence of fluid properties, e.g., density and viscosity.
- Thermal: contain blocks for the thermal domain. These blocks allow to model fundamental thermal effects like insulation and heat exchange;

- Two-phase fluid: contain blocks for the two-phase fluid domain. The working fluid line is considered a connected two-phase fluid loop. The working fluid is assumed to be part liquid and part gas.

These blocks belong to different domains, and since they work as physical interfaces, the connection of different domains is possible only under certain circumstances; it is then possible to simulate even multidomain physical systems. Anyway, a set of blocks connected with each other represent a physical system.

In the present situation, the best mean to represent liquid hydrogen gradually evaporating in tanks, pipelines and mechanical element should be the two-phase liquid, since it accurately describes the behaviour of a fluid in which the coexistence of a liquid and gas phase in non-steady equilibrium is an important feature. Unfortunately, the related library currently available in Simscape is not enough provided with elements and blocks, from both a programming and a bibliography point of view; available elements are just enough to describe a simple pipeline and its thermal interface, but it is still not possible to connect it with mechanical elements. Due to this limitation, another approach is undertaken: liquid and gaseous hydrogen are separate from the beginning, namely the storage tanks in which boil-off phenomenon takes place. Then, the evolution of the fluids is analysed separately, under the hypothesis of no further phase transition. At the end of the analysis, the results will demonstrate whether this approach could represent a suitable approximation or if more in-depth analysis is necessary.

The fixed structure of each block is another issue to overcome: available elements can normally receive as input only one predetermined kind of physical line, i.e. gas, thermal liquid, etc. This is a limitation, since in most of the cases there is no clear separation within these two states during the dynamic simulation of the system. This restriction is overcome with a proper definition of fluid properties (both gas and liquid, as seen in the devoted chapter) and the frequent use of sensors and sources blocks: it is then possible to fictitiously generate a proper mass flow in the right conditions (as evaluated from the sensors) in the physical line that allows the components to be inserted.

By this means, and specifically tailored Matlab functions, it will be possible to describe, model and simulate the dynamic behaviour of the Thermal and Energy Management System.

6.3.3. Structure of the analysis
The overall system structure is then settled, considering only the most important physical components of each pipeline: it is possible to deepen the level of detail by adding real pipeline elements, such as pipe restrictions, valves, accumulators etc, but in a conceptual design level environment this proves little use, if not obstacle, to the overall progression in the analysis. In fact, each component must be described in detail, providing many configuration choices and initial conditions: too complex design of a system whose behaviour is still not known, even in a qualitative point of view, could be harmful to the design process. Further studies could be implemented in future, using most important components of this system to build a more complex, detailed and precise model that better represent the real configuration of a pipeline.

Even considering only fundamental elements of the system, the overall architecture results to be a large and articulate model; reporting it all as a single piece could result in a readily comprehensible representation, since the blocks are barely visible themselves, and connections turn out to be excessively tangled. For the sake of clarity, the overall model will be split in three subparts, each one of them representing both a logical and physical subpart of the system. The connection in series of these elements generate the global model; generally, each part is constituted of a single physical line (gas, thermal liquid, etc). Separate analysis is consistent to the need of reduced simulation time during the design phase. Input and output physical quantities are coherent, since the same Matlab script provides the additional data processing; output information of each part is carried by sensors to next one by the introduction of fictional mass flow or pressure generators, or just setting proper initial condition within the blocks themselves. This way, the

representation of the global system is consistent and more understandable, as it is described in three subparts.

Each section will be described in its own paragraph, first analysing how the block simulates the dynamic behaviour of the physical component that it represents. Then, simulation environment is set, defining each component physical features and thermal interface with each other. In the end, simulation outputs are shown and described.

The three subparts, each one representing a logical section of the overall system, are:

- Liquid hydrogen line
- Gaseous hydrogen line
- Engine

Figure 122: analysis partition of the overall system

6.4. Liquid hydrogen line

6.4.1. General architecture

Liquid hydrogen line physical block diagram it's shown below.

Figure 123: liquid hydrogen line block diagram

It is possible to see that the block scheme matches the qualitative physical scheme shown earlier. The tank is not represented using the dedicated block within Simscape Thermal Liquid library as it represents only a fixed-volume chamber to be filled with the fluid, and it makes convergence issue arise if used as a source tank. Instead, a reservoir and a pipe are properly settled to simulate a tank behaviour. Other main components of this assembly are the fixed-displacement pump and the following "pipe", that somehow represents both the overall pipeline configuration (in terms of pipe length, friction, hydraulic losses, etc) and the heat exchanger that subtracts heat from the power plant (this last and only part will be partially set aside, as it will be described in the engine-dedicated paragraph). Grey blocks are just a set of sensors, that allow the user to understand the trend of physical quantities within the pipeline.

6.4.2. Block and components description

6.4.2.1. Reservoir (Thermal liquid)

Description

This block represents an infinite reservoir at fixed pressure and temperature. It could both represent a source and a sink: in the first case, the initial temperature of the fluid equals the starting temperature of the reservoir, which is assumed to be constant (the reservoir acts as a heat source). In the second case, if liquid flows into the reservoir, the inlet temperature equals that of the upstream liquid (the reservoir acts as a heat sink).

The block includes heat conduction across a length equal to the effective diameter of the pipe. This diameter is a function of the specified cross-sectional area of the inlet pipe.

<u>Hypothesis and limitations</u>

The reservoir is assumed to be isothermal, as no temperature variation happen inside this element. [37]

<u>Parameters and initial conditions</u>

In this case, parameters to set are the same as define initial conditions, which are:

- Pressure (MPa)
- Temperature (K)
- Cross-sectional area at inlet port (m^2)

6.4.2.2. Pipe (Thermal liquid)
<u>Description</u>

This block models the flow of a thermal liquid in a closed conduit; pipe's walls are set rigid, hence there is no expansion and contraction in the radial direction. The thermal liquid ports are set at constant elevation (vertical distance between them).

The pipe is discretised in a finite number of pipe segments: the more they are, more accurate the results will be. Total mass, momentum, and energy accumulation within its span are determined as sums over the volumes contained in the pipe: segmented pipes are treated as assemblies of smaller pipes. The appropriate number of segments to use in a model depends partly on the time scales over which temperature and pressure disturbances tend to propagate through the pipe. Pressure waves travel the fastest (they do so at the speed of sound in the fluid, c) and are often the rate-limiting factor to consider. In accordance with the Nyquist sampling theorem, in order to capture an elementary sinusoidal disturbance (described with its frequency, f), at least two computational nodes—and therefore pipe segments—must be available for sampling within one wavelength:

$$\frac{c}{f} = 2 \cdot \frac{L}{N}$$

The left-hand side represents the wavelength of the pressure disturbance and the right-hand side the length of a pipe segment (overall pipe length, L, over the number of pipe segments, N)—each providing one computational node to the pipe. Hence, it is possible to determine the required number of pipe segments (nodes) to properly describe the physical behaviour under that disturbance.

The pressure loss across the pipe is determined as a function of friction between the fluid and the pipe and of the rise or drop in height between the ports. It is possible to simulate dynamic compressibility and the inertia of the fluid; basic analysis and this more complex one will be performed in parallel to see the difference between them, but only the results of the first will be carried on, since the software response is faster, and the hypothesis of quasi-steady flow could be sufficient for accurate analysis.

The temperature profile of the fluid is determined by its interactions with the rest of the system, both by the conductive heat transfer through the dedicated thermal port and by the internal energy change due to convection between the ports.

The global description of fluid behaviour resort to Navier-Stokes equations. These equations are at the heart of fluid flow modelling: solving them, for a given set of boundary conditions, predicts the fluid velocity and its pressure in a given geometry. These equations (namely mass, momentum and energy balance) will be expressed as partial differential equations (PDEs), as explained in the next paragraphs.

<u>Mass balance</u>

Since the pipe is supposed rigid, the volume contained between inlet and outlet port is fixed. In the incompressible scenario, density is supposed constant, and then mass within the pipe can't vary over time. In terms of mass flow rate:

$$\dot{m}_A + \dot{m}_B = 0$$

Pipe walls are supposed to be rigid, hence there will be no radially compliant wall; this contribution will be neglected in this analysis.

If the thermal liquid is supposed compressible (as it should be) the mass within the pipe varies with pressure (p) and temperature (T). This dependence is captured by the bulk modulus (β) and thermal expansion coefficient (α) of the thermal liquid:

$$\dot{m}_A + \dot{m}_B = \rho_I V \cdot \left(\frac{\dot{p}_I}{\beta_I} - \alpha_I \dot{T}_I \right)$$

Subscripted variables are considered as the arithmetic mean of the variable at the beginning and at the end of the pipe segment, respectively

$$p_i = \frac{p_A + p_B}{2}$$

Momentum balance

Under the hypothesis of neglecting fluid inertia, the pipe can be treated as a quasi-steady component; its pressure balance, expressed as a pressure difference between its ports, is expressed as follows

$$p_A - p_B = p_{F,A} - p_{F,B} + \rho_1 g \Delta z$$

The left term of the equation represents the arise in static pressure. The right term of the equation is composed of the viscous friction along the pipe wall (in terms of pressure loss due to friction in half of the pipe volume) and the gravitational contribution on the volume of the pipe (in terms of mean density, gravitational acceleration and rise elevation between physical ports A and B). If the fluid is assumed incompressible, pressure varies linearly between the ports; its value at the internal node "i" was defined earlier. If the flow is treated as compressible the pressure in the pipe can vary nonlinearly between the ports. To carry out this calculation, the momentum balance is split over two control volumes, one each for half of the pipe volume. Between port A and the internal node:

$$p_A - p_i = p_{F,A} + \frac{\rho_1 g \Delta z}{2}$$

Between the internal node and port B:

$$p_B - p_i = p_{F,B} + \frac{\rho_1 g \Delta z}{2}$$

It is now necessary to evaluate pressure losses due to friction in the pipe. This calculation is lead through the Darcy-Weisbach equation

$$p_{F,j} = f_{D,j} \cdot \frac{1}{4} \cdot \frac{L_E \dot{m}_j |\dot{m}_j|}{\rho_i D S^2}$$

in which L_E is the effective length of the pipe (actual length plus the aggregate equivalent length of all local resistances like elbows, unions, fittings, and other local sources of friction), D is the hydraulic diameter, $f_{D,j}$ is the Darcy friction factor. Those variables are determined as follows:

- Darcy friction factor

- Laminar flow
  In this case, the factor is a function of Reynolds number alone

$$f_{D,j} = \frac{\lambda}{Re_j}$$

Reynold number at port j is defines as

$$Re_j = \frac{\dot{m}_j D}{\mu_I S}$$

In which μ is the dynamic viscosity of the fluid.

λ is the shape factor of the pipe, an empirical constant used to encode the effect of pipe geometry on the major pressure loss; its value is 64 in circular pipes and $48-96$ in noncircular ones.

In conclusion, the actual pressure loss in laminar flow is defines as

$$p_{F,j} = \frac{1}{4} \cdot \frac{\lambda \mu_I L_E \dot{m}_j}{\rho_I D^2 S}$$

- Turbulent flow
  In this case, the friction factor is a function also of the pipe diameter and surface roughness. The factor is evaluated from the Haaland correlation; it approximates the implicit Colebrook–White equation, valid for full-flowing circular pipe. This empirical equation consists in

$$\frac{1}{\sqrt{f_{D,j}}} = -1.8 \cdot \log\left[\left(\frac{\epsilon/D}{3.7}\right)^{1.11} + \frac{6.9}{Re_j}\right]$$

In which ϵ is the absolute roughness of the pipe (typical values are in the range $0.0015 - 3\ mm$, as it represents the height of the bumps at the pipe-fluid interface).

- Hydraulic diameter: it is an artificial quantity to allow the estimation of section area for non-cylindrical pipe. In the case of rigid pipe with circular section, the hydraulic diameter is the same as the nominal diameter.

<u>Energy balance</u>

The fluid in the pipe gains energy in several ways:

- advection and conduction through the ends of the pipe (sections A and B)
- convection at the pipe-fluid interface (heat flux, H)
- longitudinal changes in elevation.

It is possible to express the energy balance in terms of the energy accumulation rate ($\dot{E}_I$) in the pipe, accounting those contributions, as

$$\dot{E}_I = \Phi_A + \Phi_B + \Phi_H - \dot{m}_I g \Delta z$$

in which Φ is the energy flow rate. The total energy of the internal fluid volume is defined in terms of the specific internal energy (u, function of both temperature and pressure) as:

$$E_I = \rho_I u_I V$$

where V is the volume of the pipe. Deriving this equation and taking account of the compressibility

$$\dot{E}_I = \rho_I V \left(\frac{du}{dp}\frac{dp}{dt} + \frac{du}{dT}\frac{dT}{dt}\right)$$

Thus, the left term of the equation is obtained. The heat flow rate between the thermal liquid and the pipe wall is assumed to result from the superimposition of a convective exchange and a conductive exchange between the wall (H) and the internal fluid (I):

$$\Phi_H = Q_{conv} + Q_{cond}$$

Deepen those terms with simplistic analytic relations, it results that

$$\Phi_H = c_{p,average} \cdot \left| \dot{m}_{average} \right| \cdot (T_H - T_{inlet}) \left[1 - e^{\frac{hS_H}{c_{p,average} \cdot \left| \dot{m}_{average} \right|}} \right] + \frac{k_i S_H}{D} \cdot (T_H - T_i)$$

In this equation $c_{p,average}$ is the specific heat of the thermal liquid, h is the heat transfer coefficient of the pipe, k is the thermal conductivity of the thermal liquid and S_H is the surface area of pipe wall (obtained as product of the length and perimeter of the pipe).

The convective heat transfer coefficient is calculated according to the following expression

$$h = \frac{Nu_{avg} \cdot k_{avg}}{D}$$

Nu is the Nusselt number, calculated for an average temperature inside the pipe. It is evaluated as follows:

- Laminar flow
  In this case, the coefficient is assumed constant.
- Turbulent flow
  In this case, the Gnielinski correlation is used as follows

$$Nu_{avg} = \frac{\frac{f_{avg}}{8} \cdot \left(Re_{avg} - 1000 \right) \cdot Pr_{avg}}{1 + 12.7 \sqrt{\frac{f_{avg}}{g} \cdot \left(Pr_{avg}^{\frac{2}{3}} - 1 \right)}}$$

In which Pr is the average Prandtl number. [38]

Hypothesis and limitations

The hypothesis of constant elevation between physical ports lead to an approximate analysis of the system, since it operates on an aircraft, in which a roll manoeuvre can change this parameter. This perspective is not considered as there is no enough data on the mission profile regarding lateral-directional motion of the aircraft.

The design choice of not considering fluid compressibility (until hydrogen is liquid) and its inertia leads to neglect phenomena associated with rapid dynamic and fast flow changes, such as water hammer. This resolution was taken in order to simplify the model (and reducing simulation time), and to better display the macroscopic phenomena that take place within the pipeline. In addition to this, it can be considered a suitable approximation at the large time scales over which changes to flow typically occur.

The heat flow rate due to convection is computed under the assumption that temperature varies exponentially between the ends of the pipe.

6.4.2.3. Fixed displacement pump (Thermal liquid)
Description

The Fixed-Displacement Pump block represents a device that extracts power from a mechanical rotational network and delivers it to a hydraulic network. The pump displacement is fixed at a constant value: this

means that this device can let flow a fixed amount of volume per rotation (displacement is typically expressed as rad/s). This pump, as a function of rotational speed and pressure drop, can work in several modes:

1. Mode 1: forward pump, in which a positive angular shaft speed generates positive pressure gain
2. Mode 2: reverse motor, in which a negative pressure drop generates a negative shaft angular speed
3. Mode 3: reverse pump, in which a negative angular shaft speed generates negative pressure gain
4. Mode 4: forward motor, in which a positive pressure drop generates a positive shaft angular speed.

The following picture shows graphically each possible working regime. In this analysis, only the first one will be considered, being the others undesirable situations which may occur.
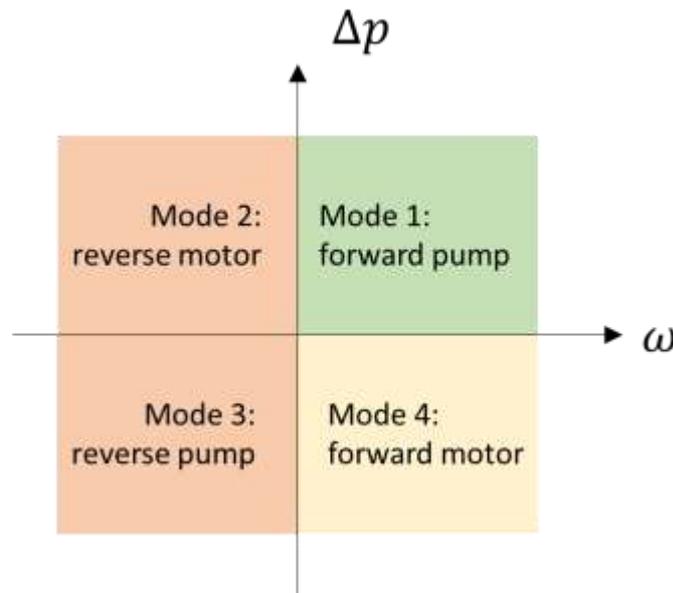

Figure 124: fixed displacement pump operation modes

It is possible, within this block choice, to choose between different kind of parametrisation of power losses due to leakage and friction; since there are not still tabulated data about efficiencies and losses available for this pump (even if this could be a future improvement of the project), the analytical model is chosen. Hence, mechanical, volumetric efficiencies and losses derive from analytical models based on nominal parameters, properly defined within the block. In the next paragraphs the analytical model will be explained, both in terms of mass flow rate and driving torque.

Mass flow rate

The actual output mass flow from the pump is constituted by the ideal mass flow rate, decreased by the internal leakage mass flow rate:

$$\dot{m} = \dot{m}_{ideal} - \dot{m}_{leak}$$

Ideal mass flow rate can be expressed in terms of average fluid density, displacement parameter (rad/s) and the shaft angular velocity, as follows

$$\dot{m}_{ideal} = \rho D \omega$$

Internal leakage mass flow rate can be expressed in terms of average fluid density, pressure drop, average dynamic viscosity and the Hagen-Poiseuille coefficient, as follows

$$\dot{m}_{leak} = \frac{K_{HP} \rho_{avg} \Delta p}{\mu_{avg}}$$

The Hagen-Poiseuille coefficient is determined from nominal fluid characteristics, namely the displacement parameter, nominal shaft angular velocity, nominal dynamic viscosity (μ_{nom}, i.e. the dynamic viscosity at which the nominal volumetric efficiency is specified), volumetric efficiency at nominal conditions ($\eta_{v,nom}$), as follows

$$K_{HP} = \frac{D\,\omega_{nom}\mu_{nom}(1 - \eta_{v,nom})}{\Delta p_{nom}}$$

Driving torque

The actual driving torque required from the pump is constituted by the ideal driving torque increased by the torque necessary to overcome the mechanical friction:

$$\tau = \tau_{ideal} + \tau_{friction}$$

Ideal torque can be expressed in terms of displacement parameter (rad/s) and the pressure drop from inlet to outlet, as follows

$$\dot{\tau}_{ideal} = D\Delta p$$

The torque necessary to overcome the friction can be expressed in terms of no-load torque (τ_0), pressure drop, angular speed, nominal shaft angular velocity (ω_{nom}, i.e. the angular speed at which the nominal volumetric efficiency is specified), and another coefficient (e, friction torque vs pressure drop coefficient), as follows

$$\tau_{friction} = \tau_0 + K_{TP} \cdot |\Delta p| \cdot tanh\left[\frac{4\omega}{(5e - 5)\omega_{nom}}\right]$$

Hypothesis and limitations

The response time of the pump is considered negligible in comparison with the system response time. The pump is assumed to reach steady state nearly instantaneously and is treated as a quasi-steady component.

The approximation of constant displacement parameter (volume disposed per rotation) is not exact strictly speaking, since fluid dynamics effects and boundary layer condition affect the volumetric flow rate in relation to rotational speed, but in the context of conceptual design of the system is still legitimate. In addition to this, some other assumptions are made:

- Effects of fluid inertia are neglected
- Effects of elevation are ignored
- The pump wall is assumed to be rigid
- External leakage is ignored [39]

6.4.2.4. Sensors (Thermal liquid)
Description

This custom block groups the main sensors in the thermal liquid library; they are necessary to measure several physical quantities, and they are placed often along the pipeline to evaluate the evolution of these variables across the components. Measured quantities are:

- Referred to the fluid
  - Internal energy $\left(kJ/kg\right)$
  - Density $\left(kg/m^3\right)$

- o Specific heat at constant pressure $\left(^{kJ}/_{kg\ K}\right)$
- o Pressure (Pa)
- o Temperature (K)
- Referred to the flow
  - o Mass flow rate $\left(^{kg}/_{s}\right)$
  - o Volumetric flow rate $\left(^{m^3}/_{s}\right)$
 - o Energy flow rate (kW)
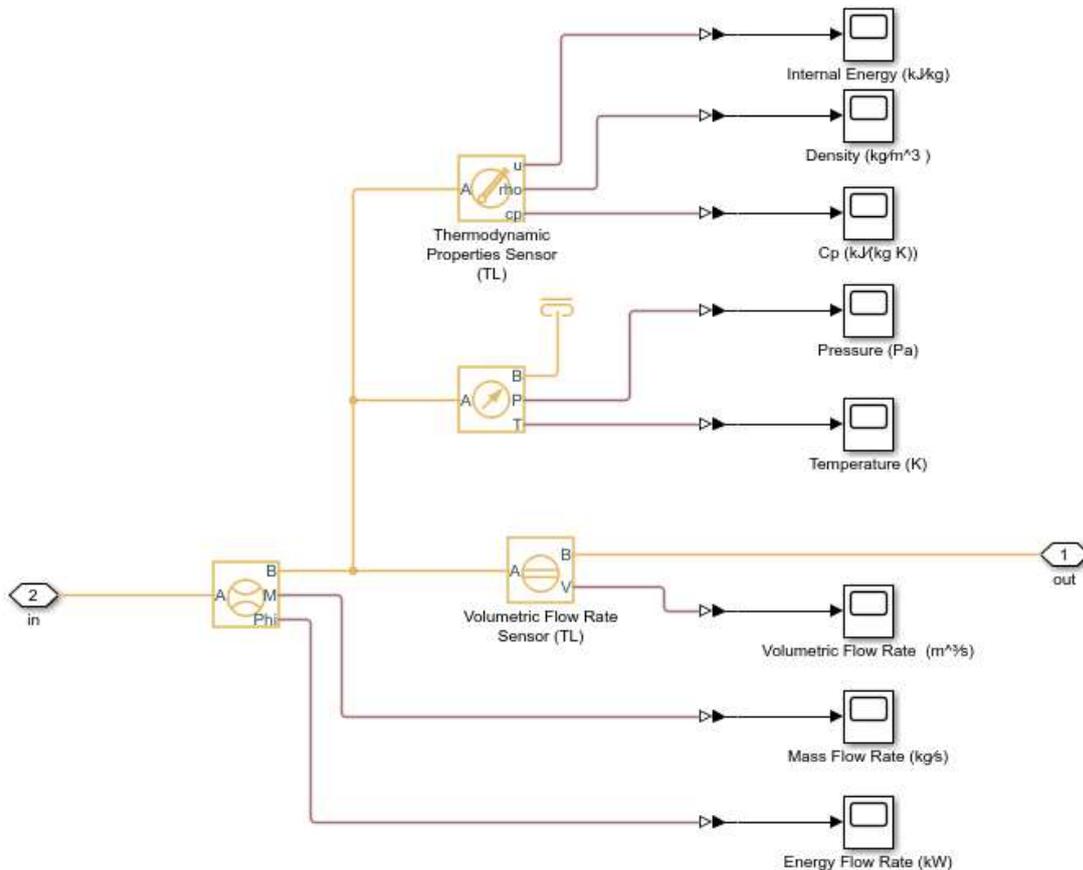
Figure 125: custom set of sensors (thermal liquid library)

<u>Hypothesis and limitations</u>

There is no mass or energy flow through the sensors related to fluid properties. There is no change in pressure or temperature across the sensors related to flow properties.

6.4.3. Settings of physical simulation

In this section, analysis and elaboration of the data will be discussed, along with all the inputs to the Simscape model.

6.4.3.1. Thermal environment

This analysis aims to deduce the effect of the environment on the aircraft, in terms of temperature. It is already known, from the mission profile analysis, the heat flux flow from the environment to the aeroshell (evaluated as an average value across the whole fuselage):
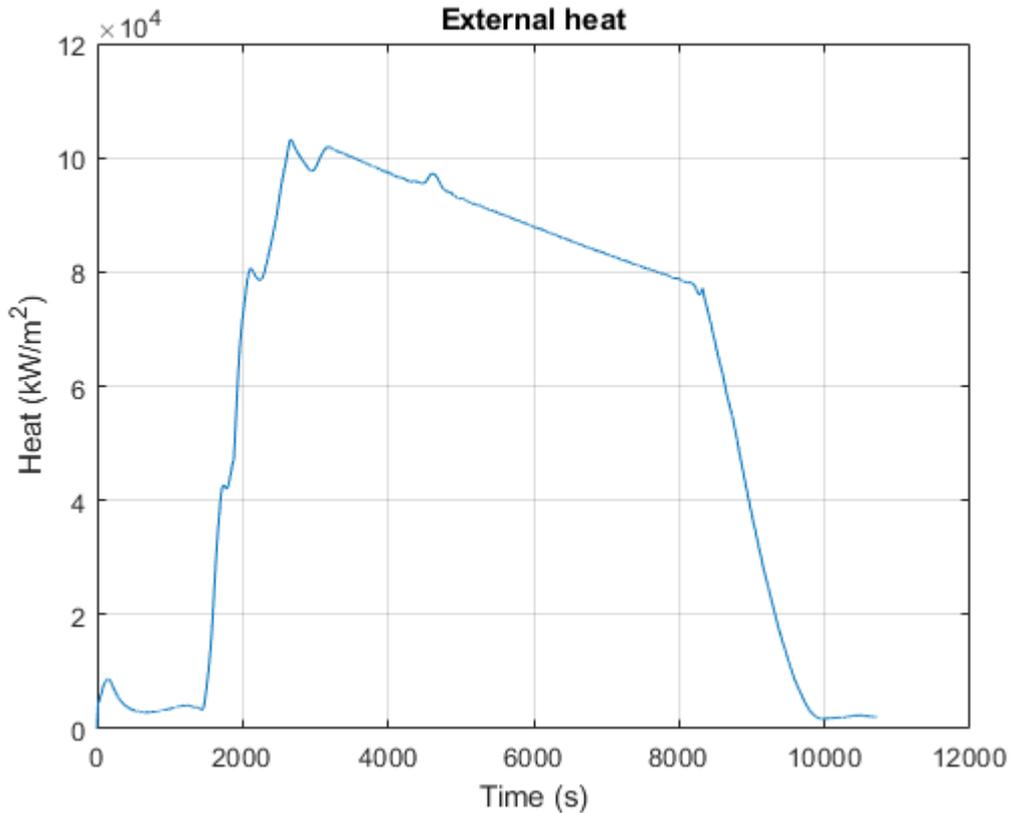
Figure 126: external heat profile

This heat profile is computed considering the friction between the aircraft and the free flow: it is evident that its trend follows the speed profile, since friction phenomenon is directly proportional to the flying velocity.

In the heat balance on the fuselage it is necessary to consider the heat dissipated in thermal radiation toward the outer environment, the heat absorbed by the fuselage (external and insulation layer) and the energy absorbed by the liquid hydrogen stored inside the tanks (in the current aircraft configuration, most of the tanks are separated from the outer environment only by the aeroshell and a layer of insulant foam). These three phenomena are processed analytically as follows.

- Radiative heat

   The fuselage acts like a "grey body" in the context of Stefan-Boltzmann law of thermal emission

$$q = \epsilon \cdot \sigma \cdot T^4$$

   Those terms are the thermal emissivity, Stefan-Boltzmann constant $\left(\sigma = 5.67 \cdot 10^{-8} \frac{W}{m^2 K^4} \right)$ and the absolute temperature (K), respectively [40]. The outer surface of the aircraft is considered to have an emissivity of $\epsilon = 0.8$ [28], in order to take account of the intermediate condition between black body (full emissivity) and white body (no emissivity). The absolute temperature refers to the external wall temperature.

- Conductive heat

   This phenomenon consists in the heat exchange between the external surfaces of a solid wall: in this case, the first one faces the free air flow, while the second is in contact with the liquid hydrogen stored in the tanks. A few assumptions are necessary:

- The wall facing liquid hydrogen is isothermal, and its conditions are the same of the liquid hydrogen
- LH_2 facing the external wall is supposed to maintain the same physical condition through the flight ($T = 20\ K$) [28].
- The wall is constituted by homogenous solid material with constant thermal properties.

Under these conditions, it is possible to predict that heat will flow through the wall from the hotter surface to the colder one, according to the second principle of thermodynamics. The differential equation with partial derivatives regulating this phenomenon is the so called "heat equation"

$$\frac{\delta^2 T}{\delta x^2} = \frac{\rho c_p}{\sigma} \cdot \frac{\delta T}{\delta t}$$

In this case, the phenomenon could be supposed quasi-steady; hence the equation becomes

$$\dot{Q} = \lambda \cdot \frac{\Delta T \cdot S}{L}$$

In which $\dot{Q}$ is the amount of transferred heat (W), λ is the thermal conductivity of the wall $\left(\frac{W}{mK}\right)$, ΔT is the temperature difference between the surfaces, S is the area and L is the distance between the faces (measured perpendicularly to the surfaces). [41]

In this case, the wall is made of a series of two different materials, with the following configuration and properties [34]:
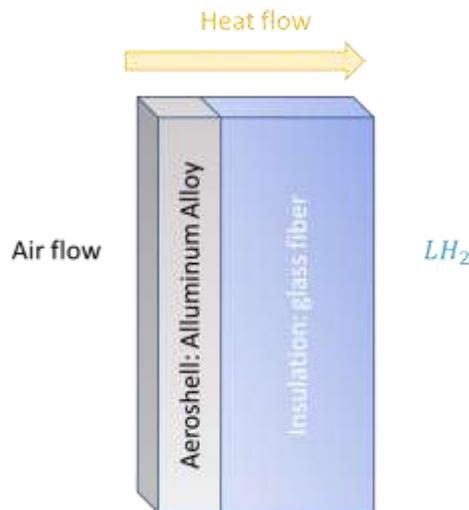

Figure 127: insulation layer between outside and tanks

	Glass fiber	Aluminium alloy
Thickness (mm)	50	1
Conductive heat coefficient, k $\left(\frac{W}{mK}\right)$	0.1	100
Thermal capacity, C $\left(\frac{kJ}{kgK}\right)$	1	0.9
Density, ρ $\left(\frac{kg}{m^3}\right)$	48	210

The evaluation of this structure thermal properties resorts to an electrical analogy. The analogue of $\dot{Q}$ is the electrical current, and the analogue of the temperature difference ΔT is voltage difference.

From this perspective the slab is a pure resistance to heat transfer and we can define the following relation

$$\dot{Q} = \frac{\Delta T}{R}$$

In which $R = \frac{L}{\lambda S}$ is the thermal resistance. In this case, the thermal resistance is calculated as series of the single resistances

$$R_{tot} = R_1 + R_2 = R_{alluminum} + R_{foam} = \frac{L_1}{\lambda_1 S_1} + \frac{L_2}{\lambda_2 S_2}$$

$$R_{tot} = \frac{L_1 \lambda_2 S_2 + L_2 \lambda_1 S_1}{S_1 S_2 \lambda_1 \lambda_2}$$

Noting that the exchange area is the same

$$R_{tot} = \frac{L_1 \lambda_2 + L_2 \lambda_1}{S \lambda_1 \lambda_2}$$

It is now possible to applicate the heat exchange equation to the whole series as follows

$$\dot{Q} = \Delta T \cdot \frac{S \lambda_1 \lambda_2}{L_1 \lambda_2 + L_2 \lambda_1}$$

Or, evaluating the heat flow per unit area

$$\dot{q} = \frac{\dot{Q}}{S} = \Delta T \cdot \frac{\lambda_1 \lambda_2}{L_1 \lambda_2 + L_2 \lambda_1}$$

The factor $\frac{\lambda_1 \lambda_2}{L_1 \lambda_2 + L_2 \lambda_1}$ is equal to 2 in case of foam only; in the whole series it is equal to 1.99996; there is no substantial difference between the two configurations in terms of thermal conduction.

- Absorbed heat

  Fuselage walls are supposed to act as a thermal capacity: a part of the external heat affecting the structure is supposed to be absorbed by the materials of which it is made, whose temperature hence rises. The reference equation is the definition of thermal capacity, hence the amount of heat to be absorbed by a body to make its temperature rise by $1\ K$

  $$Q = m \cdot C \cdot \Delta T$$

  In this case this formulation is not suitable, since it depends on the mass of the external layer. However, analysing it in terms of heat per unit-surface, a more convenient formulation is achieved

  $$q = \rho \cdot t \cdot C \cdot \Delta T$$

  In which the fuselage walls average density and thickness are taken into account. While the latter is the sum of each constituent layer (structure and insulation), equivalent average density is a weighted average of each layer density in proportion to its thickness

  $$\rho_{eq} = \sum_{i=1}^{N} \rho_i \cdot \frac{t_i}{t_{tot}}$$

It is now possible to evaluate the heat balance (i.e. the heat that affects the aeroshell) as follows:

$$\dot{q}_{external} = \dot{q}_{absorbed} + \dot{q}_{radiation} + \dot{q}_{conduction}$$

It is then possible to introduce an equation that describes heat exchange in proximity to the aerodynamic surface in a free flow; this expression is known as "Boundary layer energy equation", since it is a particular case of the general energy equation [42]:

$$\dot{q} = h_{conv} \cdot (T_{rec} - T_w)$$

In this expression appear the convection heat exchange coefficient, the recovery and the wall temperature. Since the latter is the variable of the current system, the other quantities are determined as follows.

- Heat exchange coefficient (by convection)
  This coefficient evaluates the attitude of a thermal conductor to be crossed by heat (in this case, in a situation in which the main heat transfer system is convection). It is possible to evaluate this coefficient in this dynamic situation recurring to the definition of the Stanton coefficient, which is a dimensionless number that measures the ratio of heat transferred into a fluid to the thermal capacity of fluid

$$St = \frac{h}{\rho V c_p}$$

In which h is the heat exchange coefficient, ρ is the density of the fluid, V is the speed of the fluid and the latter is its specific heat at constant pressure. [43] The heat exchange coefficient is then calculated as

$$h = \rho V c_p St$$

Stanton coefficient is also defined in terms of Reynold, Nusselt and Prandtl coefficients

$$St = \frac{Nu}{Re \cdot Pr}$$

Reynolds number in each time step of the simulation is obtained from the ASTOS output file; Prandtl number is supposed constant as pressure and speed vary, and equal to 0.71. Nusselt number, in this case of forced convection and isothermal flat plate, is expressed as a function of the Reynolds number and the Prandtl number. The empirical correlation chosen is Gnielinski's, as it covers mostly the turbulent regime (it is valid for $0.5 \leq Pr \leq 2000$, and for $3000 \leq Re \leq 5 \cdot 10^9$)

$$Nu_{avg} = \frac{\frac{f_{avg}}{8} \cdot (Re_{avg} - 1000) \cdot Pr_{avg}}{1 + 12.7 \sqrt{\frac{f_{avg}}{g}} \cdot \left(Pr_{avg}^{\frac{2}{3}} - 1\right)}$$

In this case f is the Darcy friction factor, which is obtained by Petukhov empirical relation [44]

$$f_{avg} = \frac{1}{[0.79 \cdot \ln(Re) - 1.64]^2}$$

- Adiabatic wall temperature (recovery temperature)
  This is the temperature achieved by a wall in liquid or gas flow in the condition of thermal insulation (no temperature variation along an axis perpendicular to the surface

$$\left(\frac{\delta T}{\delta n}\right) = 0$$

The difference between the adiabatic wall temperature and a characteristic flow temperature may depend on the dissipative heat release in the boundary layer, on the existence of internal heat sources and on the thermal effect of other bodies (walls). In this case, only the latter option is considered. For a compressible gas, the relation that expressed this quantity is

$$T_{rec} = T_\infty \cdot \left(1 + r \cdot \frac{\gamma - 1}{2} \cdot M_\infty^2\right)$$

Where:
- T_∞ is the static temperature of the free air flow
- γ is the isentropic exponent of thermal equations
- M_∞ is the Mach number of the external air flow
- r is a parameter that depends on the character of the flow on the surface, the flow regime, and the thermal properties of the fluid. It is possible to approximate it (under the hypothesis of turbulent flow and Prandtl number close to 1) as follows [45]

$$r \simeq \sqrt[3]{Pr}$$

In conclusion, the temperature profile on the external shell of the fuselage results to be
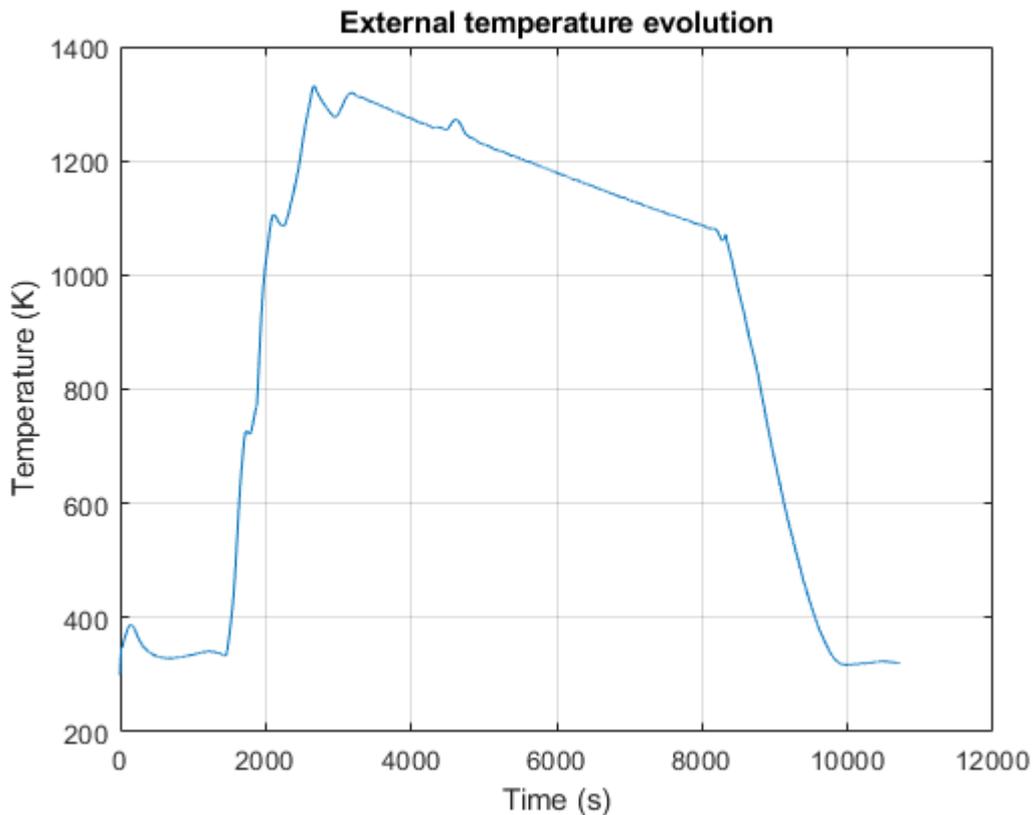
Figure 128: temperature profile on the external layer of the aircraft

6.4.3.2. Tank
6.4.3.2.1. Initial conditions
In this simulation, a single cylindrical tank will be described. As described earlier, this configuration is not realistic, and a proper emptying sequence of the multiple tanks could be provided as their position within the aircraft and geometry will be fully established. In the meanwhile, the hypothesis of a large single tank is acceptable, whereas the global result will be the same as implementing the single tanks with their own fuel transfer system.

Starting condition of the fuel will be now listed:

- Mass $170430\ kg$ [46]
- Temperature $15\ K$ [28]
- Pressure $10^5\ Pa$ [28]
- Density $76.1\ kg/m^3$
- Volume $2239.6\ m^3$

119

Cryogenic tanks are never completely filled, to prevent severe pressure drop in the tank after engine start. On the ground, the space between the top of the propellant load and the top of the tank is known as ullage space; in this case, the volume assigned for this "buffer" is the 5% of the total liquid volume. Part of LH_2 will normally tend to evaporate and fill this empty space; initial condition of this gas will be as follows:

- Mass $133.94\ kg$
- Temperature $20.26\ K$ (just above the evaporation point of hydrogen in this pressure condition)
- Pressure $10^5\ Pa$
- Density $1.34\ kg/m^3$
- Volume $111.98\ m^3$

The mass of gaseous hydrogen is computed with the perfect gas law:

$$m = \frac{p \cdot V}{\bar{R} \cdot T}$$

It is then possible to evaluate the size of the tank: since it has a volume equal to $2351.5\ m^3$, and assuming its length equal to $80\ m$, it results that it has a (circular) base of $29.39\ m^2$, with a radius of $3.06\ m$.

6.4.3.2.2. Simulation inputs
In the previous section, it was shown that the actual heat that penetrated the insulation layer by thermal conduction with the external environment was calculated as follows

$$\dot{q} = \Delta T \cdot \frac{\lambda_1 \lambda_2}{L_1 \lambda_2 + L_2 \lambda_1}$$

Now the temperature drop is defined, since the liquid hydrogen temperature is supposed to be constant at 15 K, and the outside temperature is defined. Is then possible to represent the heat that actually enters the tank
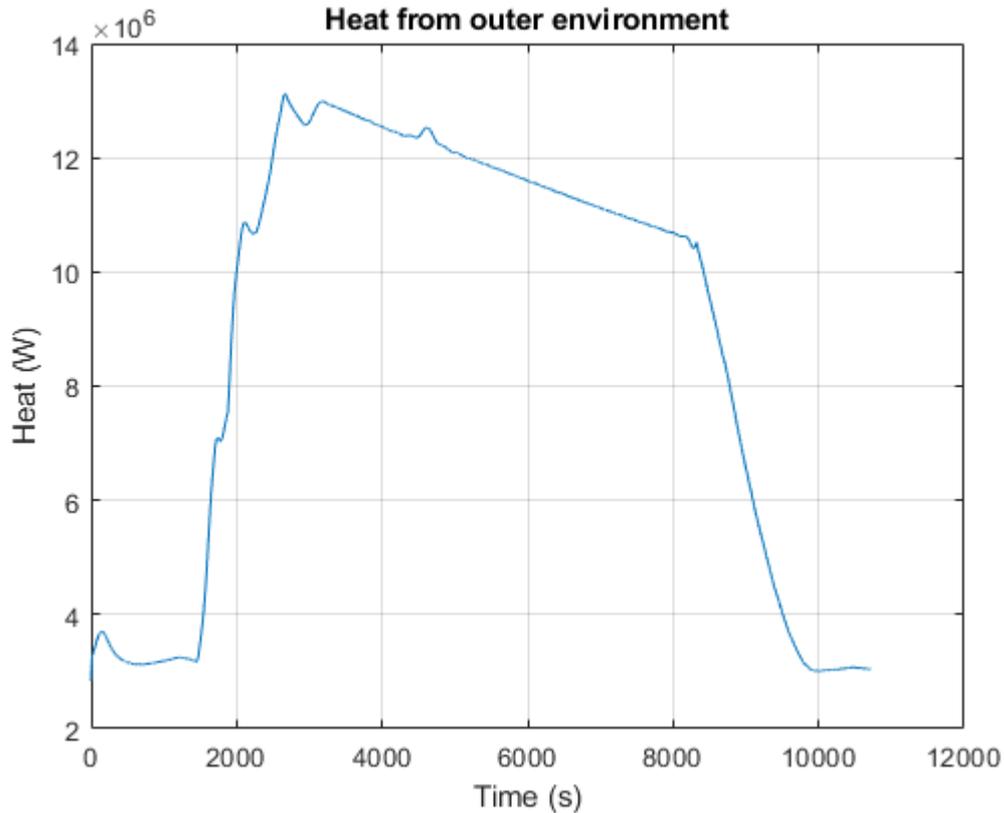
Figure 129: heat penetrating in the tank by conduction

The next analysis will permit to understand whether this heat is adequate for hydrogen boiling off purpose.

Since it is not possible (in Simscape environment, for the reasons named earlier) to dynamically simulate the behaviour of a mixture of liquid and gaseous hydrogen under the effect of a heat source, an assumption must be made. In order to analytically study what happens to both phases and then send the right input to Simscape, it is important to remember that no multiphase analysis will be made due to the lack of fundamental components in the related library: hence, the analysis of the liquid and gaseous parts will be divided. First, it is assumed that the incoming heat leaves the most of liquid hydrogen mass unchanged in pressure or temperature. It is then calculated the mass of hydrogen affected from this heat, assuming that this mass is lead to the evaporation temperature (in tanks pressure conditions, from the starting tank temperature) and then provided the heat necessary to vaporise. To sum up, it is calculated the exact mass of hydrogen that can evaporate with the external heat, while the rest of the hydrogen Is left liquid and unchanged.

First, the definition of heat capacity is recalled, as the ratio of the amount of energy transferred to a material and the change in temperature that is produced

$$C = \frac{Q}{\Delta T}$$

The equation can be written in terms of specific heat capacity $\left(c, \frac{kJ}{kgK} \right)$

$$Q = mc\Delta T$$

The total amount of heat that is necessary to boil a certain amount of hydrogen is given as the sum of the heat necessary to rise his temperature until the boiling point and the heat to shift the phase from liquid to gas. The latter quantity is expressed in terms of latent heat, i.e. the energy released or absorbed, by a body

121

or a thermodynamic system, during a constant-temperature process. It can be expressed as specific latent heat $\left(L, \frac{kJ}{kg}\right)$

$$Q = mL$$

In which Q is the amount of energy released or absorbed during the change of phase of the substance.

It is assumed that the whole process happens at constant pressure (the tank is supposed to be at constant, atmospheric pressure), so the specific heat can be approximated as the specific heat at constant pressure, c_p.

The whole thermodynamic process can be summed up as follows

$$Q_{ext} = mL + mc\Delta T$$

Since the variable is the evaporating mass, the equation is rearranged

$$m_{evaporating} = \frac{Q_{ext}}{L + c\Delta T}$$

The evaporating mass can follow a double path: part of it tends to take up the space left free from the evaporating liquid, and the rest will be vented out the tank in order not to increase its pressure. The mass that remains in the tank is evaluated in its pressure condition, fill the volume left free, according to the perfect gas law.
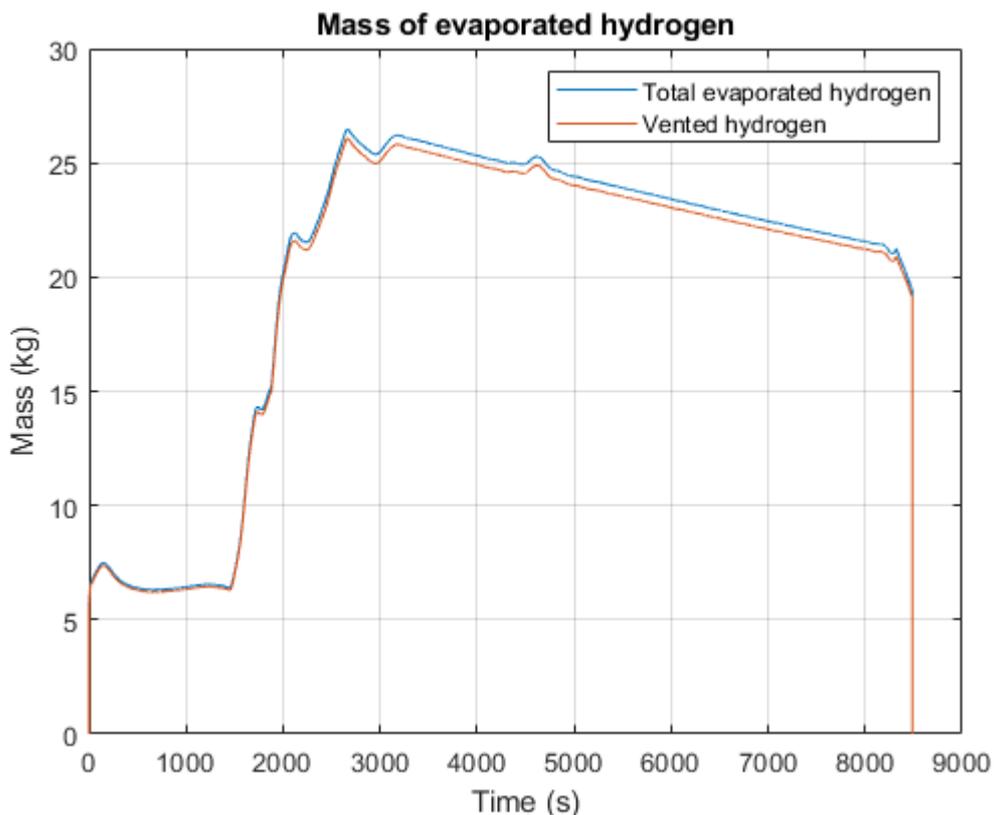
Figure 130: mass of hydrogen evaporating due to external heat

The plot of the evaporating hydrogen abruptly stops before the end of the flight, since the last part of the mission is thought to be unpropelled and requires no more fuel. During the rest of the mission, gaseous

hydrogen ends up feeding the engine, just like its liquid counterpart. It is then natural to compare the available boiled-off hydrogen with the fuel required by the engine

Fuel mass
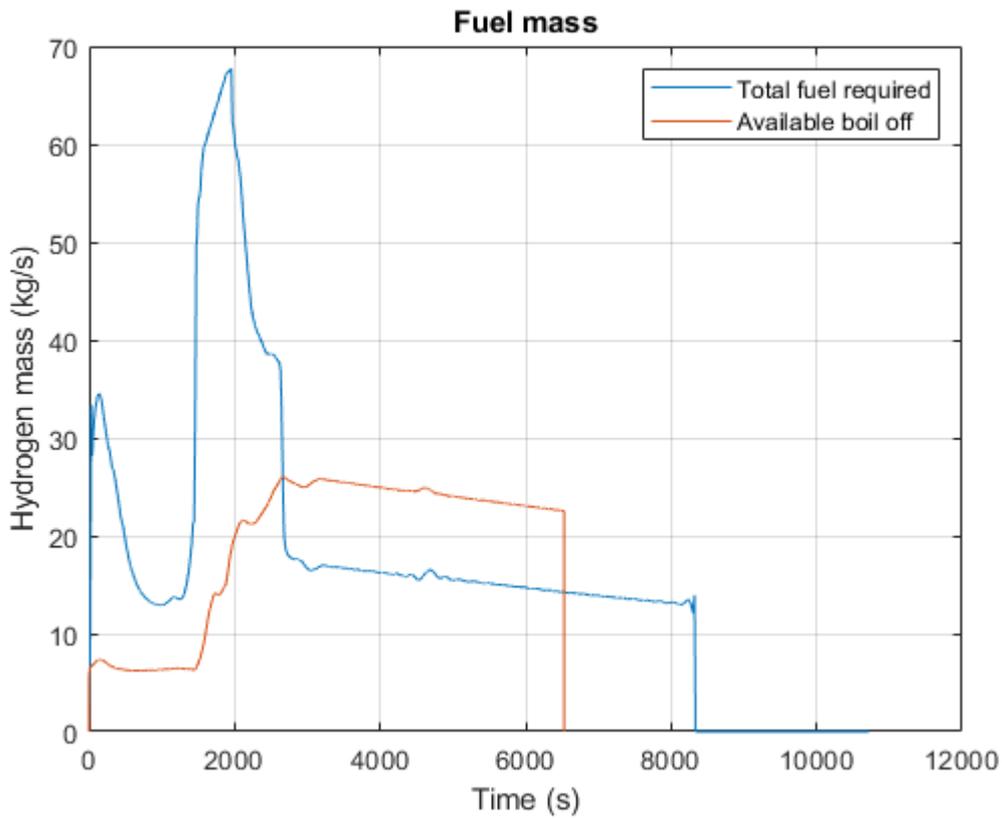
Figure 131: comparison between required fuel and available boil off

It is evident that in the in the first part of the mission (until 2662 seconds from the start) the boil off is not enough to provide the full feeding of the engine. On the other hand, after that moment, the available gaseous hydrogen is enough to guarantee the correct fuelling of the engine until a certain point (approximatively 6529 seconds). Before the latter point the boiled off hydrogen seems even too much to feed the engine, but then boil-off mass flow abruptly interrupts, since there is no remaining fuel to vent. In the graph it is shown an approximate situation, given that the evaporated hydrogen should not be damped in the exact moment it is created. However, in the latter case, the constant pressure in the tank cannot be guaranteed, since it should become a source of gas whose generation rate is greater than its damping rate (at least in the time range $2662 \leq t \leq 6529 \; seconds$).

A possible solution to keep the pressure inside the tank constant is to provide a better thermal insulation of the tanks: if a thicker layer of foam is inserted, less heat can flow into the tank, and thus make hydrogen evaporate. For example, a situation with a $72 \; mm$ thick insulation layer is shown

123
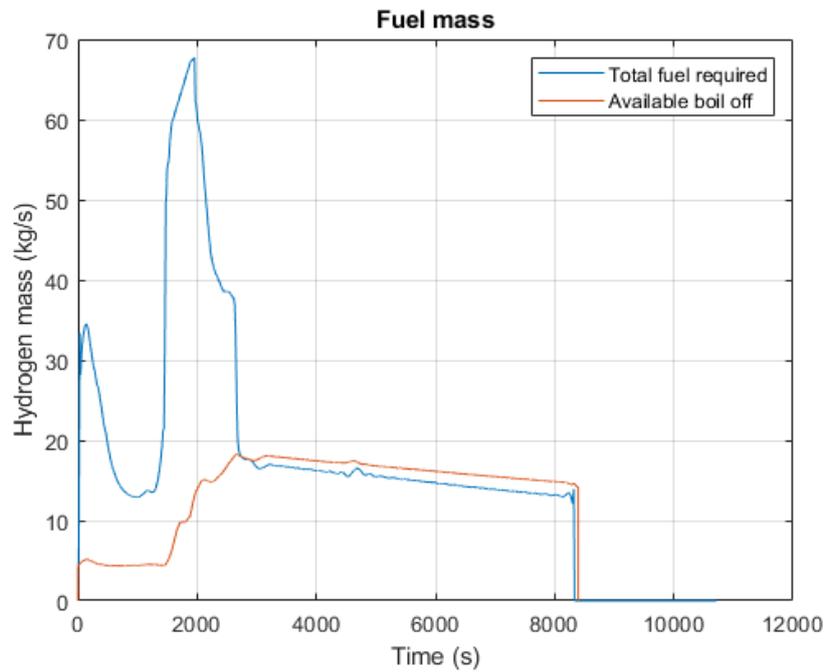
Figure 132: boil off management with thicker insulation layer

It is clear that this configuration provides better fuel feeding for the engine (no excessive amount of gas accumulating within the tank) until the end of the engine required working time. In this work, from now on, this average thickness of the insulation will be considered.

In the next picture is shown the amount of liquid hydrogen necessary to fuel the engine in the first mission time range, until when boiled off hydrogen becomes enough to feed the power plant.
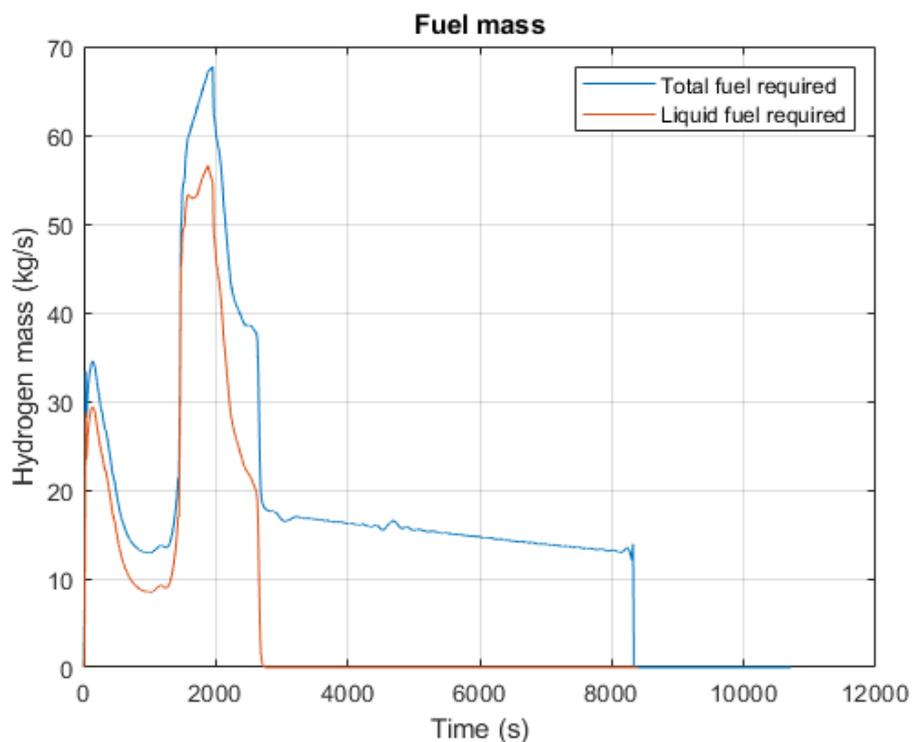
Figure 133: liquid fuel management

Unfortunately, it is necessary to provide a pump to set the liquid hydrogen in motion toward the engine. This mechanical element is not optimised, since it must work in a wide variety of mass flow rates (no fixed design point). If the pump is fixed displacement type, it will perform the pressure drop with a great set of angular velocities, hence non guaranteeing the maximum efficient during most of its working time. In addition to this, the pump must be oversized in comparison to the mission, since

- The peak mass flow required is substantially greater than the rest of the mass request
- The pump stands completely unused for the greater part of the mission (i.e. when the boil-off hydrogen can manage the whole fuel supply itself).

6.4.3.3. Pump

The fixed displacement pump requires a geometrical and performance characterisation, consisting mostly in:

- Nominal shaft angular velocity: a value of $150 \ ^{rad}/_s$ is chosen, as a well-tested working point in similar conditions;
- Displacement parameter: a value of $2.1 \cdot 10^{-3} \ ^{m^3}/_{rad}$ is chosen, in order to guarantee a proper fuel mass flow rate without exceeding the maximum speed ($\sim 4000 \ rpm$) [47];
- No-load torque: this is related to the moment of inertia of the pump, which is its resistance to changes in angular velocity as it rotates about its shaft. Knowledge of the moment of inertia of a pump, motor and associated components is required for transient analysis of a pumped system. In this case only pump impeller inertia will be considered, since motor inertia will be evaluated in a subsequent paragraph, and shaft and transmission inertia are negligible. Wylie relation is used

$$I_P = 1.5 \cdot 10^7 \cdot \left(\frac{^{\rho \cdot Q \cdot h \cdot g}/_{\eta \cdot 10^3}}{N(rpm)^3} \right)^{0.9556} = 2.5 \cdot 10^{-3} \ kg \cdot m^2$$

It takes account of rotational speed and pump power, evaluated in terms of volumetric flow rate, differential heat and pump efficiency [48];
- Efficiency: typical efficiency for high performance centrifugal pumps, $\eta = 0.8$ [49].

6.4.4. Simulation outputs

The simulation is launched under the above-mentioned hypothesis. The results are shown in the following paragraphs.
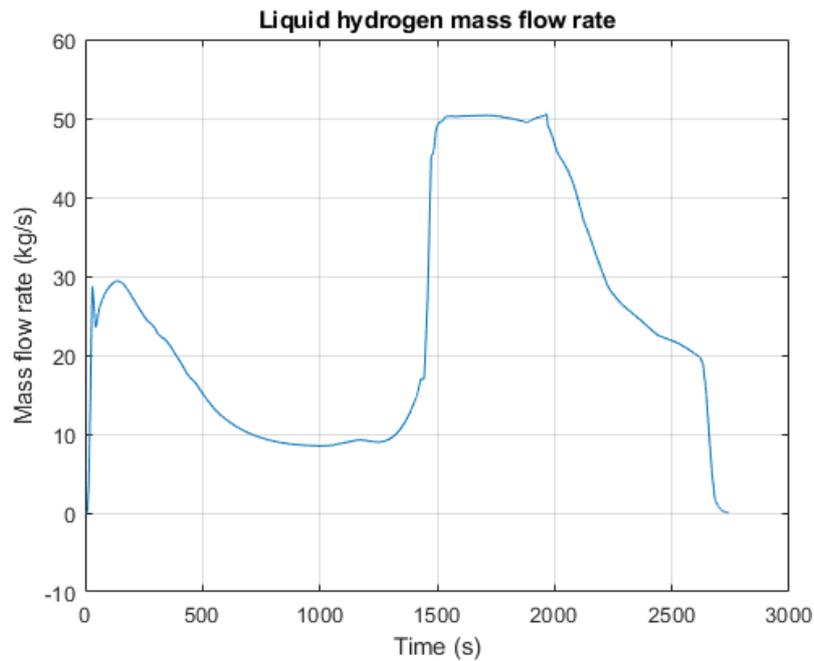
Figure 134: liquid hydrogen mass flow rate

As expected, the pump is able to manage the exact amount of required mass flow rate of liquid hydrogen within the pipeline.

6.4.4.2. Temperature
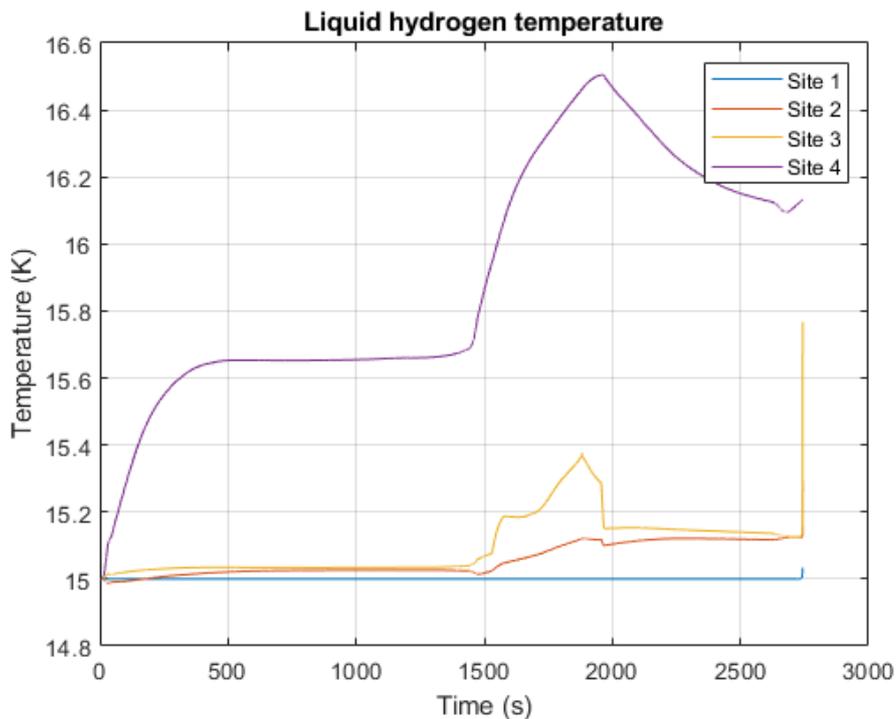
Figure 135: liquid hydrogen temperature in several stations across the pipeline

It is possible to see the temporal evolution of temperature in 4 stations scattered along the pipeline (as seen in the global model picture). Clearly, the temperature profile in every station tends to increase following mass rate profile, since more fuel in the same time interval means more speed, and hence more friction

(which increases the temperature). In addition to see, each station measures a greater temperature, since in the gap between them there are major physical components (pump or pipes) which simulate real thermal effects. The greater rise in temperature is in the fourth station, since it follows the propulsion plant heat exchanger; however, temperature stays almost unchanged for most of the time, ensuring the liquid phase to persist.

6.4.4.3. Pressure
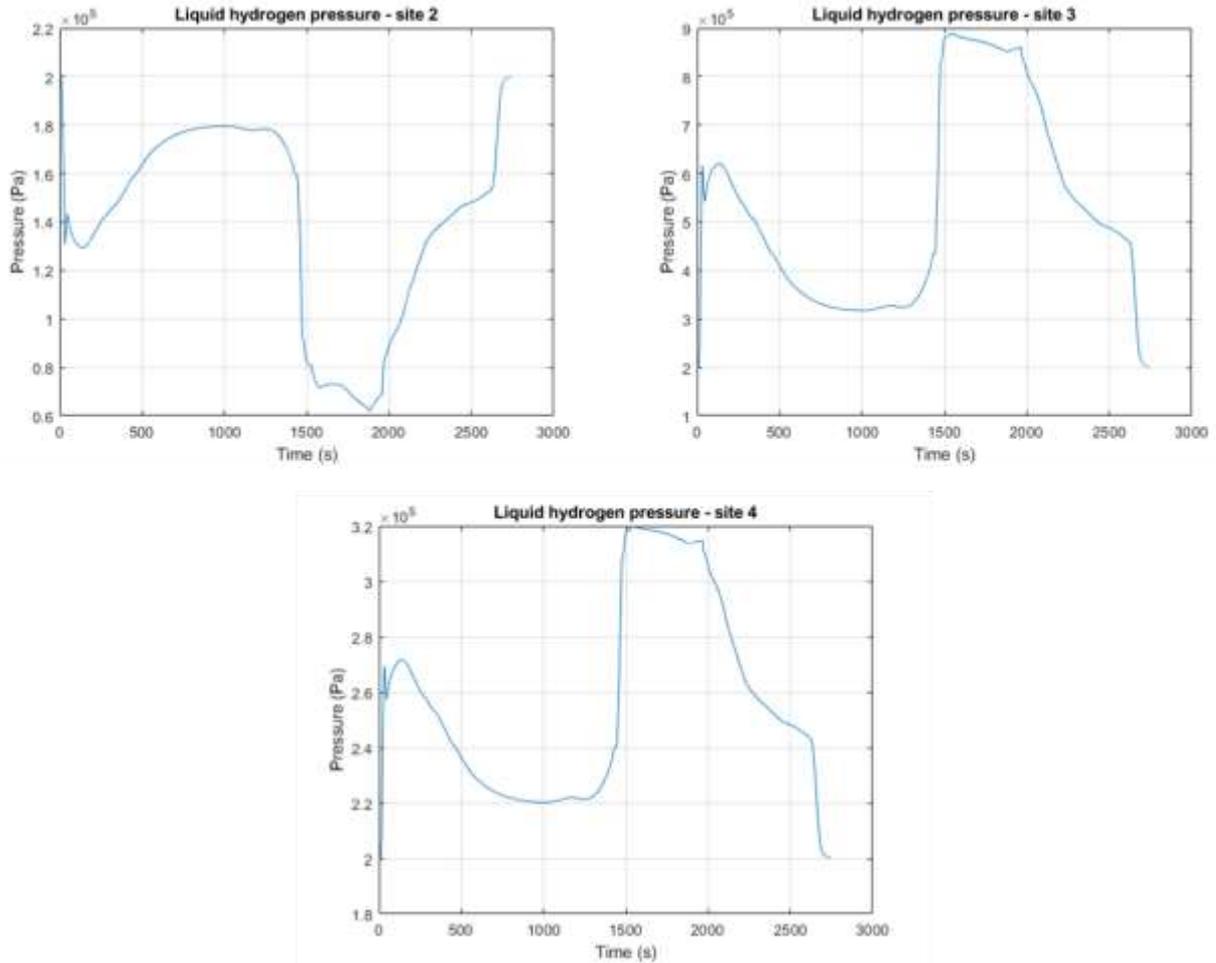
Figure 136: liquid hydrogen pressure in 3 stations

The picture shows the evolution of pressure in three sites along the pipeline. The first one is placed immediately before the pump, and it is evident the pressure reduction due to the pump aspiration. The second graph shows the pressure rise due to the pump power. In the last one, the effect of increasing temperature across the heat exchanger is clear.

6.4.4.4. Density
This quantity follows accurately temperature and pressure trends as follows
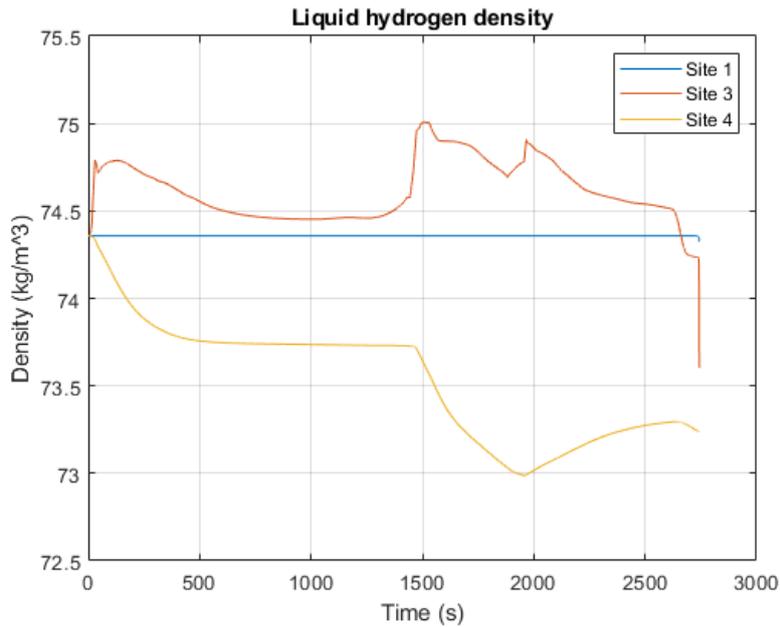
*Figure 137: liquid hydrogen density variation in sites 1,3,4*
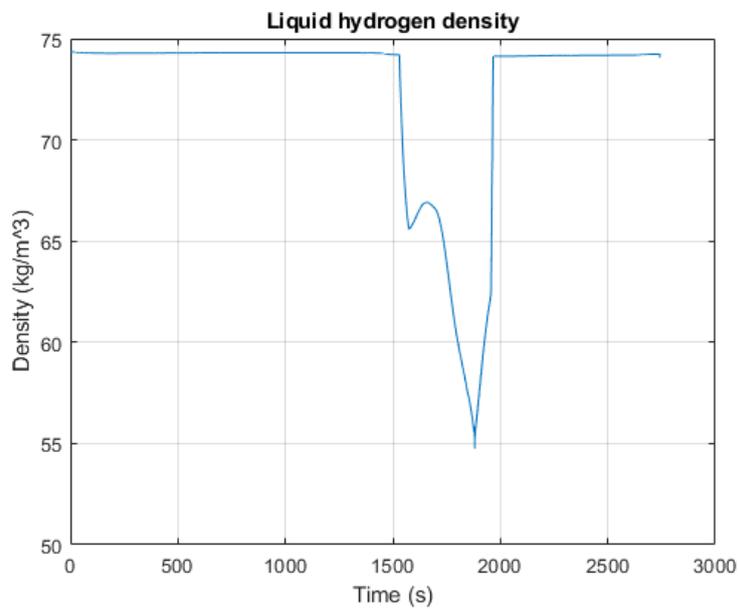
Figure 138:liquid hydrogen density variation in site 2

This representation is split in two to better show the small variation in stations 1 (in which, as temperature and pressure, is measured in tank condition), 3 (after the pump) and 4 (after the heat exchanger). In the second station the situation is different, since the simultaneous pressure drop and temperature rise cause the density to fall rapidly, still maintaining hydrogen in is liquid state.

6.4.4.5. Pump
Next pictures show the actual dynamic behaviour of the pump from the mission start to the moment in which the liquid hydrogen mass flow rate is no longer necessary to feed the power plant.
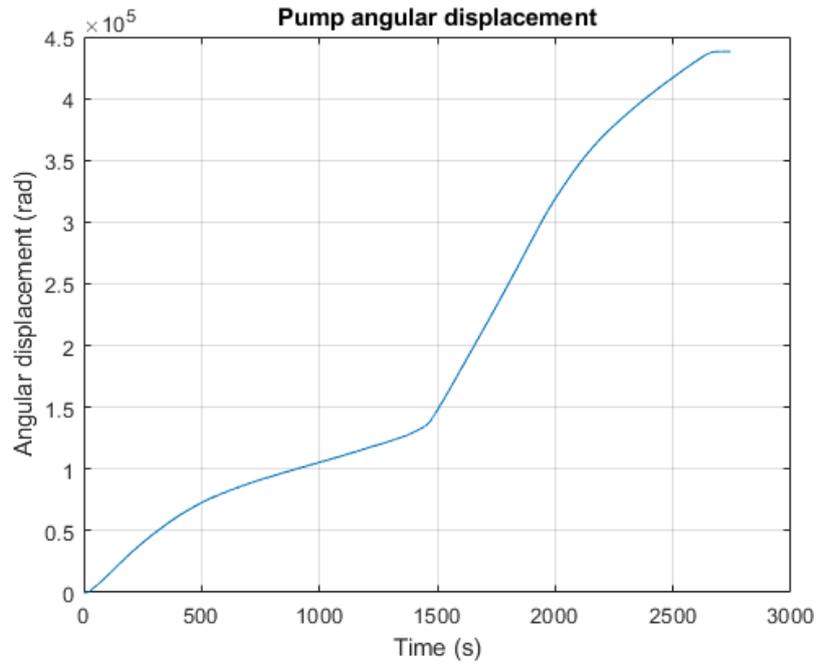
*Figure 139: cumulative pump angular displacement*
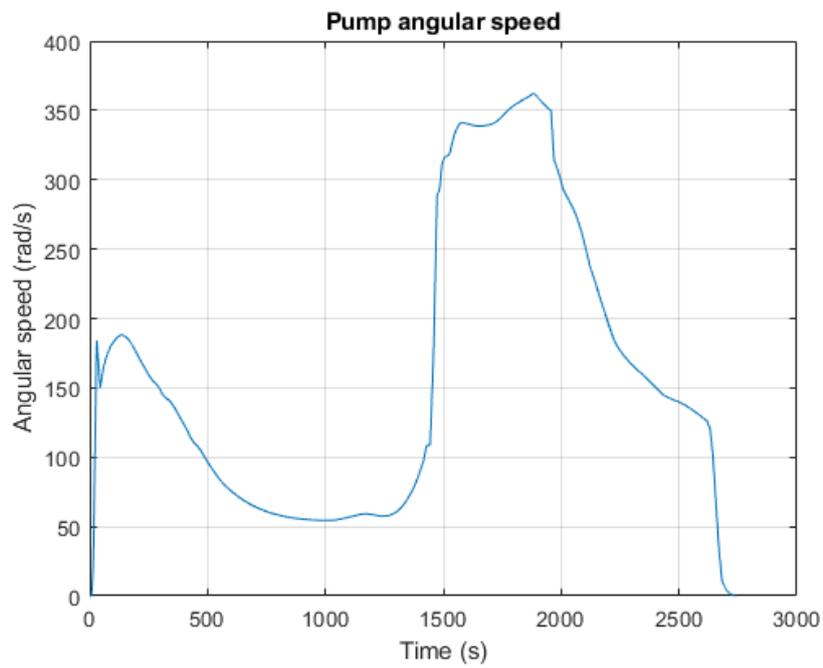

Figure 140: pump angular speed
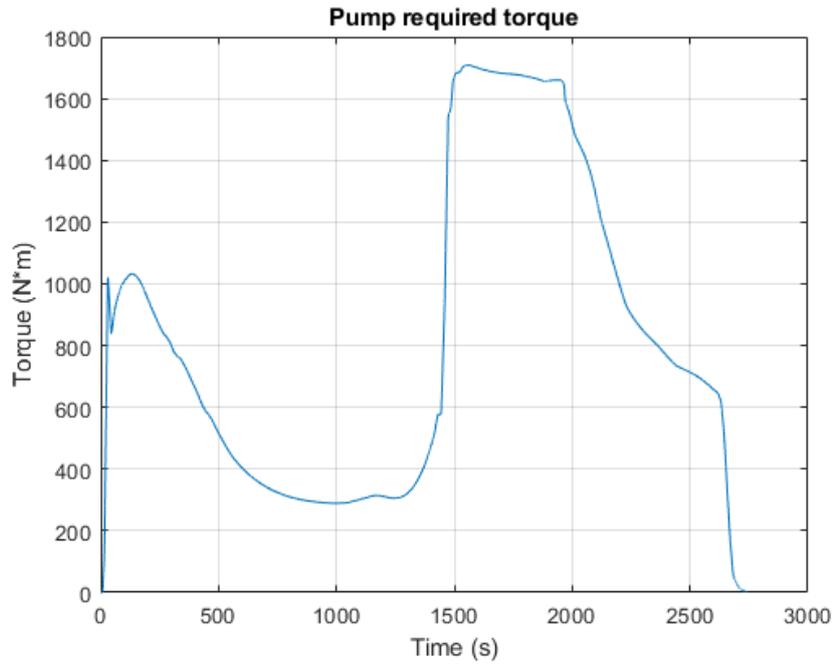
Figure 141: pump required torque
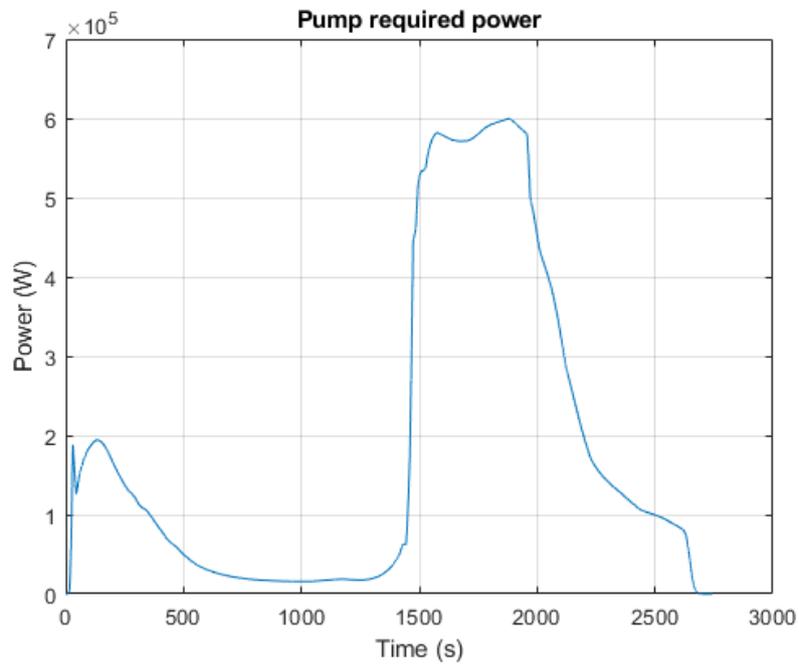
Figure 142: power absorbed by the pump

Required power of the pump is obtained as the product of the torque and the angular speed, as follows

$$P = \tau \cdot \omega$$

This power should be provided an external energy source; the following chapter will investigate whether the electrical power obtained as an output of the free turbine will be enough to feed the pump and the rest of the aircraft power budget.

6.5. Gaseous hydrogen line
The overall working scheme of this section will be divided in three parts for the sake of clarity.

6.5.1. Air Pack

6.5.1.1. General description
The environmental control system of an aircraft provides air supply, thermal control and cabin pressurisation as main functions. In the following paragraph all of those purposes will be investigated. Secondary functions of the ECS, such as smoke detection, cooling of avionics, gearboxes, transmissions, and fire suppression will be neglected in this analysis, as they are left open for further and more detailed studies.

- Air supply: typically, it is provided by the aircraft pneumatic system; in particular, it is supplied by bleed air tap-offs on each engine compressor section or from the APU pneumatic supply. Bleeding air is extracted upstream the combustor, and its condition depend on the compressor stage chosen, the power setting of the engine and the operating mode of a manifold pressure regulating shut-off valve. Sometimes this flow passes through a first heat exchanger, known as "pre-cooler", that cools it down by energy exchange with an air flow bled from the turbine.
- Thermal control: in many cases, this function is carried out by a subsystem named PACK (pressurisation air conditioning kit). The quantity of bleed air flowing to the A/C pack is regulated by the "flow control valve" (FCV). Downstream of the FCV is the actual Air Cycle Machine (ACM), whose working principle are listed below:
    - bleed air is guided through the primary ram air heat exchanger, where it is cooled by either ram air, expansion or a combination of both;
    - the air flux then enters the compressor, which add heat and rises the pressure;
    - the secondary ram air heat exchanger cools the air while maintaining the high pressure;
    - the air then passes through a turbine which expands the air to further reduce heat and lower the pressure. The energy extracted from the air passing through the turbine is used to power the compressor;
    - the air flow then is directed to the re-heater before it passes to the condenser for water extraction. Water separator operates with no moving parts: air is forced through a fiberglass sock that condenses and coalesces the mist into larger water drops. The convoluted interior structure of the separator swirls the air and water. The water collects on the sides of the separator and drains down and out of the unit, while the dry air passes through. This water removal process prevents ice from forming and clogging the system and keeps the cabin from fogging on low altitudes. This stage provides a filter as well, to remove dirt and oil from the engine bleed air;
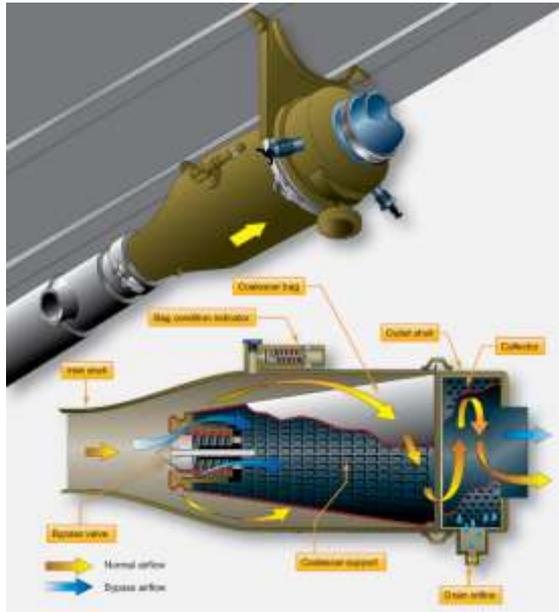
Figure 143: water separator working scheme [50]

o the temperature is controlled by the adjusting flow through the ram air system and modulating a temperature control valve (TCV), which bypasses a portion of the hot bleed air around the Air Cycle Machine and mixes it with the cold air downstream of the ACM turbine.
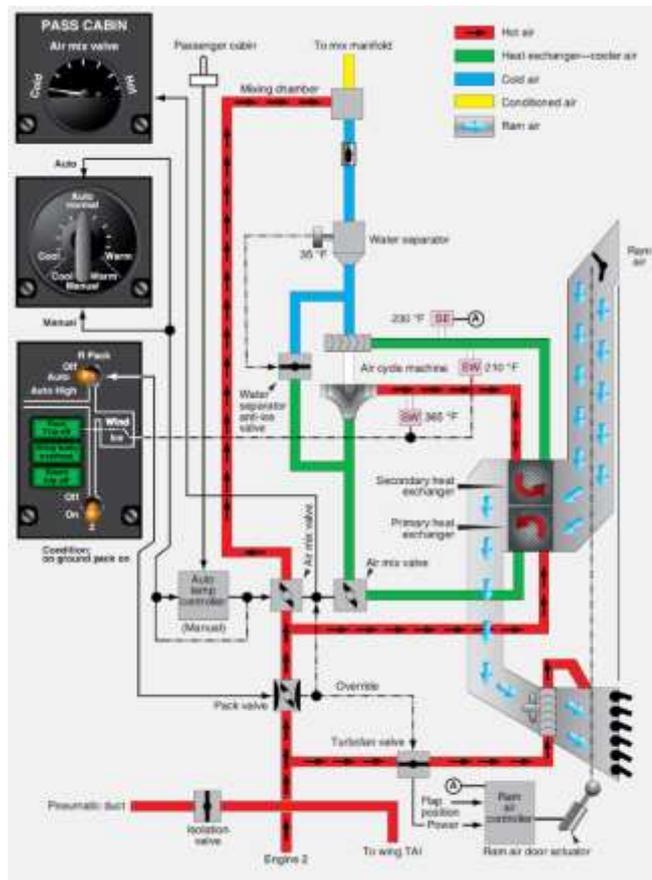

Figure 144: air cycle air conditioning system on a Boeing 737 [50]

- Cabin pressurisation: the airflow entering the cabin rather constant, and requested pressure is maintained by varying the opening of the out-flow valve. To prevent pressure rise due to OFV valve

failure, at least two positive pressure relief valves (PPRV) and at least one negative pressure relief valve (NPRV) are provided to protect the fuselage from over- and under- pressurization. Aircraft cabin pressure is commonly pressurized to a "cabin altitude" of 2400 m; hence nominal cabin pressure and temperature are.

$$p_{cabin} = 75 \; kPa$$
$$T_{cabin} = 300 \; K$$

6.5.1.2. Architecture

The following picture show a simplified model of the cold air unit subsystem.
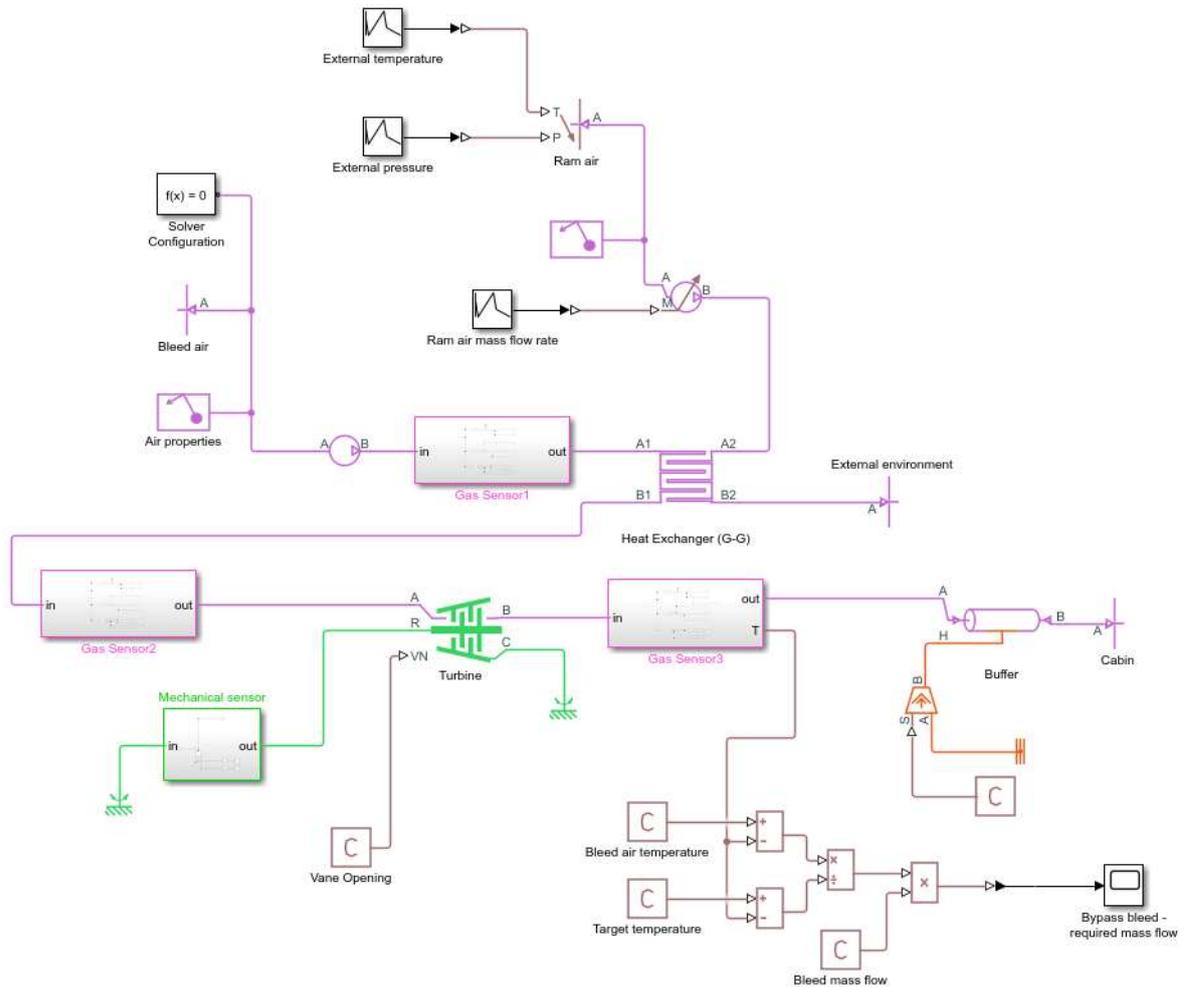

Figure 145: cold air unit Simscape model

The scheme shown above comprises only the most important element of a real air pack, since there is only one ram air heat exchanger, no compressor and no water separator.

The left branch of the picture shows the bleeding air exacted from the propulsion plant combustion stages in the following conditions [34]

	Temperature (K)		Pressure (bar)		Mass flow (kg/s)
	In	Out	In	out	
Air Pack	1000	300	10	0.75	3.6

The right branch shows the ram air mass flow, evaluated simplistically as

$$\dot{m} = \rho \cdot A \cdot u$$

133

In which ρ is the atmospheric air density, u is the flight path speed (both of them derive from Astos mission profile), and A is the surface of a hypothetical opening on the aeroshell into which air can flow with no distortion and further compression.

These streams couples in the heat exchanger; after that, the free flow from the outer environment is released, while the main stream expands and cools in a turbine; in the end, the fluid is at the right pressure, but rather cooler than the target cabin temperature. It is finally obtained upon mixing this flow with air which is spilled from the intake (as well) but bypassed the air cycle machine. The thermal balance is stated by the convection heat transfer law

$$\dot{Q}_{in} = \dot{Q}_{out} = \dot{m} \cdot c \cdot \Delta T$$

6.5.1.3. Components description

Turbine block working principles will be shown in the next section for a logic of prescribed continuity (since it will be coupled with a compressor).

The Heat Exchanger block models the complementary cooling and heating of fluids held briefly in thermal contact across a thin conductive wall. The model used is the Effectiveness-NTU method, in which the heat transfer of flowing fluid is computed as a fraction of the steady configuration (under the hypothesis of flows kept each as their inlet temperature, and cleared of every thermal resistance in between)

$$Q_{actual} = \epsilon \cdot Q_{max}$$

ϵ is known as "heat exchanger effectiveness", which is the fraction of the ideal heat rate, as long as losses are considered. Those quantities are defined as follows:

- maximum possible heat transfer (Q_{max}): achievable in a counter-flow heat exchanger of infinite length. One of the two fluids experience the maximum possible temperature difference, namely the difference between the inlet temperature of the hot stream and the inlet temperature of the cold stream, $T_{h,i} - T_{c,i}$. In terms of heat capacity (mass flow rate multiplied by specific heat)
$$Q_{max} = C_{min} \cdot (T_{h,i} - T_{c,i}) = \min|\dot{m}_c c_{p,c}, \dot{m}_h c_{p,h}| \cdot (T_{h,i} - T_{c,i})$$
  The minimum heat capacity must be used as it is the fluid with the lowest heat capacity rate that would, in the hypothetical infinite length exchanger, actually undergo the maximum possible temperature change.
- actual heat transfer (Q_{actual}). It can indifferently for each fluid, considering his heat capacity and temperature drop between inlet and outlet
$$Q_{actual} = C_h \cdot (T_{h,i} - T_{h,o}) = C_c \cdot (T_{c,o} - T_{c,i})$$

This quantity is a function of the number of transfer unit (NTU), that quantifies how efficient is the heat exchanged between flows, in relation to fluid's ability to absorb that heat; basically, is the ratio between the actual heat transfer rate and the maximum possible heat transfer rate

$$NTU = \frac{UA}{C_{min}}$$

Where U is the overall heat transfer coefficient and A is the heat transfer area. Effectiveness is also function of the geometry, in terms of heat capacity ratio C_r [51]

$$C_r = \frac{C_{min}}{C_{max}}$$

And also, of the relative disposition of the flows, the number of passes between them, and the mixing condition for each.

Flow arrangement

This parameter describes how the flows meet in the heat exchanger. The chosen configuration is known as "shell-and-tube". This type of heat exchanger consists of a shell (a large pressure vessel) with a bundle of tubes inside it.

Two fluids flow through the heat exchanger. One flows through the tubes (the tube side) and the other flows outside the tubes but inside the shell (the shell side). Heat is transferred from one fluid to the other through the tube walls, either from tube side to shell side or vice versa. In order to transfer heat efficiently, a large heat transfer area should be used, leading to the use of many tubes [52].
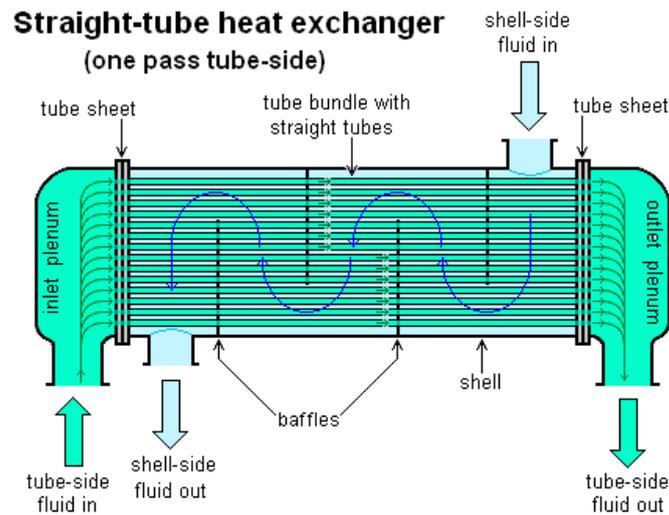

Figure 146: shell-and-tube heat exchanger configuration [52]

In this case, unmixed flows will be considered; this configuration is characterised by variable temperature in both the transverse and longitudinal planes. Shell-and-tube exchangers with multiple are the most effective configuration (compared with parallel and cross flow exchangers), as shown below
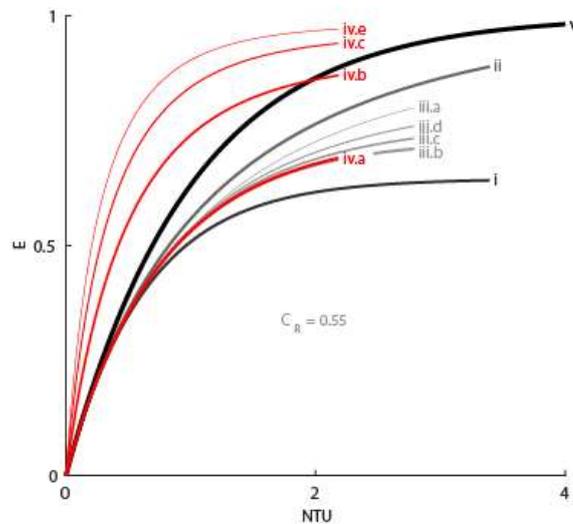

Figure 147: heat exchangers effectiveness for several configuration. Shell-and-tube is the series iv., and b, c, e stand for 2, 3 or 4 passes, respectively [51]

Thermal transmission

The transmission of heat between fluids can be considered in analogy with an electrical circuit, in which each component represents a "thermal resistance"; the total resistance to the heat transfer path is obtained as a series of the single ones
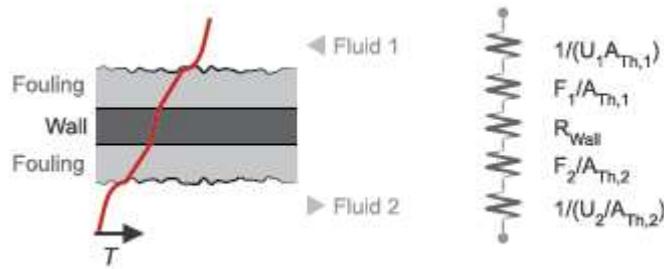

Figure 148: thermal resistances lining the heat transfer path

The expression is then

$$R = \frac{1}{h_1 A_{th,1}} + \frac{F_1}{A_{th,1}} + R_w + \frac{F_2}{A_{th,2}} + \frac{1}{h_2 A_{th,2}}$$

In which the single components represent respectively:

- Convection at the surfaces of the wall: it takes account of the convective heat transfer coefficients (h) and the heat transfer surface area. The first are computed as a function of fluid properties, flow geometry and wall friction; used equations are empirical correlations between Reynolds, Nusselt, and Prandtl numbers, whose choice depends on the flow arrangement and mixing conditions;
- Conduction through the wall: it simply accounts the wall as a single thermal resistance. A more complex model taking account of wall thermal capacity is available: heat storage slows the transition between steady states so that a thermal perturbation on one side does not promptly manifest on the side across. The lag persists for the short time that it takes the heat flow rates from the two sides to balance each other. This phenomenon is not considered in this analysis, since the actual mass of the pipes of the heat exchanger is required to proceed;
- Conduction through the layers of fouling: it takes account of the Fouling factor and the heat transfer surface area. Fouling consists in the accumulation of residuals on pipe wall; heat exchanger performances decrease over time as a result of accumulation of deposits on heat transfer surfaces, since this layer represents additional resistance to heat transfer. Since the flowing fluid is hydrogen, most common compounds are metal hydrates, that make the pipe material more brittle too; any residual and impurity can also be part of this layer.
  The phenomenon is quantified in terms of fouling factor, which is a measurement of the additional thermal resistance; it is 0 for a new heat exchanger, and rises as a function of operating temperature, velocity of the fluid and length of service. For this analysis a representing value is considered $F_1 = F_2 = 10^{-4} \frac{m^2 \cdot K}{W}$ [53] [54].

6.5.1.4. Results
In this section, the most important results of the simulation are shown.
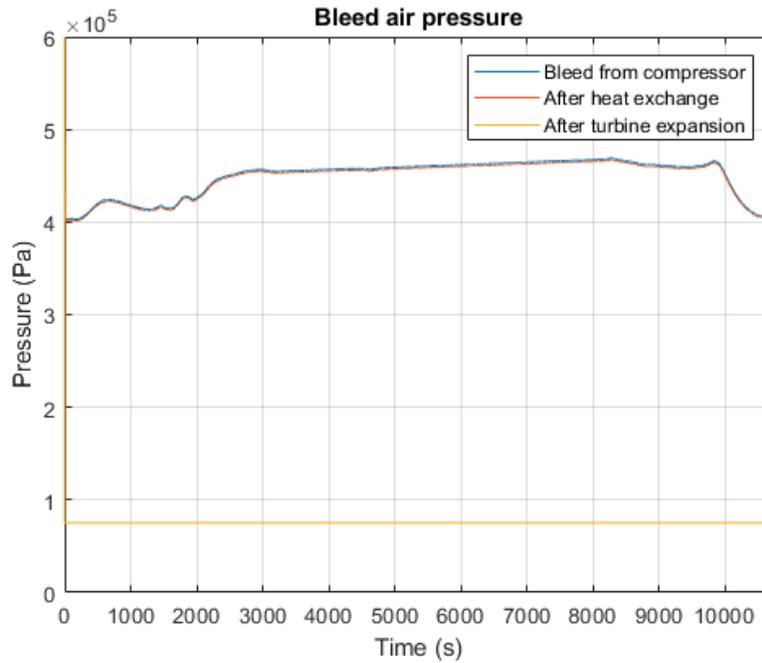
Figure 149: pressure evolution of bleed air through the air pack

First, the temporal evolution of pressure through the pipeline is shown. The heat exchanger provides only a negligible pressure drop ($\sim 2\ kPa, constant$), compared to the following turbine, in which most of the expansion happens. The components are set for the final pressure to be $75\ kPa$, namely cabin pressure.
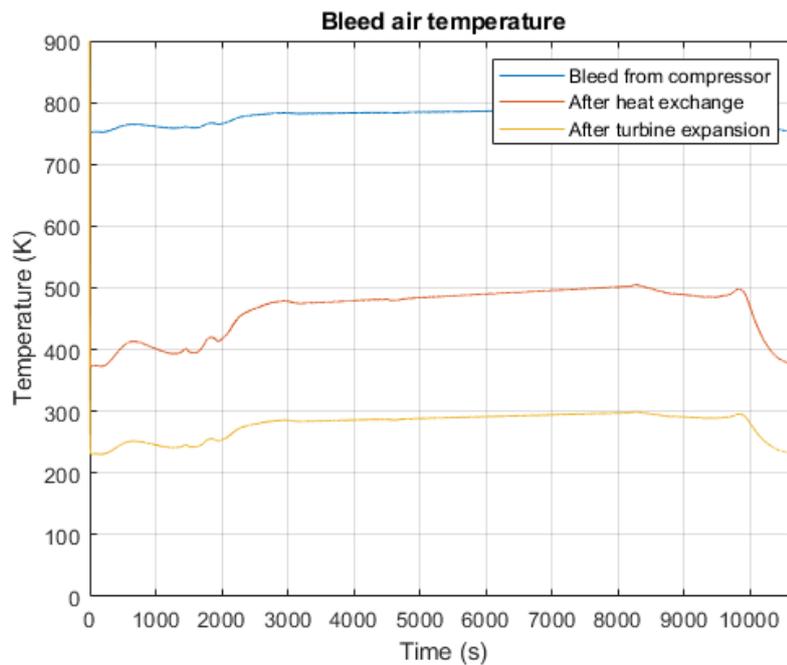

Figure 150: temperature evolution of bleed air through the air pack

The temporal evolution of temperature through the pipeline is shown. The heat exchanger provides a first temperature drop; it is followed by turbine expansion, in which air reaches sub-freezing temperature. Cabin temperature is obtained upon the mixing with a desired amount of bleed air that bypasses the whole air pack (and then keeping high temperature and pressure). The necessary air mass flow to be mixed with the main stream to enter the cabin is shown in the picture below

137
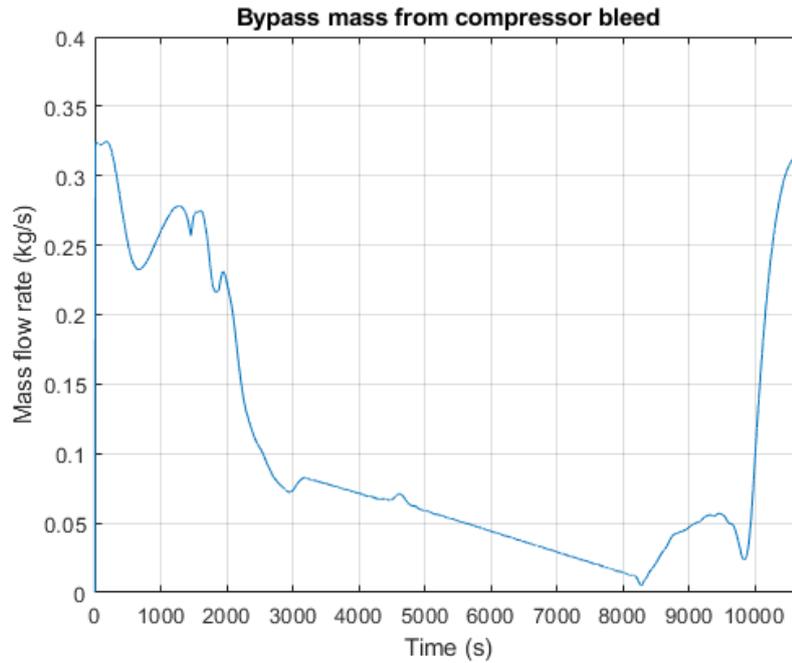
Figure 151: required mass flow rate from the compressor for final mixing

The amount of bypassed mass flow rate changes as a function of main stream temperature (whose mass flow rate is constant): low temperatures require a great amount of hot air to be mixed with, and vice versa.
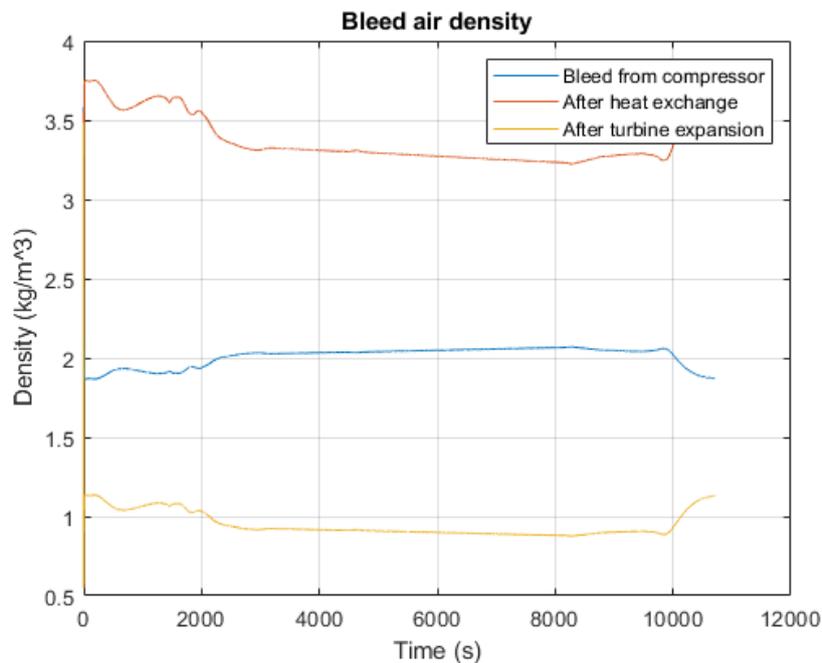

Figure 152: density evolution of bleed air through the air pack

The temporal evolution of density in the pipeline is shown. Final density is compatible with cabin environment, as it is both function of pressure and temperature. The graph shows that air density is greater after the passage through the heat exchanger: the pressure remains rather constant, and this is an immediate consequence of temperature drop.
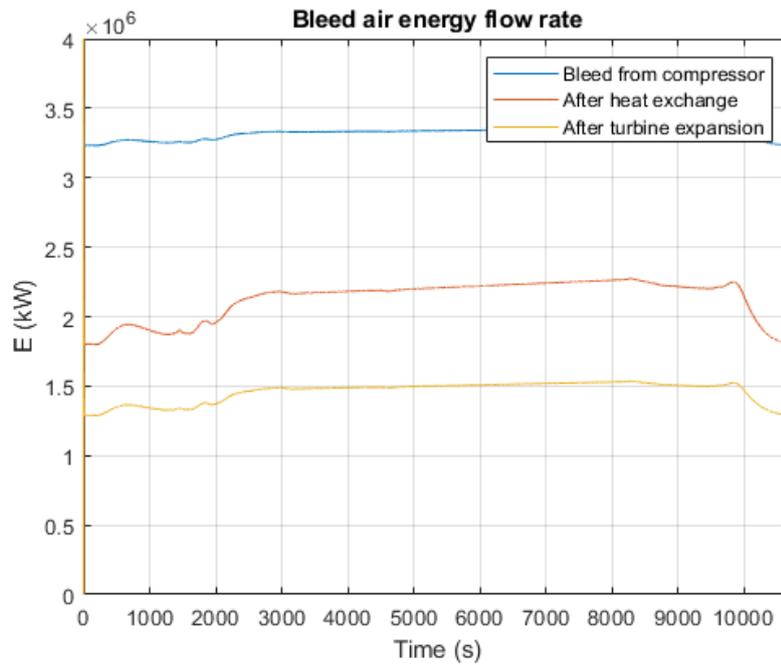
Figure 153: energy flow rate evolution of bleed air through the air pack

In conclusion, the temporal evolution of energy flow rate in the pipeline is shown. This physical quantity summarises the trends of temperature and pressure through those physical elements.

6.5.2. Heat exchangers

6.5.2.1. General architecture

The following picture shows the configuration of a part of the gaseous hydrogen pipeline, in particular the one involving the heat exchangers.
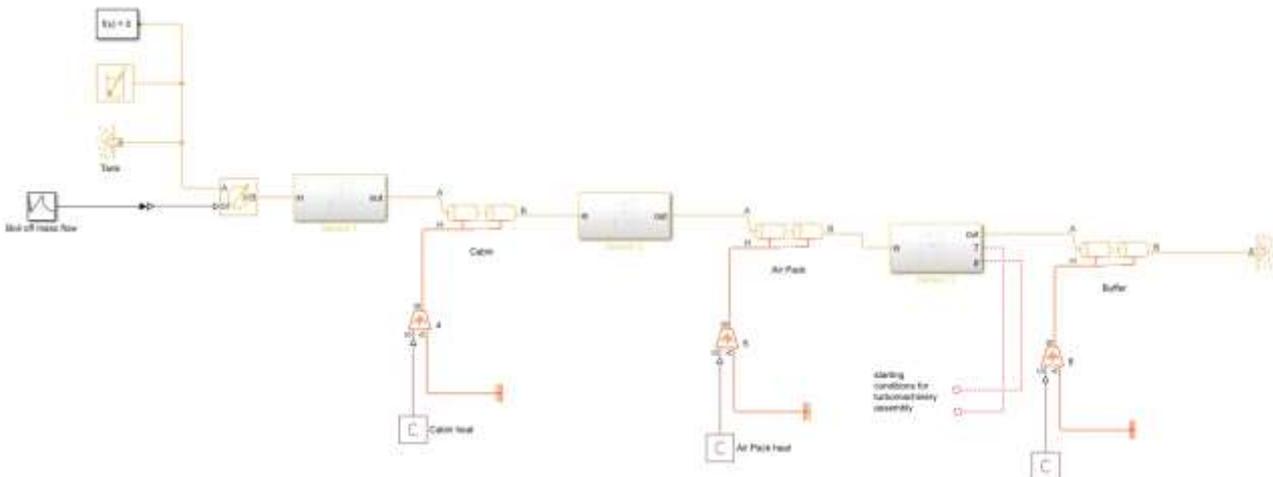

Figure 154: heat exchangers overall scheme

This scheme represents the ramification of the heat exchanging system, that enclose a large part of the aircraft: in this case, cabin and air pack heat are considered. This analysis is carried out in a conceptual design standpoint, since physical interfaces between actual aircraft component are not yet know with enough precision to better simulate a more complex heat exchanger model. By now, the geometrical configuration is known only macroscopically; for example, the cabin volume and air turnover inside and outside are known, but no further information are available about their interfaces and possible heat exchanger configuration. In

this case, each component will be considered as a simple interface with the fluid, and their interaction will generate heat exchange and several changes in fluid properties; basically, the interaction between fluid and each aircraft subsystem will be considered only by the energy exchange, which will be applied and distributed over the subsystem whole interface.

Eventually, fluid most important physical information (i.e. temperature and pressure) will be transmitted to the last part of this subsystem (the turbomachinery assembly) by fictional signals: this expedient is necessary to cope the lack of fluid interface components within Simscape libraries.

6.5.2.2. Description
6.5.2.2.1. Cabin
Passenger cabin is considered as a cylinder of appropriate volume ($\sim 300 \ m^3$) [55] which contains only air in proper condition of temperature and pressure (as prescribed from international regulations [56]). Heat exchange happens all along the fuselage length, as shown in the following picture
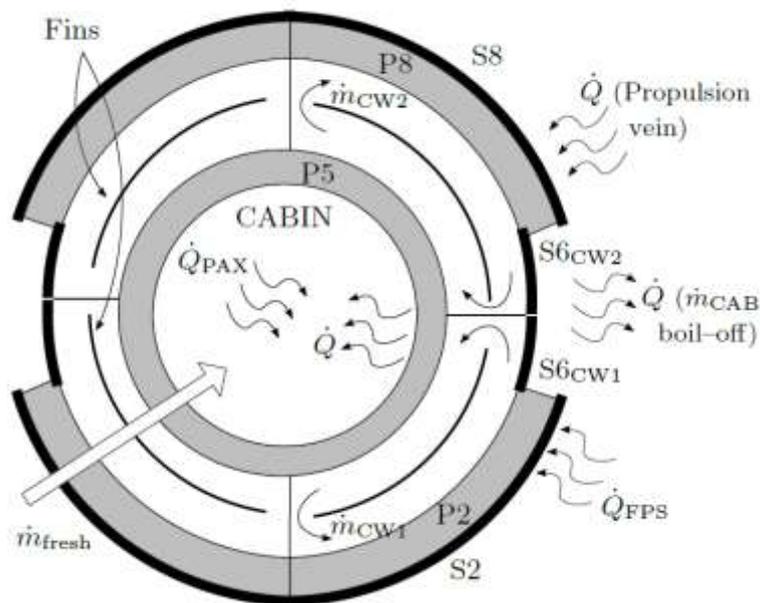
Figure 155: heat exchange between cabin and external insulating layer [28]

Hence, the thermal exchange surface will be considered as the whole cabin outside layer. Three main heat sources will be considered:

- Passengers body heat: the amount of heat generated by people organism depends on the "total metabolism", that consists in two main contributions.
  - Basal metabolism: the amount of energy used for vegetative activities. An average weight adult (75 kg) consumes 1720 $kCal/day$;
  - Extra-basal metabolism: the amount of energy used for routine activities. It burns 25% of daily calorie requirement;
- As first attempt estimation, an average of 130 $W/person$ will be considered (moderate office activity [57]);
- On board passenger services: the small amount of power necessary to entertainment and lighting. This amount is estimated as 70 $W/person$ [58].

Hence, it will be necessary to throw out a total amount of 200 $W/person$, namely 60 kW.

6.5.2.2.2. Air pack

As described in the previous paragraph, the air pack need a heat exchanger to dump the excessive temperature of air flowing into the cabin. This component simulates this coupling by a pipe (in which gaseous hydrogen flows) subject to heat input, which is spread on a reasonable surface (taken as reference from existing cold air units from civil aviation).

6.5.2.3. Results

At the beginning of this pipeline, gaseous hydrogen has just left the tank as it boiled off ($p = 1.01 \cdot 10^5 \ Pa, T = 20.26 \ K$). The evolution of some physical quantities, due only to heat absorption by the hydrogen flow, is shown in the next pictures.
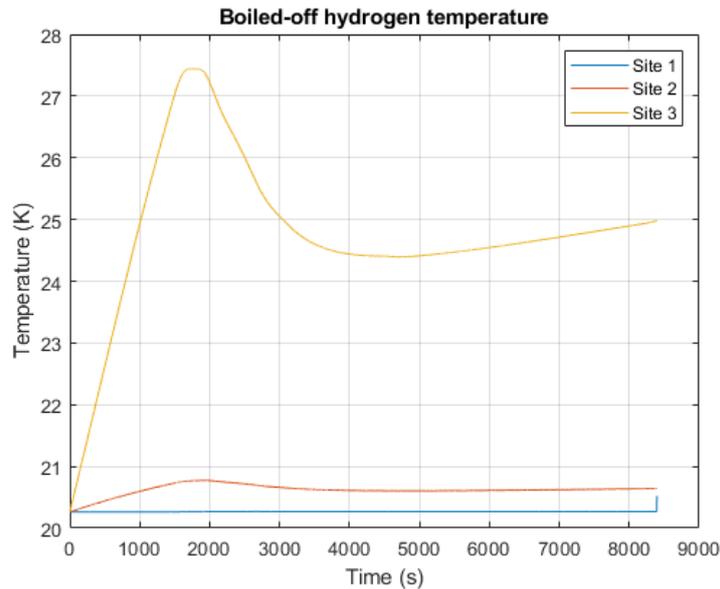
Figure 156: hydrogen temperature variation in three sites

Temperature evolution reflects heat introduction inside the system. Site 1 represents tank conditions' evolution in time, while site 2 measures hydrogen temperature after the cabin heat exchanger: as expected, a temperature increase is detected. Site 3 reveals the impact of the heat absorbed from the air pack heat exchanger, whose numerical value is much greater than cabin's.
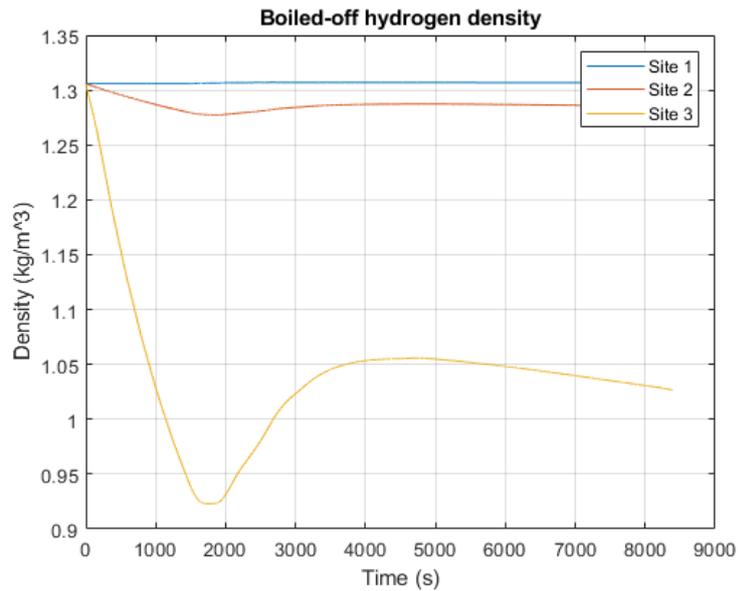
Figure 157: hydrogen density variation in three sites

Hydrogen density reflects temperature's trend, revealing that after the whole heat exchanging assembly the is a remarkable reduction of its density.

In conclusion, a comparison between fuel mass flow rate and its temperature is made.
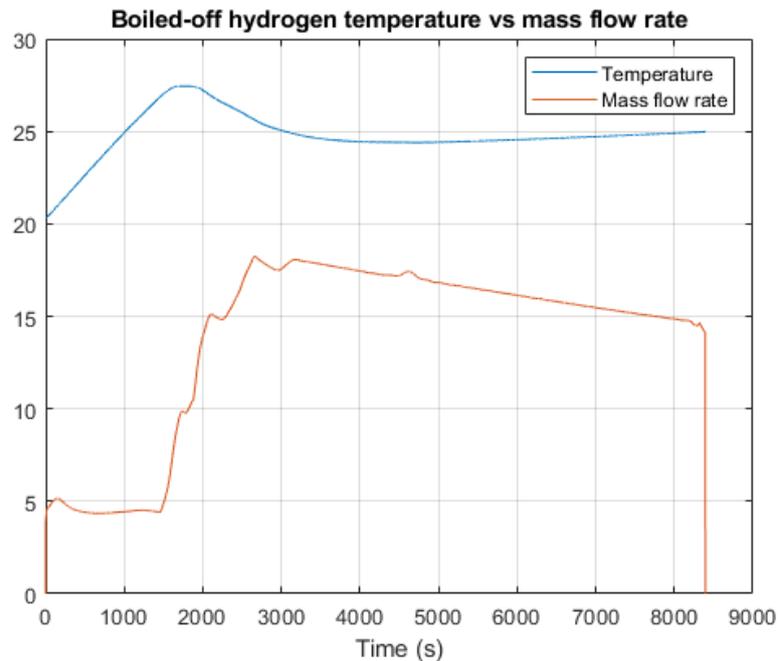

Figure 158: comparison between mass flow rate and temperature trends

The whole system can be described as a variable mass flow source subject to constant heat input. It is logical that the fluid temperature and the flow rate show a complementary trend: the same amount of heat can increase less the temperature of a greater mass per second flowing into the pipes. In particular, temperature increases since mass flow rate is rather constant, but start decreasing as the mass flow rate is greater. Local minimum of temperature is in correspondence with mass flow maximum, and then, as mass per second decrease, temperature start rising again. According to this logic, temperature trend shows some delay compared to mass flow too.

142

6.5.3. Turbomachinery and power generation

This subpart represents the core of the TEMS subsystem; the architecture described in the following paragraphs will be the new one, as it was mentioned qualitatively earlier.

6.5.3.1. Turboshaft architecture

The overall architecture of the system is reminiscent of that of a dual-shaft turboshaft engine with free power turbine, which will be taken as a reference in the next discussion. The presence of the free power turbine separated from the gas generator group, although not the only existing configuration, was preferred in this case for the advantage of being relatively independent of the operation of the rest of the engine and for greater flexibility in a wide range of operating ranges. [59] Moreover, this configuration allows to make the rotation speed of the shaft of power independent from that of the gas generator, allowing a more regular operation and a constant rotation speed.

The purpose of a turboshaft engine is exclusively the production of shaft power; the generation of hot gases with a certain speed at the exit of the turbine is a consequence to be minimized, since it is a symptom of further potential unexploited expansion in the turbine, and thus a possible unused enthalpy drop.

The next figure is a diagram of the operation of a typical turboshaft engine
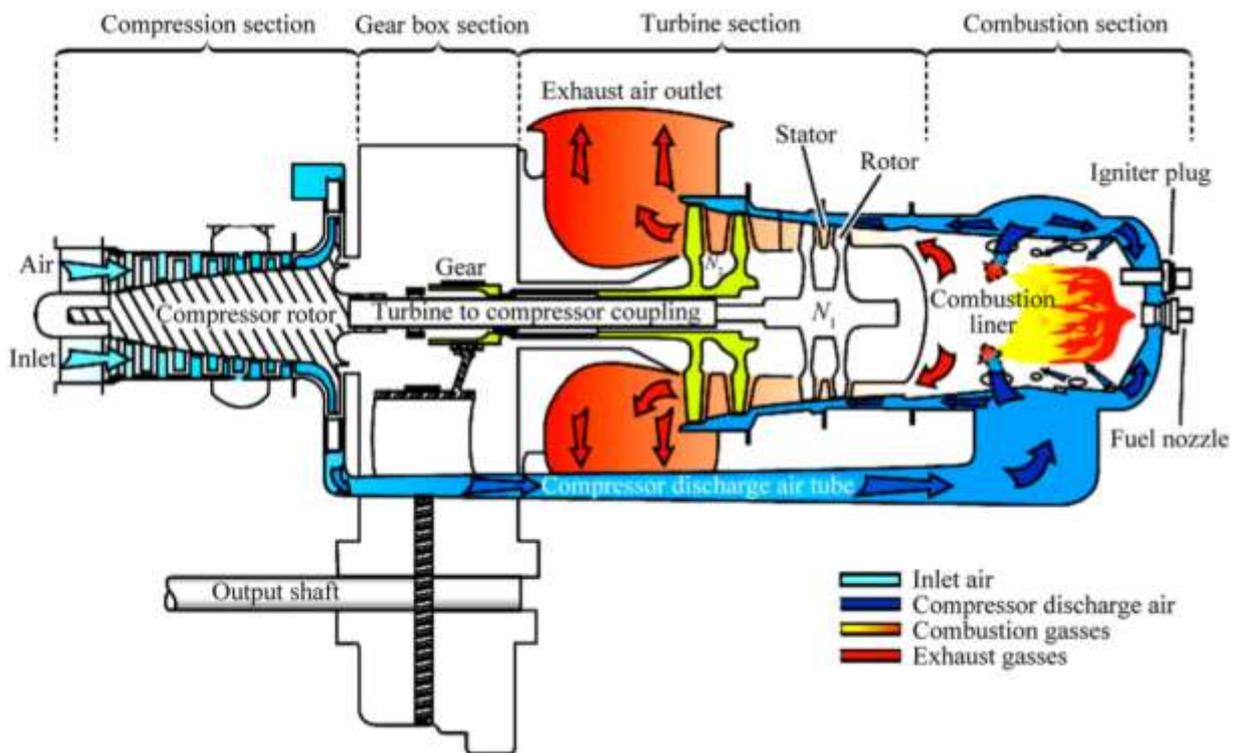

Figure 159: turboshaft engine schematics [60]

A typical architecture consists in a dual-shaft turboshaft engine with free power turbine, in which a low-pressure compressor and a high-pressure compressor are driven by the high-pressure turbine.

6.5.3.2. Brayton cycle

The Brayton cycle is the thermodynamic cycle commonly used in aircraft engines. Its turboshaft version mainly consists of:

- Compression stage: boiled-off hydrogen is compressed, ideally by an isentropic process (in the model, it will be considered adiabatic, but a compression efficiency η_c will be foreseen);

- Heat addition: gaseous hydrogen will be mixed with a proper amount of air (spilled from the intake) to reach combustion conditions (for further details, see the engine paragraph). The mixture is then ignited in a dedicated combustor, in which an ideal isobaric process happens;
- Expansion in the gas generator turbine: the heated gas mixture expands to provide mechanical power to the preceding compression stage, ideally by an isentropic process (in the model, it will be considered adiabatic, but an expansion efficiency $\eta_{t,T}$ will be foreseen).;
- Expansion in the free turbine: the mixture further expands in a following free turbine to provide shaft power, ideally by an isentropic process (in the model, it will be considered adiabatic, but an expansion efficiency $\eta_{t,FT}$ will be foreseen).

The efficiency of the overall Brayton cycle is calculated as a function of temperature (or compressor pressure ratio, $\beta = \frac{P_3}{P_1}$) as follows [61]

$$\eta_g = 1 - \frac{T_1}{T_3} = 1 - \frac{1}{\beta^{\frac{\gamma-1}{\gamma}}}$$

The highest temperature in the cycle occurs at the end of the combustion process, and it is limited by the maximum temperature that the turbine blades can withstand. This also limits the pressure ratios that can be used in the cycle. For a fixed-turbine inlet temperature, the net work output per cycle increases with the pressure ratio (thus the thermal efficiency).

The following picture shows the temperature-entropy diagram of a typical turboshaft engine with no cycle modifications (recuperation or intercooling)
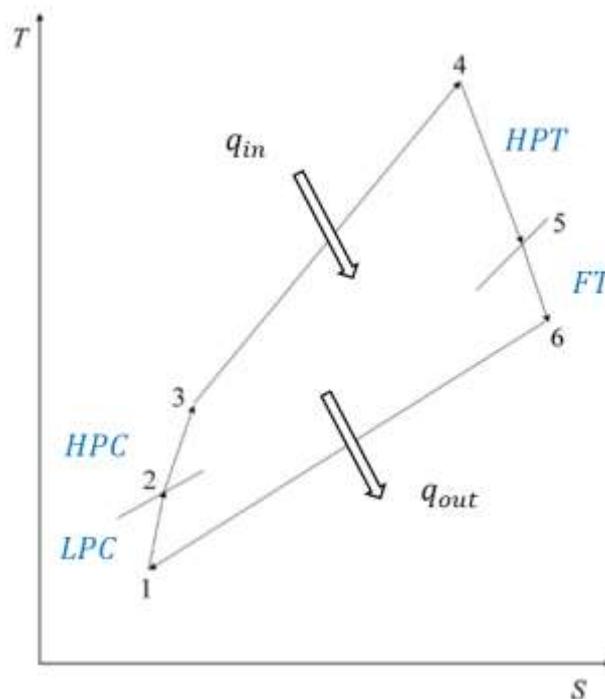

Figure 160: T-s diagram of a simple cycle of a two-spool engine with free power turbine

Each part is now briefly described:

- Compression (low pressure compressor) $(1 \rightarrow 2)$
  The compressor work of the low-pressure stage is defined as
  $$L_{c,LPC} = \dot{m}(h_2 - h_1) = \dot{m}c_p(T_2 - T_1)$$

It considers the unit air mass flow and the enthalpy drop, which is in turn the product of the specific heat at constant pressure and the temperature drop.

- Compression (high pressure compressor) (2 → 3)
  The compressor work of the high-pressure stage is defined as
  $$L_{c,HPC} = \dot{m}(h_3 - h_2) = \dot{m}c_p(T_3 - T_2)$$

- Combustion (3 → 4)
  The heat flow inside the cycle is defined as
  $$q_{in} = \dot{m}(h_4 - h_3) = \dot{m}c_p(T_4 - T_3)$$

- Expansion (high pressure turbine) (4 → 5)
  The expansion work of the high-pressure turbine is defined by
  $$L_{t,HPT} = \dot{m}(h_4 - h_5) = \dot{m}c_p(T_4 - T_5)$$

- Expansion (free turbine) (5 → 6)
  The expansion work of the free turbine is defined by
  $$L_{t,FT} = \dot{m}(h_5 - h_6) = \dot{m}c_p(T_5 - T_6)$$

- Exhaust (6 → 1)
  The heat rejected at constant pressure is defined by
  $$q_{out} = h_6 - h_1 = c_p(T_6 - T_1)$$

The overall efficiency of the cycle is calculated as the net work obtained, related to the input heat flow

$$\eta_\theta = \frac{L_{tot}}{q_{in}} = \frac{L_{expansion} - L_{compression}}{q_{in}} = \frac{L_{HPT} + L_{FT} - L_{c,LPC} - L_{c,HPC}}{q_{in}}$$

$$= \frac{(T_4 - T_5) + (T_5 - T_6) - (T_2 - T_1) - (T_3 - T_2)}{(T_4 - T_3)} = \frac{(T_4 - T_6) - (T_3 - T_1)}{(T_4 - T_3)} = 1 - \frac{T_1 - T_6}{T_4 - T_3}$$

6.5.3.3. Components description

In this section, the physical behaviour of the turbomachinery involved in this architecture will be explained, with a focus on the global performance rather than the evaluation of local design choices, like blade geometry and consequent speed triangles. This choice is undertaken due to the conceptual design nature of this project, and also because the overall configuration is not yet defined: in this perspective, a more detailed analysis could be unprofitable.

6.5.3.3.1. Compressor

In this paragraph, compressor performance will be evaluated through a powerful tool, namely the compressor map; it is a chart based on experimental analysis of a specific turbomachinery, but it refers to non-dimensional or corrected parameters, making it useful to describe a whole group of compressors associated in terms of aerodynamic and geometric similarity. This graph will be analysed in dept, since the dynamic simulation will be based on the coupling of compressor and turbine maps.

The following picture shows a typical compressor map
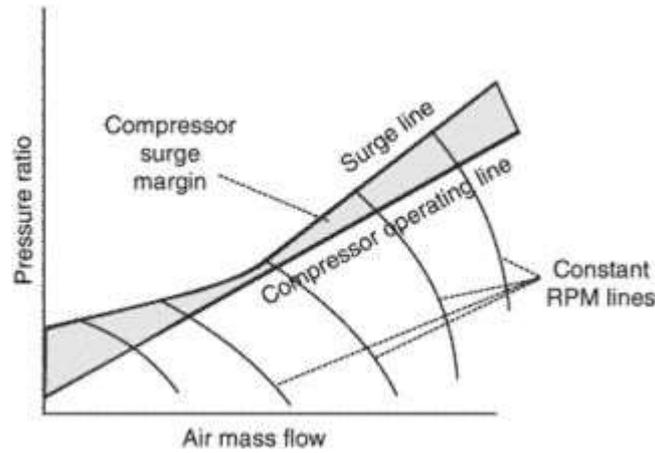
Figure 161: compressor map example [62]

The x-axis represents the corrected mass flow, namely the mass flow that would pass through the compressor if the inlet pressure and temperature corresponded to ambient conditions (temperature and pressure) at sea level [63]

$$m_{corr} = \frac{\dot{m}\sqrt{\theta}}{\delta} = \frac{\dot{m}\sqrt{T/T_{ref}}}{p/p_{ref}}$$

The higher the corrected mass flow is, the higher the axial Mach number of the flow through the device is. The y-axis is the pressure ratio, that is the ratio of the compressor discharge pressure to the compressor suction pressure. It is expressed as a function of stagnation pressure in exit and inlet conditions, respectively

$$\beta = \frac{p_2}{p_1}$$

The dashed line represents the surge line, i.e. a limit condition over which the compressor is stalled, and its flow is unstable.

It can be also outlined a working line, namely the locus of the operating points of the engine, which defines the typical steady state of working and the optimal design point. This line should be appropriately distant from the surge line, since there are some transient conditions (such as slam-accelerations) in which the working line temporarily translates closer to the surge line (due to the inertia of the shaft). Compressor surging usually causes flameout of the combustor, and the violent changes in aerodynamic load on the compressor blades during the surge period may cause them to fail. The surge margin is hence defined as a measure of how close an operating point is to surge. The definition currently used is

$$SM = 100 \cdot \frac{\dot{m}_{WL} - \dot{m}_S}{\dot{m}_{WL}}$$

Where $\dot{m}_{WL}$ is the mass flow at the operating point, and $\dot{m}_S$ is the mass flow at surge, at the same corrected speed. The compressor map is limited also on the right by the choke line: in this situation, the maximum flow rate through the device is reached. The choke line is a rapidly descending line on the right of the compressor map [64].

There are also corrected speed lines, which measure the angular rotational speed of the compressor in terms of corrected speed, namely

$$N_{corr} = \frac{N}{\sqrt{\theta}} = \frac{N}{\sqrt{\dfrac{T}{T_{ref}}}}$$

Ultimately, it is possible to cross-plot on the same map also the variation of isentropic efficiency with flow, at constant speed. Usually the efficiency islands converge to the centre of the compressor map, where the efficiency is at its maximum [65].

6.5.3.3.2. Turbine

In this paragraph, turbine performance will be evaluated through a powerful tool, namely the turbine map; it is a chart based on experimental analysis of a specific turbomachinery, but it refers to non-dimensional or corrected parameters, making it useful to describe a whole group of turbines associated in terms of aerodynamic and geometric similarity.

The following picture shows a typical turbine map
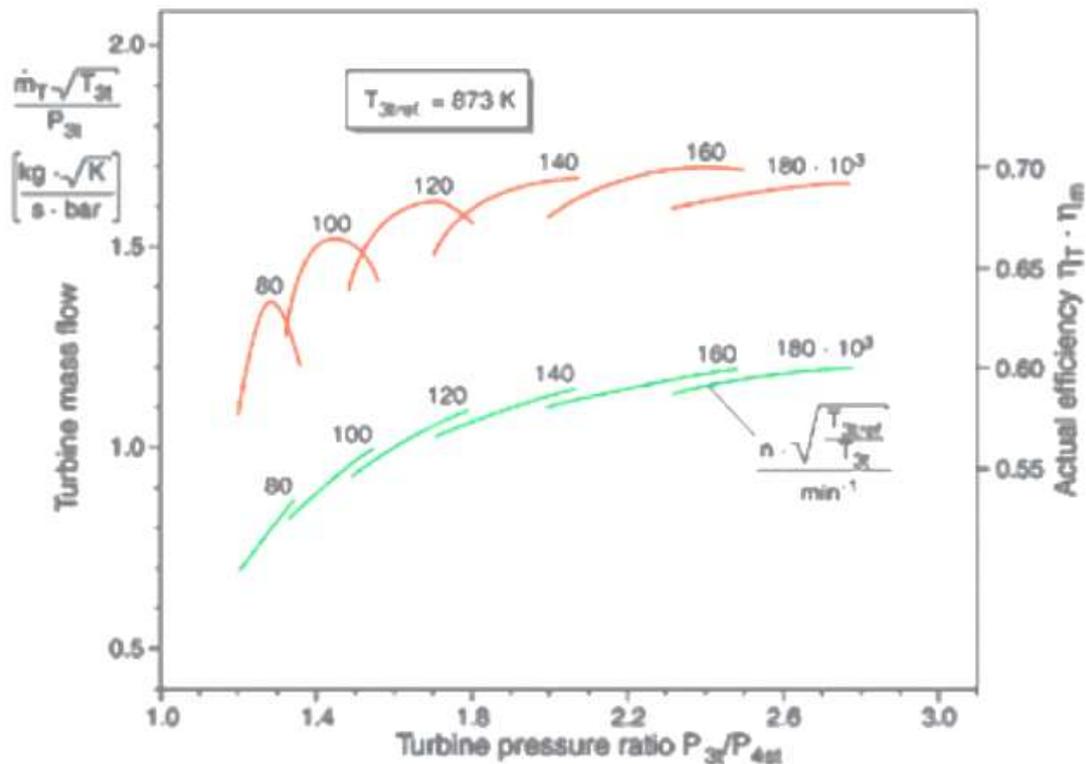
Figure 162: example of turbine map [66]

The x-axis represents the pressure ratio (also known as expansion ratio), as a function of total pressure at the turbine inlet and static pressure at the turbine outlet., respectively

$$\beta = \frac{p_3}{p_4}$$

The y-axis is the corrected mass flow, expressed as

$$m_{corr} = \frac{\dot{m}\sqrt{\theta}}{\delta} = \frac{\dot{m}\sqrt{T/T_{ref}}}{p/p_{ref}}$$

It is represented by green lines, that are labelled with the corresponding shaft speed.

147

Unlike a compressor, surge does not occur in a turbine; consequently, there is no surge line marked on a turbine map. If the throat Mach number reaches sonics conditions, the turbine becomes chocked, and then there is no variation in mass flow even with an increase of corrected speed. [67]

Turbine efficiency also looks different as compared to the compressor map; there are efficiency lines (red) which correspond to each compressor speed line with the efficiency values also plotted on the vertical axis.

6.5.3.4. Simulation blocks description
In this section, the blocks used to simulate the dynamic behaviour of the system are explained.

General architecture

The following picture shows the block scheme of the gas generator and free turbine assembly
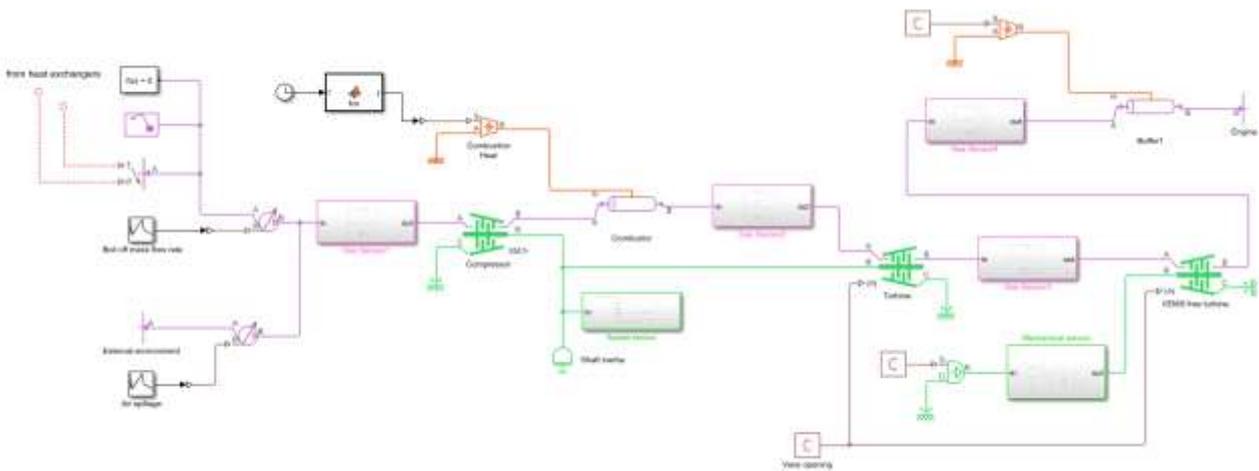
Figure 163: turbomachinery in TEMS subsystem, block scheme

First, gaseous hydrogen starting conditions (temperature and pressure) are directly measured in the heat exchanger assembly (as described previously), and the available amount of boil-off enters the turbomachinery, upon mixing with an appropriate amount of clear air; the latter has been spilled from inlet port, that is the same source of Air Pack (its initial conditions are assumed identical as stated in the preceding paragraph [58]).

The mixture follows the Brayton cycle path: compression, burning in the combustor (the amount of burnt hydrogen will be defined shortly), and then expanded twice; it is then injected in the engine for its final purpose of providing thrust. It is noted that the shaft connecting the gas generator elements (compressor and first turbine) in direct drive is characterised by an appropriate value of rotational inertia, taken as reference from existing turboshaft engine in helicopter applications. Vane opening of the turbine is chosen to maximise the efficiency in the most working conditions.

The most sensitive part in this design is the estimation of the amount of hydrogen to use in the pre-burner as fuel (and not as working fluid like the rest) in order to achieve the optimal efficiency of the whole assembly, since this aspect is not known a priori. In addition to this, the blocks do not allow an interpolate sequence of numbers to be the input of the heat introduced in the combustor.

First, the required onboard power is estimated. Since no further power budget analysis has been made, a rough estimation of this quantity will be made taking account of the liquid hydrogen fuel pump (a single fictional logical component that represents all the active fuel pumps on board) and main subsystem

requirements, whose power consumption is estimated to be approximately $200\,W/passenger$, hence $60\,kW$. The following picture represents the power target to be produced by the TEMS
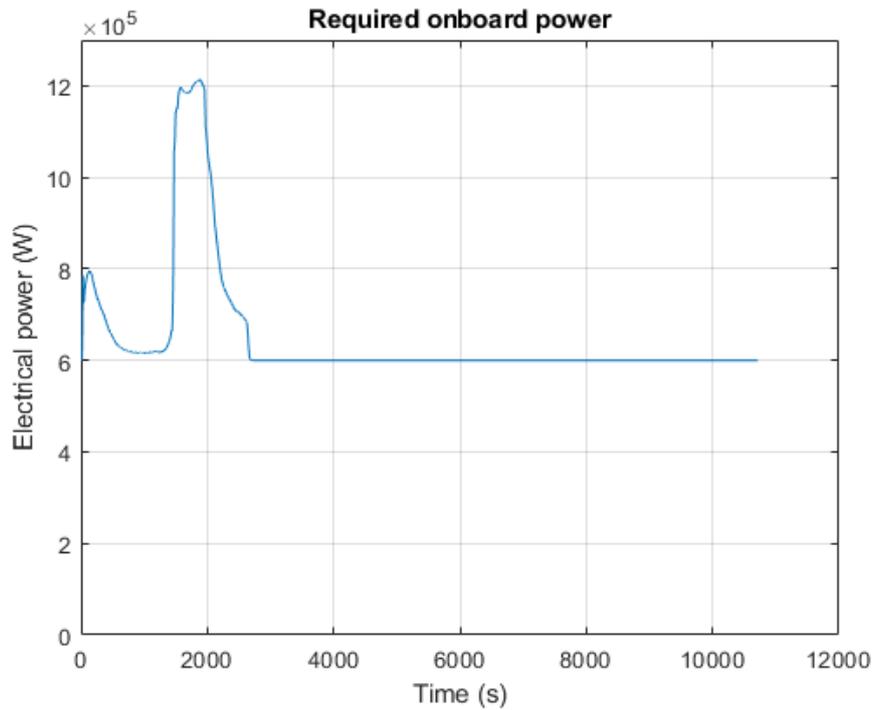

Figure 164: power budget

As a first attempt, the amount of hydrogen to be consumed to produce the necessary raw chemical power is estimated, together with the quantity of air to be spilled from the inlet to have the oxidation reaction
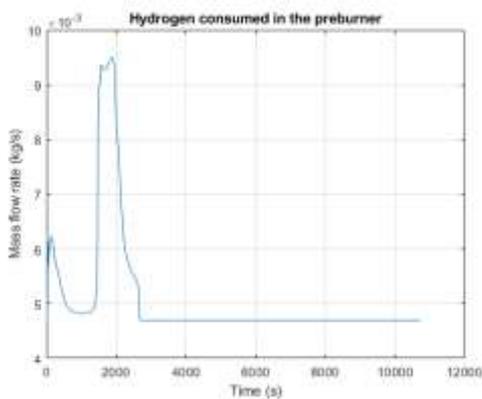

Figure 165: air used in the preburner
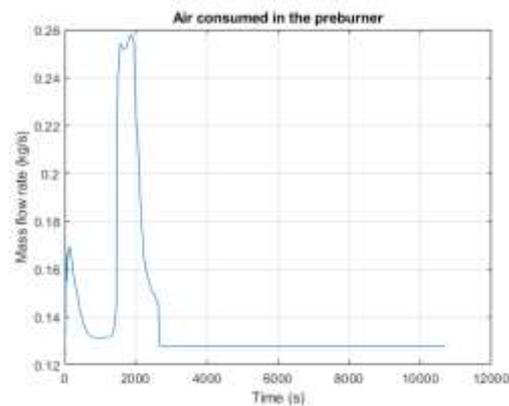
Figure 166: hydrogen used in the preburner

This data is used as a first attempt value for the amount of air to be mixed with the boiled off hydrogen to obtain the desired reaction. As a second and more deepen step, an iterative and recursive method is applied: the actual mechanical power output from the free turbine is compared to the power request; depending on their relationship, on the following simulation step more or less fuel is used in the preburner to increase the gas mixture temperature and, in the end, power output.

Compressor

The overall definition of this block requires the acquisition of the following data:

- Surge line

- o Corrected shaft speed vector
- o Pressure ratio vector
- Working line
  - o Corrected shaft speed vector
  - o Surge margin vector
  - o Corrected mass flow rate table
- Efficiency
  - o Corrected shaft speed
  - o Surge margin vector
  - o Isentropic efficiency table
- Other
  - o Reference pressure for corrected flow
  - o Reference temperature for corrected flow
  - o Mechanical efficiency

The definition of this vectors and tables contributes to define univocally the compressor map, as showed in the following chart
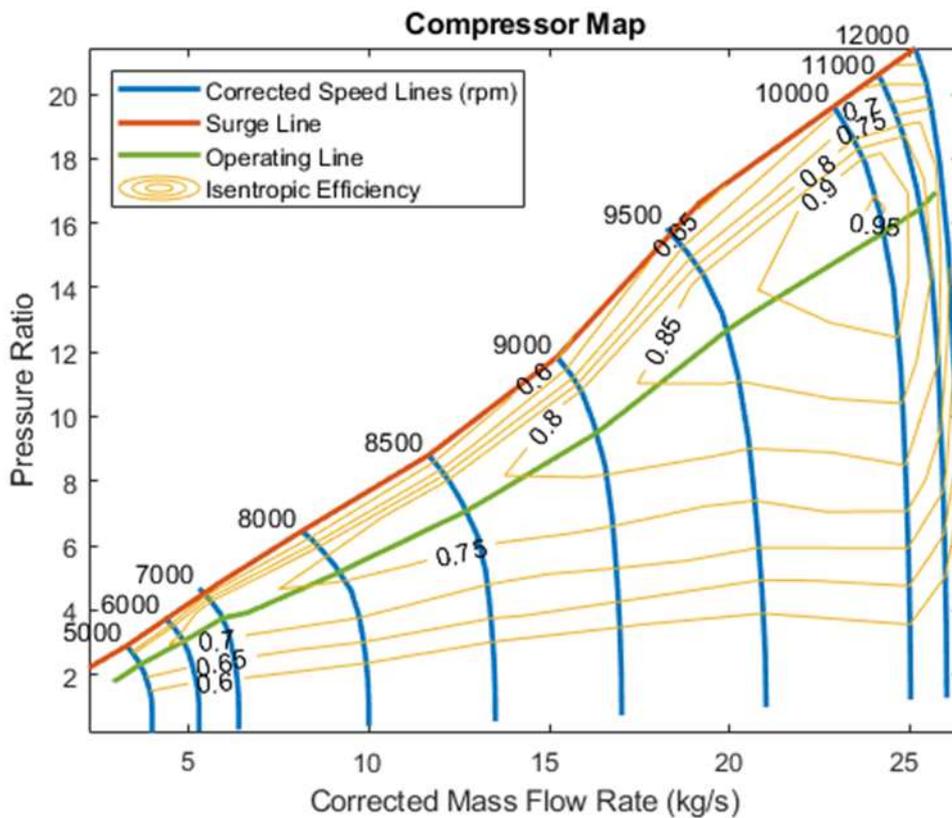
Figure 167: compressor map

Turbine

The overall definition of this block requires the acquisition of the following data:

- Working line
  - o Pressure ratio vector
  - o Corrected mass flow rate vector
- Efficiency

- o Pressure ratio vector
- o Isentropic efficiency table
- Other
  - o Reference pressure for corrected flow
  - o Reference temperature for corrected flow
  - o Mechanical efficiency
  - o Vane opening

The definition of this vectors and tables contributes to define univocally the turbine map, as showed in the following charts, for both the high pressure and the free turbine
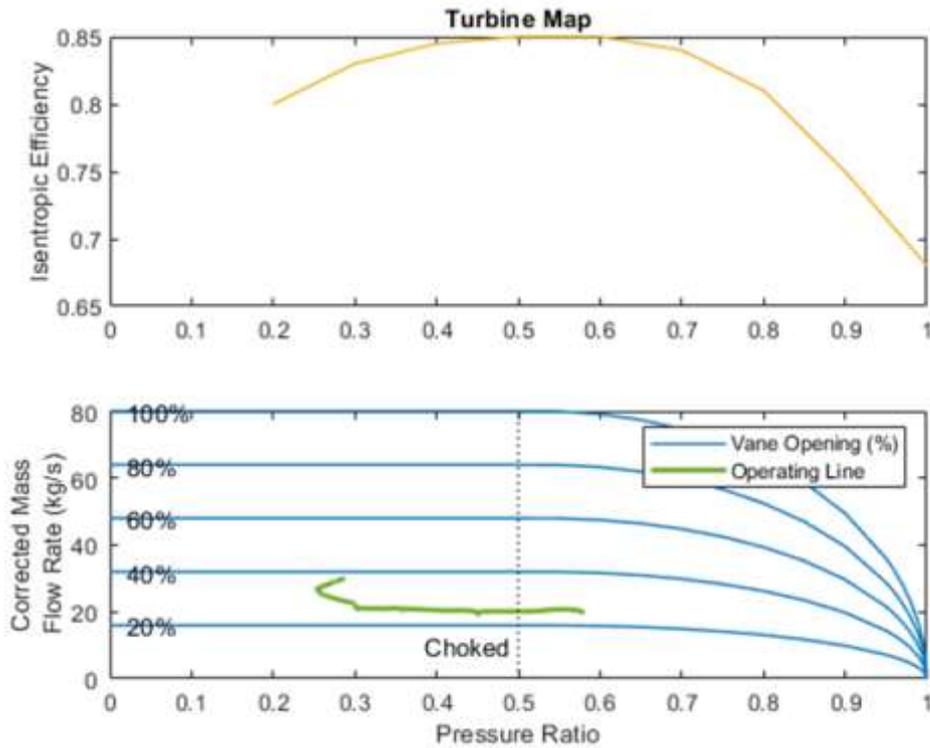

Figure 168: gas generator turbine map
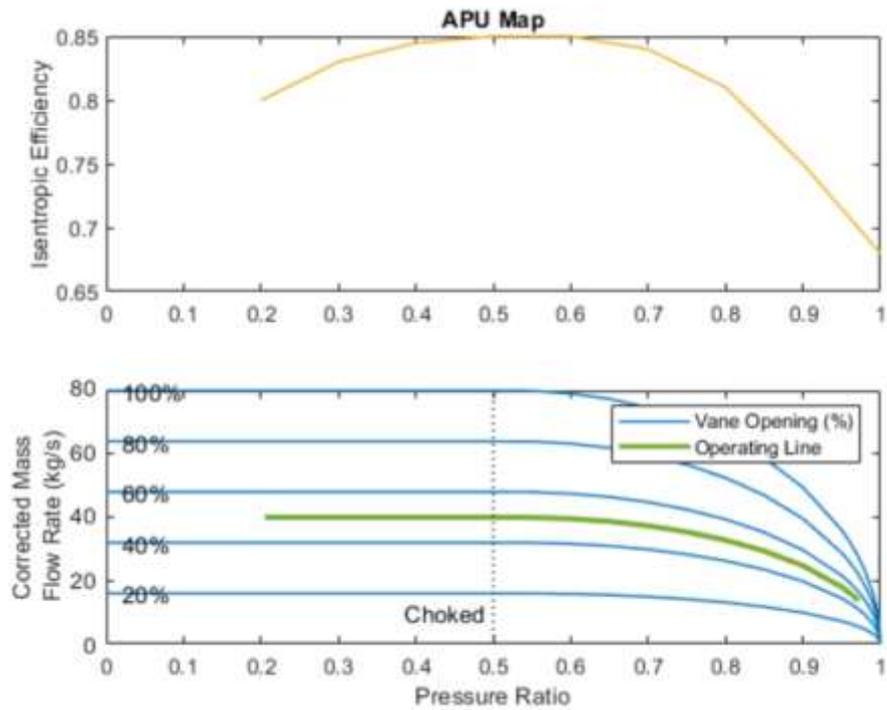
Figure 169: free turbine map

6.5.3.5. Simulation results

The following picture shows the reference for the sizing of turbomachinery inlets and outlets, and pipes hydraulic diameter. It is important to note that each part is sized according to the most demanding flight phase in terms of mass flow rate or pressure rise
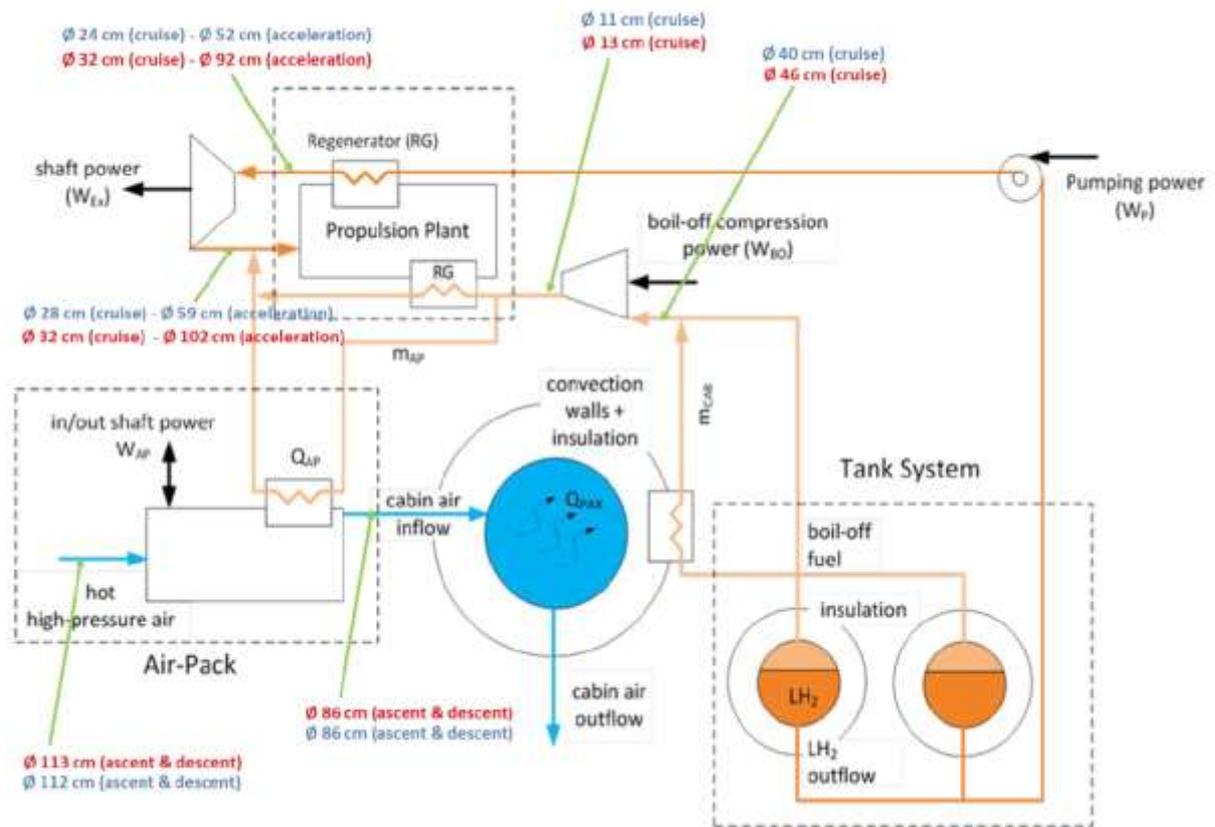
Figure 170: preliminary non-optimized pipes diameter (red) [34]

The next pictures show the pressure and temperature trend during the mission in several checkpoint scattered along the pipeline (before the compressor, after the burner, after the gas generator turbine)
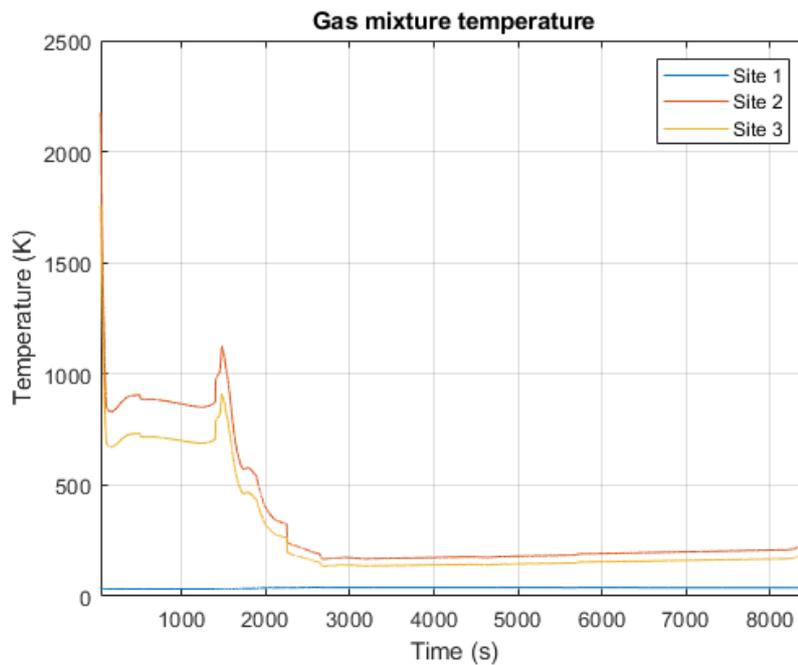

Figure 171: temperature of the gas mixture in three stations along the pipeline: before the compressor, after the burner and after the turbine, respectively

The following charts show that just a relatively limited amount of fuel and oxidizer is necessary, since the gas assembly should just elaborate a quite small amount of working fluid. The overall cost in terms of liquid hydrogen of the entire assembly along the whole mission is $591.78\ kg$, that is a negligible amount compared to the tank capacity and engine request; however, this quantity should be considered as part of the tanks design and the overall vehicle performance evaluation.
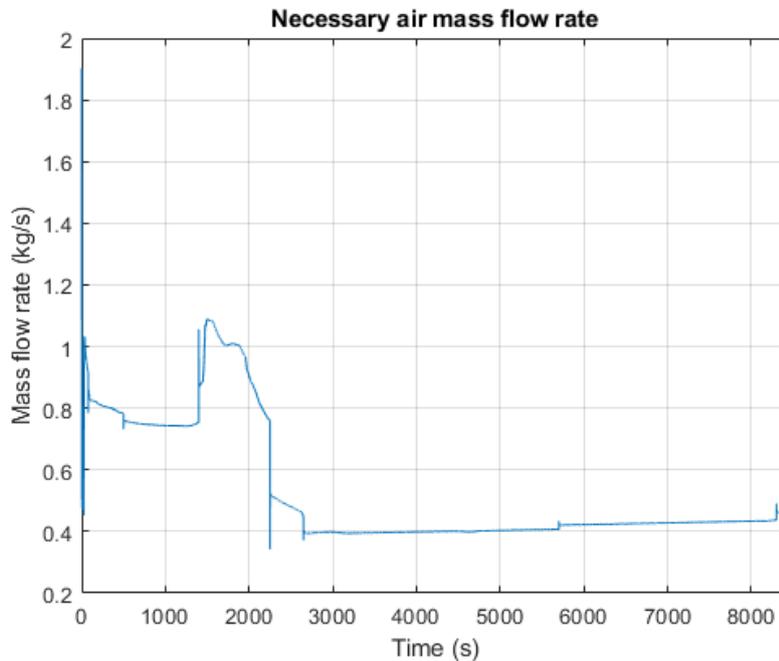

Figure 172: air flow rate necessary for combustion in the pre-burner
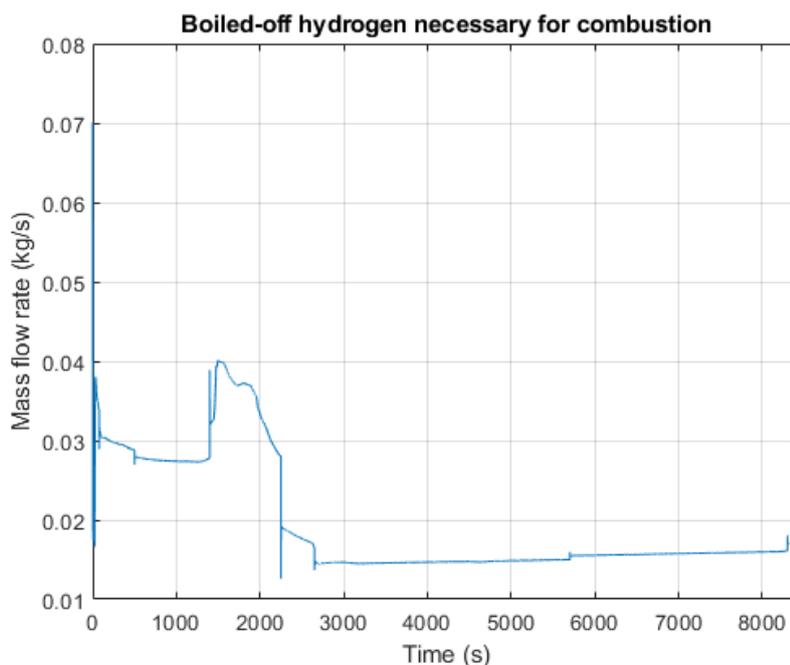

Figure 173: gaseous hydrogen to burn for the combustion in the pre-burner

The previous chart shows the amount of energy released in the combustion chamber due to the chemical reaction between hydrogen and air oxygen.

The following chart shows the amount of energy released in the combustion chamber due to the chemical reaction between hydrogen and air oxygen.
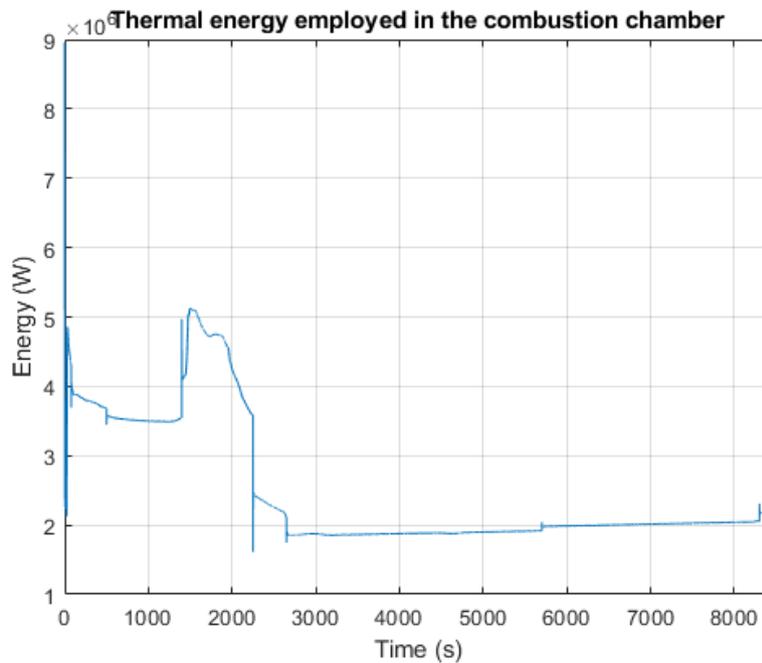

Figure 174: thermal energy release in the pre-burner by the combustion

The following chart shows the pressure variation as an evolution of both time and pipeline stage: the blue line defines the condition upstream the compressor, namely the boiled-off hydrogen after evaporating from the tanks and passing through the heat exchangers; the red one describes the gas mixture properties after the combustion, which increases both pressure and temperature. The yellow line defines the situation after the expansion in the gas generator turbine: the gas mixture made enough work to feed the direct-driven compressor but has still some pressure and temperature for further expansion through the free turbine.
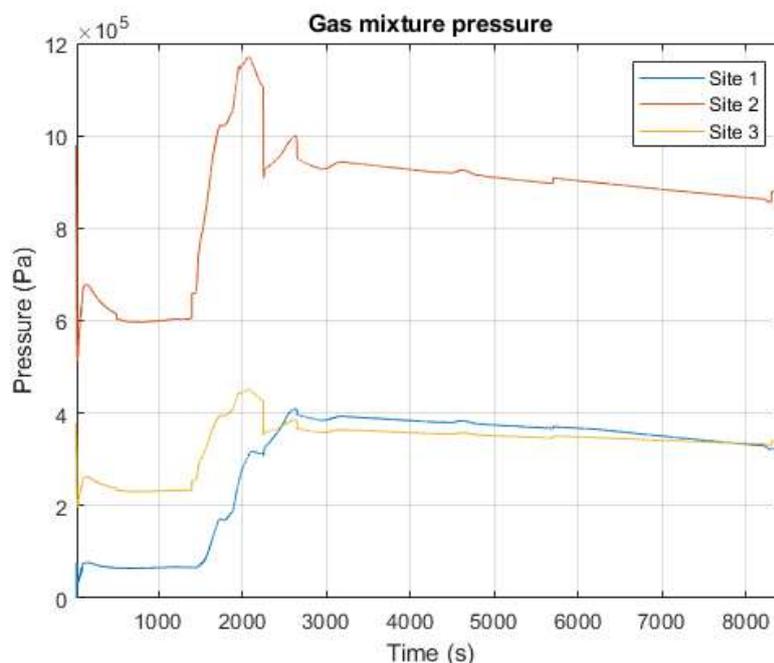

Figure 175: pressure of the gas mixture in three stations along the pipeline: before the compressor, after the burner and after the turbine, respectively
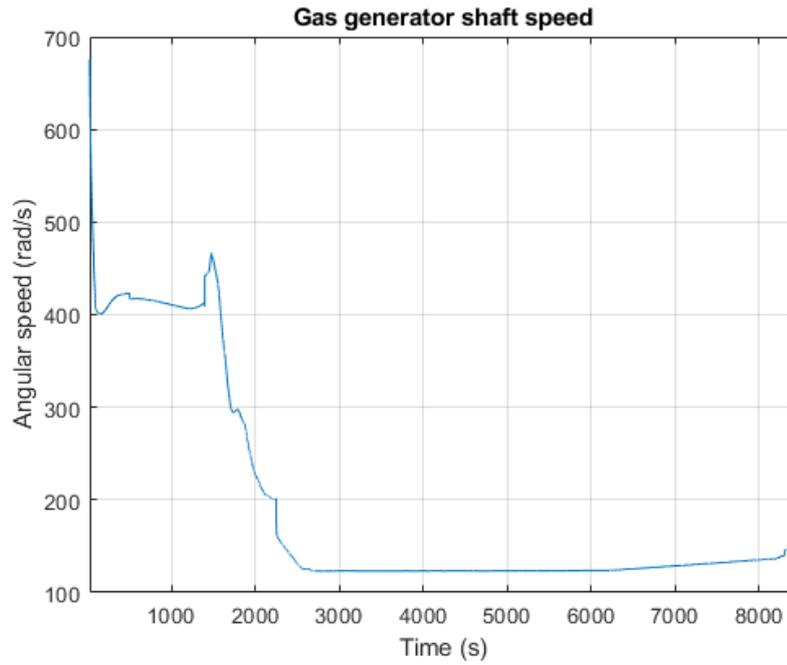
Figure 176: gas generator shaft speed, hence compressor and turbine rotational speed

Rotational speed of the whole compressor-turbine assembly shows a proportionality with the mass flow rate which go through the pipeline.
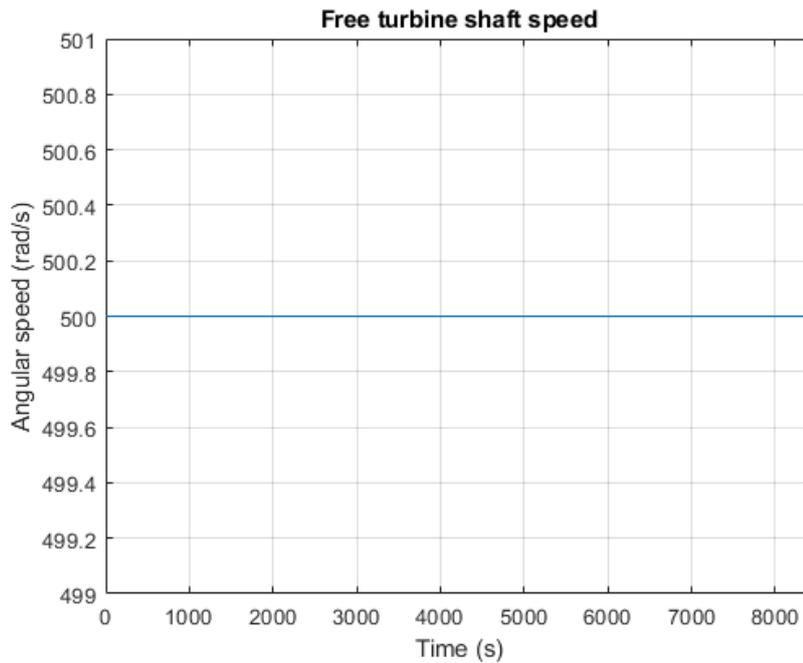

Figure 177: free turbine shaft speed

The free turbine shaft angular speed is assumed constant for more regularity in the power output and relative independence from the gas generator assembly working regime.
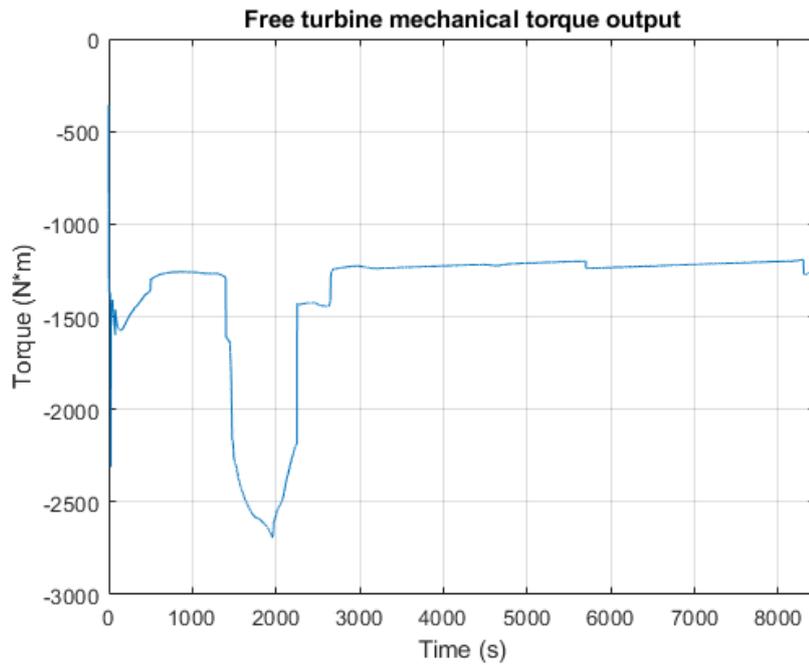
Figure 178: free turbine torque output
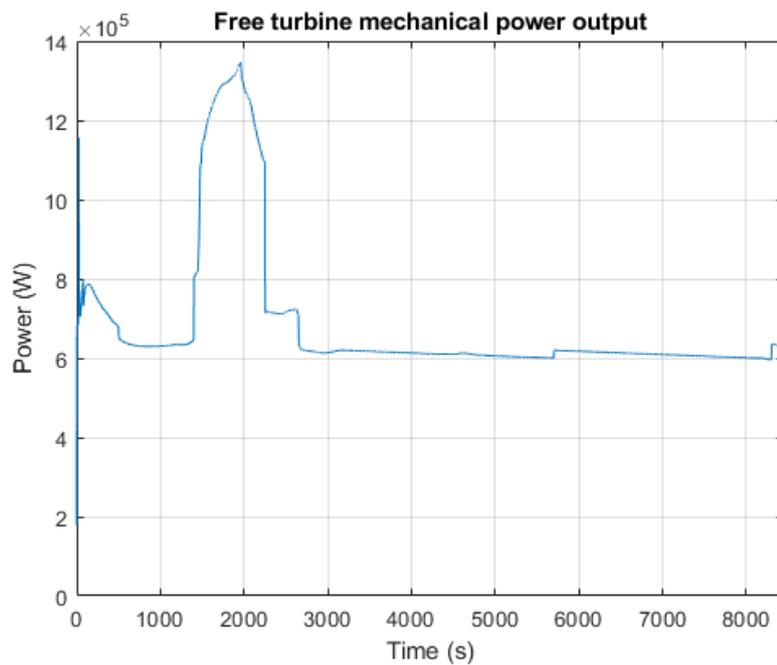
Figure 179: free turbine power output

The previous charts show the torque produced by the free turbine and the mechanical power generated, respectively. The latter quantity is calculated as

$$P = C \cdot \omega$$

Therefore, the generated mechanical power is calculated as the product of the torque and the angular speed. It is possible to see that torque is plotted negative since, according to the selected sign convention, the output work is considered negative. The output power is instead plotted positive even if it respects the same norm, but this choice is made for the sake of clarity.

In closing, a recapitulatory argument about the vehicle power budget is necessary. Since no further information about on-board systems energy consumption alongside the flight path and mission phases is available, the power requests are limited to:

- Pump to manage the fuel system
- Gas assembly compressor (this contribution has been already considered within the analysis of the TEMS in turboshaft configuration)
- On-board passenger and aircraft power requests, that are estimated to be $200 \, W/passenger$, namely $60 \, kW$.

This negative contribution should be balanced by the power generated from the TEMS free turbine. this last analysis is made iteratively and recursively, since no other analytic technique is provided in this stage of design. In addition to this, the efficiency of the electric machines powered by the turbine for the actual power generation is not considered; in fact, a provision of the performance of the final electric power generator could be premature, and no literature data is available so far. On the other hand, it is possible to suppose a high-efficiency generator, and by now its efficiency and performance are believed ideal and perfect: hence, the whole mechanical output is completely converted in electrical power.

The following chart shows a comparison between the total power request and the power output; a design effort was made to esteem manually, through many simulations, trials and error, to define a satisfactory power output, that is in any point of the mission greater than the requested energy. There is little margin for uncertainties, and only further studies can property define the right amount of energy necessary to prevent all aircraft power requests, even in case of failure. The setting of the output power is made by the repeated definition of the amount of hydrogen burnt in the combustor compared to the total mass flow rate; the latter should behave only as a working fluid, since there are no stoichiometric condition for chemical burning reaction to happen (it will then be used in the propulsion plant for the final and most relevant combustion).
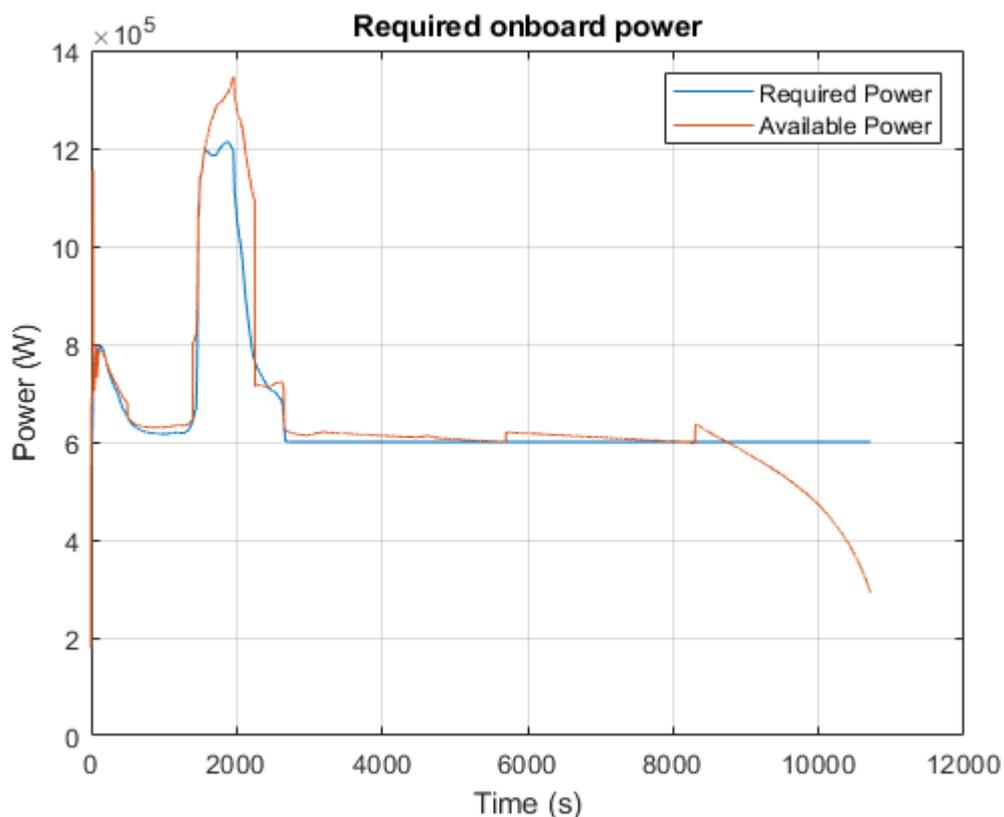

Figure 180: available vs required on-board power

It is possible to see that the last part of the mission, which still claims energy for aircraft manoeuvre and sustenance, could not be fed by the free turbine since, as seen before, that the on-board fuel ends when the aircraft starts its unpropelled descent. This is a serious matter of concern, since the last part of the mission is then left unpropelled and with no energy generated. This issue will be solved with the development of a new vehicle configuration and mission profile, which provides a continuous propulsion (hence engines and TEMS operating) alongside the whole trajectory.

6.6. Engine

6.6.1. General description

The propulsion plant designed for the aircraft is a complex combination of Air Turbo Ramjet (ATR) and Dual Mode Ramjet (DMR) engines. The purpose of this work is not to deepen engine description and evaluation, since that study is already been carried on and it is still under investigation with dedicated analysis and tools. The propulsion plant will be then analysed only as much as it concerns the TEMS subsystem, since it interfaces with the power plant for cooling purposes. In particular, only the combustion chamber will be considered (since it is the most important heat source in the engine, and it will surely need a regenerative cooling system due to the high energy release of hydrogen). This study will be performed from a conceptual design standpoint, since only its main phenomena will be considered; a chemical approach will be undergone, since the detailed behaviour of the fluid in the combustion chamber cannot still be simulated in greater detail due to lack of data.

6.6.2. Combustion chamber

Before this chemical reaction can occur, the liquid fuel must be injected into the airstream, atomized, and vaporized, and the vapor must be mixed with the air. In aerospace field, the combustion rate in gas turbines at sea level is of the order of $5 \cdot 10^6 \ \frac{kJ}{m^3 s}$ (for hydrocarbon-based fuels), which is more than 100 times as intense as the combustion in a large stationary power plant furnace, due to several reasons:

- The density of the reactants is around 10 times as high as standard ISA conditions;
- The fineness of atomization of the injected fuel is very refined to improve combustion efficiency;
- The air flow inside the combustion chamber is characterised by intense turbulence, which improves the mixing of vaporised fuel and air, and a faster propagation of flame through the unburned mixture.

In this case of study, combustion chamber has been designed for supersonic combustion, since this condition will persist for most of the mission time. In particular, the combustion chamber geometry has been optimised to improve the flame stability in all flight conditions (working fluid speed has to be as high as possible without incurring excessive losses due to shocks, wall friction, and viscous mixing). A limitation is imposed by the combustor since it is necessary to maintain a stationary flame within a moving airstream; in addiction to this, if the velocity is too high, the flame will be "blown out" the exit, and if too low, the flame will travel upstream and be extinguished. It is not necessary, however, that the mixture velocity be exactly equal to the flame speed since the flame front need not be normal to the flow.

This engine design involves a ramjet in hypersonic flight: experimental evidence show that additional problems arise because of extremely high temperature at the entrance to the combustion chamber. This not only makes vehicle cooling very difficult, but it leads to severe combustion loss due to dissociation. The following graph shows adiabatic deceleration from a high-altitude ambient temperature of 220 K and from hypersonic flight to a chamber pressure of either 1 or 10 atm. The temperature of the air in the chamber is quite dependent on the pressure: the higher the pressure, the less dissociation and the higher the temperature of the mixture.

Supersonic combustion involves favourable phenomena from the point of view of the engine interfaces with the rest of the aircraft: fluid temperatures are relatively lower than subsonic combustion characterized as almost stationary; from a propulsive point of view, there is a reduction of losses due to dissociation, since this phenomenon depends on the static temperature. The wall heat exchange instead depends on the stagnation temperature of the fluid, of which the definition is remembered

$$T_0 = T \cdot \left(1 + \frac{\gamma - 1}{2} \cdot M^2\right)$$

In which the total temperature in the stagnation point (T_0) depends on the static temperature on a point of the streamline, fluid properties (γ) e and it velocity, expressed in terms of Mach number (M). [68]

This is why supersonic combustion does not solve the problem of the need to cool the engine walls. The stagnation pressure loss due to supersonic heating depends on the extent to which the fluid is being accelerated while combustion is taking place. The solution envisaged here is the adoption of a liquid hydrogen regenerative cycle that removes heat from the combustion chamber externally, preserving the engine walls and allowing interfaces between the propulsion plant and other on-board systems.
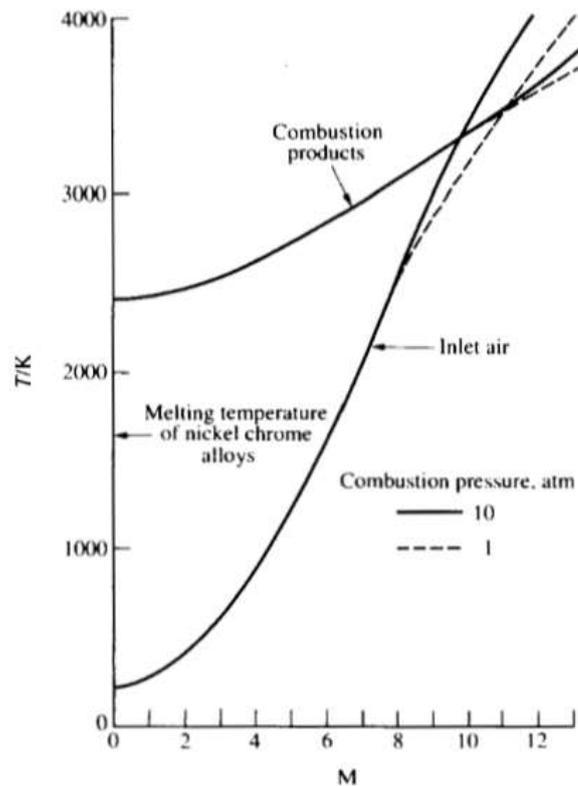

Figure 181: hypersonic ramjet, adiabatic compression and combustion [27]

The figure shows that, at sufficiently high Mach number, the temperature of the combustion products can be lower than that of the incoming air. This result, that seems apparently paradoxical, is justified by the assumption of equilibrium composition of the mixture in the combustion chamber, but this hypothesis is not justified in this case study. As a matter of fact, during the subsequent expansion in the nozzle, the equilibrium composition is not granted: it is quite possible that the expansion will be too rapid for the composition to readjust, after each step of temperature and pressure reduction, to a new equilibrium composition. If the expansion is extremely rapid, the mixture may be effectively "frozen" with the initial (high-temperature) composition. This would mean that little of the combustion energy of the fuel would be available for acceleration of the combustion products to provide thrust. The chemical kinetics of the recombination processes in the nozzle would, in general, have a strong effect on the thrust and the propulsion efficiency of the engine.

The configuration adopted has been defined, in first approximation, as follows
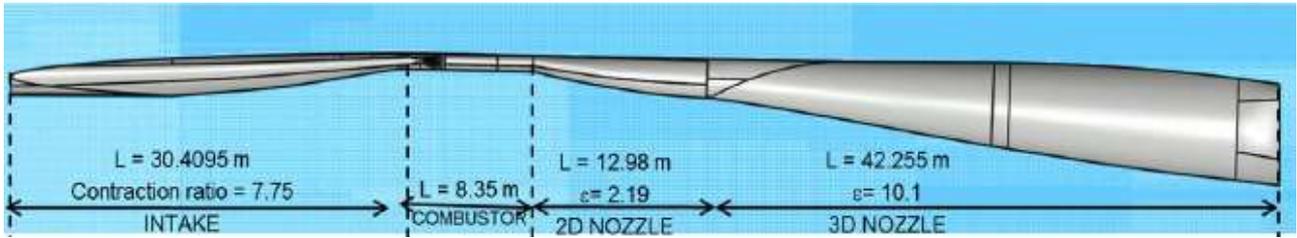
Figure 182: schematic of Dual Mode Ramjet (DMR) internal flow path and flow stations [37]

Hence, the combustion chamber will be treated as a cylinder with a height and diameter of [69]

$$L = 8.35 \; m$$

$$D = 0.88 \; m$$

The combustion chamber (in the scramjet model) has been modelled as a constant area duct; the applied conservation relationships between the combustor input (1) and output (2) are

- Continuity equation

$$\frac{\dot{m}_1}{\dot{m}_2} = \frac{1}{1 + \Phi} = \frac{\rho_1 u_1}{\rho_2 u_2}$$

    Where:

    - $\dot{m}$ is the mass flow rate $\left(\frac{kg}{s}\right)$
    - Φ is the fuel-to-air mass ratio
    - ρ is the fluid density $\left(\frac{kg}{m^3}\right)$
    - u is the fluid speed $\left(\frac{m}{s}\right)$

- Momentum equation

$$p_1 A_1 + \dot{m}_1 u_1 + \dot{m}_1 \Phi u_f \cos(\beta) = p_2 A_2 + \dot{m}_2 u_2 + \dot{m}_2 u_2 + F_{wc}$$

    o Where:
        - p is the fluid pressure (Pa)
        - A is the reference area (m^2)
        - u_f is the fuel speed in the combustor $\left(\frac{m}{s}\right)$
        - β is the fuel injection angle in the combustor (rad)
        - F_{wc} is the combustor wall drag due to skin friction, expressed as follows

$$F_{wc} = \frac{C_f}{2} \cdot \dot{m}_1 \cdot u_1 \cdot \frac{A_w}{A_1}$$

        - A_w is the combustor wetted area (m^2)
        - C_f is the skin friction coefficient ($C_f = 0.003$)

- Energy equation

$$\dot{m}_1 \cdot \left(h_1 + \frac{u_1^2}{2}\right) + \dot{m}_1 \Phi h_{of} = \dot{m}_2 \cdot \left(h_2 + \frac{u_2^2}{2}\right) + \dot{Q}$$

    Where:

    - h_{of} is the fuel stagnation entalphy, evaluated at the stagnation temperature T_{of}
    - $\dot{Q}$ is the heat transfer rate to the combustor walls (W), given by

162

$$\dot{Q} = St \cdot \dot{m}_1 \cdot \frac{A_w}{A_1} \cdot (h_{aw} - h_w)$$

- h_{aw} is the enthalpy of clean air at the adiabatic wall temperature $\left(\sfrac{J}{kg}\right)$
- h_w is the enthalpy of clean air at the static wall temperature (T_w).

Further analysis of engine performance will not be made, as it is beyond the target of this thesis. Instead, the analysis of heat transfer rate to the combustor walls will be considered: the Reynolds analogy will be implemented with the following conditions

- Recovery factor: $r = 0.9$
- Mean value of the combustor Stanton number: $\quad St = \frac{c_f}{2} = 0.0015$

To account for the presence of un-reacted fuel in the combustor exit, the exhaust products are considered as two separate streams. One stream contains an equilibrium mixture of the consumed fuel and air, and the second contains the remaining un-burnt pure fuel. The overall composition of the mixture is calculated by adding the unburnt fuel to the equilibrium mixture and the overall enthalpy is then evaluated from the known enthalpy of each component. A combustion efficiency is used to calculate the mass fraction of unburnt fuel: a value of 0.8 was used, which implies 20% of the fuel remained unburnt [69].

6.6.3. Chemical methodology

It should be noted ,first of all, that an accurate and detailed analysis of the thermo-fluid dynamic phenomena within the propulsion plant (and in particular the combustion chamber) is outside the scope of this thesis, the objective of which is the analysis of the behaviour of the TEMS subsystem. However, as this system interfaces with the engine to relieve part of its thermal loads, a simplified treatment of the combustion process will take place, to evaluate the intensity of heat transmitted through the walls to the external environment.

Firstly, the phenomenon of hydrogen combustion is analysed from a purely chemical point of view. In this discussion reference will be made to the following simplifying hypotheses:

- Chemical reactions in propulsion plant occur between gases whose behaviour is approximate to that of perfect gases;
- Chemical processes take place between equilibrium states. This hypothesis is true unless there are rapid expansion processes, which will not be considered in this analysis;
- Heat exchanges are considered to have occurred at constant pressure.

In general, this is considered a steady-flow process; if energy is not fed into the form of work, the heat transfer into a liquid flowing through a volume control is equal to the variation in enthalpy; or

$$Q = \Delta H = H_{products} - H_{reactants}$$

In this equation, velocity variations and relative elevation have been neglected.

The complex chemical reaction is broken down as follows
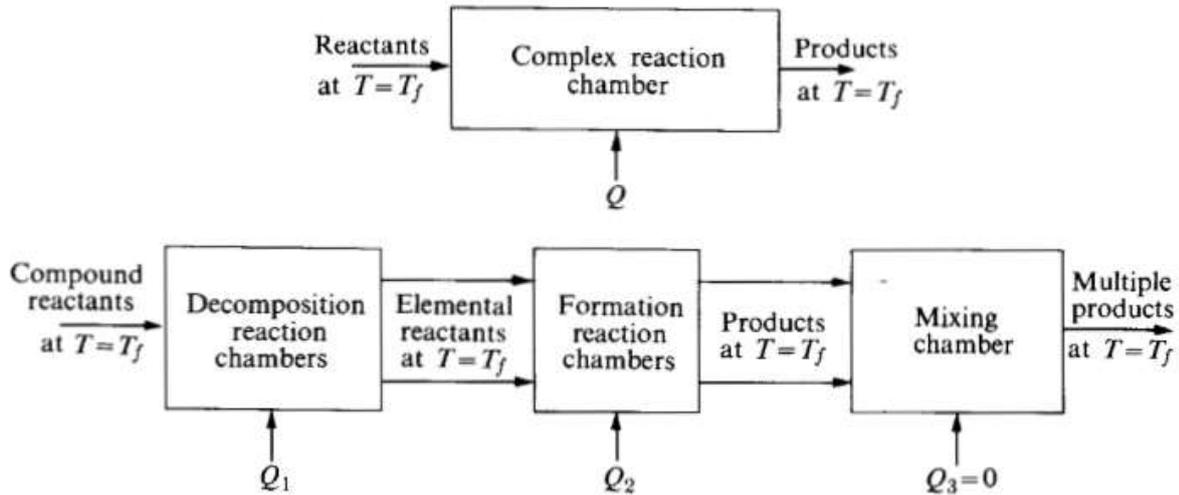
Figure 183: schematic of complex chemical reaction, and its equivalent in terms of elementary reactions [27]

In which Q is the heat to be supplied in order to maintain constant the temperature in the combustion chamber; the overall reaction is considered as linear overlap of the effects of more simple reactions of composition and decomposition. In particular, each reaction provides a heat input of

$$Q_i = \pm n_i \cdot Q_{f,i}$$

In which the heat generated (or absorbed) by the reaction is equivalent to the product of the number of moles of reactant (n_i) and molar heat formation. The sign preceding the expression is determined by the tendency of the reaction to emit heat towards the external environment (exothermic reaction, positive sign) or vice versa (endothermic reaction, negative sign). In general, therefore, the heat produced in the combustion chamber by decomposition of the reagents is given by

$$Q_1 = - \sum_{i=1}^{n° \text{ reactants}} \left(n_i \cdot Q_{f,i} \right)_{reactants}$$

In this case the minus sign is applied to respect the convention that the heat supplied by the reaction to the environment is negative (this is assumed to be the case, since the fuels are selected mainly on the basis of the energy released during the combustion reaction). On the other hand, the heat absorbed in product formation is equivalent to

$$Q_2 = \sum_{j=1}^{n° \text{ products}} \left(n_j \cdot Q_{f,j} \right)_{products}$$

Assuming the mixing process in the third adiabatic chamber, the net heat emitted by the reaction is equivalent to

$$Q_R = Q_1 + Q_2 = \sum_{j=1}^{n° \text{ products}} \left(n_j \cdot Q_{f,j} \right)_{products} - \sum_{i=1}^{n° \text{ reactants}} \left(n_i \cdot Q_{f,i} \right)_{reactants}$$

In terms of enthalpy

$$H_{RP,f} = H_{P,f} - H_{R,f} = Q_R$$

That is, the difference in enthalpy is equivalent to the change in enthalpy between products and reagents at the reference temperature (assumed constant). These values are tabulated over a wide range of reagents and environmental conditions.

In the present case, the considerable energy involved in the reaction and the extreme temperatures in the combustion chamber make the reaction hypothesis at constant temperature unlikely. For this reason, in the course of the simulation, the following approach will be adopted
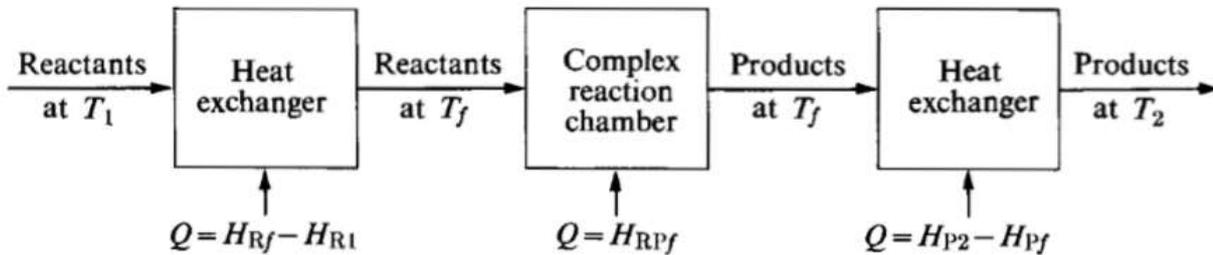

Figure 184: complex reaction scheme without constant temperature hypothesis [27]

It is supposed to be able to model the process through 3 distinct phases (that in reality happen simultaneously): first the reagents are brought to the desired temperature for the reaction by means of a fictitious heat supply; the reaction takes place at constant temperature (the same as described in the previous method, this step consists of the above process), and finally the products by appropriate heat exchange reach the final temperature. In formulas

$$Q = \left(H_{P,2} - H_{P,f}\right) - \left(H_{R,1} - H_{R,f}\right) + H_{RP,f}$$

Reference temperature $\left(T_f\right)$ is selected according to the conditions under which combustion takes place in the specified boundary conditions (tabulated by experimental tests). Subscripts refer to the temperature at which the enthalpy change occurs. The adiabatic combustion process is therefore graphically represented
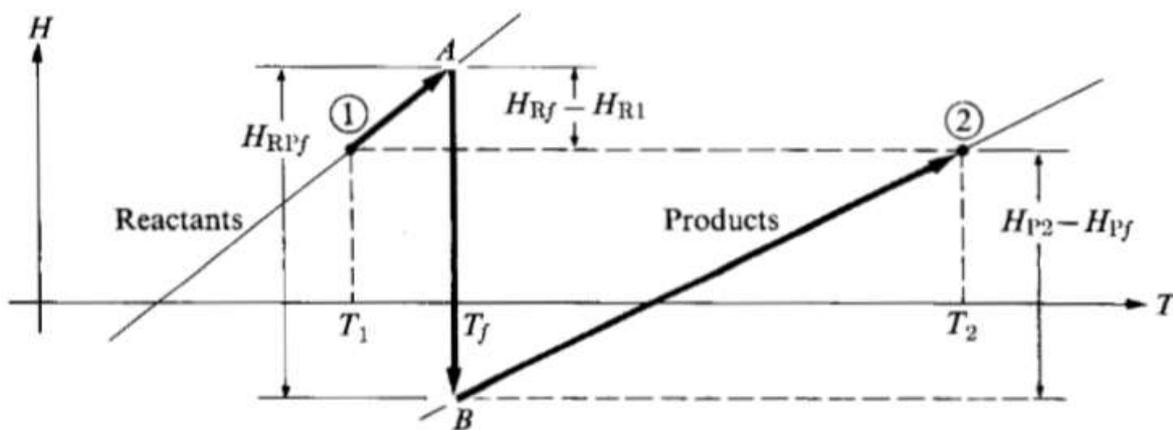

*Figure 185: enthalpy-temperature diagram for adiabatic combustion [27]*

Reactants in condition 1 are brought to temperature T_f by thermal exchange; in this condition (A) the isothermal reaction of the reagents takes place in products along line AB. The products are then brought to the situation B by appropriate thermal input. Since overall there is no heat exchange, $H_{R,1} = H_{P,2}$. [59]

6.6.4. Chemical reaction
The advantages of using liquid hydrogen as a fuel are numerous, such as

- wide range of flammability: it can be ignited in a wide range of fuel-air mixtures, even lean mixtures (those in which fuel fraction is less than stoichiometric);
- low ignition energy: the amount of energy needed to ignite hydrogen is about one order of magnitude less than that required for gasoline, and it ensures prompt ignition. This could be also a drawback, since the wide flammability range can make a generic hot spot to become the source of premature ignition and flashback;
- high flame speed at stoichiometric ratios: under the same conditions, hydrogen flame speed is nearly an order of magnitude higher (faster) than that of gasoline. This means that hydrogen engines can more closely approach the thermodynamically ideal engine cycle;
- high diffusivity: it facilitates the formation of a uniform mixture of fuel and air and improves safety in case of leakage.

Theoretical stoichiometric combustion of hydrogen and oxygen for complete combustion happens according to the following reaction

$$2H_2 + O_2 \leftrightarrow 2H_2O$$
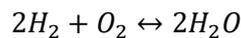
In the combustion chamber, the oxidant will not be pure oxygen, but clear air. The percentage of moisture in air is neglected, simulating the behaviour of the aircraft in cruise conditions, which is through the low stratosphere; it is important to remember that it represents about 0.25% by mass over full atmosphere, and its presence strongly varies locally. The composition of air (on average) is [70]

Gas	Volume fraction (%)
Nitrogen (N_2)	78.084
Oxygen (O_2)	20.946
Water vapour (H_2O)	0-3
Argon (Ar)	0.9340
Carbon dioxide (CO_2)	0.041332
Neon (Ne)	0.001818
Helium (He)	0.000524
Methane (CH_4)	0.000187
Krypton (Kr)	0.000114

As said before, atmospheric moisture will be neglected, along with other gases but nitrogen and oxygen, due to their negligible presence. The result is air as a mixture of two diatomic gases, who have therefore similar thermodynamic properties. The most important features of those gases are now listed:

Gas	Molar weight (g/mol)	Number of moles considered	Weight (molar weight $\cdot$ number of moles)(g)
Air	28.96	$1 + 3.73 = 4.73$	136.98
Nitrogen (N_2)	$14.0067 \cdot 2 = 28.0134$	$1 \cdot \dfrac{78.084}{20.946} = 3.73$	104.49
Oxygen (O_2)	$15.9994 \cdot 2 = 31.9988$	1	32.00

In the previous table, a mole of oxygen is considered (and the related amount of air); according to the chemical reaction, it requires two moles of H_2 to fully react, hence

$$fuel_{mass} = 2 \, mol \cdot M_H \frac{g}{mol} \cdot 2 \ = 2 \cdot 1.008 \cdot 2 = 4.032 \, g$$

Hence, the mixture ratio (based on mass) is

$$MR_{mass} = \frac{m_{air}}{m_{fuel}} = \frac{136.98}{4.032} \sim 34.33 : 1$$

Because of hydrogen's wide range of flammability, hydrogen engines can run on A/F ratios of anywhere from 34:1 (stoichiometric) to 180:1. The A/F ratio can also be expressed in terms of equivalence ratio: Φ is equal to the stoichiometric A/F ratio divided by the actual A/F ratio [71].

The correct air-fuel ratio determines whether a mixture is combustible at all, how much energy is being released, and how much unwanted pollutants are produced in the reaction. The range is limited in range in which the reaction can chemically take place, namely the lower and upper explosive limits. Different choices can be made:

- stoichiometric mixture: in theory, it provides the exact amount of reactant to allow the complete reaction. In practice this is never quite achieved, due primarily to the very short time available within the combustion chamber to the complete reaction to happen. In addition to this, it burns very hot and can damage engine components.
- fuel shortage (lean): the combustion reaction is more complete. The final combustion temperature is generally lower, reducing the amount of pollutants, but the power output is significantly reduced due to a reduction in the volumetric heating value of the air/fuel mixture.
- fuel surplus (fuel rich): are less efficient but may produce more power and burn cooler [72].

As stated before, fuel rich mixture will be used, since it is estimated that 20% of total fuel will not react. In those conditions, the reaction heat produces is $515.2 \ ^{kJ}/_{mol}$, related to hydrogen moles, with an average flame temperature of $2318 \ K$ [73]: hence, the combustion of liquid hydrogen (H_2) produces $127.78 \ ^{MJ}/_{kg}$.

The following picture shows the effect of mixture ratio and distance from the injectors on flame temperature, considered on a model who evaluates the performance of high Mach number combustion systems.
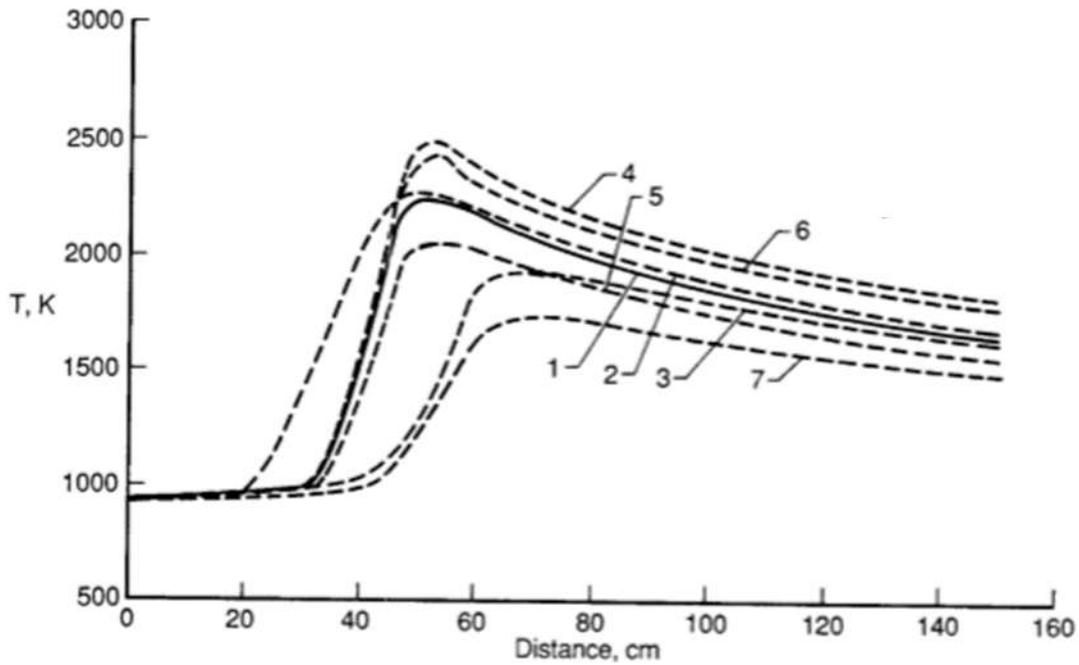
Figure 186: chemical kinetic effect at Mach 8 condition for various mixture ratios [33]

6.6.5. System architecture

The system architecture in the form of block diagrams is shown in the following image.
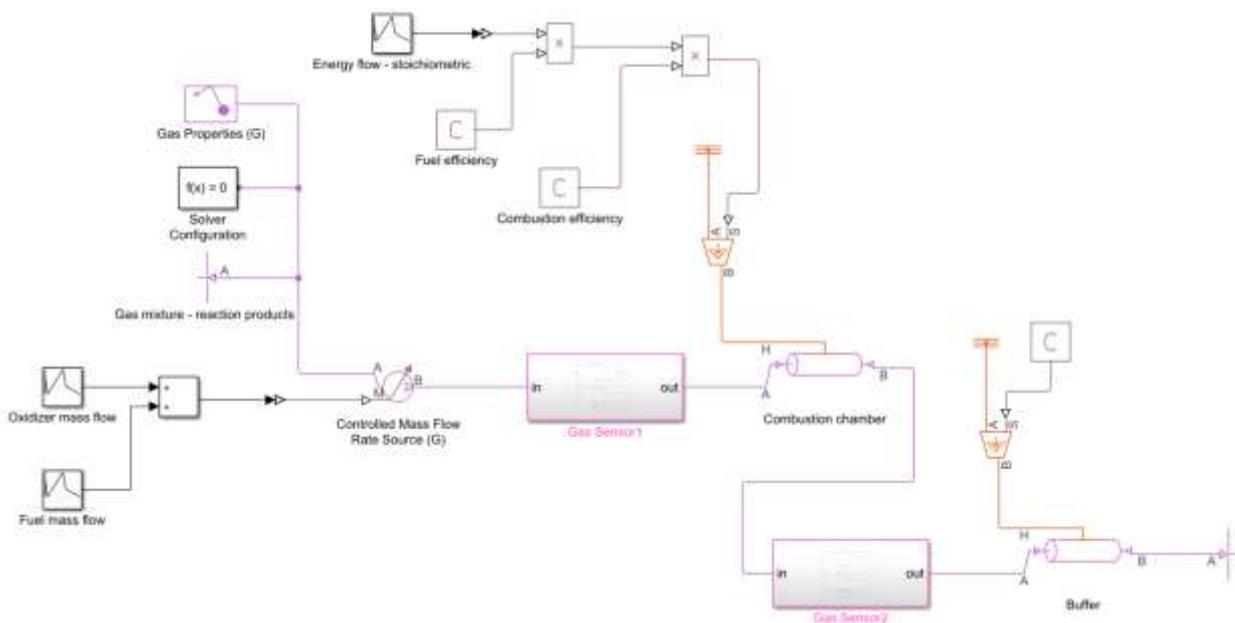
Figure 187: block scheme of the combustion chamber

The mass flow rate of reaction products is equal to that of reagents (hydrogen and air) for the law of mass conservation; please note that the amount of air needed to burn only 80% of the entire fuel flow, since a fuel rich mixture is desired. For this reason, 2 moles of hydrogen react with 0.8 moles of oxygen (for stoichiometric equilibrium); the amount of air required (moles number) in relation to the amount of oxygen is therefore

$$n_{air} = n_{O_2} + n_{N_2} = 0.8 \cdot \left(1 + \frac{78.084}{20.946}\right) = 3.78 \; mol$$

In terms of mass, therefore, each mole of hydrogen liquid H_2 (4,032 grams) requires 109.47 grams of air for combustion to take place under the desired conditions. This ratio is explained in the fictional source of mass flow, as the sum of the amount of fuel required by the engine (which takes into account the type of mixture and the fuel not burned) and the appropriate oxidant flow rate.

The fluid therefore passes through the combustion chamber, considered cylindrical according to the above hypotheses, and the heat produced by the combustion reaction is supplied. It should be remembered that the latter must be reduced to 80% for the non-complete reaction, and a thermal efficiency of 90% is also applied: it is the ratio of the rate of addition of kinetic energy to the propellant to the total energy consumption rate $\dot{m}_f Q_R$, where $\dot{m}_f$ is the fuel mass flow rate and Q_R is the heat of reaction of the fuel. In general, it is defined as follows

$$\eta_{th} = \frac{\dot{m}_e \left[(1+f)\left(\frac{u_e^2}{2}\right) - \frac{u^2}{2}\right]}{\dot{m}_f Q_R}$$

6.6.6. Simulation outputs
In this section, the most remarkable results of the simulation are shown.

The following picture shows the amount of fuel compared to the necessary mass flow rate of air for the chemical reaction to happen
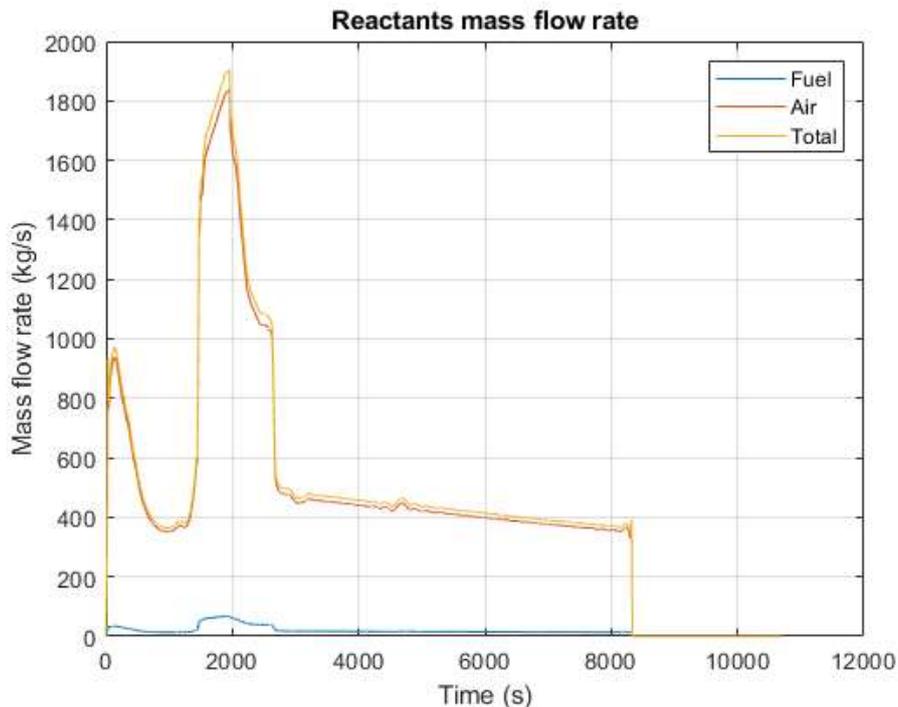

Figure 188: mass flow rate of air and fuel inside the combustion chamber

The next graph shows the amount of heat generated in the combustion chamber through the chemical reaction between hydrogen and air (oxygen)
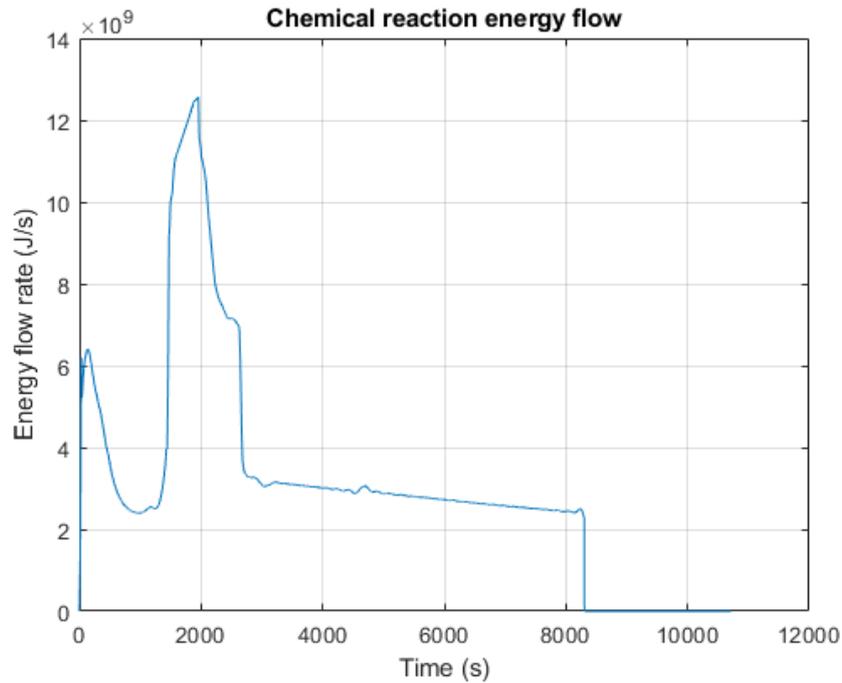
Figure 189: energy generated through the burning reaction

The following picture shows the amount of heat flowing into the combustion chamber walls, that must be disposed by the Thermal and Energy Management System; in fact, both the liquid hydrogen line and the gas assembly contain an ideal heat exchanger to absorb this extra heat and prevent the overheating of the combustion chamber. The calculation is carried out by Reynolds analogy, as stated before
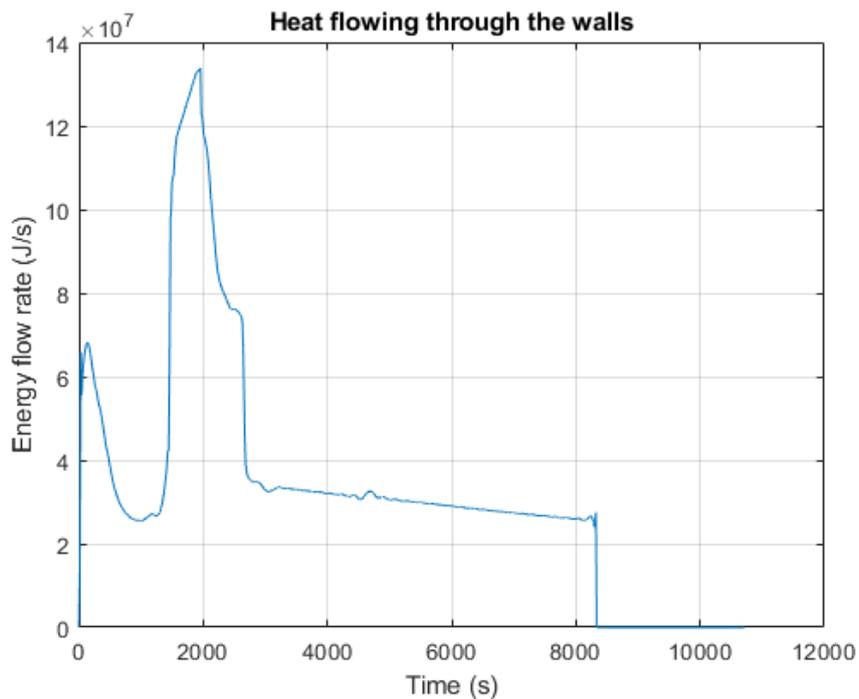

Figure 190: heat that flows through the combustion chamber walls

The following graph shows the evolution of temperature of reaction products inside the combustion chamber. It is noted that there is a temperature peak in correspondence of the maximum fuel mass flow, since the increasing mass cannot absorb the increasing amount of heat generated. As the simulation ends,

the temperature inside the combustion chamber tends to room temperature, since there is no more fuel available to burn.
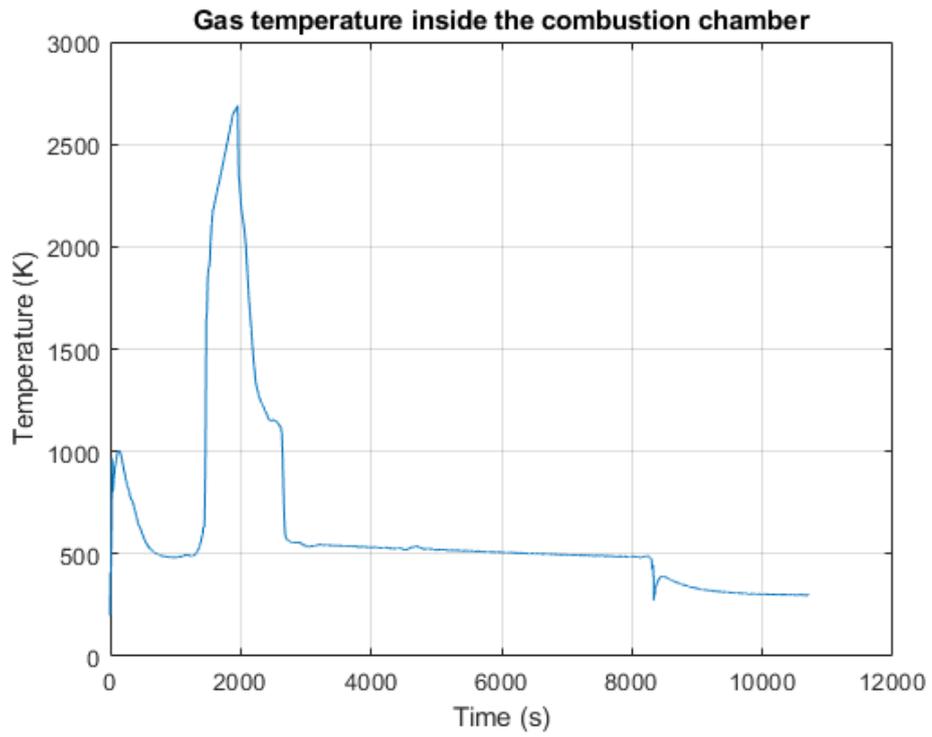

Figure 191: evolution of temperature of the gases within the combustion chamber

Conclusions and future steps

This work has been carried out with the aim of introducing new ideas, perfecting and deepening the definition of the TEMS system, within the framework of the STRATOFLY project. Being an innovative, complex and highly integrated on-board system, the research process has taken a long time, since a linear and logical analysis of the subject has required the deepening of several aspects of the classic aeronautical project, some of which are absolutely pioneering in the sector. The subject has been approached with a design point of view: the elaboration of the concept of VEMS, of which there is currently no prototype or in-depth study, has left ample room for creativity, making this work highly personal. Where possible, attempts were made to follow tried and tested design paths (as in the case of the definition of mission profile, which draws on current performance estimation techniques in civil aviation), but in most cases it was necessary to create a dedicated model or algorithm and to establish the limits of its application, then colliding with the physical reality through the dynamic simulations. Through a complex iterative and recursive study of the input parameters and their subsequent processing to the final result, an algorithm for the preliminary estimation of the performance with a relatively straightforward system has been developed, which can also be applied in the future at a later stage of refinement of the project.

Thesis summary

First, the main steps that make up this work are briefly retraced:

- Overall acknowledgement of the project as a whole
- Review of available literature, both concerning the previous LAPCAT MR2.4 project, and new STRATOFLY results
- Definition of a database containing the main aerodynamic coefficients, represented in a wide range of speed and angles of attack values
- Definition of a database containing the main performance indices of the propulsive plant, in a wide range of altitude and speed values
- Aerothermodynamic study on the leading edge of the inlet
- Mission simulation with flight mechanics equations and interpolation of previous databases
- In-depth analysis of the chemical and physical characteristics of hydrogen, mainly cryogenic. Definition of a database containing the most important properties of the fluid in a wide range of pressure and temperature values. Definition of boil-off phenomenon
- Elaboration of analytical methods (semi-empirical and analytic) for the estimation of the performance of the main components (active and passive) of turbomachinery
- Definition of thermal equilibrium at the interface between fuel and external environment, and assessment of the behaviour of hydrogen stored on board
- Dynamic design and simulation of a hydraulic system for onboard fuel transport
- Definition of the main interfaces of the VEMS system with other on-board subsystems, design and performance estimation of the thermal control system by dynamic simulation
- Design and dynamic simulation of the Environmental Control System
- Definition of a turboshaft architecture for fuel use on board, estimation of component performance. Dynamic system simulation and definition of a concept of operation for its use, in order to satisfy the demand for power;
- Estimated operation of the aircraft propulsion system and interface with the VEMS system.

Final results

In the last chapter, the results regarding the performance of turbo machines operating in the VEMS system were presented. The main components analysed from this point of view were the compressor and the turbine of the gas generator, the free power turbine, and the fuel management turbopump. Such turbomachinery has been characterized in terms of speed of rotation, torque produced/required, and therefore power

developed or absorbed. Then, the static sizing method described in Chapter 4 may be used, in order to provide a first-approximation estimation of the geometrical and physical characteristics of the components studied. This estimate could be approximate, but at conceptual design stage it is more necessary than ever to provide estimates as accurate as possible but easy to use for the preliminary definition of the whole aircraft; these evaluations will then be refined during the project together with all other components progress. In fact, in the aeronautical project, and especially in the definition of highly integrated systems, it is impossible to proceed blindly in the development of a single component in itself, but the project must evolve harmoniously, or with the same degree of deepening for each part, so as not to create imbalances and integration difficulties as the research progresses, and the changes become more difficult to implement.

From the static analysis the following graphs are obtained, respectively for the three main components, from which it is possible to make the dimensioning for each component, separately.

Compressor

Literature review states that a possible diameter for the gas assembly compressor could be $D_c = 0.3\ m$. Hence, the sizing of the compressor is only function of rotational speed (settled in the dedicated chapter) and of the number of compression stages. Since there is no literature review reference for the estimation of the latter, this will be assumed as a variable.
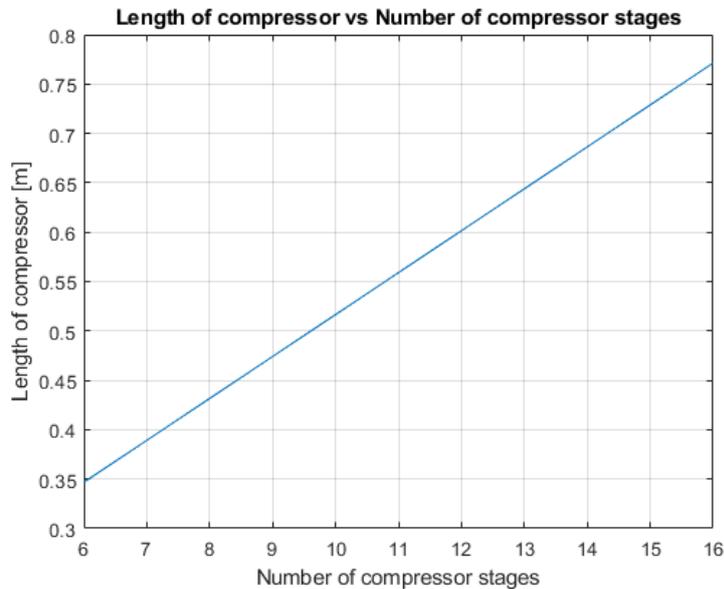

*Figure 192: compressor length vs number of compression stages*
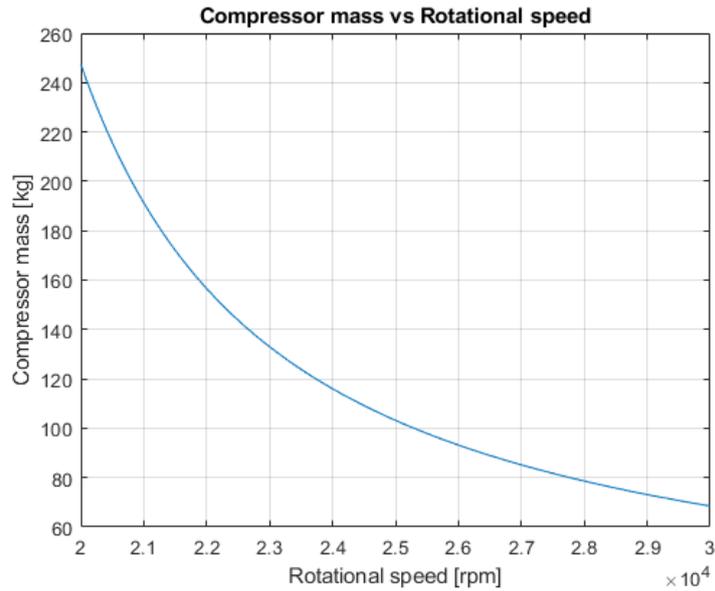
*Figure 193: compressor mass vs rotational speed*
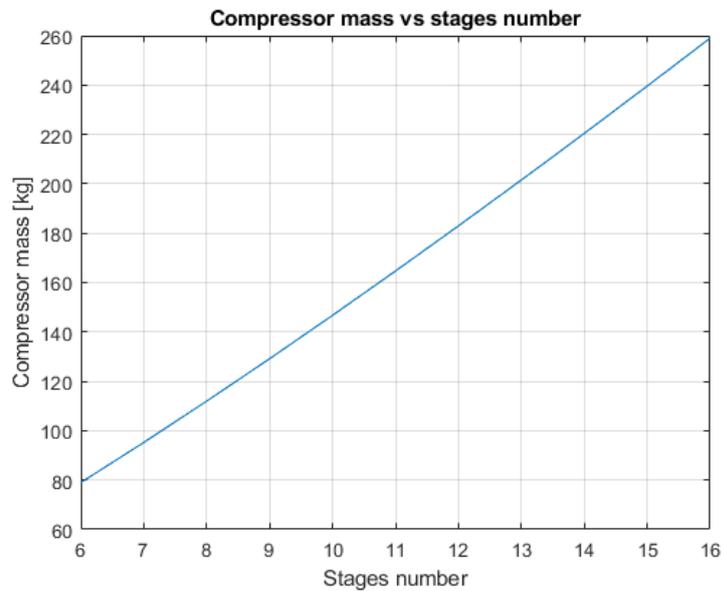
Figure 194: compressor mass vs number of compression stages

Turbine

Literature review states that a possible diameter for the gas assembly turbine could be $D_t = 0.8\,m$, while the free turbine is supposed to have a large diameter, $D_{ft} = 1.02\,m$. Hence, the sizing of the turbine is only function of rotational speed (settled in the dedicated chapter) and of the number of turbine stages. Since there is no literature review reference for the estimation of the latter, this will be assumed as a variable.
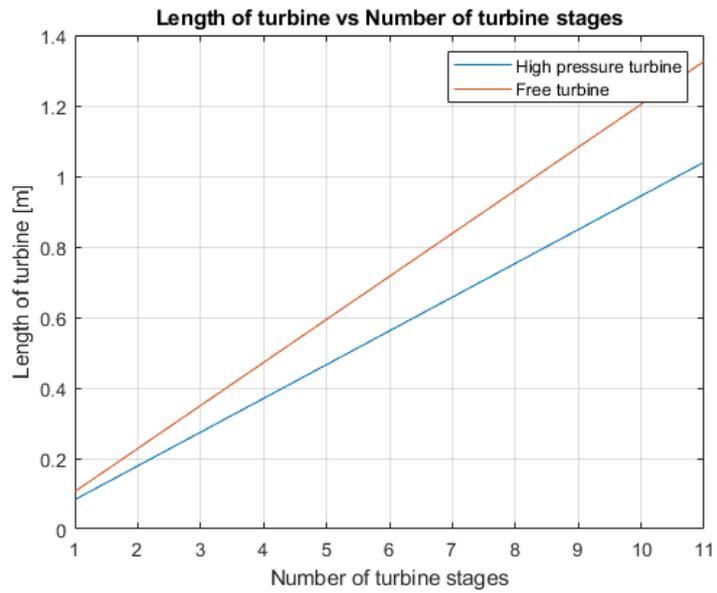
*Figure 195: turbine length vs number of expansion stages*
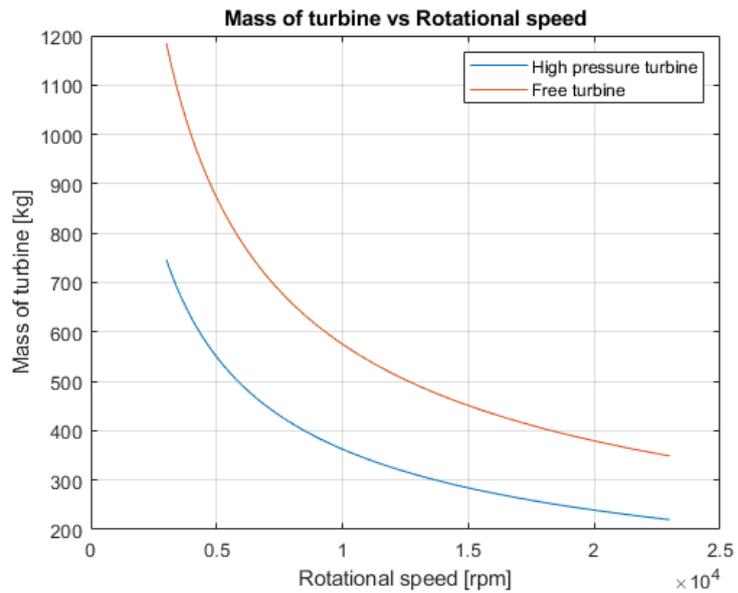
*Figure 196: turbine mass vs rotational speed*
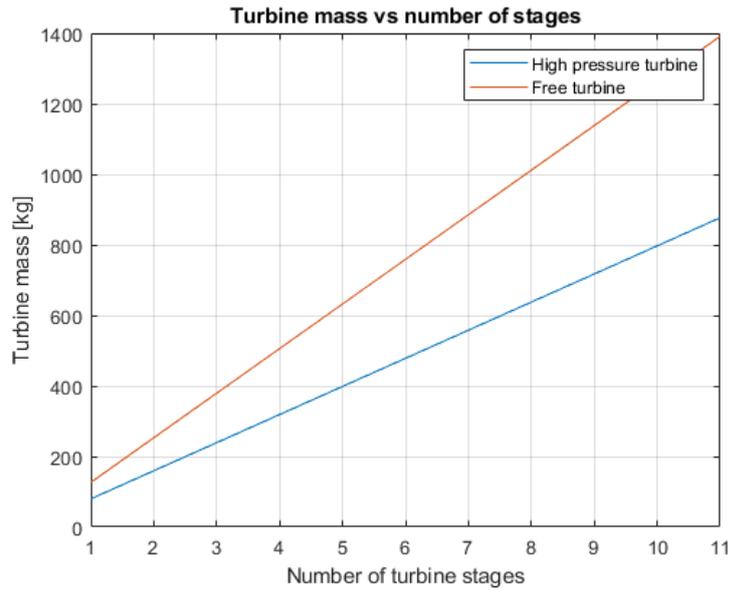
Figure 197: turbine mass vs number of expansion stages

Turbopump

In this case, a statistical analysis is available. Hence, the sizing of the turbopump will happen with a criterion of similarity with other existing hardware with the same physical characteristics.
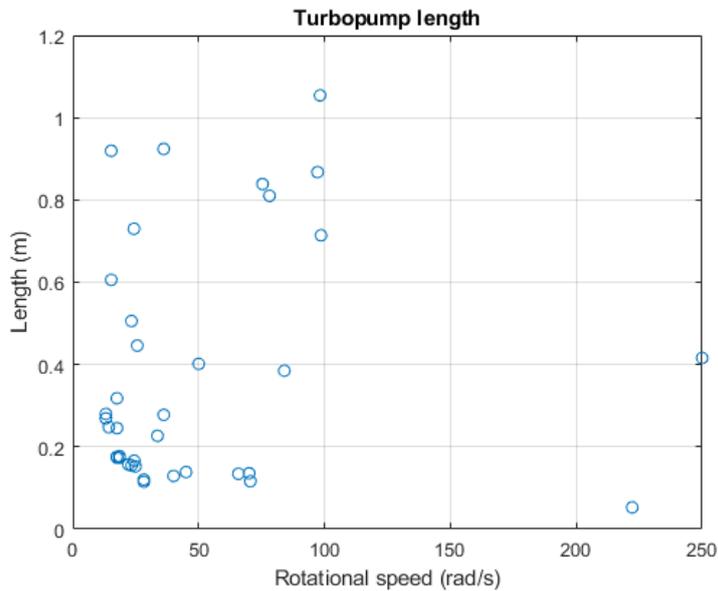

*Figure 198: statistical analysis of spacecraft turbopumps length*

176
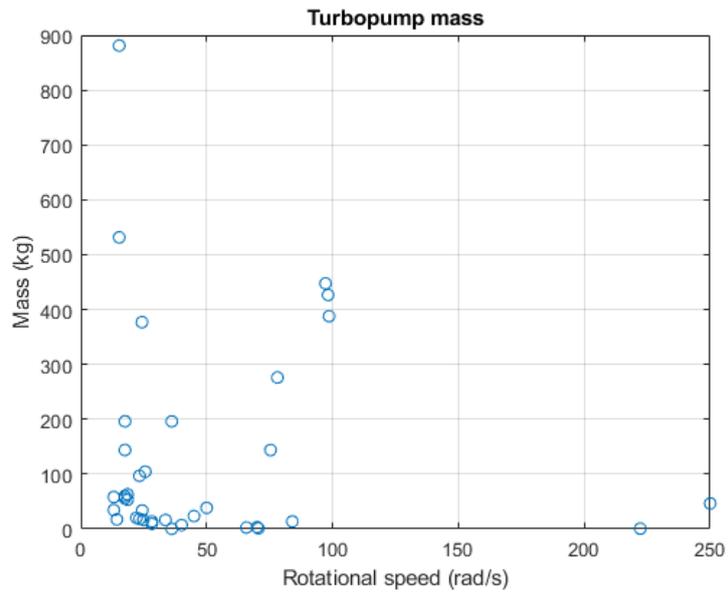
*Figure 199: statistical analysis of spacecraft turbopumps mass*
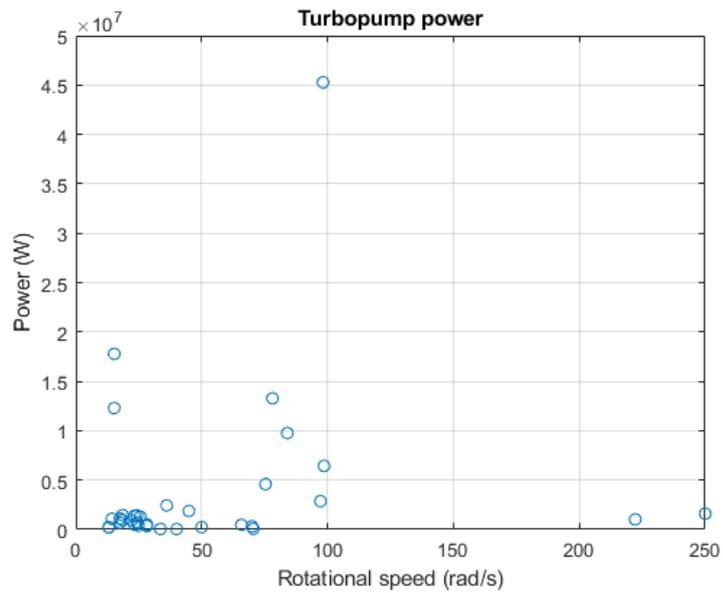
Figure 200: statistical analysis of spacecraft turbopumps consumed power

177

Future steps

It is important to remember that the analysis currently carried out, as it is performed at conceptual design level, presents some approximations due partly to the study techniques used and partly to the lack of information concerning the interfaces of the VEMS system with the external environment and other on-board subsystems. Please note that a design of a system, in the sense of heuristic sum of single components, follows an iterative and recursive process to be improved and deepened; in the present case, it is first necessary to refine the physical definition of components. For example, in the dynamic model of VEMS, the complexity of tanks (that characterizes this aircraft, and that is offering the design team a real challenge) has been approximated as a single cylindrical element containing the entire volume of liquid hydrogen. The same concept can be expressed for all components of TEMS, in which the representation of the component has been carried out according to its ultimate purpose; for the sake of clarity of the preliminary analysis, the design point was considered, sometimes neglecting the element actual physical layout and complexity. The physical models of simulated components itself can be further improved in order to simulate a wide range of real phenomena occurring in turbo machines which have not been considered during this analysis, whose purpose was a general characterization of the performance of the entire system. From the point of view of system inputs, it is necessary to update the technique of estimating thermal flow rates on the fuselage with the new trajectory data, and where possible obtain a subdivision of the heat flows for each section of the aeroplane (and not as a total average), so that the thickness of the insulation layer can also be characterised for each section. A further possible investigation could be an accurate study of the amount of heat generated in the combustion chamber of the main engine, and in general of its configuration, so that it is possible to hypothesize the architecture of the heat exchangers and the regenerative cycle: this study, together with the choice of insulation materials of the combustion chamber and the dedicated cooling techniques, could allow a more accurate estimation of the thermal loads from the propulsion plant to be disposed of by exchange with liquid (and gaseous) hydrogen. A useful step towards a more accurate definition of the amount of hydrogen evaporated in the tanks is a better estimate of the thermal flows entering from the outside; however, this process is the result of an iterative study includes various, often contrasting, needs of optimization of weights and thermal loads.

References

[1] [Online]. Available: http://www.horizon2020news.it/.

[2] [Online]. Available: http://www.horizon2020news.it/horizon-europe.

[3] [Online]. Available: http://www.horizon2020news.it/horizon-europe-3.

[4] [Online]. Available: https://ec.europa.eu/inea/en/horizon-2020/projects/h2020-transport/aviation/stratofly.

[5] [Online]. Available: https://www.h2020-stratofly.eu/index.php?option=com_content&view=article&id=55&catid=13&Itemid=233.

[6] D. R. S. D. N. Passin, «Aerodynamic Analisys of Hypersonic Waverider Aircraft.,» *Tech. rep. NASA,* vol. Ames Research Center, 1993.

[7] A. B. L. Vigevano, «Preliminary design of waverider aircraft,» *MA thesis,* vol. Politecnico di Milano, 2016.

[8] ESA-ESTEC, «Preliminary Mach 8 Turbo-Based/DMR Vehicle Analysis: Update of the LAPCAT-MR2.4 Waverider based Vehicle,» *LAPCAT II - Long-Term Advanced Propulsion Concepts and Technologies II,* 2008, October 1st .

[9] A. A. S. H. S. Mohammad Sadeghi, «A Novel Integrated Guidance and Control System Design in Formation Flight,» *Journal of Aerospace Technology and Management,* December 2015.

[10] D. A. Caughey, «Introduction to Aircraft Stability and Control - Course Notes for M&AE 5070,» Ithaca, New York , Sibley School of Mechanical & Aerospace Engineering, Cornell University , 2011.

[11] D. Krempus, «CFD study of the LAPCAT MR2 hypersonic cruiser,» ESA/ESTEC, 2017.

[12] J. S. V. F. Villace, «The Thermal Paradox of Hypersonic Cruisers,» *20th AIAA International Space Planes and Hypersonic Systems and Technologies Conference,* 6-9 July 2015.

[13] J. Anderson, Hypersonic and High-Temperature Gas Dynamics, AIAA, 2006.

[14] G. P. A. Viviani, Aerodynamic and Aerothermodynamic Analysis of Space Mission Vehicles, Springer Aerospace Technology.

[15] E. V. Zoby, «Empirical stagnation-point heat-transfer relation in several gas mixtures at high enthalpy levels,» *NASA TECHNICAL NOTE,* n. Ldngley Research Ceater, October, 1968.

[16] J. Steelant, «LAPCAT: High-Speed Propulsion Technology,» *Educational Notes RTO-END-AVT-150,* 2008.

[17] S. E. J. S. T. Langener, «Trajectory Simulation and Optimization of the LAPCAT-MR2 Hypersonic Cruiser concept,» *29th Congress of the International Council of the Aeronautical Sciences,* 7-12 September 2014.

[18] P. S. D. R. L. Jenkinson, Civil Jet Aircraft Design, London: Arnold, 1999.

[19] EUROCONTROL, «Aircraft Performance Database - A320,» [Online]. Available: https://contentzone.eurocontrol.int/aircraftperformance/details.aspx?ICAO=A320&ICAOFilter=a320 .

[20] B. Bajeli, «STRATOFLY Project: analysis of the Concept of,» *MSc. Thesis. Politecnico di Torino.*

[21] A. S. P. D. R. Barbucci, Tavola periodica e proprietà degli elementi, Edizioni V. Morelli, 1998.

[22] J. d. P. P- Atkins, «Atkins' Physical Chemistry,» W.H.Freeman, 2006.

[23] Hydropole, «About hydrogen,» [Online]. Available: https://hydropole.ch/en/hydrogen/abouth2/.

[24] W. U. N. W. L. J. T. M. T. A. M. Swanger, «Integrated Refrigeration and Storage for Advanced Liquid Hydrogen Operations,» *19th International Cryocooler Conference (ICC 19); June 20, 2016 - June 23, 2016; San Diego, CA; United States ,* June 20, 2016 .

[25] B. Granath, «Innovative Liquid Hydrogen Storage to Support Space Launch System,» NASA, [Online]. Available: https://www.nasa.gov/feature/innovative-liquid-hydrogen-storage-to-support-space-launch-system.

[26] J. Z. C. R. G. Helenbrook, «Development and validation of purged thermal protection systems for liquid hydrogen fuel tanks of hypersonic vehicles,» *NASA Contractor Report,* June, 1977.

[27] J. H. H. M. R. R. D. McCarty, Selected Properties of Hydrogen (Engineering Design Data), February, 1981.

[28] J. S. Victor Fernandez Villace, «The Thermal Paradox of Hypersonic Cruisers,» *20th AIAA International Space Planes and Hypersonic Systems and Technologies Conference,* 6-9 July 2015.

[29] E. Buckingham, On physically similar systems; illustrations of the use of dimensional equations, 1914.

[30] D. Pastrone, Dispense del corso di Motori per Aeromobili, 2018.

[31] C. P. P. Hill, Mechanics and Thermodynamics of Propulsion, Pearson, 2010.

[32] R. F. V. V. D. Ferretto, «Mathematical Description of the VEMS models,» 12 July 2018.

[33] S. L. R. P. K. D.A. Sagerser, «Empirical expressions for estimating length and weight of axis-flow components of VTOL powerplants,» *NASA technical memorandum,* December, 1973.

[34] V. F. V. J. S. Sarah Balland, «Thermal and Energy Management for Hypersonic Cruise Vehicles Cycle Analysis,» *20th AIAA International Space Planes and Hypersonic Systems and Technologies Conference,* 6-9 July 2015.

[35] F. D. R. Christian D. Bodemann, «THE SUCCESSFUL DEVELOPMENT PROCESS WITH MATLAB SIMULINK IN THE FRAMEWORK OF ESA'S ATV PROJECT,» 2004.

[36] I. The MathWorks, «Simscape : User's Guide,» 2019.

[37] The MathWorks, Inc., «https://it.mathworks.com/help/physmod/simscape/ref/reservoirtl.html,» [Online].

[38] T. M. Inc, «https://it.mathworks.com/help/physmod/hydro/ref/pipetl.html?s_tid=doc_ta,» [Online].

[39] T. M. Inc, «https://it.mathworks.com/help/physmod/hydro/ref/fixeddisplacementpumptl.html,» [Online].

[40] N. V. Mazzoldi, Fisica - Volume 1, 2001.

[41] «https://web.archive.org/web/20081006105349/http://www.kayelaby.npl.co.uk/general_physics/2_3/2_3_7.html,» [Online].

[42] «http://thermopedia.com/content/596/,» [Online].

[43] C. W. Hall, Laws and Models: Science, Engineering, and Technology.

[44] Y. A. Çengel, Heat and Mass Transfer, McGraw-Hill., 2002.

[45] J. Anderson, Modern compressible flow, with historical perspective, McGraw Hill, 2003.

[46] R. F. V. V. D. Ferretto, «Mathematical Description of the VEMS models,» 2018.

[47] Turolla, «Gear Pumps - Group 2 - Technical information,» [Online]. Available: https://www.turollaocg.com/files/Catalogs/Turolla_Group_2_Gear_Pumps_L1016341_Web.pdf.

[48] Neutrium, «https://neutrium.net/equipment/estimation-of-pump-moment-of-inertia/,» [Online].

[49] Nautrium, «https://neutrium.net/equipment/pump-power-calculation/,» [Online].

[50] A. Guide, «Aircraft Air Conditioning Systems,» [Online]. Available: https://www.aircraftsystemstech.com/2017/05/aircraft-air-conditioning-systems.html.

[51] D. P. D. F. P. Incropera, Fundamentals of Heat and Mass Transfer, New York: Wiley, 1990.

[52] H. L. Sadik Kakaç, Heat Exchangers: Selection, Rating and Thermal Design, CRC Press, 2002.

[53] T. M. Inc, «Heat Exchanger (G-G),» [Online]. Available: https://it.mathworks.com/help/physmod/hydro/ref/heatexchangergg.html.

[54] Y. A. Çengel, Heat Transfer: A Practical Approach, McGraw-Hill.

[55] «LAPCAT II - Long-Term Advanced Propulsion Concepts and Technologies II,» in *Preliminary Mach 8 Turbo-Based/DMR Vehicle Analysis: Update of the LAPCAT-MR2.4 Waverider based Vehicle*, 2008.

[56] E. A. S. Agency, Certification Specifications for Large Airoplanes - CS-25, 2007.

[57] «Valori rappresentativi degli apporti di calore sensibile e latente rilasciati dalle persone in diversi stati di attività,» 26 11 2004. [Online]. Available: http://www.idronicaline.net/admin/tiny_mce/plugins/filemanager/files/software/tmf/apporti_delle_personex__tfm.pdf.

[58] V. F. V. J. S. Sarah Balland, «Thermal and Energy Management for Hypersonic Cruise Vehicles - Cycle Analysis,» *International Space Planes and Hypersonic Systems and Technologies Conferences,* 6-9 July 2015.

[59] C. P. P. Hill, Mechanics and Thermodynamics of propulsion, Pearson Education, 1992.

[60] P. P. T. N. B. Nkoi, «Performance assessment of simple and modifies cycle turboshaft gas turbines,» Cranfield University, UK, 15 April 2013.

[61] M. Edu, «Brayton Cycle,» [Online]. Available: http://web.mit.edu/16.unified/www/SPRING/propulsion/notes/node27.html.

[62] [Online]. Available: https://i.stack.imgur.com/4iEPw.jpg.

[63] «Performance Corrections for Compressor Maps,» Concepts NREC, [Online]. Available: https://www.conceptsnrec.com/blog/performance-corrections-for-compressor-maps.

[64] «Compressor Map,» Performance Trends Inc, [Online]. Available: http://performancetrends.com/Definitions/Compressor-Map.htm.

[65] «Compressor Maps,» EnggCyclopedia, [Online]. Available: https://www.enggcyclopedia.com/2012/01/compressor-maps/.

[66] K. Dinh, «Compressor and Turbine Map Details,» Turbo Tech, [Online]. Available: https://motoiq.com/turbo-tech-compressor-and-turbine-map-details/.

[67] K. B. R. Kurz, «Gas Turbine: what makes the map?».

[68] S. Van Wylen, Fundamentals of Classical Thermodynamics.

[69] «LAPCAT II - Long-Term Advanced Propulsion Concepts and Technologies II. Collaborative Project: Small or Medium-Scale Focused Research Project. Theme 7: TRANSPORT,» 2008.

[70] T. E. ToolBox, «Air - Composition and Molecular Weight,» [Online]. Available: https://www.engineeringtoolbox.com/air-composition-d_212.html.

[71] C. o. t. Desert, «Module 3: Hydrogen use in internal combustion engines,» December 2001.

[72] M. B. M. K. Y. Cengel, Thermodynamics: An Engineering Approach, McGraw-Hill, 2019.

[73] C. J. Jachimowski, «An A.nalytica1 Study of the Hydrogen-Air Reaction Mech-anism With Application to Scramjet Combustion,» NASA, 1988.